THE EFFECT OF THE PARTICLE SIZE DISTRIBUTION ON NON-NEWTONIAN TURBULENT SLURRY FLOW IN PIPES

by

GARY SVEN THORVALDSEN

ABSTRACT

THE EFFECT OF THE PARTICLE SIZE DISTRIBUTION ON NON-NEWTONIAN TURBULENT SLURRY FLOW IN PIPES

The handling of solid-liquid suspensions is an important concern within the chemical and processing industries and many theoretical models have been proposed to try and explain and predict turbulent flow behaviour. However, the prediction of turbulent flow from only the viscous properties of non-Newtonian suspensions has over the years been questioned by researchers. This thesis considers theoretical models well established in the literature and the Slatter model, which uses both the rheology of the suspension and the particle size distribution of the solids. These models are used to analyze the experimental data and the effect that particle size and the particle size distribution has on turbulent flow behaviour.

The literature concerning the rheological fundamentals relevant to fluid flow in pipes has been examined. The Newtonian turbulent flow model as well as the non-Newtonian models of Dodge & Metzner, Torrance, Kemblowski & Kolodziejski, Wilson & Thomas and Slatter have been reviewed.
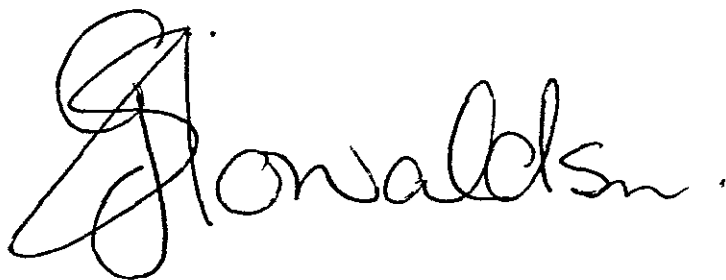
Test work was conducted at the University of Cape Town's Hydrotransport Research Laboratory using a pumped recirculating pipe test rig. The test apparatus has been fully described and calibration and test procedures to enable collecting of accurate pipeline data have been presented. Three slurries were used in test work namely kaolin clay, mixture 1 (kaolin clay and rock flour) and mixture 2 (kaolin clay, rock flour and sand) with a d_{85} particle size ranging from $24\mu m$ to $170\mu m$.

The yield pseudoplastic model has been used to model and predict the laminar flow of the suspensions that were tested and the method adopted by Neill (1988) has been used to determine the rheological constants. The pipeline test results have been presented as pseudo-shear diagrams together with the theoretical model lines providing a visual appraisal of the performance of each model. The Slatter model predicts the test data best with the other theoretical models that were considered tending to under predict the head loss. The reason the Slatter model performs better than the other theoretical models is because this model can account for the wall roughness and particle roughness effect. Evidence to support this statement has been presented.

This thesis highlights the fact that the particle size distribution is a vitally important property of the suspension and that it does influence turbulent flow behaviour. It shows that turbulence modelling using the particle roughness effect (eg Slatter, 1994) is valid and can be adopted for non-Newtonian slurries. It is concluded that the particle size distribution must be used to determine the particle roughness effect and this effect must be incorporated in the turbulent flow analysis of non-Newtonian slurries.

DECLARATION

I, Gary Sven Thorvaldsen, hereby declare that to the best of my knowledge and belief, this thesis is essentially my own work and has not been submitted for the award of any other diploma or degree at any university or technikon.

G S Thorvaldsen

October 1996

DEDICATION

to my parents

and to those who have shown and taught me to celebrate life to the fullest, to seize the day, to be educated - not simply to fill the mind with knowledge but to open the mind to all possibilities, for learning produces change, change produces surprise and surprise, joy.

"I am a survivor of a concentration camp. My eyes saw what no person should witness. Gas chambers built by learned engineers, children poisoned by educated physicians, infants killed by trained nurses, woman and babies shot and killed by high school and college graduates. So I am suspicious of education. My request is, help your students to be human. Your efforts must never produce learned monsters, skilled psychopaths or educated Eikmans. Reading and writing and spelling and history and arithmetic are only important if they serve to make our students HUMAN."

Quotation taken from a book by H Genard

"Each of us has a time for life.
There is a misconception that we have forever.
In reality we have such a brief moment in time
but remember even that brief moment is yours.
It's yours to celebrate - to misuse it, to loose
it, is to devalue our greatest gift - the gift of
life.

It's our personal celebration with so much to
be joyous over, like the right to love, the
wonder of mingling with unique people, of
smiles, of hugging each other, of good food, of
flowers, of trees, of sunlight, of green grass
and cool summer breezes, of high flying
balloons - oh and so much more. This is our
time, the time of our lives. Don't miss a
minute of it, it passes so quickly. The time to
live and celebrate is NOW."

Leo Buscaglia

ACKNOWLEDGEMENTS

PUBLICATIONS

The following paper was presented by the author in support of this thesis:

"Particle Roughness Turbulence", 13th International Conference on Slurry Handling and Pipeline Transport, Johannesburg, South Africa, September 1996, BHR Group Conference Series - edited by J F Richardson, Mechanical Engineering Publication Limited, UK, pg 237-257.

CONTENTS

LIST OF FIGURES

LIST OF TABLES

Page

NOMENCLATURE

Symbol	Description	Unit
a	constant	
A	constant	
	cross sectional area	m^2
A_r	area ratio	
b	constant	
B	constant	
	roughness function	
c	constant	
C	concentration	
C_D	drag coefficient	
d	particle diameter	μm
D	internal pipe diameter	m
E	error function	
	rheological parameter	
f	Fanning friction factor	
F	force	N
k	constant	
	hydraulic roughness	μm
K	fluid consistency index	$Pa.s^n$
K′	apparent fluid consistency index	$Pa.s^{n'}$
l	average amplitude of the liquid oscillation	
$\mathscr{L}$	Prandtl mixing length	m
L	pipe length	m
m	slope	
	rheological parameter	
M	mass	kg
n	flow behaviour index	

n'	apparent flow behaviour index	
N	number of items	
p	mixing length factor	
	pressure	Pa
q	ratio of solid to liquid oscillation amplitude	
Q	volumetric flow rate of slurry	m^3/s
r	radius at a point in the pipe	m
	correlation coefficient	
R	radius of the pipe	m
Re	Reynolds number	
S	relative density	
u	point velocity	m/s
u^+	dimensionless velocity	
V	average slurry velocity	m/s
V_*	shear velocity	m/s
X	unknown quantity	
	abscissa value	
y	distance from the pipe wall	m
y^+	dimensionless wall distance	
Y	ordinate value	
α	proportional to	
	shape factor	
	shear stress ratio	
δ	viscous sub-layer thickness	μm
Δ	increment	
ϵ	relative roughness	
η	coefficient of rigidity for Bingham fluid	Pa.s
λ	friction factor $= 4f$	
μ	dynamic viscosity	Pa.s
μ'	apparent dynamic viscosity	Pa.s
ρ	slurry or fluid density	kg/m^3

τ	shear stress	Pa
τ_y	yield stress	Pa
Φ	function of	
	rheological parameter	
χ	von Karman constant	
Ω	velocity function	

Subscripts

0	at the pipe wall
85	85th percentile of the particles passing
ann	refers to the annulus
c	critical
calc	calculated
l	loss, liquid
m	mixture (slurry)
max	maximum
N	Newtonian
NN	non-Newtonian
obs	observed (experimental)
p	particle
plug	of the plug
r	roughness
res	residual
s	solids
shear	zone over which shear occurs
v	volumetric
w	water
x	representative size

CHAPTER 1

CHAPTER 1

INTRODUCTION

1.1 STATEMENT OF THE PROBLEM

The handling of solid-liquid suspensions is an important concern within the chemical and processing industries and hence the study of fluid flow is essential if fluids are to be efficiently and economically transported in a pipeline system. The pumping of these suspensions in the chemical processing industry normally takes place both in the plant and over long distances and includes various foodstuffs, chemicals, chemical and industrial wastes, sewage and mine and quarry products. Slurries of high concentration are also frequently encountered in the petroleum and detergent industries and virtually every mineral processing installation has a tailings pipeline to transport waste to the mineral disposal site. A large number of these industrial suspensions encountered do not follow the simple laws of flow (Alves, 1949) and are therefore referred to as non-Newtonian suspensions ie. they do not obey Newton's law of viscosity (Govier and Aziz, 1972).

A design engineer is thus faced with many problems when designing a system for the transportation of non-Newtonian suspensions. Some problems encountered are the determination of the pressure gradient, the sizing of the pipeline and pump selection. The most accepted method used by industry today, for the efficient design of pipeline systems, is by conducting large scale pipe tests. In carrying out large scale pipe tests designers try to simulate normal operating conditions in order to determine required parameters and data for design. This is widely accepted by industry provided prototype diameter and velocity are used (Moodie et al, 1994). Even though designers try to simulate normal operating conditions, usually a range of variables are covered as desired flow rates cannot be exactly matched (Cheng, 1970).

In fluid engineering design, the laminar flow behaviour of non-Newtonian suspensions is reasonably well understood and can be predicted using theoretical models from the literature.

Data obtained can be used for design and if in the form of a curve of shear stress vs shear rate (as presented in this study) can be used directly for scale-up (Alves *et al*, 1952 & Metzner, 1956).

Turbulent flow of non-Newtonian suspensions on the other hand is complex and is often considered problematic for design. However, in many situations it has beneficial characteristics, preventing suspensions settling and enabling higher throughputs (Mun, 1988). Many commercial slurry pipes operating in the turbulent flow regime operate close to the transition region and therefore any error in prediction of the transition velocity will cause large errors in pressure drop predictions (Thomas, 1976).

Many theoretical models have therefore been proposed to try and explain and predict turbulent flow behaviour. The benefit to industry would be tremendous if turbulent flow behaviour could be accurately predicted as it would greatly reduce the cost of the energy requirements for pumping the solids. Inaccurate predictions could result in the wrong size pump or pipe diameter being specified or even that the system will not operate at the required throughput (Slatter, 1994). From the above it can be seen that efficient design of pipe and pump plant is of paramount importance. This is reinforced when it is considered that 15% to 25% (Aude *et al*, 1971) or even up to 30% (Bunker, 1954) of the investment in chemical plants is for piping. In fact the final choice of pipeline characteristics is often governed by the capital cost of pipework and pump and also the installation and maintenance costs (Cheng, 1970).

1.1.1 Solid Particle Effect

The prediction of turbulent flow or pipe flow energy requirements from only the viscous properties of non-Newtonian suspensions has over the years been questioned by researchers. It has been found that flow behaviour and rheology of these suspensions can be and is influenced by such factors as particle size, shape, weight and distribution (Philippoff 1944, Hedström 1952, Orr & Blocker 1955, Zettlemoyer & Lower 1955, Maude and Whitmore 1956, 1958, Thomas 1963, Thomas 1983, Mun 1988, Slatter 1994).

For example:

- In experiments carried out by Maude & Whitmore (1956) it was postulated that in determining the turbulent flow behaviour of suspensions, particle size is a significant factor. Maude & Whitmore (1958) hence performed a study on dilute mono-disperse systems and their subsequent correlation took account of the particle size. They also reported that the viscous sub-layer was significantly affected by particle size.

- Orr & Blocker (1955) concluded that particle size is of no relevance in determining the flow behaviour of suspensions, although the particle size distribution (PSD) is. However, in the very next paper of the same journal, Zettlemoyer & Lower (1955) documented the exact opposite conclusion.

- D G Thomas (1963) reported that there was evidence to suggest that particle shape affected turbulent flow data which could not be predicted from simple laminar-flow measurements.

- The effect of particle size was also reported by A D Thomas (1983) and illustrated by plotting the ratio of the suspension pressure drop to the water pressure drop against the average particle size of the suspension.

- An extensive study was conducted by Mun (1988) in which twenty four correlations found in the literature were compared with experimental data obtained using a fine and coarse liminite suspension and a coal suspension. A definite variation in turbulent flow behaviour of the suspensions tested was found, dependent upon their particle size. It was thus concluded by Mun (1988) that the particle size and hence the PSD of a suspension is important in describing turbulent flow behaviour.

- Slatter (1994) found that the particle size will have an effect on the turbulent flow head loss of that particular slurry and that the size of the particle plays a pivotal role in the interaction at the pipe's surface in producing a roughness effect in turbulent

flow, which in turn affects the viscous sub-layer.

However, even with findings such as these, most of the theoretical models which have been proposed to predict turbulent flow behaviour have not taken into account the size of the particles inherent in the fluid. In fact Mun (1988) states that particle size is the most frequently overlooked piece of data in published literature data. Only as recently as 1994 was a new model been proposed by Slatter (1994) to account for not only the rheology of the slurry but also the representative particle size of the solids.

1.2   OBJECTIVE

The aim of this study is to model turbulent flow using Slatter's model as well as other models already well established in the literature, to determine the effect of the PSD on non-Newtonian flow in pipes and to analyze the results.

The majority of the test work conducted by Slatter (1994) was done using kaolin clay as the solids material with only 15% of the tests having a representative particle size exceeding 50μm. The average representative particle size of the remaining tests was 29μm.

This study is essentially a continuation of work conducted by Slatter (1994) and hence tests were conducted using kaolin clay to first confirm the accuracy of Slatter's model. Further tests were then carried out using a mixture of kaolin clay and rock flour (mixture 1) and a mixture of kaolin clay, rock flour and sand (mixture 2) in order to obtain a representative particle size higher than that tested by Slatter (1994) and to observe the influence of the particle size and the particle roughness effect on turbulent flow predictions using the various theoretical models.

1.3 METHODOLOGY

The following steps were undertaken with the above objective in mind.

1.3.1 Literature Review

The literature review covers the following theoretical models:

- Newtonian approximation
- Dodge and Metzner (1959)
- Torrance (1963)
- Kemblowski & Kolodziejski (1973)
- Wilson & Thomas (1985)
- Slatter (1994)

The correlation of Maude & Whitmore (1956, 1958) is also reviewed as it is the only correlation previous to Slatter's theoretical model to take any account of the particle size of the suspension.

1.3.2 Experimental Work

Experimental work was conducted at the University of Cape Town's Hydrotransport Facility using a pumped recirculating pipe test rig consisting of pipe diameters 25mm, 80mm, 150mm and 200mm.

1.3.3 Analyses of Data

The aforementioned theoretical models were used to analyze the data obtained.

1.4   BENEFITS

Slatter's model is mainly theoretical at this stage and it is envisaged that through applying practical research to the model that it will go some way to establishing a new model for industry and to make it more acceptable.

CHAPTER 2

CHAPTER 2

LITERATURE REVIEW

2.1   INTRODUCTION

The presentation in this chapter deals with the rheological fundamentals relevant to fluid flow in pipes. These fundamentals include the classification, measurement and interpretation of non-Newtonian behaviour.

2.2   FLOW PATTERNS

The nature of flow of a fluid depends on a number of factors. Factors influencing flow are:

- the physical properties of the fluid and its mass flow rate,

- the geometry of the container or pipeline.

The flow of a fluid can be characterized into one of three categories namely laminar flow, transitional flow or turbulent flow.

2.2.1 Laminar Flow

In laminar flow layers of fluid move relative to each other without any macroscopic intermixing (Holland, 1973) ie. there are no components of velocity normal to the direction of flow (Govier & Aziz, 1972). From the above statement it can be understood why laminar flow is also referred to as viscous or streamline flow in the literature.

For the purpose of this study the yield pseudoplastic model has been used for laminar flow predictions (section 2.6), although other models in the literature may also be used.

2.2.2 Transition from Laminar to Turbulent Flow

There are several methods in the literature that can be used to identify the transition between

laminar and turbulent flow. However, the transition between these two regimes is very rapid and is often difficult to identify. It is known that below a certain velocity laminar flow will exist and above a certain velocity turbulent flow exists. The transition region can therefore be expressed as a region acting between these two critical velocities ie. at a certain critical velocity the relationship between energy loss and velocity changes fundamentally (Slatter, 1994). It must however be expressed that this region is not only a function of the velocity but also of the Reynold's number and depends on the average pipe roughness size relative to the thickness of the viscous sub-layer (Sabersky & Acosta, 1966). Slatter (1994) showed how the Torrance Reynolds number, which excludes the yield stress of the fluid, is unable to predict the transition and hence he states that full rheology should be used in determining the transition point.

Some of the well known methods in the literature for determining the transition region are as follows:

● For Bingham plastic fluids Binder & Busher (1946), Hedström (1952) and Hanks (1963) have proposed methods based on modification of Reynolds numbers.

● For pseudoplastic fluids proposed methods are given by Dodge & Metzner (1959), Ryan & Johnson (1959), Clapp (1961), Kemblowski & Kolodziejski (1973), Hanks & Ricks (1975).

● For yield pseudoplastic fluids Slatter (1994) developed a new non-Newtonian Reynolds number which uses the complete rheology and the unsheared core geometry (section 2.10.5).

● Cheng (1970) proposed a general method for determining the transition region based on the proposal of Ryan & Johnson (1959).

● An intersection method, using the laminar and turbulent lines as the critical point has been proposed by Shook & Roco (1991).

2.2.3 Turbulent Flow

Turbulence is a natural form of fluid motion which is characterized by irregular, random movement of fluid both parallel and transverse to the direction of the main flow. Turbulent flow behaviour, which is the main emphasis of this study, and the modelling of non-Newtonian slurries are discussed further in section 2.8, section 2.9 and section 2.10.

2.3   REYNOLDS NUMBER

The Reynolds number can be used to determine what mode of flow exists under given conditions. The famous dye experiment conducted by Osborne Reynolds in 1883, a study of the head losses associated with the flow of water through pipes, showed clearly the distinction between laminar and turbulent flow. He stated that the transition between these two regimes was characterized by a dimensionless group,

$$Re = \frac{\rho \ V \ D}{\mu} ,$$
(2.1)

called the Reynolds number in his honour. The end of the stable laminar flow region usually occurs around Re=2100 (Alves 1949, Metzner 1956, Ryan & Johnson 1959, Govier & Aziz 1972).

2.4   RHEOLOGY

Rheology can be defined as "the study of the deformation and flow of matter" (BS 5168) as termed by the late Prof E C Bingham. It is that branch of science which deals with relationships between a shear stress and the resulting shear rate of a fluid in the laminar flow region and any variable influencing these relationships (Metzner, 1956).

2.4.1 Shear Stress

Under laminar flow conditions when adjacent layers of fluid are displaced laterally over each other the deformation of the fluid is called shearing (Duncan 1982, Holland 1973). Thus shearing stresses are involved when there is flow or motion of a fluid.

2.4.2 Yield stress

Yield stress can be defined as the force per unit area required to break down the rigid structure of the material and initiate laminar flow (Mun, 1988). The yield stress is an important consideration in the design of pipelines for suspensions due to the following:

- Slurries with a high yield stress often require higher pumping pressures to obtain a given flow rate. The pumping of slurries with a high yield stress can be uneconomical due to the high energy consumption and capital cost of the pumps (Mun, 1988).

- However, it can be advantageous for a slurry to have a high yield stress as this usually implies that it can be safely transported in laminar flow without danger of solid deposition problems (Cheng, 1975).

2.4.3 Newton's Law of Viscosity
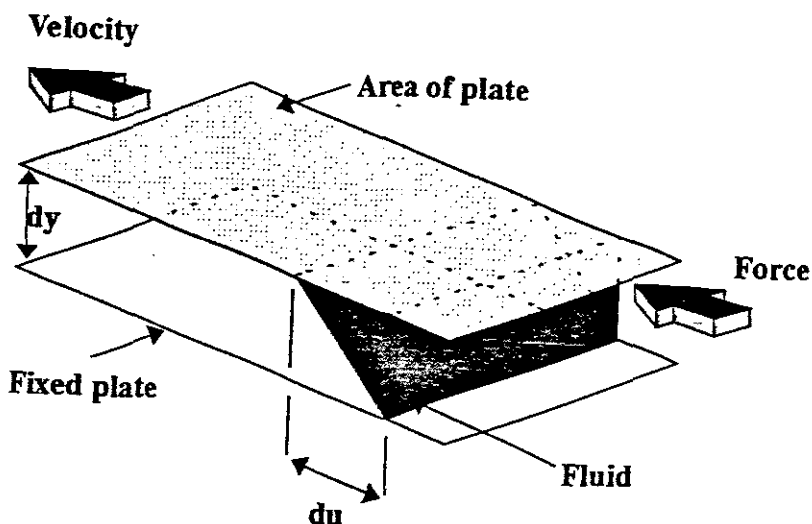
Figure 2.1: Illustration of Newton's law of viscosity

Newton postulated that for a given fluid an applied shearing stress will be proportional to the

velocity gradient, provided laminar flow conditions exist. This can be illustrated (Miller, 1989) by the experiment as shown in Figure 2.1 where two parallel plates, of equal area, are separated by a distance denoted by dy. The space between the plates is filled with a fluid. A constant force is applied to the top plate causing it and the adjacent fluid to have a velocity du. No slip occurs at the bottom of the fixed plate and thus the fluid at this point has no velocity. The relationship between force, area and displacement, as Newton postulated, is given by:

$$F = A \, \mu \, \frac{du}{dy} \quad \text{or,} \tag{2.2}$$

$$\tau = \mu \, \frac{du}{dy} \quad \text{ie.} \quad \frac{F}{A} = \tau \, \alpha \, \frac{du}{dy} \, , \tag{2.3}$$

where μ is the coefficient of absolute or dynamic viscosity.

For the flow of a fluid in a pipe, the above relationship becomes:

$$\tau = \mu \left[- \frac{du}{dr} \right] . \tag{2.4}$$

2.5   FLUID CLASSIFICATION

Fluids are classified according to the relationship expressed in equation 2.4. Fluids obeying this relationship are termed Newtonian and those which do not, non-Newtonian.

2.5.1 Newtonian Fluids

The viscous properties of a Newtonian fluid undergoing shear can be defined by one rheological constant, the viscosity. As can be seen from Figure 2.2 a plot of shear stress against shear rate yields a straight line for Newtonian fluids. The straight line has a slope equal to the coefficient of dynamic viscosity (equation 2.4).

However, even though the above statements can be taken to be true for Newtonian fluids there are times when certain fluids deviate from the Newtonian behaviour. From theoretical considerations as presented by Grunberg & Nissan (1945) it can be concluded that at high rates of shear the viscosity of these fluids (eg. n-pentane) may become a function of the shear rate. Other fluids which behave as Newtonian at lower shear stresses also exhibit non-Newtonian behaviour above certain shear stresses. In experiments conducted by Weltmann (1948) it was shown that several oils have a non-Newtonian behaviour above a limiting shear stress of approximately 958 Pa. This seems to contradict the fact that normally at high Reynolds numbers non-Newtonian behaviour decreases (see section 2.5.3.d).

Examples of Newtonian behaviour include:

- all gases,
- all liquids or solutions of low molecular weight (Metzner, 1956).

2.5.2 Non-Newtonian fluids

Unlike Newtonian fluids, the term viscosity has no meaning for a non-Newtonian fluid unless it is related to a particular shear rate (Holland, 1973). However, an apparent viscosity can be defined as (Holland 1973, Wilson 1986):

$$\mu' = \frac{\tau_0}{\left[-\dfrac{du}{dr} \right]_0} \quad . \tag{2.5}$$

Non-Newtonian fluids are normally divided into one of two categories (Metzner, 1956):

(a)   Fluids with properties independent of tome or the duration of shear.

(b)   More complex fluids where the relationship between shear stress and shear rate depends on the duration of shear.

A graphical representation of several possible relationships between shear stress and shear rate for non-Newtonian fluids, called a rheogram, is shown in Figure 2.2.

Most of the engineering work in industry today deals with the first category into which non-Newtonian fluids fall ie. time independent fluids (Metzner 1956, Aude *et al* 1971).

2.5.3 Characteristics of Non-Newtonian Behaviour.

In general, solutions of high-molecular-weight polymeric materials are non-Newtonian (Metzner, 1956). However, a number of factors can influence the degree of non-Newtonian behaviour.
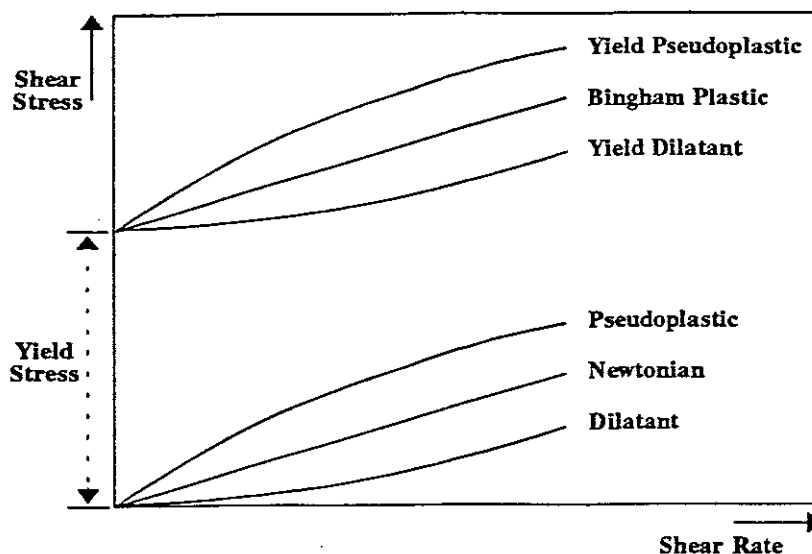
Figure 2.2: Rheological models for non-Newtonian fluids

Some of the factors influencing non-Newtonian behaviour include:

(a)   Particle Size

The probability of a solid-liquid suspension displaying non-Newtonian behaviour is increased as the particle size of the solids decreases. Very small particles, however, which are suspended by Brownian motion may flocculate and thus decrease the extent of non-Newtonian behaviour (Lazarus, 1992).

⟋(b)   Particle Shape

In a Newtonian liquid, if the solid particles are rigid spherical particles, they impart pseudoplastic behaviour. Rigid ellipsoidal and elastic spherical particles will normally result in visco-elastic behaviour (Charles & Kenchington, 1976).

⟋ (c)   Concentration

The increase of solids concentration increases the degree of non-Newtonian behaviour and larger particles may form a non-Newtonian mixture at increased concentration (Lazarus, 1992). Thomas (1963) showed that for particles in the range 0,35 to 13 μm the yield stress is inversely proportional to the particle diameter and proportional to the cube of the volumetric concentration.

ι (d)   Reynolds Number

At high Reynolds numbers non-Newtonian behaviour decreases (Lazarus, 1992). This is due to the fact that turbulent flow of non-Newtonian fluids at high Reynolds numbers is characterized by increased inertial forces compared with the viscous forces. This is in contradiction to the findings of Weltman (1948) (see section 2.5.1). In laminar flow and at low Reynolds numbers the non-Newtonian characteristics or behaviour becomes more prominent.

2.6   SLURRY CLASSIFICATION

Solid-liquid suspensions (ie. slurries) can be classified in one of two regimes according to the manner in which they flow.

2.6.1 Homogeneous Slurries

This type of slurry often exhibits non-Newtonian rheology (Thomas 1976, Lazarus 1992) and although it is characterized by a uniform concentration of particles about the axis of the pipe, it flows as a single-phase fluid (Thomas 1976). This definition encompasses non-settling

slurries as well as those requiring turbulent flow to maintain homogeneity. This study will concentrate on homogeneous slurries.

2.6.2 Heterogeneous Slurries

By contrast, heterogeneous slurries do not behave as single-phase fluid ie. the fluid and solid phase retain their separate identities. Hence, these slurries will flow with a non-axisymmetric concentration distribution. The solids phase tends to have larger particles than homogeneous slurries.

2.7   TIME-INDEPENDENT FLUIDS

2.7.1 Introduction

Bingham plastic, pseudoplastic and dilatant fluids all fall into this category. However, all of these rheological relationships as well as the Newtonian and yield dilatant relationships can be described by the yield pseudoplastic model (sometimes referred to in the literature as the generalised Bingham model). The rheological assumption for the yield-pseudoplastic model, as suggested by Herschel & Bulkley (1926), is as follows:

$$\tau = \tau_y + K \left[-\frac{du}{dr} \right]^n , \tag{2.6}$$

where τ_y is the yield stress,

   K is the fluid consistency index which characterizes the "thickness" of a fluid and is similar to the viscosity of a Newtonian fluid,

   n is the flow behaviour index and characterizes the extent of deviation of a fluid from Newtonian behaviour (Metzner,1956).

The above mentioned rheological relationships can be described using the yield pseudoplastic model depending on the values of τ_y and n:

(a)	Bingham plastic	$\{\tau_y > 0 \text{ and } n=1\}$
(b)	Yield pseudoplastic	$\{\tau_y > 0 \text{ and } n < 1\}$

(c)	Yield dilatant	$\{\tau_y > 0 \text{ and } n > 1\}$
(d)	Newtonian	$\{\tau_y = 0 \text{ and } n = 1\}$
(e)	Pseudoplastic	$\{\tau_y = 0 \text{ and } n < 1\}$
(f)	Dilatant	$\{\tau_y = 0 \text{ and } n > 1\}$

Using the above settings the yield pseudoplastic can be simplified to the Bingham plastic and power law models. The Bingham plastic model is an ideal case of the yield pseudoplastic model and substituting η for K the rheological assumption becomes:

$$\tau = \tau_y + \eta \left[-\frac{du}{dr} \right]^n , \qquad (2.7)$$

The yield pseudoplastic and yield dilatant, with the settings as given in (b) and (c), keep the rheological assumptions as described in equation 2.6.

For the Newtonian, pseudoplastic and dilatant models, with the settings as given in (d), (e) and (f), equation 2.6 will revert to what is termed the Ostwald-de Waele power law model (Heywood,1980)

$$\tau = K \left[-\frac{du}{dr} \right]^n . \qquad (2.8)$$

2.7.2 Laminar Flow Regime

The above models (yield pseudoplastic - equation 2.6, Bingham plastic - equation 2.7 and Ostwald-de Waele power law - equation 2.8) have been put forward to relate shear stress to shear rate in the laminar flow regime. Volumetric flow rate as a function of the pressure gradient and other relevant variables can be obtained from the models. They can also be used to develop methods by which turbulent flow data may be predicted from laminar flow data.

The equations for laminar pipe flow can be derived as follows (Cheng 1970, Heywood 1980 and Benedict 1980). The flow rate through a pipe is given by:

$$Q = \int_0^{\frac{D}{2}} 2\pi r \ V \ dr \qquad\qquad (2.9)$$

The relationship between shear rate and the velocity distribution is given by

$$\dot{\gamma} = - \frac{dV}{dr} \qquad\qquad (2.10)$$
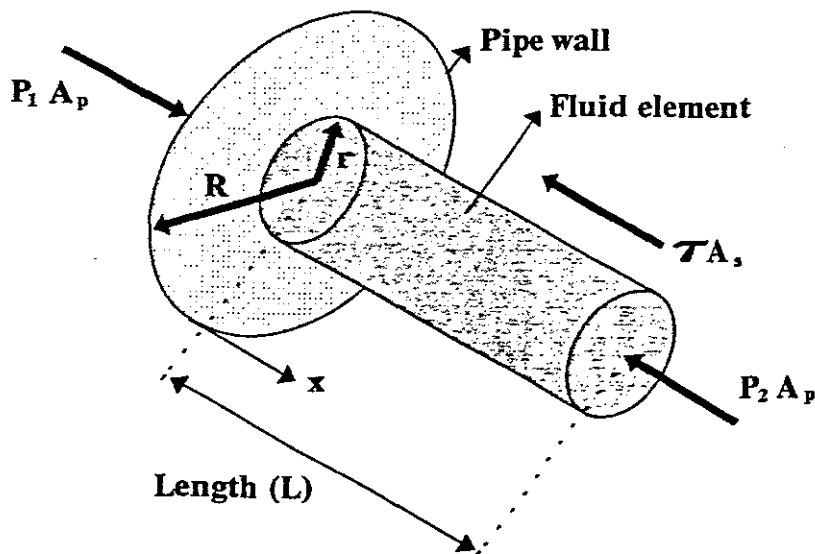
Figure 2.3: Forces acting on a fluid element in laminar flow

A force balance on the cylindrical element in Figure 2.3 will yield the relationship of the shear stress at a radial position r to the overall axial pressure drop over the pipe of length L:

$$(p_1 - p_2)\pi r^2 = \tau(2\pi r L) \qquad\qquad (2.11)$$

or,

$$\tau = \frac{\Delta p \; r}{2 \; L} \; . \tag{2.12}$$

The partial integration of equation 2.9 using equation 2.10 and equation 2.12 leads to:

$$Q = \frac{\pi}{8} \left[\frac{D}{\tau_0} \right]^3 \cdot \int_0^{\tau_0} \tau^2 - \frac{du}{dr} \; d\tau \; , \tag{2.13}$$

where the shear stress at the wall is given by:

$$\tau_0 = \frac{D \; \Delta p}{4 \; L} \; . \tag{2.14}$$

The flow rate for the yield pseudoplastic model, the Bingham plastic model or the power law model can hence be obtained by substitution of the relevant rheological equation ie. equation 2.6, equation 2.7 or equation 2.8 respectively. As mentioned, the yield pseudoplastic model is to used for this study therefore substituting equation 2.6 into equation 2.13 yields:

$$\frac{32Q}{\pi D^3} = \frac{8V}{D} = \frac{4n}{K^{\frac{1}{n}} \tau_0^3} \left(\tau_0 - \tau_y \right)^{\frac{1+n}{n}} \left[\frac{(\tau_0 - \tau_y)^2}{1+3n} + \frac{2\tau_y(\tau_0 - \tau_y)}{1+2n} + \frac{\tau_y^2}{1+n} \right] \; . \tag{2.15}$$

2.7.3   Generalized Approach for Laminar Flow

Metzner & Reed (1955) proposed a generalized correlation for any time independent fluid. This is based upon a relationship developed by Rabinowitsch (1929) and Mooney (1931) for the calculation of shear rates at the wall of a pipe, where:

$$\left[-\frac{du}{dr} \right]_0 = \frac{3}{4} \left[\frac{8V}{D} \right] + \frac{1}{4} \frac{8V}{D} \tau_0 \; . \tag{2.16}$$

Rearranged the equation becomes:

$$\left[-\frac{du}{dr}\right]_0 = \frac{3n' + 1}{4n'} \left[\frac{8V}{D}\right] \qquad ,$$

(2.17)

where

$$n' = \frac{d(\ln \tau_o)}{d\left[\ln\dfrac{8V}{D}\right]} \ .$$

(2.18)

Rabinowitsch (1929) and Mooney (1931) also clearly showed that the relationship between the wall shear stress and the term 8V/D is independent of the diameter of the pipe in laminar flow as shown in Figure 2.4.
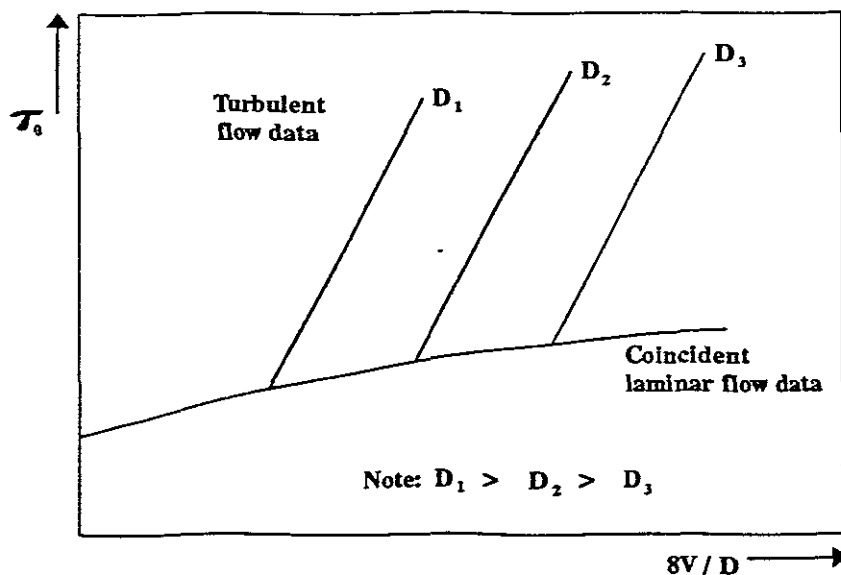
Figure 2.4: Typical pipeline test data for three pipe diameters

Metzner & Reed (1955) continued with the fact that the derivative of Equation 2.18 represents the slope of the line:

$$Ln\ \tau_0 = n'\ \ln\ \left[\frac{8V}{D}\right] + \ln\ K' \qquad \text{or ,}$$

$$\tau_0 = K'\ \left[\frac{8V}{D}\right]^{n'} . \tag{2.19}$$

If n' is a constant then the mathematical relationship between shear stress and shear rate in equation 2.18 is given by equation 2.19. If n' is not a constant but varies with wall shear stress then equation 2.19 represents the tangent to the curve at any chosen value of shear stress or shear rate. Their approach is shown graphically in Figure 2.5.

Note n' must be evaluated for the differing values of wall shear stress (τ_o) occurring in the laminar flow region if the yield-pseudoplastic model is used.

Metzner & Reed (1955) went further to develop a generalized Reynolds number for non-Newtonian pipe flow. By analogy with Newtonian flow they related the Fanning friction factor, given by:

$$f = \frac{2\ \tau_0}{\rho\ V^2} , \tag{2.20}$$

to the Reynolds number in laminar flow as:

$$f = \frac{16}{Re_{MR}} . \tag{2.21}$$

Combining equations 2.19, equation 2.20 and equation 2.21 the following Reynolds number Re_{MR} is obtained:

$$Re_{MR} = \frac{8\ \rho\ V^2}{K'\left[\dfrac{8V}{D}\right]^{n'}} . \tag{2.22}$$

At Newtonian conditions ie. $n'=n=1$ and $K'=\mu$ the equation reverts back to equation 2.1

as stated by Osborne Reynolds.
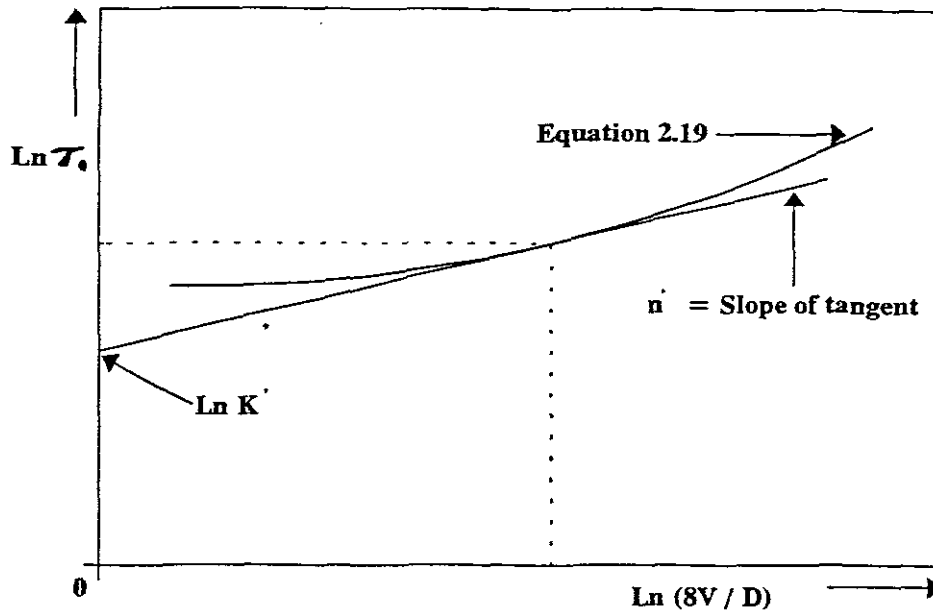
Figure 2.5: Graphical presentation of the Metzner & Reed approach

2.8   RHEOLOGICAL CHARACTERIZATION

The following rheological models can be used to characterize a non-Newtonian time independent fluid in the laminar flow regime:

- Bingham plastic
- Yield pseudoplastic
- Yield dilatant
- Newtonian
- Pseudoplastic
- Dilatant

The model which best fits the data should be used to determine the values of τ_y, K and n for a particular slurry. As mentioned previously the yield-pseudoplastic model was used in this study and all slurries tested were successfully characterized using this model. The constants (τ_y, K and n) were determined using the method adopted by Neill (1988).

At fixed values of τ_y, K and n, a root mean square error of fit function E can be defined for a series of N data points in the laminar flow region,

$$E = \sqrt{\frac{\sum_{i=1}^{N} \left[\left[\frac{8V}{D}\right]_{i\ obs} - \left[\frac{8V}{D}\right]_{i\ calc} \right]^2}{N-1}} \ . \tag{2.23}$$

The K value for minimum error K_{min} can be found by setting $\partial E/\partial K=0$ for a fixed value of τ_y and n,

$$K_{min} = 1 \ / \ \left[\frac{2 \sum_{i=1}^{N} \left[\frac{8V}{D}\right]_i / 8}{n \sum_{i=1}^{N} \left(\tau_{0\ i} - \tau_y\right)^{\frac{1+n}{n}} \left[\frac{(\tau_{0\ i} - \tau_y)^2}{1+3n} + \frac{2\tau_y(\tau_{0\ i} - \tau_y)}{1+2n} + \frac{\tau_y^2}{1+n} \right]} \right]^n \ . \tag{2.24}$$

The τ_y and n values are then optimized to give a global minimum for E.

2.9   VELOCITY DISTRIBUTION FOR TURBULENT FLOW

Turbulent flow models for non-Newtonian fluids are normally based on the analytical methods adopted for Newtonian fluid turbulent behaviour (eg. Torrance 1963, Wilson & Thomas 1985, 1987, Slatter 1994). In this section turbulent flow for Newtonian fluids is covered although the effect of solid particles is also considered as it is felt that this should form part of the basis for turbulent flow analysis of any non-Newtonian flow model.

2.9.1 Wall Roughness

The type of turbulent flow encountered depends on the wall roughness (Govier & Aziz, 1972). Under microscopic investigation it can be seen that the inner wall of the pipe is not smooth but many protrusions exist. The term wall, pipe or surface roughness is used to describe the complex size, shape and spacing of these protrusions. The extent of roughness will depend on the material used in manufacturing the pipe and the method of its manufacture. For a given fluid and velocity, roughness in a pipe increases the pressure drop

At fixed values of τ_y, K and n, a root mean square error of fit function E can be defined for a series of N data points in the laminar flow region,

$$E = \sqrt{\frac{\sum_{i=1}^{N} \left[\left[\frac{8V}{D} \right]_{i\,obs} - \left[\frac{8V}{D} \right]_{i\,calc} \right]^2}{N-1}} \;.$$

(2.23)

The K value for minimum error K_{min} can be found by setting $\partial E/\partial K = 0$ for a fixed value of τ_y and n,

$$K_{min} = 1 \Big/ \left[\frac{2 \sum_{i=1}^{N} \left[\frac{8V}{D} \right]_i / 8}{n \sum_{i=1}^{N} \left(\tau_{0i} - \tau_y \right)^{\frac{1+n}{n}} \left[\frac{(\tau_{0i}-\tau_y)^2}{1+3n} + \frac{2\tau_y(\tau_{0i}-\tau_y)}{1+2n} + \frac{\tau_y^2}{1+n} \right]} \right]^n \;.$$

(2.24)

The τ_y and n values are then optimized to give a global minimum for E.

2.9   VELOCITY DISTRIBUTION FOR TURBULENT FLOW

Turbulent flow models for non-Newtonian fluids are normally based on the analytical methods adopted for Newtonian fluid turbulent behaviour (eg. Torrance 1963, Wilson & Thomas 1985, 1987, Slatter 1994). In this section turbulent flow for Newtonian fluids is covered although the effect of solid particles is also considered as it is felt that this should form part of the basis for turbulent flow analysis of any non-Newtonian flow model.

2.9.1 Wall Roughness

The type of turbulent flow encountered depends on the wall roughness (Govier & Aziz, 1972). Under microscopic investigation it can be seen that the inner wall of the pipe is not smooth but many protrusions exist. The term wall, pipe or surface roughness is used to describe the complex size, shape and spacing of these protrusions. The extent of roughness will depend on the material used in manufacturing the pipe and the method of its manufacture. For a given fluid and velocity, roughness in a pipe increases the pressure drop

compared with conditions existing in a "smooth" pipe (Bowen 1961a, Cheng 1975). Dimensional analysis shows that the effect of roughness is not due to its absolute dimensions but rather to its dimensions relative to that of the pipe. The relative roughness (ϵ) is defined as:

$$\epsilon = \frac{k}{D} , \qquad (2.25)$$

where k = roughness size

   D = diameter of the pipe concerned

The effectiveness of wall roughness in turbulent flow depends not only the relative roughness but also on the Reynolds number (Govier and Aziz, 1972). This is attributed to the viscous sub-layer which exists in contact with the wall.

The viscous sub-layer, as postulated by Prandtl (1926), is a thin layer next to the pipe wall where turbulent mixing stresses are suppressed (velocity at the wall being zero) and where viscous forces predominate. The thickness of the viscous sub-layer, for Newtonian turbulent flow in pipes, which exists for a finite thickness, can be expressed as (Wilson, 1986):

$$\delta = \frac{11,6 \, \mu}{\sqrt{\rho \, \tau_0}} . \qquad (2.26)$$

At low Reynolds numbers when the viscous sub-layer is sufficiently thick to cover the protrusions on the pipe wall, the roughness will not be effective (Figure 2.6). At high Reynolds numbers when the viscous sub-layer is not sufficiently thick to cover the protrusions, roughness will be effective. A roughness Reynolds number can hence be used to determine various regions of turbulent flow in a pipe,

$$Re_r = \frac{k}{D} Re \sqrt{\frac{f}{2}} = \frac{\rho \, V_* \, k}{\mu} . \qquad (2.27)$$

At $Re_r < 3$ smooth wall turbulence exists.

At $3 < Re_r < 70$ partially rough wall turbulence exists.

At $Re_r > 70$ fully rough wall turbulence exists (Schlichting 1968, Govier & Aziz 1972).

Viscous Sub-layer Thickness $Re_r < 3$

$3 < Re_r < 70$

$Re_r > 70$
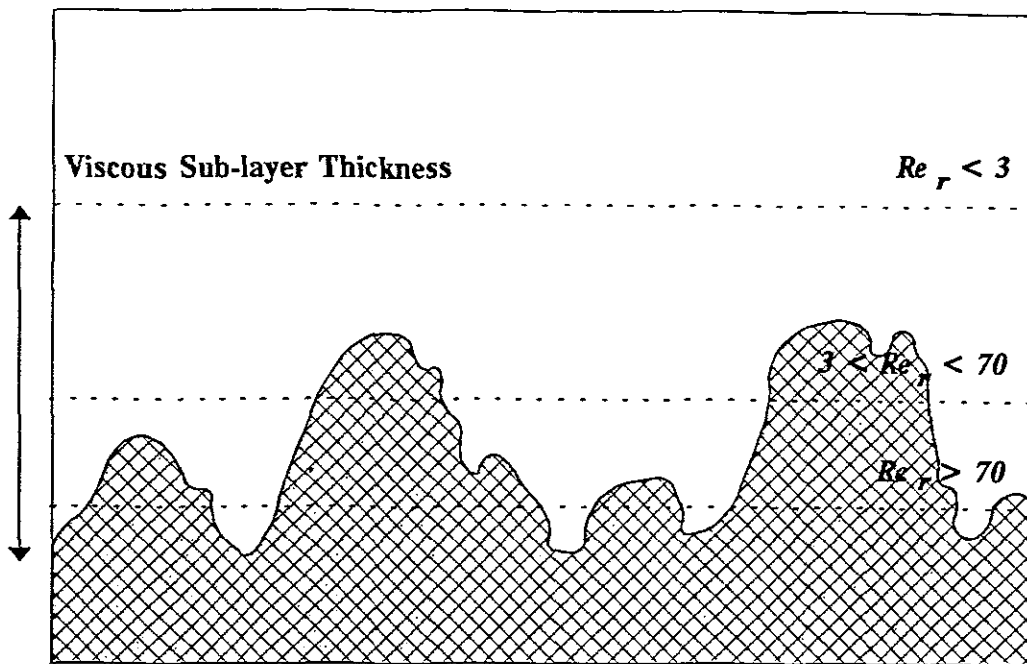
Figure 2.6: Magnified view of a rough wall pipe showing regions of turbulent flow

2.9.2   The Effect of Solid Particles

Although a particle size effect on energy gradients in turbulent flow has been reported by Maude & Whitmore (1956, 1958), Mun (1988) and Slatter (1994), it is still customary in homogenous non-Newtonian slurries to ignore the fact that solid particles are present. As previously mentioned in Chapter 1 it has been found that particle size and distribution do influence flow behaviour (Philippoff 1944, Hedström 1952, Orr & Blocker 1955, Zettlemoyer & Lower 1955, Maude & Whitmore 1956, Thomas 1983, Mun 1988, Slatter 1994) and yet it is the most overlooked piece of data in turbulent flow analysis (Mun, 1988). Particles will cause a decrease in the velocity gradient similar to the effect of the wall roughness (Slatter, 1994) and should therefore be taken into account in turbulent flow analyses. This can be understood if the following is considered.

The change in velocity as the pipe wall is approached is very rapid. The magnitude of change in the region of the pipe wall is in the order of 1m/s (Slatter, 1994) over the diameter of a typical particle. If solid particles are present in the fluid they will resist shear and hence impede the rapid changes in velocity.

2.9.3 Continuum Approximation

From section 2.9.1 and section 2.9.2 it can be seen that wall roughness and the presence of solid particles will affect the velocity gradient. This fact should be stressed as virtually all researchers in the field of hydrotransport describe homogeneous solid-liquid suspensions using continuum models. The definition of continuum as given by Parker (1994) is:

"The study of distributions of energy, matter and other physical quantities under circumstances where their discrete (composed of separate and distinct parts) nature is unimportant and they may be regarded as (in general, complex) continuous functions of position."

The problem with using continuum models is that homogeneous solid-liquid suspensions can never be truly homogeneous. The continuum nature of these slurries is an approximation and is a state to which the slurries tend asymptotically (Shook & Roco, 1991). Although this approximation is deemed to hold good, it only does so as long as the scale of fineness required by the subsequent modelling is not surpassed by the particle size (Lumley, 1978). Hence, when considering the viscous sub-layer, the continuum approximation MUST be compromised (Slatter 1994, Slatter *et al* 1996). This can clearly be seen in Figure 2.7, a magnified view of a rough pipe wall showing the viscous sub-layer thickness and the slurry particles, which indicates that the solid particles are large compared with the scale of modelling. It is therefore imperative that the theoretical model account for the effect of the particles in turbulent flow.

Maude & Whitmore (1956, 1958) and Slatter (1994) are at the time of writing the only known researchers to have taken particle size into account in the turbulent flow analyses of their theoretical models. Their analyses are presented in section 2.11.6 and section 2.11.5 respectively.

2.9.4 Turbulence

Blasius (1913) was the first to suggest a standard empirical relationship between the Reynolds number and the friction factor for fully developed turbulent Newtonian flow.
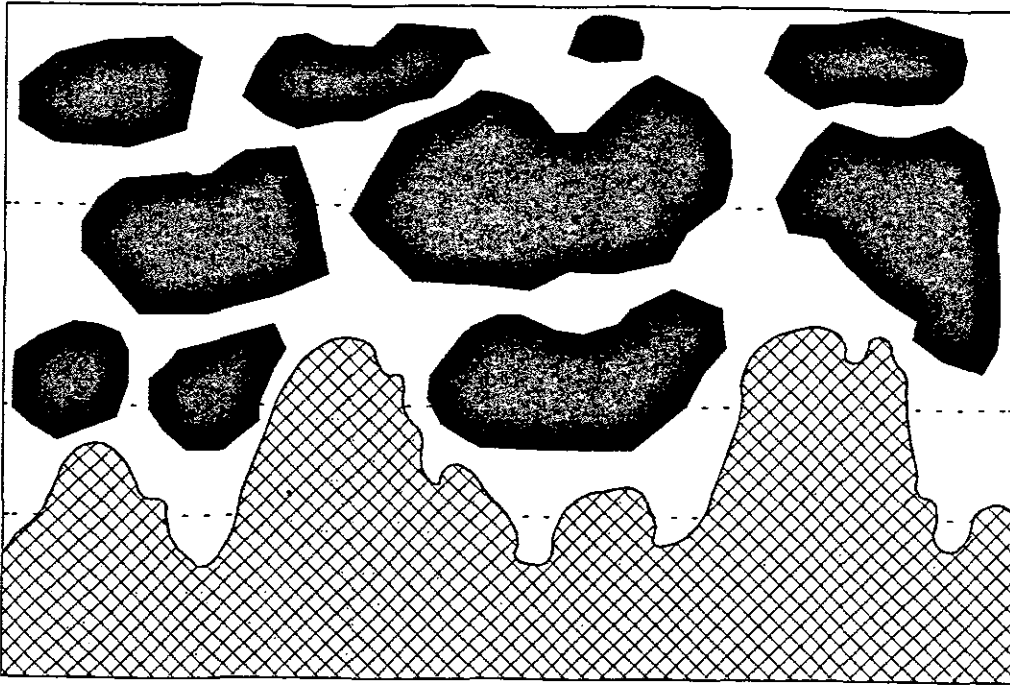
Figure 2.8: Magnified view of a rough pipe wall showing the viscous sub-layer
and the slurry particles

The Blasius equation is applicable to the range 3000 < Re < 100 000 where,

$$f = 0{,}079 \ Re^{0.25} \ .$$ (2.28)

Knudsen & Katz (1958) proposed a similar equation for fully developed turbulent Newtonian flow supposedly applicable to the range 5000 < Re < 200 000 where,

$$f = 0{,}046 \ Re^{0.2} \ .$$ (2.29)

Equation 2.29 is about 10% below equation 2.28 at low Reynolds numbers but meets it at higher Reynolds numbers (Bowen, 1961). A logarithmic plot of f vs Re (Figure 2.8) for the above equations yields a straight line and over the years evidence has supported this single line correlation. For example, Cadwell & Babbitt (1941), who studied the flow of muds, sludges and suspensions in circular pipes concluded that head loss in the turbulent flow regime can be calculated from the Blasius equation if the density of the slurry and a proper viscosity (defined under laminar flow conditions) are used.

The von Karmen equation (1930) based on the Prandtl (1926) mixing length model was proposed to represent more exactly the experimental data for Reynolds numbers for the range 3000 < Re < 300 000 where,

$$\sqrt{\frac{1}{f}} = 4 \log\left(\text{Re} \sqrt{f}\right) - 0,4 \ . \tag{2.30}$$

Even though this equation was proposed for a much wider range of Reynolds numbers, the Reynolds numbers of the vast majority of non-Newtonian fluids rarely exceeds 100 000 due to the viscous nature of these fluids.

However, even though the simple Blasius type equations can be used, most of the work to develop semi-theoretical models for turbulent flow of Newtonian fluids in pipes has centred around the mixing length model of Prandtl (1926).
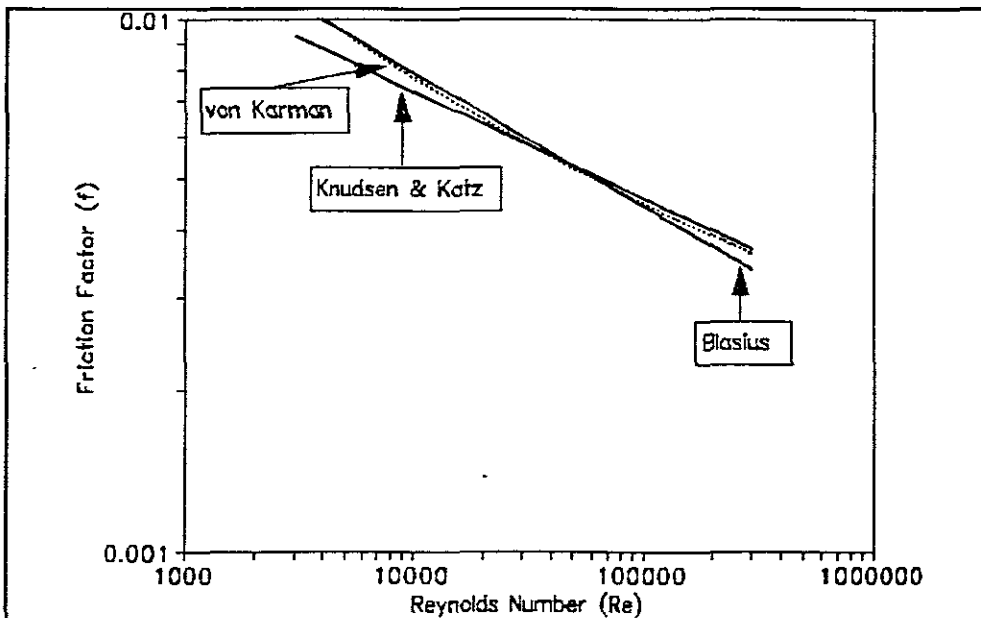
Figure 2.9:   Graphical comparison of Blasius, Knudsen & Katz and von Karmen friction factor equations for turbulent flow

2.9.5 Smooth Wall Turbulence

In turbulent flow, the interchange of momentum between layers, due to eddy formation, sets up shear stresses, also known as Reynolds stresses (Schlichting, 1968). The shear stress in the turbulent core must be related to the shear rate in order to obtain the velocity distribution and flow rate (Janna, 1983).

Prandtl (1926) developed a mixing length theory as a means of estimating the Reynolds stress. Considering the shear stress at any radial position to have two components he derived the expression:

$$\tau = \mu \frac{du}{dr} + \rho \left[\mathscr{L} \frac{du}{dy} \right]^2 . \qquad (2.31)$$

The first term of equation 2.31 is the viscous contribution to the total shear stress and the second, the turbulent portion. Neglecting the viscous shear stress in turbulent flow we have an expression for the turbulent shear stress between any two layers of fluid in terms of Prandtl's mixing length: ·

$$\tau = \rho \left[\mathscr{L} \frac{du}{dy} \right]^2 , \qquad (2.32)$$

and

$$\mathscr{L} = \chi \, y , \qquad (2.33)$$

where $\chi = 0{,}4 = $ von Karmen constant

        $y = $ distance from the wall.

Prandtl further asserted that at any y near the wall, the turbulent shear stress was given by the wall shear stress. Hence equations 2.32 and equation 2.33 were combined,

$$V_\bullet = \sqrt{\frac{\tau_0}{\rho}} = \mathscr{L} \frac{du}{dy} = \chi \, y \, \frac{du}{dy} , \qquad (2.34)$$

which yields

$$\frac{du}{V_\bullet} = \frac{1}{\chi} \frac{dy}{y} . \qquad (2.35)$$

The smooth pipe turbulent velocity distribution is obtained by integrating equation 2.35:

$$\frac{u}{V_\bullet} = \frac{1}{\chi} \ln y + \text{constant} . \qquad (2.36)$$

The von Karmen constant specifies the rate at which turbulence develops at points progressively further from the wall. Nikuradse (1932) made the first experimental determination of the constant in equation 2.36, determining it to be 5,5. Thus equation 2.36 becomes:

$$\frac{u}{V_\bullet} = 2,5 \ln \left[\frac{\rho \, V_\bullet \, y}{\mu} \right] + 5,5 \; . \tag{2.37}$$

The mean velocity for smooth wall turbulence can found by integrating the above velocity distribution over the cross sectional area (Schlichting, 1968),

$$\frac{V}{V_\bullet} = 2,5 \ln \left[\frac{\rho \, V_\bullet \, R}{\mu} \right] + 1,75 \; . \tag{2.38}$$

2.9.6 Fully Developed Rough Wall Turbulence

Roughness has a profound effect on the velocity profile and hence for turbulent flow in rough pipes Prandtl (1926) modified his smooth pipe equation to the form:

$$\frac{u}{V_\bullet} = A \ln \frac{y}{k} + B \; . \tag{2.39}$$

Nikuradse (1933) provided the first numerical evaluation for the constant B for flow in rough pipes, yielding:

$$\frac{u}{V_\bullet} = 2,5 \ln \frac{y}{k} + 8,5 \; . \tag{2.40}$$

A generalized plot that compares smooth and rough pipes can be given in terms of the roughness Reynolds number and the factor:

$$B = \frac{u}{V_\bullet} - 2,5 \ln \frac{y}{k} \; . \tag{2.41}$$

From equations 2.37 and 2.41, for smooth pipes we have,

$$B_{smooth} = 2.5 \ln Re_r + 5.5 ,$$

(2.42)

which represents the equation for smooth wall turbulent flow.

And from equations 2.40 and 2.41, for rough pipes we have,

$$B_{rough} = 8.5 .$$

(2.43)

A comparison of the law of the wall for smooth and rough pipes (taken from Benedict, 1980) using Nikuradse's data points (1932, 1933) is shown in Figure 2.9.
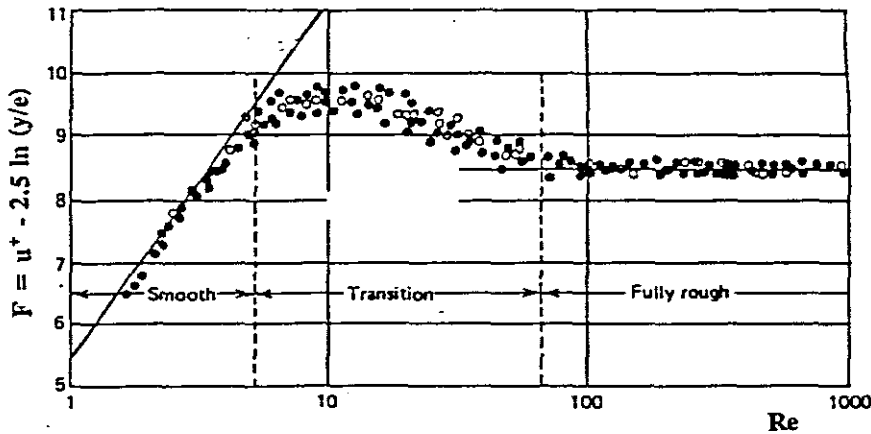
Figure 2.9: Comparison of the law of the wall for smooth and rough pipes

The mean velocity for fully developed rough wall turbulence can be found by integrating the velocity distribution over the cross sectional area to yield (Schlichting, 1968),

$$\frac{V}{V_\bullet} = 2.5 \ln \frac{R}{k} + 4.75 .$$

(2.44)

2.10   THE FRICTION FACTOR

An evaluation of the flow resistance of a particular fluid flowing through a pipe is essential
for design. The pressure loss due to a fluid flowing through a straight pipeline can be
expressed as a function of the Fanning friction factor f, (Weltman, 1956),

$$\Delta p = f \left[\frac{2 \rho V^2 L}{D} \right] . \qquad (2.45)$$

However, dimensional analysis indicates that the friction factor, in general, is a function of
the pipe Reynolds number and the relative roughness.

2.10.1   Laminar Flow

In terms of the Reynolds number the friction factor in laminar flow is given by

$$f = \frac{16}{Re} . \qquad (2.46)$$

2.10.2   Smooth Wall Turbulence

Reformulating equation 2.38 in terms of the Fanning friction factor and the Reynolds
number, Prandtl's universal law for smooth pipes (Schilichting, 1968) is obtained,

$$\frac{1}{\sqrt{f}} = -4 \log \left[\frac{1,26}{Re \sqrt{f}} \right] . \qquad (2.47)$$

2.10.3   Fully Developed Rough Wall Turbulence

Reformulating equation 2.44 in terms of the Reynolds number and the relative roughness,
equation 2.48 is obtained,

$$\frac{1}{\sqrt{f}} = -4 \log \left[\frac{k}{3,7 \, D} \right] \, . \tag{2.48}$$

2.10.4   Partially Developed Rough Wall Turbulence

The transitional flow between smooth and rough pipes as shown in Figure 2.10 was investigated by Colebrook and White (Colebrook, 1939). The following empirical equation was proposed:

$$\frac{1}{\sqrt{f}} = -4 \log \left[\frac{k}{3,7 \, D} + \frac{1,26}{Re \, \sqrt{f}} \right] \, . \tag{2.49}$$

2.10.5   Moody Diagram

Moody (1944) was the first to present a composite diagram of all the regions of interest for Newtonian flow in pipes. The chart, termed the Moody diagram, as shown in Figure 2.10, represents the effect of Re and k/D on the friction factor and includes:

- the straight line laminar friction factor curve
- the smooth pipe turbulent friction factor curve
- the various fully rough turbulent friction factor curves
- the transition friction factors

2.11   NON-NEWTONIAN TURBULENT FLOW MODELS

Data obtained by Slatter (1994) was analyzed and compared using his new model with the Torrance (1963) and Wilson & Thomas (1985, 1987) models, theoretical models which have a stronger analytical background. It was decided to use these two models for analysis and comparison of data for this thesis seeing that this is a continuation of work conducted by Slatter (1994). It was, however, also decided to incorporate into the analysis the models of Dodge & Metzner (1959) and Kemblowski & Kolodziejski (1973), models having a more and empirical approach.
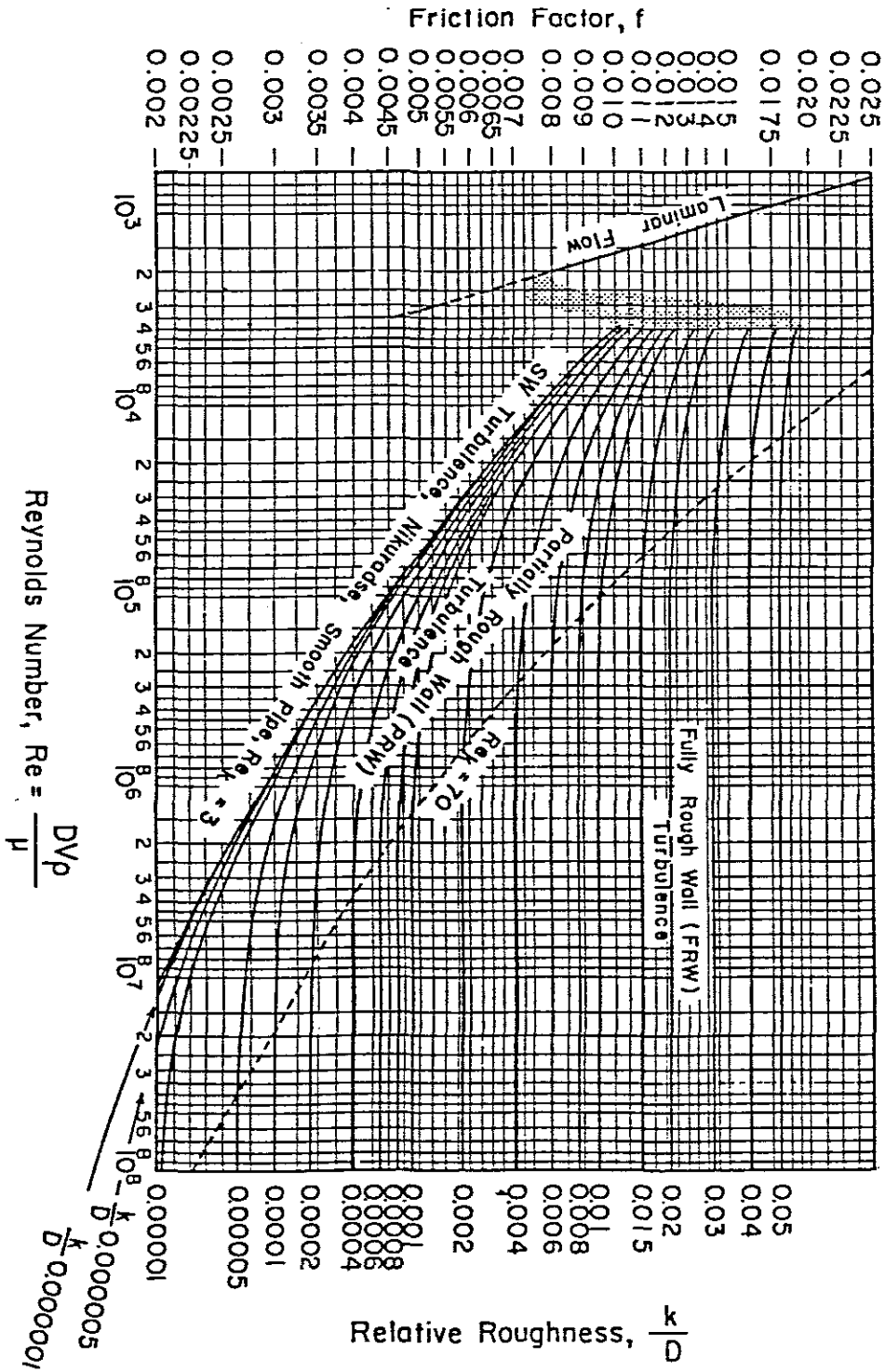
Figure 2.10: Moody Diagram (taken from Govier & Aziz, 1972)

2.11.1   The Dodge & Metzner Model

The non-Newtonian turbulent flow model of Dodge & Metzner is probably the most quoted and used of all flow models due to its simplicity and applicability to a wide range of non-Newtonian fluids (Mun, 1988). The model was developed from the laminar flow work of Metzner & Reed (1955) in which sixteen different non-Newtonian materials were studied. Both Metzner & Reed (1955) and Dodge & Metzner (1958) stated that standard Newtonian procedures could be used for turbulent flow predictions. In order to obtain a velocity profile equation Dodge & Metzner assumed the existence of a discrete boundary layer (viscous sublayer), transition zone and turbulent core in the pipe. They also assumed that the apparent flow behaviour index n' influences the point velocity in the turbulent core which means that the turbulent flow head loss is dependant on n'.

Their relationship for turbulent flow is:

$$\frac{1}{\sqrt{f}} = A_n \log\left[Re_{MR} \, f^{\left(1 - \frac{n'}{2}\right)}\right] + C_n \, , \tag{2.50}$$

where

$$A_n = \frac{4}{(n')^{0.75}} \, , \tag{2.51}$$

and

$$C_n = -\frac{0.4}{(n')^{1.2}} \, . \tag{2.52}$$

From the assumptions made by Dodge & Metzner (1959) the above relationship will revert to the smooth wall Newtonian model when n'=1. The above relationship can also be represented graphically as shown in Figure 2.11.

2.11.2   The Torrance Model

Torrance developed a relationship between the fanning friction factor and the Reynolds number for Herschel-Bulkley model fluids ie. the yield pseudoplastic rheological model.
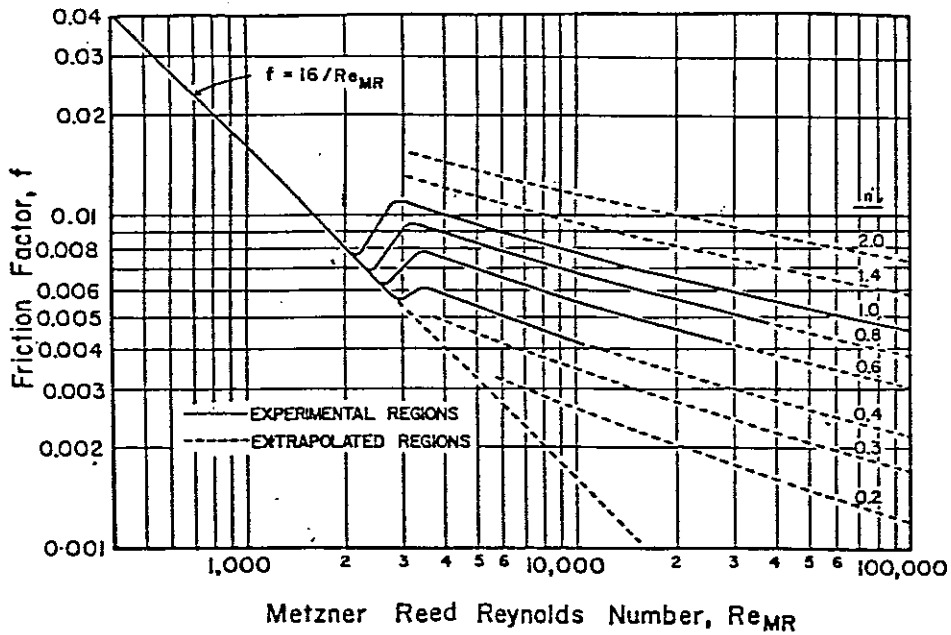
Figure 2.11: The Dodge & Metzner correlation shown on a friction factor
Reynolds number diagram

His analysis was based on the work of Clapp (1961) where Prandtl's mixing length theory
was used. For the purpose of his analysis Torrance made two assumptions:

- that transition from laminar to turbulent flow occurs at some finite distance
  from the pipe wall and,

- the value of the dimensionless velocity is constant for turbulent flow in any
  size of pipe at the finite distance were transition occurs.

Torrance derived relationships for both smooth and rough walled pipes. The relationship for
smooth walled pipes is:

$$\sqrt{\frac{2}{f}} = (a - 1,5\ n\ b) + b\ \ln\left[1 - \left[\frac{u_*}{V_*}\right]^2 \left[\frac{2}{f}\right]\right] + b\ \ln\left(Re\ \sqrt{f^{2-n}}\right)$$

$$+\ 0.347\ (5n - 8)\ b\ . \qquad (2.53)$$

The two constants a and b were assumed to be identical to those evaluated by Clapp (1961) and hence taken to be:

$$a = \frac{3,8}{n} ,$$
(2.54)

and

$$b = \frac{2,78}{n} .$$
(2.55)

For rough walled pipes the velocity profile was modified using Prandtl's assumption that $u(y) \propto y/k$ and the constants re-evaluated using the Newtonian data of Nikuradse (1933).

The relationship for rough wall pipes is:

$$\sqrt{\frac{2}{f}} = \frac{2,5}{n} \log \left[\frac{Re}{k} \right] - \frac{3,75}{n} + 8,5 .$$
(2.56)

The Reynolds number formulation as given by Torrance is:

$$Re_{NN} = \frac{8 \rho V^2}{K \left[\frac{8V}{D} \right]^n} .$$
(2.57)

The Torrance model is unable to predict the onset of turbulence (as shown by Slatter, 1994) and thus it was assumed (Mun, 1988) that the transition occurs at the intersection of the laminar and turbulent curves.

2.11.3   The Kemblowski & Kolodziejski Model

Kemblowski & Kolodziejski (1973) developed an empirical equation of the Blasius type to predict the behaviour of power law fluids. Tests undertaken related the flow resistances of 10%, 20%, 30%, 40% and 50% by weight aqueous suspensions of kaolin in pipes of circular cross-section. The test results are given in the form of the dependence of the coefficient of flow resistance on the generalized Reynolds number

$$\lambda = 4f = f (Re) . \hspace{6cm} (2.58)$$

This forms a relatively flat f-Re line. At higher values of Re all lines of equation 2.58 approach the curve described by the equation

$$\lambda = 4f = \frac{0,3164}{Re_{MR}^{0,25}} . \hspace{5cm} (2.59)$$

Kemblowski & Kolodziejski (1973) compared their work extensively with the Dodge & Metzner model and found that it did not accurately describe the behaviour of these aqueous kaolin suspensions. In fact they found that the data lay on a relatively flat f-Re line between the lines of equation 2.59 and the Dodge & Metzner prediction as can be seen in the figure below (Figure 2.12).
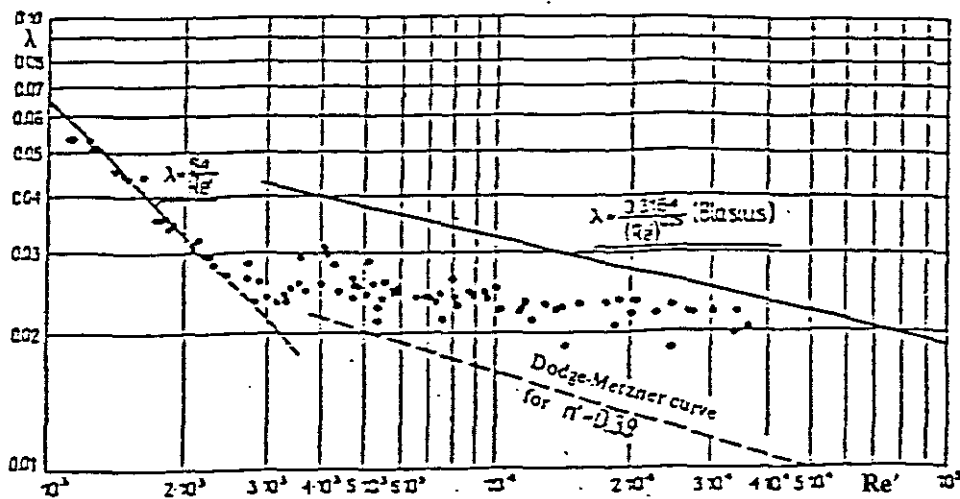
Figure 2.12: Comparison of Dodge & Metzner prediction curve and Kemblowski & Kolodziejski experimental data for the flow of a 30% aqueous kaolin suspension at n=0,39 (taken from Kemblowski & Kolodziejski, 1973)

The data was hence empirically modelled as:

$$\lambda = 4f = \frac{E}{Re_{MR}^{m}} \; \Phi^{1/Re_{MR}} \; ,$$

(2.60)

where

$$E \approx 8,9 \times 10^{-3} \exp \left[3,57 \; (n')^2 \right] \; ,$$

(2.61)

and

$$m = 0,314 \; (n')^{2,3} - 0,064 \; . ,$$

(2.62)

and

$$\Phi = \left[\exp \left[0,572 \; \frac{1 - (n')^{4,2}}{(n')^{0,435}} \right] \right]^{1006} \; .$$

(2.63)

2.11.4   The Wilson & Thomas Model

Wilson & Thomas (1985) produced an analysis of the turbulent flow of non-Newtonian fluids based on enhanced micro-scale viscosity effects. Their analysis predicts a thickened viscous sub-layer, over and above that for an equivalent Newtonian fluid. This leads to an increased throughput velocity and reduced friction factor and flow parameters can be determined directly from rheograms, without pipe flow data.

Wilson & Thomas (1985, 1987) turbulent flow theory was applied to:

- Power law fluids (Wilson & Thomas, 1985). The theory showed markedly different trends to that of Dodge & Metzner (1959) for power law fluids, although no supporting data was provided.

- Bingham plastic fluids (Wilson & Thomas, 1985). The theory in this case predicted that the turbulent flow line would fall below the Newtonian line until it converged at a Reynolds number some five times the transition value.

- Yield pseudoplastic fluids (Thomas & Wilson, 1987). Their analysis showed that as the value of the flow behaviour index decreases from unity, the plot of friction factor vs Reynolds number converges towards the Newtonian line. The plot then parallels the Newtonian line and eventually diverges downwards from the Newtonian line. It was found that the converging behaviour was exhibited by low concentration slurries compared to the diverging behaviour, exhibited by high concentration slurries.

The equations of their turbulent flow model as applying to pseudoplastic fluids is presented below.

The thickness of the viscous sub-layer increases by a factor called the area ratio A_r shown graphically in Figure 2.13. The figure shows that the area ratio is defined as the ratio of the integrals of the non-Newtonian and assumed Newtonian rheograms under identical shear conditions.
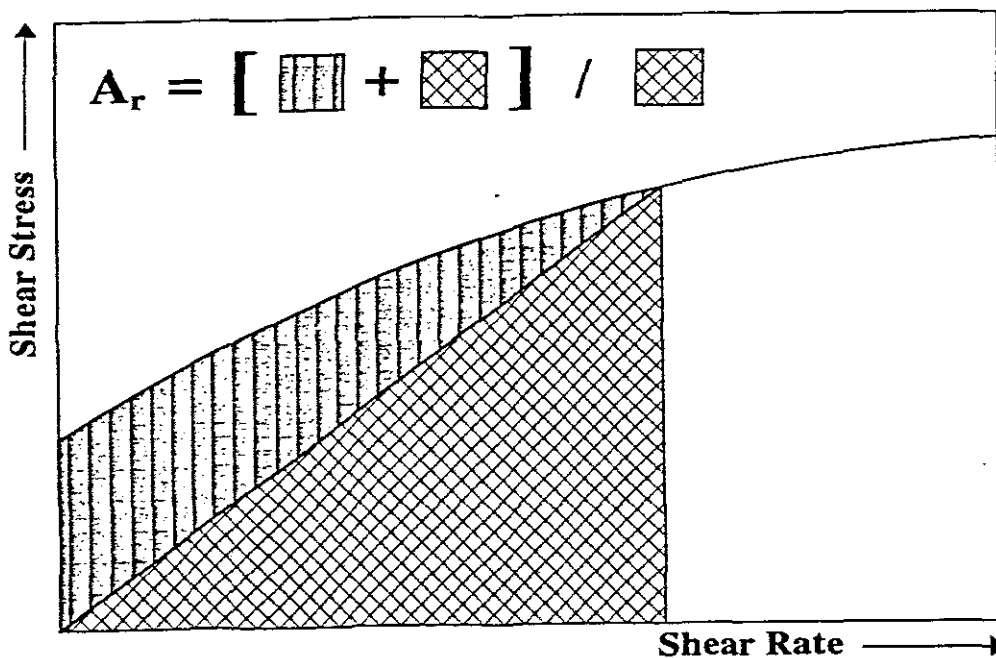
Figure 2.13: Illustration of the area ratio

The area ratio A_r is thus given by:

$$A_r = 2 \left[\frac{1 + \frac{\tau_y}{\tau_0} n}{1 + n} \right] ,$$

(2.64)

and hence the viscous sub-layer thickness is:

$$\delta_{NN} = A_r \, \delta_N ,$$

(2.65)

where δ_N and δ_{NN} are equivalent Newtonian and non-Newtonian viscous sub-layer thicknesses respectively.   .

The velocity distribution is given by:

$$\frac{u}{V_*} = 2,5 \ln \left[\frac{\rho \, V_* \, y}{\mu'} \right] + 5,5 + 11,6 \, (A_r - 1) - 2,5 \, \ln(A_r) .$$

(2.66)

The mean velocity is given by:

$$\frac{V}{V_*} = \frac{V_N}{V_*} + 11,6 \, (A_r - 1) - 2,5 \, \ln A_r - \Omega ,$$

(2.67)

where V_N is the mean velocity for the equivalent Newtonian fluid and Ω is given by:

$$\Omega = -2,5 \ln \left[1 - \frac{\tau_y}{\tau_0} \right] - 2,5 \frac{\tau_y}{\tau_0} \left[1 + 0,5 \frac{\tau_y}{\tau_0} \right] .$$

(2.68)

2.11.5   The Slatter Model

As mentioned in Chapter 1 Slatter (1994) is one of the few researchers to have taken into account the size of the particle contained in the fluid for turbulent flow analysis.

A new Reynolds number was developed for predicting the onset of turbulence. It was modelled using the assumption that the unsheared plug present due to the yield stress acts as a solid at the pipe axis and inhibits turbulence (Figure 2.14).

Direction of flow
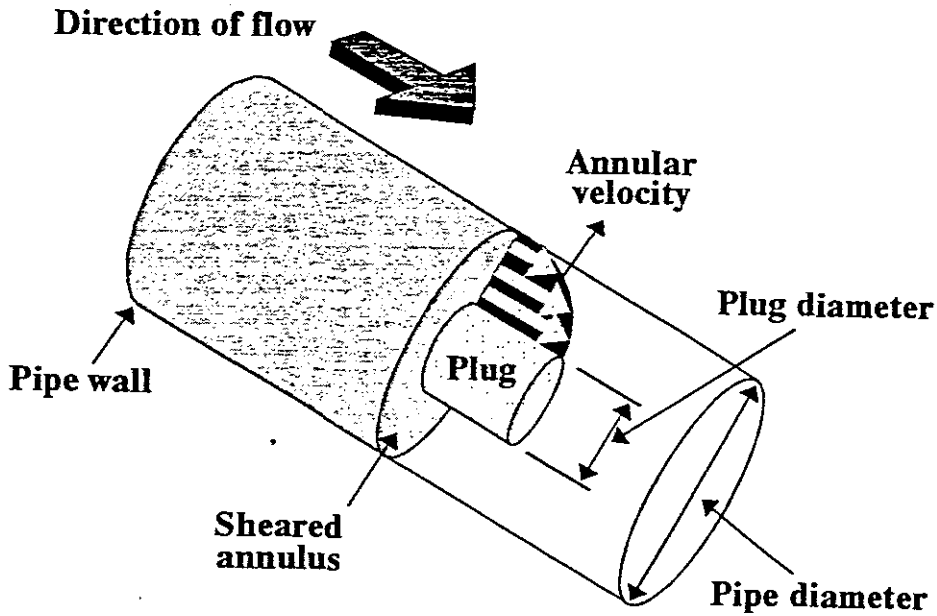
Figure 2.14: Unsheared plug geometry

The Reynolds number is given by

$$Re = \frac{8\,\rho\,V_{ann}^2}{\tau_y + K\left[\dfrac{8\,V_{ann}}{D_{shear}}\right]^n}\ ,$$

(2.69)

where

$$V_{ann} = \frac{Q_{ann}}{A_{ann}}\ ,$$

(2.70)

and

$$D_{shear} = D - D_{plug}\ .$$

(2.71)

Slatter (1994) used the following precepts as the basis of his turbulent flow model:

- The velocity distribution is logarithmic and similar to the classic Newtonian turbulent velocity distribution over the entire core region.

- A roughness effect is caused by the solid particles.

- Fully developed rough wall turbulent flow does exist and the partially rough wall turbulent region is much narrower than for Newtonian fluids.
- Fully developed turbulent flow is independent of the viscous characteristics of the slurry.
- Plug flow does not occur.

In order to determine whether smooth wall turbulent flow or fully developed rough wall turbulent flow exists a roughness Reynolds number was formulated in terms of the yield pseudoplastic model.

The roughness Reynolds number is:

$$Re_r = \frac{8 \rho V_*^2}{\tau_y + K \left[\dfrac{8 V_*}{d_x}\right]^n} ,$$

(2.72)

where d_x is the representative particle size. $d_x = d_{85}$ was found to be good representative particle size for the slurries tested.

If $Re_r < 3,32$ then smooth wall turbulent flow exists and the mean velocity is given by:

$$\frac{V}{V_*} = 2,5 \ln \left[\frac{R}{d_{85}}\right] + 2,5 \ln Re_r + 1,75 .$$

(2.73)

If $Re_r > 3,32$ then fully developed rough wall turbulent flow exists and the mean velocity is given by:

$$\frac{V}{V_*} = 2,5 \ln \left[\frac{R}{d_{85}}\right] + 4,75 ,$$

(2.74)

which reduces to

$$\frac{1}{\sqrt{f}} = 4,07 \log \left[\frac{3,34\ D}{d_{85}} \right] .$$

(2.75)

This correlation produces a transition from the smooth to the rough flow condition which is abrupt.

The thickness of the viscous sub-layer for the Slatter model is taken to be the point of intersection between the viscous sub-layer zone and the turbulent core zone as shown in Figure 2.15 where $u^+ = u/V^*$ is dimensionless velocity.
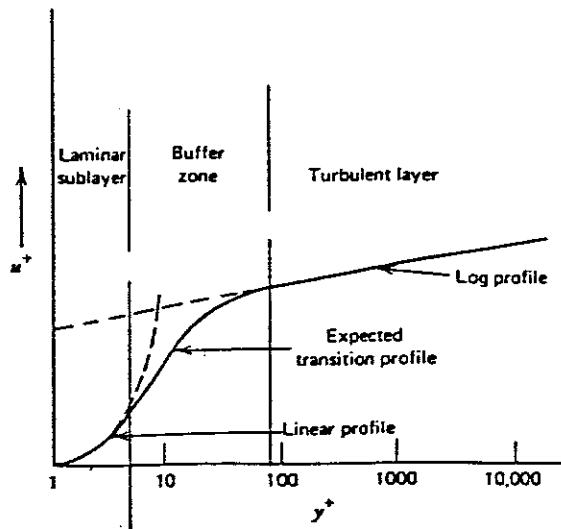
Figure 2.15: Velocity profile in turbulent flow

Equation (I) in Figure 2.15, the point velocity of the viscous sub-layer, is given by:

$$u = y \left[\frac{\tau_0 - \tau_y}{K} \right]^{\frac{1}{n}} .$$

(2.76)

Equation (II) in Figure 2.15, the point velocity of the turbulent flow core, is given by:

The viscous sub-layer thickness is the point of intersection between equation 2.76 and equation 2.77.

$$u = V_* \left[2,5 \ln \left[\frac{y}{d_x} \right] + 2,5 \ln Re_r + 5,5 \right] . \qquad (2.77)$$

Tests conducted by Slatter (1994) confirmed the model to be more accurate than the Torrance (1963) model and Wilson & Thomas (1985, 1987) model against which experimental data was compared. This model was also supported by the experimental data of Park *et al* (1989) and Xu *et al* (1993).

2.11.6   Maude & Whitmore Correlation

Maude & Whitmore (1956, 1958) are two of the few researchers, if not the only two before Slatter (1994), to take any account of the effect particles play in turbulent flow.

Tests were conducted in thin vertical 2,2mm, 3,5mm and 5mm diameter tubes using emery slurries at six different concentrations. The particle size distribution of the emery slurries fell within the range 20 to 40μm. Data was presented in the form of curves of friction factors against Reynolds numbers.

The main observation of Maude & Whitmore (1958) was that the turbulent friction factor (based on the wall viscosity) was initially higher than the Newtonian friction factor but fell below at increased Reynolds numbers. This observation is contradictory to the more widely publicised finding that the non-Newtonian friction factor is always less than the Newtonian friction factor (eg Wilson, 1986).

The phenomena encountered by Maude & Whitmore (1958) were explained in the following theoretical terms. The mixing length, as developed by Prandtl, is defined as the mean distance which fluid elements move at right angles to the direction of flow before they acquire the velocity of the layer they have entered. Hence, the fluid element would pursue an oscillating passage down the tube. However, inertial forces would prevent any high density particles from following exactly the velocity changes of the fluid. The particles would instead oscillate with a smaller amplitude and the mean mixing length of the suspension would decrease with an increase in solids concentration as compared to that of the raw fluid. They postulated that the effective mixing length is reduced by a theoretical

mixing length factor p

$$p = \frac{\rho_l (1 - C_v) + q \, \rho_p \, C_v}{\rho_l (1 - C_v) + \rho_p \, C_v} \,, \tag{2.78}$$

where C_v = volume of particles per unit volume of suspension

   q = the ratio of the amplitude of the particles to the amplitude of fluid, given by:

$$q = \frac{1}{\kappa l} \ln \left[1 - \left[(1 + (\kappa l)^{-2})^{\frac{1}{2}} - (\kappa l)^{-1} \right]^2 + \frac{2}{\kappa l} \left[(1 + (\kappa l)^{-2})^{\frac{1}{2}} - (\kappa l)^{-1} \right] \right]^2$$

$$\times \left[1 - \left[(1 + (\kappa l)^{-2})^{\frac{1}{2}} - (\kappa l)^{-1} \right]^2 \right]^{-1} \,. \tag{2.79}$$

where $l = v_0 t_l$ = average amplitude of the liquid oscillation and K is given by:

$$K = \frac{C_D}{2} \frac{\rho_l}{\rho_p} \frac{3}{2} \frac{1}{d} \frac{1}{(1 - C_v)^\alpha}, \tag{2.80}$$

where α = shape factor.

Maude & Whitmore (1958) hence stated that the pressure loss and friction factor should be reduced in turbulent flow. It must be noted however, that while this accounts for flow behaviour at high Reynolds numbers, the approach does not take into account low Reynolds number behaviour.

In order to account for low Reynolds number behaviour and to explain why higher-than-Newtonian equivalent friction factors were being observed, Maude & Whitmore (1958) considered the effect of the suspended particle on the viscosity of the medium forming the viscous sub-layer. It is known that as the Reynolds number increases the viscous sub-layer becomes narrower to the extent that the mean particle diameter is greater. Thus the viscous sub-layer is said to consist only of the suspending medium. At lower Reynolds numbers, the viscous sub-layer thickens and the whole suspension is sheared by the viscous flow in the sub-layer. Hence, the effective viscosity becomes that of the suspension and explains the higher friction factors.

Two equations were postulated by Maude & Whitmore (1958) for turbulent flow. The criterion as to which equation to use being when the particle diameter is greater than half the thickness of the viscous sub-layer. The equation for determining the thickness of the viscous sub-layer was given by:

$$\delta = \left[\frac{11,7\,\mu}{\rho_s\,V_*} - \frac{1}{2}k'\ c\ d \right]\ (1 - k'c)^{-1}.$$ (2.81)

The turbulent flow equations for $\delta \geq \frac{1}{2}d$ is given by:

$$\frac{1}{\sqrt{f}} = \frac{-0,815}{0,408p}\ \log_{10}\left[\frac{66,3}{Re\ \sqrt{f}}\ \frac{1}{(1 - k'c)} - \frac{d}{D}\ \frac{k'c}{(1 - k'c)} \right] - \frac{0,531}{0,408p} + 4,14\ .$$ (2.82)

The turbulent flow equations for $\delta < \frac{1}{2}d$ is given by:

$$\frac{1}{\sqrt{f}} = \frac{-0,815}{0,408p}\ \log_{10}\left[\frac{66,3}{Re\ \sqrt{f}} \right] - \frac{0,531}{0,408p} + 4,14\ .$$ (2.83)

2.11.7   The Bowen Correlation

Bowen (1961) noted that no universal correlation had been suggested for non-Newtonian fluids and hence published a method which appeared to be applicable to all fluids. The basis of his method was his finding that on a log-log pseudo-shear diagram the turbulent branches of different diameters appeared to describe similar straight lines, with each branch appearing to be almost parallel to the next. He suggested that if the shear stress or shear rate were multiplied by a function of the diameter, a correlation of the turbulent data might be obtained. Hence, he was able to correlate the diameter effect by adapting the Blasius equation (equation 2.28) for Newtonian fluids and obtain the following correlation:

$$D^{1+b}\ \left[\frac{\Delta p}{L} \right] = k\ V^{2-b}\ ,$$ (2.84)

where k and b are constants.

Bowen presented four worked examples to substantiate his method.

Although this correlation does not provide an explanation of the behaviour of the slurry in terms of the physical properties of the slurry, it does produce a good correlation of non-Newtonian turbulent flow pipe data (Harris & Quader, 1971 and Quader & Wilkinson, 1980).

2.12   EVIDENCE OF PARTICLE ROUGHNESS

Many researchers report similarity between the turbulent behaviour of Newtonian fluids and non-Newtonian slurries (Caldwell & Babbitt 1941, Hedström 1952, Metzner & Reed 1955, Dodge & Metzner 1959, Tomita 1959, Michiyoshi et al 1966, Edwards & Smith 1980, Thomas & Wilson 1987 and Sive 1988). One of the more interesting pieces of evidence to date on the similarity between Newtonian and non-Newtonian slurry turbulent flow is presented by Park et al (1989).

Park et al (1989) investigated the turbulent structure of a non-Newtonian slurry using laser doppler anemometry and concluded that the transition region is much narrower than for Newtonian fluids. Their non-Newtonian slurry turbulent flow velocity profile (Figure 2.16) agrees well with measurements with air (Newtonian fluid). However, they reported higher relative turbulence intensities in the wall region for the slurry, when compared with air (Figure 2.17). This would support the concept of particle roughness. Pokryvalio & Grozberg (1995) confirmed the findings of Park et al (1989) using electro-diffusion techniques for measuring velocity profiles of Bentonite clay suspensions at concentrations of 4% and 6% and comparing it with air. They reported a significant increase in turbulence intensities in the wall region for the Bentonite clay suspension (Figure 2.18), providing further support of the concept of particle roughness.

2.13   DATA FROM THE LITERATURE

Experimental data obtained by Sive (1988) was used in the analysis of the various models under consideration. The tests conducted by Sive (1988) were done using a mixture of kaolin clay and a relatively coarse quartz sand, which resulted in a heterogeneous, settling slurry. The purpose of using this data was to see if the coarse, settling particles contributed to the turbulent flow headloss, as proposed by the Slatter model.

-
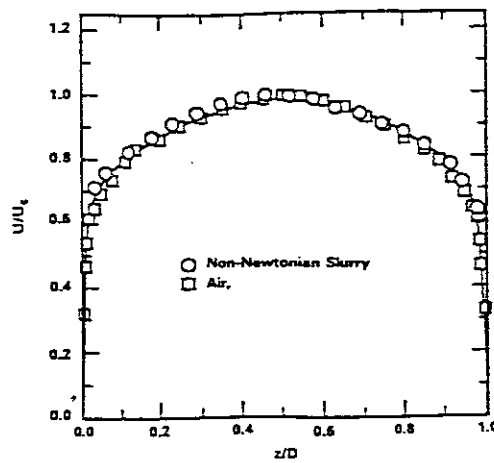
Figure 2.17: Comparison of turbulent velocity distribution between a non-Newtonian
slurry and air at Re = 40 600 (Taken from Park *et al*, 1989)
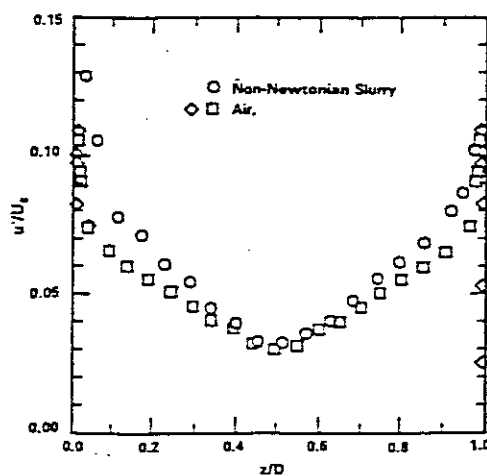
Figure 2.18: Comparison of relative turbulent intensities between a non-Newtonian
slurry and air at Re = 40 600 (Taken from Park *et al*, 1989)
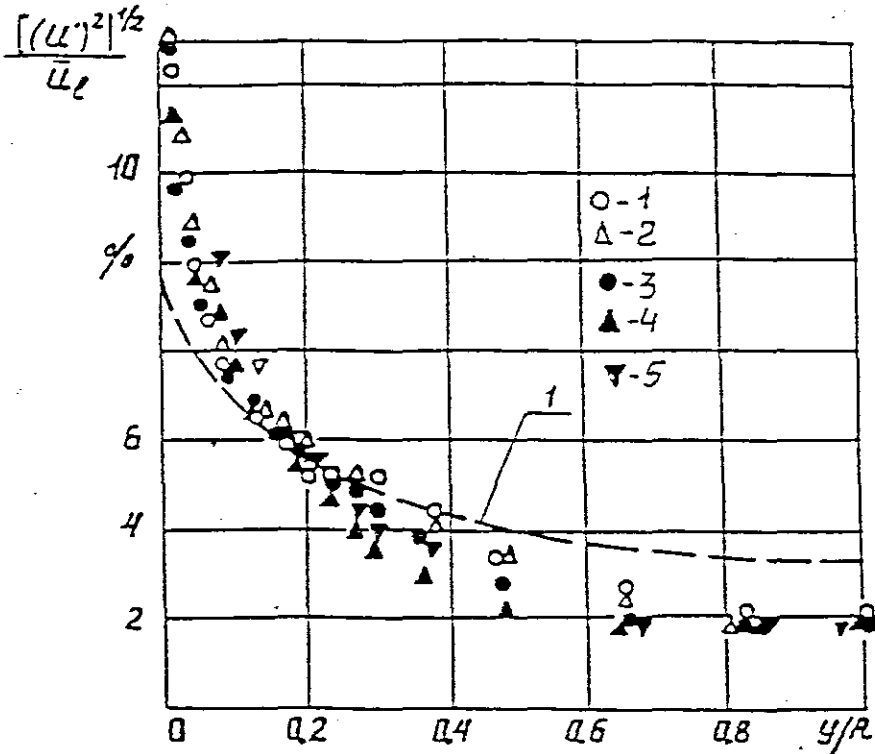
Figure 2.19: Comparison of relative turbulent intensities between bentonite
clay suspensions (C_v=4% and C_v=6%) and water
(Taken from Pokryvalio & Grozberg, 1995)

2.14   CONCLUSIONS

The rheological fundamentals relevant to fluid flow in pipes have been presented and the
theoretical models under consideration have been reviewed

2.14.1   Laminar Flow

The yield pseudoplastic model can be used to model and predict the laminar flow of non-
Newtonian slurries. The rheological constants can be accurately determined using the method
adopted by Neill (1988).

2.14.2   Transition from Laminar to Turbulent Flow

There are several methods in the literature to determine the transition between laminar and turbulent flow. However, the full rheology should be used.

2.14.3   Turbulent flow

The Blasius type equations can be used to determine turbulent flow. However, most of the work to develop semi-theoretical models for turbulent flow has centred around the mixing length model of Prandtl. Hence, the logarithmic velocity distribution can be used to model smooth wall Newtonian turbulent flow. A logarithmic velocity distribution with a roughness function and a roughness Reynolds number to correlate the roughness function can be used to model fully developed rough wall Newtonian turbulent flow. The Colebrook White relation can be used to model partially rough wall Newtonian turbulent flow.

There are three approaches in the literature for modelling non-Newtonian turbulent flow data:

- empirical approach eg Bowen (1961),
- approach based on the slurry rheology eg Torrance (1963) or Wilson & Thomas (1985, 1987),
- approach based on the particle effect or particle roughness effect eg Slatter (1994).

The continuum approximation must be compromised as the solid particles contained in the slurry are large compared with the scale of modelling of the viscous sub-layer thickness. Theoretical models must therefore account for the effect of the particles in turbulent flow and hence from the three possible approaches that can be adopted, the approach using the particle roughness effect should be used. Although Bowen's method does produce good correlation of non-Newtonian turbulent flow pipe data it cannot provide an explanation of the behaviour of the slurry in terms of the physical properties of the slurry.

A wall roughness effect, particle effect or particle roughness effect has been reported in the literature (Maude & Whitmore 1956, 1958, Mun 1988, Slatter 1994). This effect has been

supported by data from Park *et al* (1989) and Pokryvalio & Grozberg (1995).

There are reported differences in the literature as to when the viscous sub-layer breaks down.

Although the particle roughness effect has been reported in the literature there is no published limit of the validity of the effect.

2.14.4   Objectives of Thesis

Having reviewed the relevant literature the following areas for investigation can be noted:

- There is a lack of published literature on the particle roughness effect. Slatter (1994) has developed a new general approach to turbulence flow modelling and concluded that the particle roughness effect was valid for the slurries that were tested. However, research is required to determine if Slatter's model is accurate with increasing particle size and whether the d_{85} size (as suggested by Slatter) does produce a good representation of the particle roughness effect.

- To investigate if the PSD does affect the turbulent flow behaviour of the slurry.

- To determine if the correlation of Maude & Whitmore (the only other model to incorporate particle size besides the Slatter model) can accurately predict turbulent flow behaviour of non-Newtonian homogeneous slurries.

- To determine if increasing particle size has an effect on turbulent flow behaviour. This can be achieved by using the theoretical models (as described in this chapter) to model experimental data and to observe and analyze any effects particle size has on turbulent flow behaviour.

CHAPTER 3

CHAPTER 3

EXPERIMENTAL WORK

3.1 INTRODUCTION

The test work was conducted at the University of Cape Town's Hydrotransport Research Facility. The test facilities used included a pumped recirculating pipe test rig known as the East Rig and a pipeline rig known as the Mini Rig.

In large scale pipe testing (as used for this study), slurry is pumped in a looped circuit normally consisting of two pipe diameters, over a wide range of velocities. This is done in order to measure the behaviour of the slurry (rheology) and the turbulent pipe flow head loss which are needed in designing a piping system. Rheological data which is obtained from laminar flow data can be used to predict turbulent pipe flow head loss (Slatter, 1994).

The test facilities which were used consisted in total of four different pipe diameters namely a 25mm, 80mm, 150mm and 200mm nominal bore. Slurries were tested at mean velocities ranging from 0,1m/s to 6.2m/s. Slurries tested included kaolin clay, a mixture of kaolin clay and rock flour (mixture 1) and a mixture of kaolin clay, rock flour and silica sand (mixture 2) at varying ratios.

3.2 TESTING FACILITIES

3.2.1 The East Rig

Figure 3.1 depicts a schematic diagram of the pumped recirculating pipe test rig.

(a)   Pump Specification

Slurry is supplied to the East Rig by a four bladed Mather and Platt 8x6, solids handling pump, which is driven by a variable speed hydraulic drive (Figure 3.2).
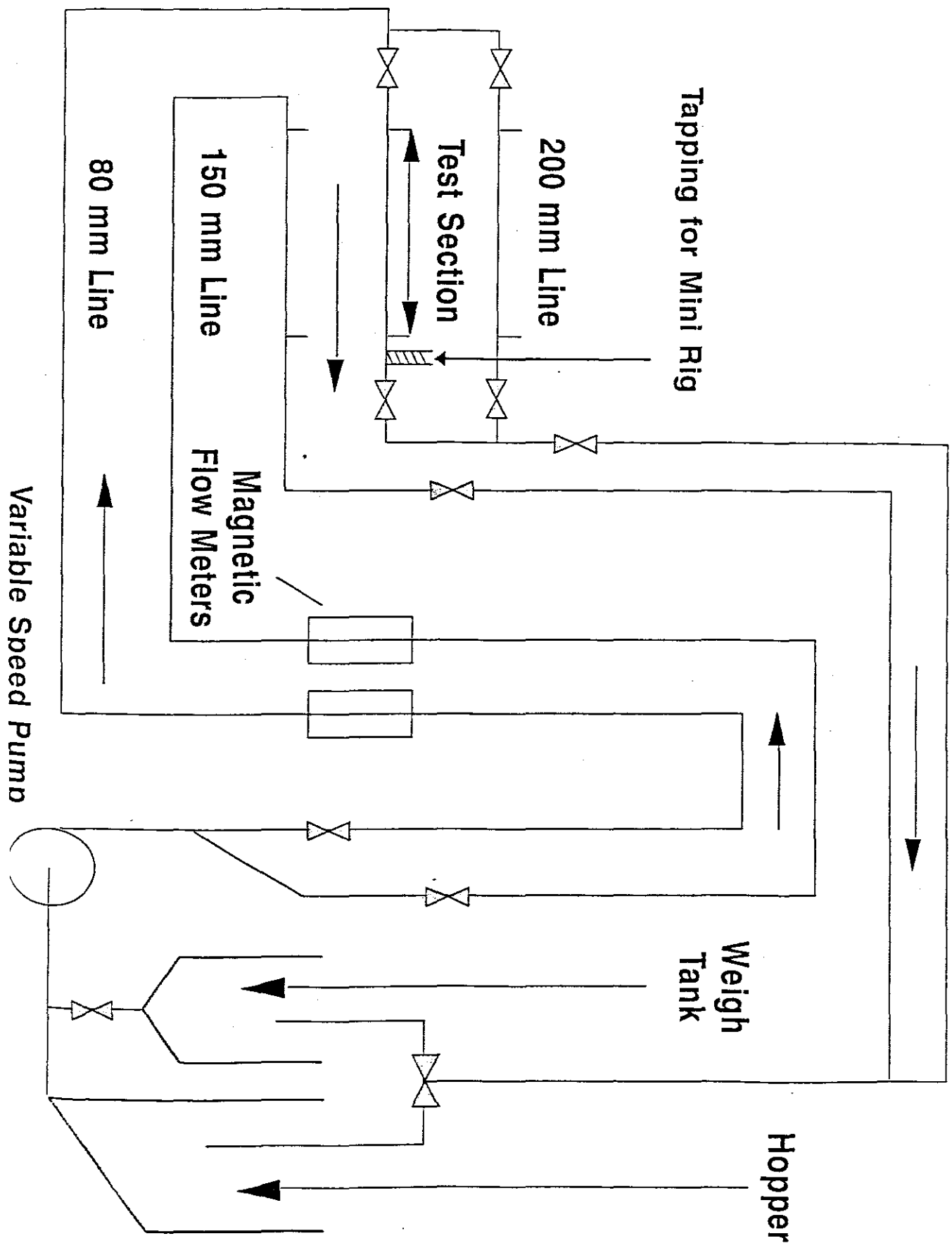
Figure 3.1: Schematic diagram of the pumped recirculating pipe test rig
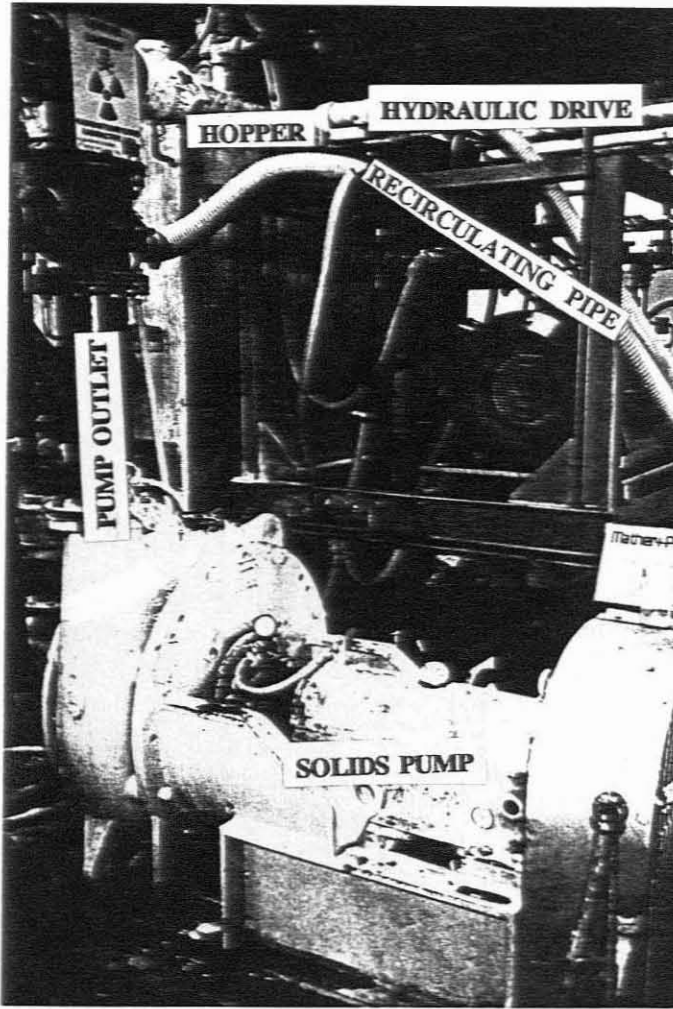
Figure 3.2: Solids handling pump & variable speed hydraulic drive

(b)   Layout

Slurry to be used for a test run is collected in a steel hopper which has a capacity $2m^3$ from where it is pumped through a looped circuit. Directly after the pump the 150mm line splits up into an 80mm and 150mm pipeline. These two pipelines have a vertical counterflow section (Figure 3.3) and horizontal section (Figure 3.4), the flow rate being measured in both downcomer sections by means of magnetic flux flow meters. The horizontal section is approximately 30m in length, with the return pipelines passing through an in-line heat exchanger and pneumatic diverter valve before being re-routed back into the hopper.
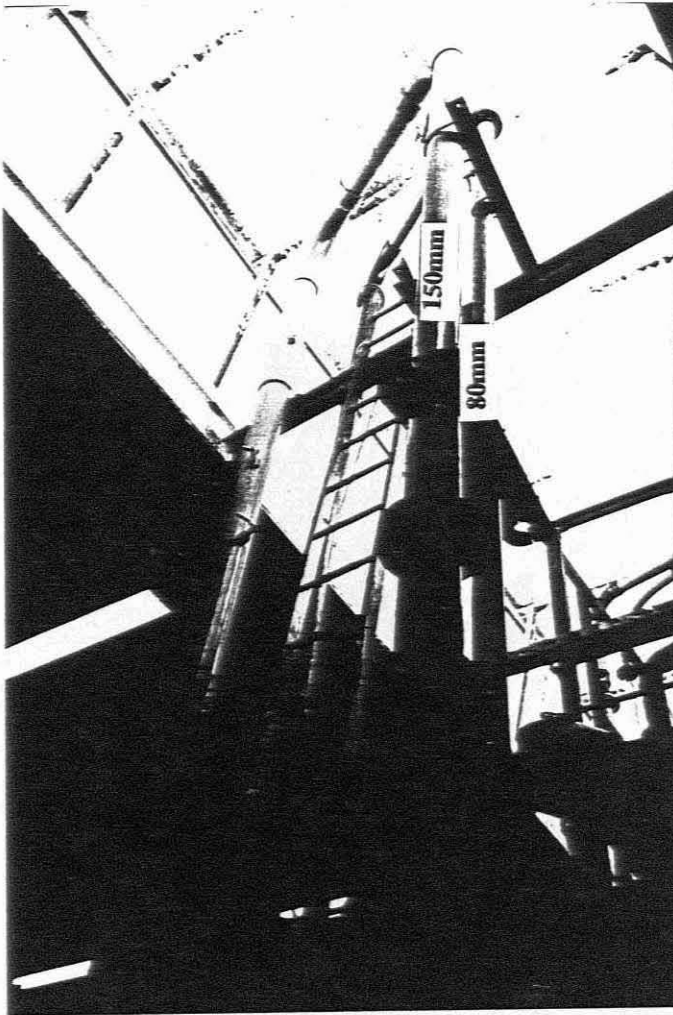
Figure 3.3: Vertical counterflow section

The 150mm horizontal return pipeline splits into a 150mm line and a 200mm pipeline the two joining together after 12m (Figure 3.5). The 80mm and 150mm pipelines are PVC with clear viewing and test sections located in the horizontal return pipelines. The 200mm line is steel.

Flow rate can also be determined by diverting the slurry by means of a pneumatic diverter valve into a weigh tank (Figure 3.6) which is located alongside the hopper. The weigh tank which has a capacity of 1,5m³ and is placed on a 1750kg mass scale is used to calibrate the magnetic flux flow meters. After flow rate determinations the slurry is directed back into the looped circuit.

Figure 3.4: Horizontal test section
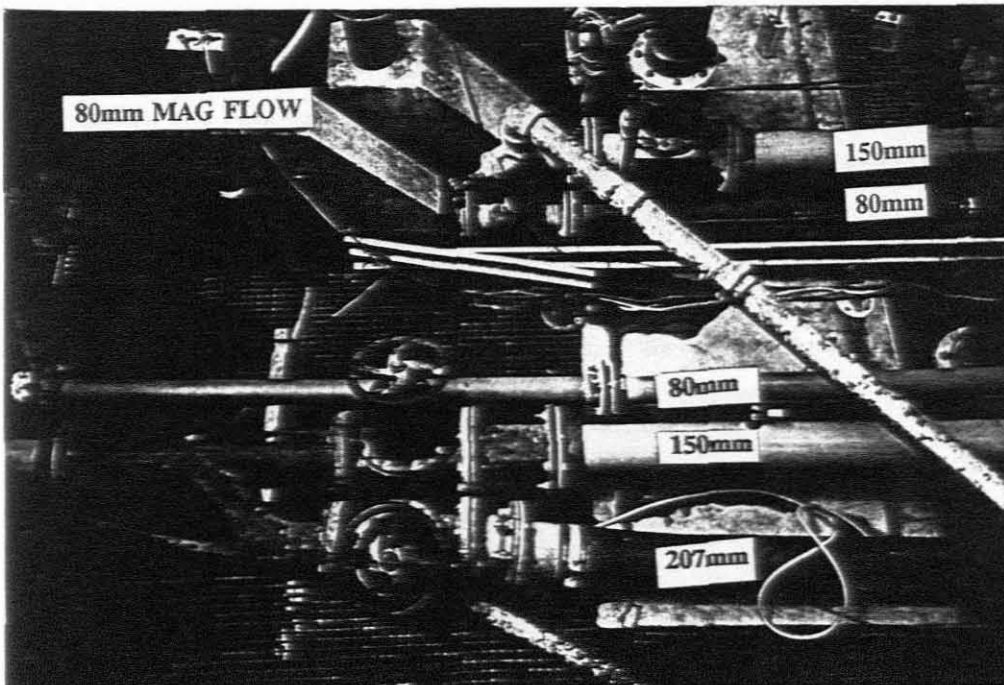
Figure 3.5: The 80mm, 150mm and 200mm horizontal return pipelines
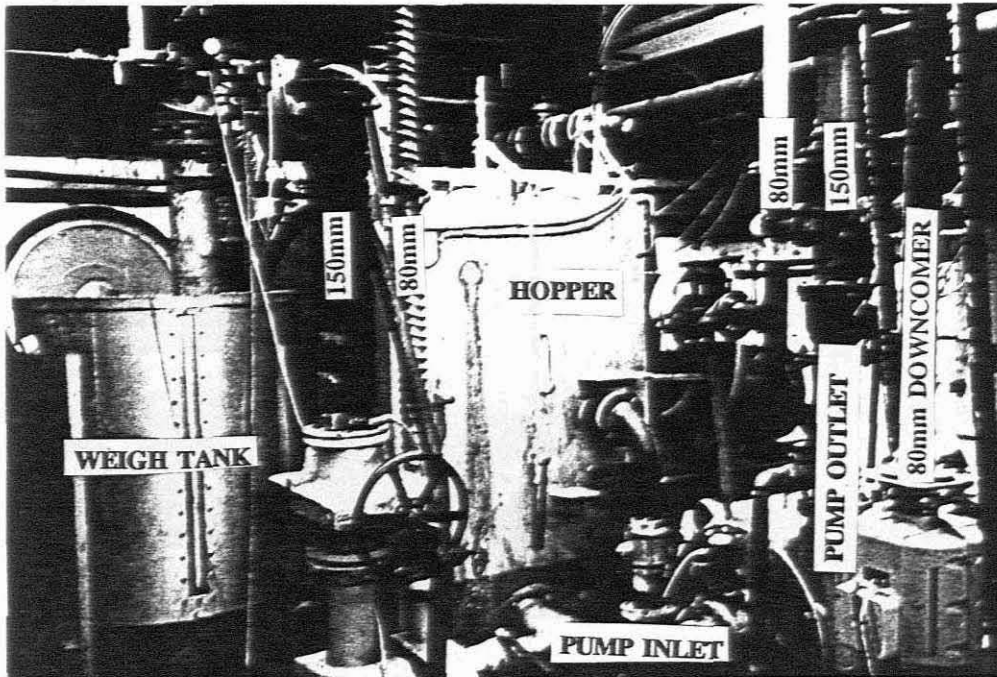
Figure 3.6: Steel hopper and weigh tank

3.2.2 Mini Rig

The purpose of the Mini Rig was to obtain accurate measurements of velocity and head loss in laminar flow for the determination of the rheology of the slurry. Slurry was tapped off from the 150mm pipeline on the East Rig through a 25mm section of PVC piping, which included a 25mm Altometer magnetic flux flowmeter, and the slurry directed into the weigh tank. The weight of slurry passing into the weigh tank during a data test point, and the time taken for that specific volume to fill the weigh tank, were recorded, in order to ensure that accurate velocity readings were being obtained from the flowmeter.

The back pressure from the 150mm pipeline was used as the driving force for the slurry to pass through the Mini Rig.

Using slurry from the East Rig ensured that the same slurry is tested in both rigs ie. East and Mini Rigs. Figure 3.7 depicts the Mini Rig used for testing purposes.
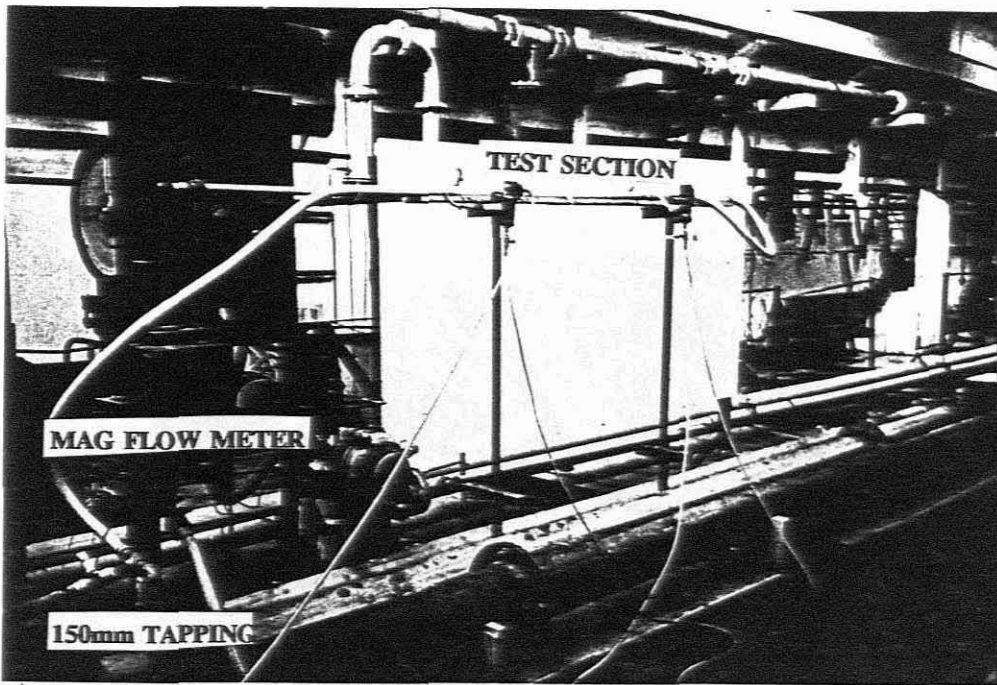
Figure 3.8: The Mini Rig

3.3   MEASURED VARIABLES

3.3.1 Pressure Measurement

(a)   Pressure Tappings

Pressure tappings located in the horizontal test section in the pipe wall are used for differential pressure measurements.   Figure 3.8 shows a typical pressure tapping arrangement that was used.

The tapping hole diameter is 3mm and as reported by Hanks (1981) the length to diameter (L/D) ratio (ie. length of tapping hole to tapping diameter), which is considered critical, was designed according to the ratio

$$\frac{L}{D} = 4 \; , \tag{3.1}$$

to ensure accurate readings.   All burrs on the inside edge of the tappings were removed.
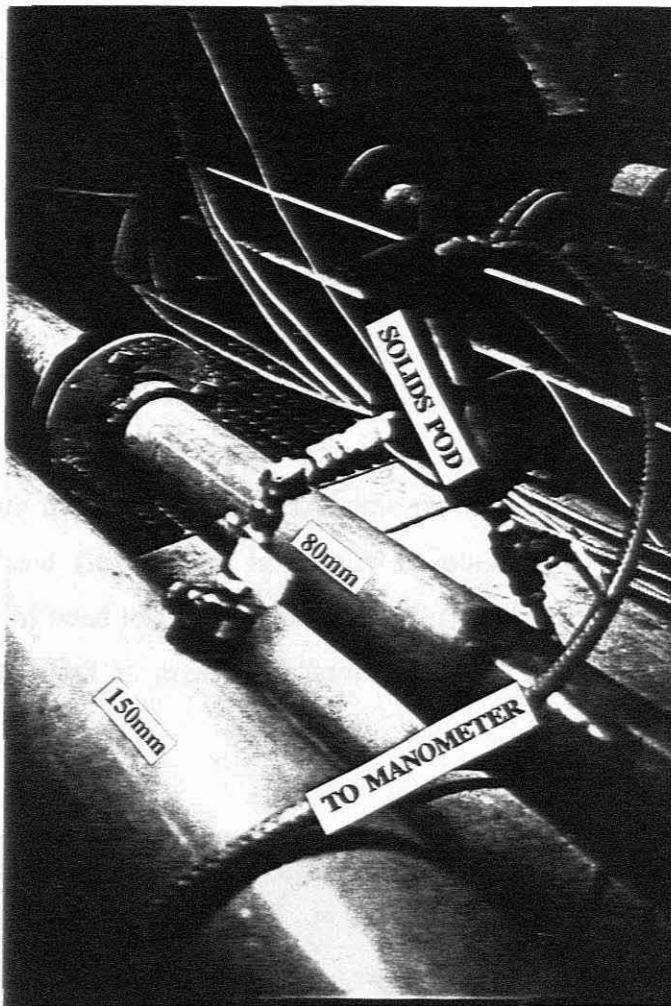
Figure 3.8: Pressure tapping and solids collecting pod

Pressure measurement points are located at 45° to the horizontal to ensure that the ingestion of solid particles or air bubbles into the solids trap (see Figure 3.9) is kept to a minimum. There is, however, a valve located on each solids trap for flushing away any unwanted solids which may accumulate.

The manometer and differential pressure transducer (DPT) are connected by clear water lines to the solids trap.

The test sections which are 2,995m in length are preceded by unobstructed straight pipe of at least 50 pipe diameters (Govier & Aziz, 1972 and Hanks 1981). The only

exception is the 200mm nominal bore pipe which has a straight entry length of 35 pipe diameters.

(b)   Manometer Board

The manometer board serves as a centralised point for measuring pressure and flow. There are six differential water manometers and the layout is shown in Figure 3.9 and Figure 3.10. Electrical signals from the DPT and flow meters are output from the board to the data logging system (Figure 3.11). Head loss measurements can be measured with manometer menisci visible or masked, although the air over water manometer head (ie. visible) is usually maintained during a test run to provide confirmation of head loss measurements. Flushing water is supplied from the water main (400 kPa) and air pressure is supplied at 800 kPa by a compressor.

Figure 3.9: Manometer Board
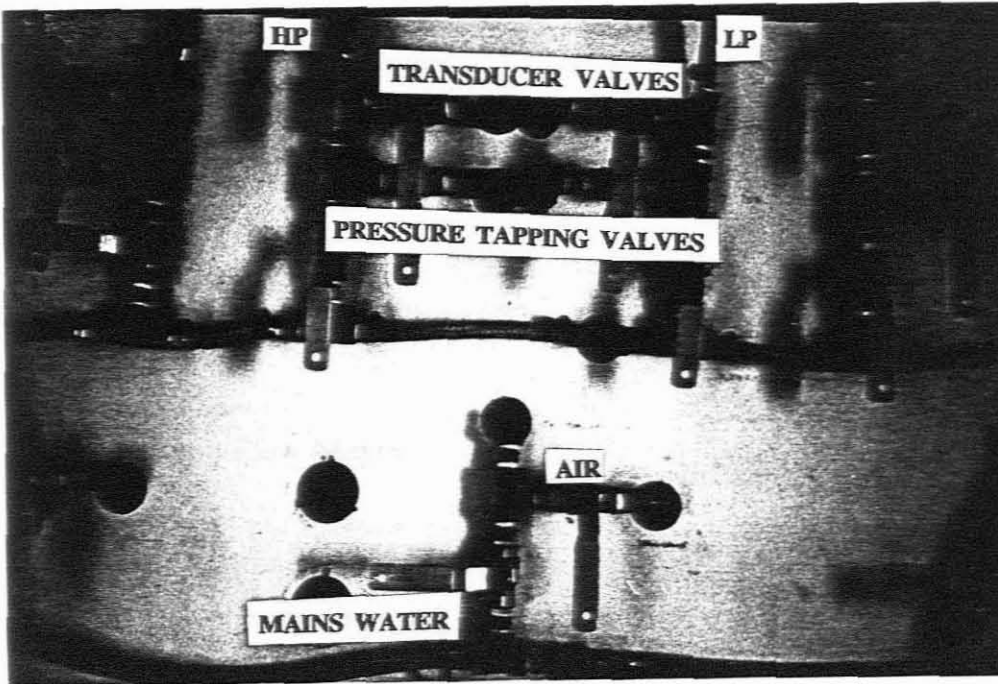
Figure 3.10: Layout of valves for a manometer for the East and Mini Rigs
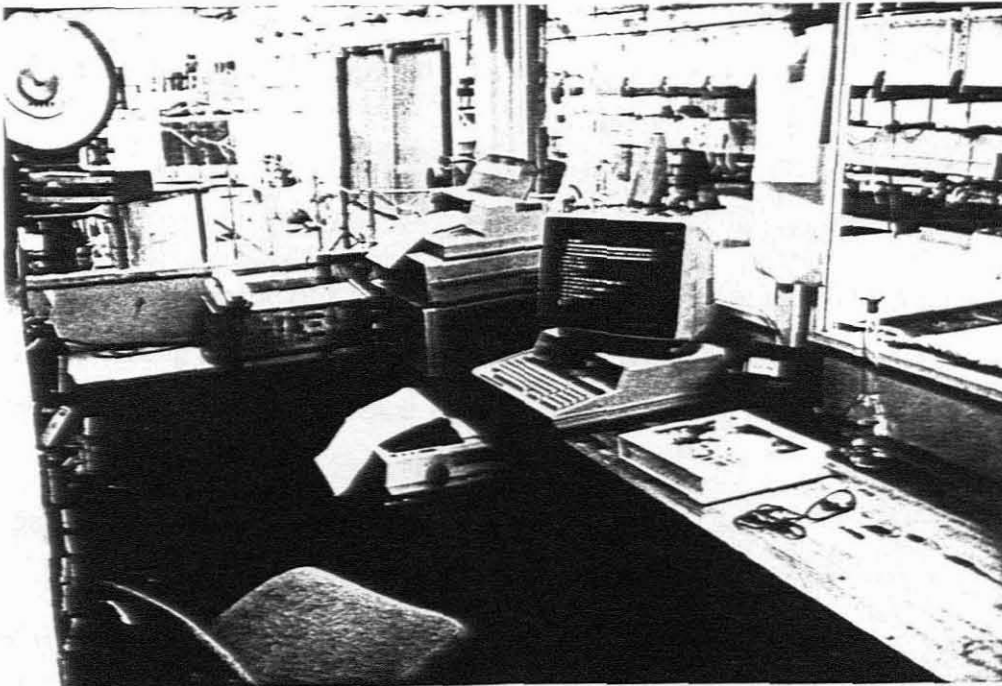
Figure 3.11: Data logging set-up

(c)   Pressure Transducers

A Gould PD3000 pressure transducer was used for differential pressure measurement. The transducer employs a strain gauge bridge to convert differential pressure to an electrical output which can then be read. The diaphragm is made of Hastelloy C with a 316 stainless steel body.

3.3.2 Flow Measurement

(a)   Magnetic Flow Meters

The magnetic flow meters that were used for the East Rig were manufactured by Kent Instruments (80mm pipeline) and Krone Instruments (150mm & 200mm pipelines).

The principle of operation of both magnetic flow meters used is similar. Firstly, a magnetic field is set up across the bore of the magnetic flow meter. Liquid flowing through the metering tube will cut the magnetic field and thus develop an induced emf in the liquid. This emf is detected by two electrodes in the wall of the metering tube. The emf is proportional to the flow velocity multiplied by the magnetic field strength. The transducer signal is digitised by a data logger.

3.4   CALIBRATION

The transducers and magnetic flux flow meters are re-calibrated at regular intervals to ensure accuracy for collecting research data. The transducers are calibrated at the start of each day and the flow meters at the start of each week as well as during a test run.

3.4.1 Pipeline

(a)   Pipeline Diameter

The internal pipeline diameter (D) is measured by filling a known length (L) of pipe with water. The amount of water required to fill the pipe is weighed (M_w) and the

diameter is then calculated from

$$D = \sqrt{\frac{4 \, M_w}{\pi \, \rho_w \, L}} \; .$$

(3.2)

Results obtained from pipeline diameter determination are presented in Table 3.I.

Table 3.I: Pipeline Diameters

Nominal Diameter (mm)	Actual Inside Diameter (mm)	Nominal Wall Thickness (mm)
25	21,6	2
90	79,0	5
150	140,7	5
230	207,0	12

(b)   Roughness Test

The pipeline hydraulic roughness (k) is calculated by comparing the measured energy gradients of clear water tests in the four pipeline diameters with the values calculated using the Colebrook-White equation. This procedure thus establishes the Colebrook-White equation as the datum for all tests, the equation given as follows

$$\frac{1}{\sqrt{f}} = -4 \, \log \left[\frac{k}{3,7 \, D} + \frac{1,26}{Re \, \sqrt{f}} \right] \; .$$

(3.3)

The pipeline roughness as determined for the four pipeline diameters is presented in Table 3.II.

Table 3.II: Pipeline Roughness

Actual Inside Diameter (mm)	Pipeline Roughness (μm)
21,6	4
79,0	7
140,7	9
207,0	130

3.4.2 Calibration of Differential Pressure Transducer

The following procedure is used to calibrate the DPT on the East and Mini Rig.

1.   The transducer and manometer that are to be calibrated are flushed with mains water to ensure that air and any solids have been removed from the lines.

2.   Air over water manometer head ie. a differential head (H) is set up in the glass manometer tubes.

3.   This head is measured and the DPT output is logged at the same time.

4.   Steps 2 and 3 are repeated for different manometer heights over the full differential head test range until enough data points have been collected for calibration.

A least squares linear regression is performed on the measured head and transducer readings in order to obtain the calibration equation. A set of N observed measurements Y on the corresponding set of N transducer readings X will yield the least squares regression line of (Spiegel, 1972)

$$Y = m X + c \ ,$$

                                                                                      (3.4)

where

$$m = \frac{N \, \Sigma XY - (\Sigma X)(\Sigma Y)}{N \, \Sigma(X^2) - (\Sigma X)^2} \, , \tag{3.5}$$

and

$$c = \frac{\Sigma Y \, \Sigma(X^2) - \Sigma X \, \Sigma(XY)}{N \, \Sigma(X^2) - (\Sigma X)^2} \, . \tag{3.6}$$

An objective measure of how well the line represents the data is given by the correlation coefficient (r) equation:

$$r = \frac{N \, \Sigma XY - (\Sigma X)(\Sigma Y)}{\sqrt{\left[N \, \Sigma(X^2) - (\Sigma X)^2\right]\left[N \, \Sigma(Y^2) - (\Sigma Y)^2\right]}} \, . \tag{3.7}$$

Calibrations were accepted for r values in the range $0,99 < r < 1$, a value of $r = 1$ implying a perfect fit.

In general the fit is not perfect and at each point there remains a small but finite difference or residual error E_{res} which is defined by:

$$E_{res} = [\, Y_{obs} - (m \, X + c) \,] \, . \tag{3.8}$$

The highest residual error from a calibration provides a measure of the absolute error involved in the use of the transducer under the test conditions (Slatter, 1994). A typical output obtained from the calibration programme is shown in Figure 3.12.

3.4.3 Calibration of Magnetic Flow Meters

The calibration of the magnetic flow meters was undertaken with the test slurry over the complete test range as the output can be influenced by the velocity profile (Heywood et al, 1993). This is due to the fact that the magnetic flux lines can never be perfectly parallel. It has been shown by Mehta (1993) that this is the only method of ensuring accurate readings over the laminar turbulent and transition regimes.

TRANSDUCER C

PLOT OF CURRENT SIGNAL VS DIFFERENTIAL HEAD

LINEAR REGRESSION
R SQUARED = 1.00

Y = - 0.4842 + 1.2015 X

X (I)	Y (I)	Y	RESIDUAL
0,402943	0,000	0,000	0,000
0,689331	0,343	0,344	-0,001
0,795483	0,471	0,472	-0,001
0,893752	0,589	0,590	-0,001
0,947572	0,653	0,654	-0,001
1,051085	0,778	0,779	-0,001
1,104898	0,843	0,843	0,000
1,189980	0,946	0,946	0,000
1,304870	1,084	1,084	0,000
1,205970	0,966	0,965	0,001
1,116196	0,857	0,857	0,000
1,018119	0,740	0,739	0,001
0,914735	0,615	0,615	0,000
0,822246	0,504	0,504	0,000
0,768191	0,439	0,439	0,000
0,650622	0,298	0,298	0,000
0,542588	0,168	0,168	0,000
0,447548	0,054	0,054	0,000
0,402496	0,000	-0,001	0,001
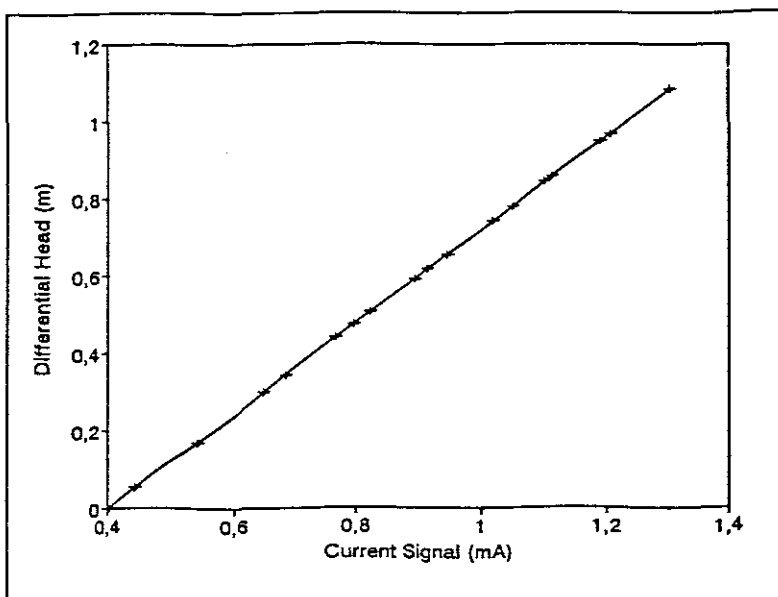
Figure 3.12: Typical output obtained from calibration programme

The following procedure was undertaken for calibrating the magnetic flow meters.

1.   The pump speed was set to the desired speed.

2.   The weigh tank scale reading was noted (M_1).

3.   The data logger was first started and then the diverter valve was opened and the stopwatch started at the same time.

4.   The diverter valve was closed and the stopwatch stopped at the same time when sufficient slurry had been collected. The data logger ran for a pre-set time, enough to cover the whole procedure.

5.   The weigh tank reading .was noted (M_2).

The flow rate for each reading is given by the equation:

$$Q = \frac{(M_2 - M_1)}{\rho\ t} .$$

(3.9)

The average transducer reading cannot be used for calibration purposes as it is not accurate. In order to obtain the correct transducer reading for each point a graph of current signal vs time was plotted. Figure 3.13 shows a typical output.

As can be seen from the graph the current signal drops sharply after the diverter valve is opened (point A) before constantly decreasing (point B to point C). After the diverter valve is closed (point C) the current signal reading returns to the original value (point D). The slope of the line BC remains constant at the varying pump speeds. The transducer reading is thus read by extending a line EF from the slope of line BC halfway during the time taken to divert the slurry to the weigh tank (point A to point C).

The calibration equation is then derived by performing a linear regression on the flow rate and the transducer readings in each case.

No difference was found between the laminar and turbulent flow data when calibrated in this way, as indicated by Fig 3.14 showing a typical calibration.
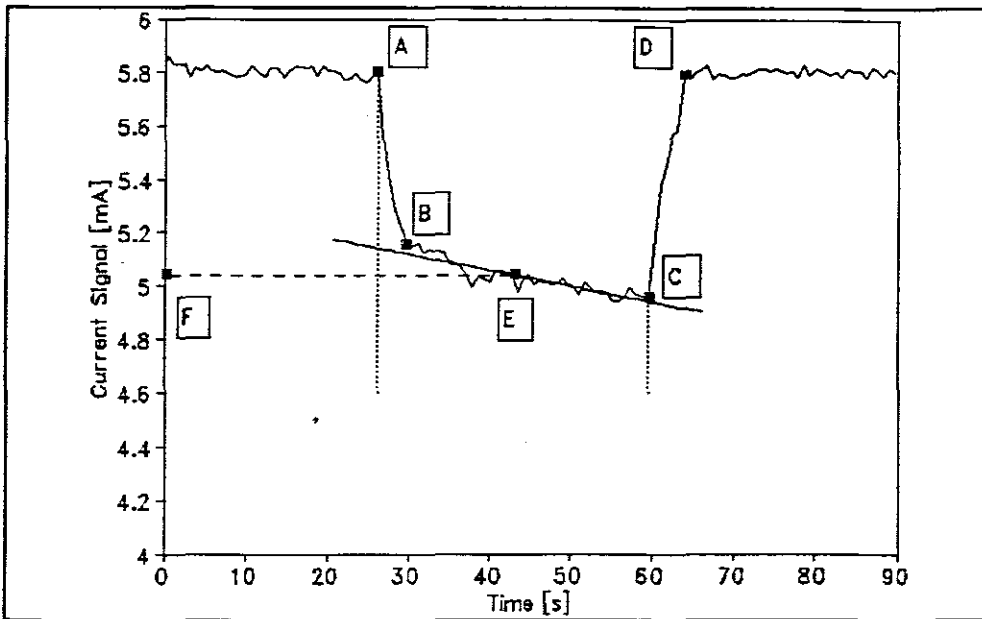
Figure 3.13:   Current signal vs time for the 150mm magnetic flow meter
for a desired speed
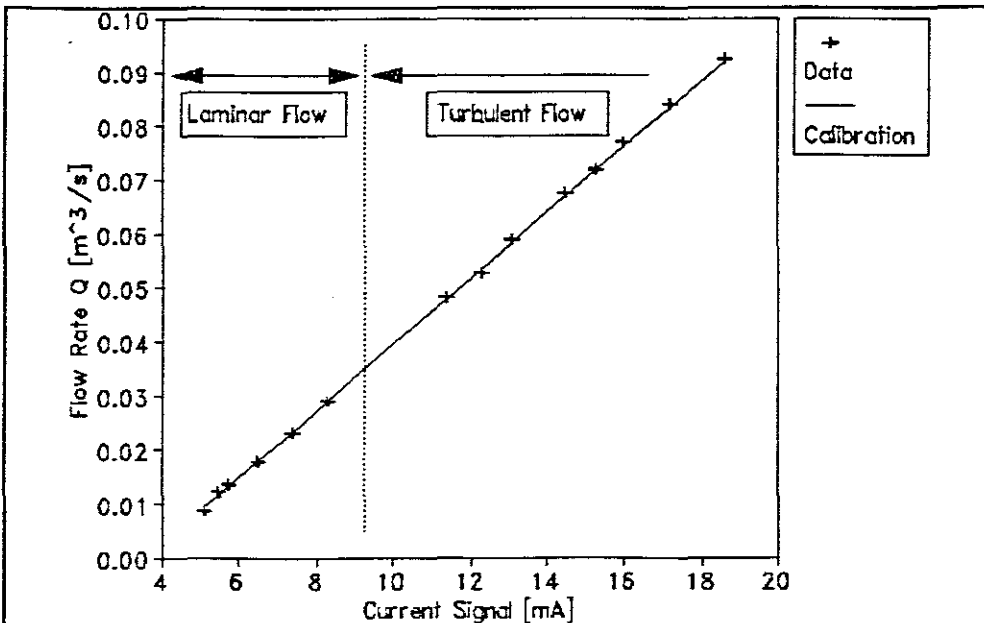
Figure 3.14:   Calibration of the 150mm magnetic flow meter, showing
laminar and turbulent flow data over the full test range

3.5   OTHER MEASURED VARIABLES

3.5.1   Slurry Density

Slurry density and relative density are determined by performing the following steps.

1.   A clean, dry one litre volumetric flask is weighed (M_1).

2.   The volumetric flask was filled with slurry from a tapping in the pipe wall on the vertical section above the pump before it splits into the 80mm and 150mm pipelines. The volume of slurry is approximately 990ml.

3.   The flask plus slurry are weighed (M_2).

4.   The flask is then filled with water up to the graduated mark and weighed (M_3).

5.   The flask is emptied, filled with clear water and weighed again (M_4).

6.   Steps 1-5 were repeated except that in step 2 slurry was taken from a tapping in the horizontal test section.

The relative slurry density S_m is defined as:

$$S_m = \frac{\text{mass of slurry sample}}{\text{mass of equal volume of water}} = \frac{M_2 - M_1}{(M_4 - M_1) - (M_3 - M_2)} \ . \tag{3.10}$$

S_m is calculated using the above equation and slurry density is calculated from:

$$\rho = S_m \, \rho_w \ . \tag{3.11}$$

Normally the use of tappings for sampling slurries is not a good procedure to follow however in this particular case the following should be noted:

●   the slurry being tested was homogeneous;

●   the point at which slurry was tapped was from an area where the slurry had been well mixed;

●   Slatter (1994) compared this method against samples taken from other points in the pipe system and hopper and found no discrepancies.

3.5.2 Solids Relative Density

The relative density of the solids (S_s) is determined using test method 6B for fine grained soils from BS 1377 (1975).

3.5.3 Slurry Temperature

A mercury thermometer was used to measure the temperature of the slurry in the hopper. The temperature very rarely went above 20°C, with a temperature of between 19°C and 20°C being the norm. A rise of approximately 2°C is usually experienced during a test run. If a temperature rise exceeding 2°C is experienced, data at the extreme temperatures is compared to detect for any temperature effects (Slatter, 1994).

3.5.4. Particle Size Distribution

The ASTM (American Standard Testing Method), which is recognized worldwide, was used to determine the particle size distributions and were conducted at Gibbs Africa laboratories. In this procedure a sample of slurry is thoroughly dried and the courser particles are screened to determine the distribution. The distribution of finer particles is determined using a hydrometer. The particle size distributions for the kaolin clay test sets however, were determined using the Malvern 2600/3600 Particle Sizer VF.6 instrument, which if used correctly produces more accurate results for finer material (Robertson, 1996). Ideally it would have been preferable to use only one PSD method however, the testing method of the Malvern instrument was not suitable for determining the courser particles of the slurry and hence it was decided to use the ASTM method for Mixture 1 and Mixture 2 and the Malvern instrument for the finer kaolin clay particles. The particle size distributions are presented in Appendix A.

Any comparison of particle size distributions should be undertaken with caution as those produced by methods other than the ASTM or the Malvern 2600/3600 Particle Sizer VF.6 instrument may not necessarily agree. An example of this can be seen in Figure 3.15 where the same slurry (mixture of kaolin, rock flour and sand) used for the ASTM, was used on the Malvern instrument for particle size distribution determinations. As can be seen from

Figure 3.15 these methods yield significantly different results.
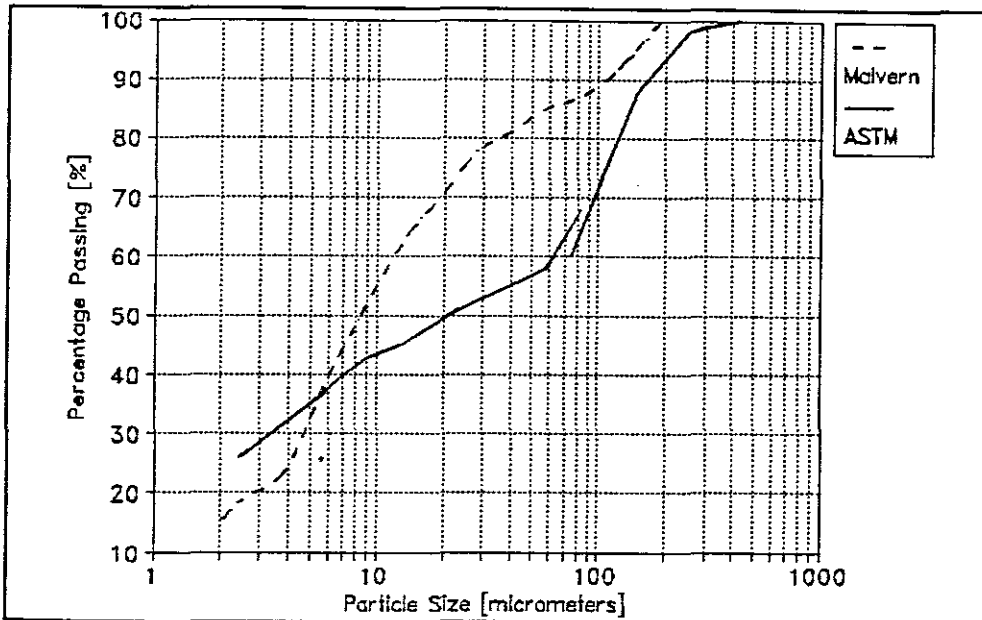
Figure 3.15:   Particle size distribution using the ASTM and Malvern
              Particle Sizer for the same mixture of kaolin clay rock flour
              and sand

The representative particle size used by Slatter (1994) was the d_{85} size and this was determined from the particle size distributions. The values obtained are presented in the table below.

Table 3.III: d_{85} Sizes for the Various Data Test Sets

Data Test Set	d_{85} Size	PSD Method
K_10	30,1	Malvern
K_20	24,6	Malvern
RF_10	51,9	ASTM
RF_20	77,4	ASTM
RF_30	83,7	ASTM
S_10	137,1	ASTM
S_20	158,5	ASTM
S_30	170,4	ASTM

3.6   MATERIAL

The solids materials used for testing purposes were kaolin clay, rock flour and silica sand (Figure 3.16). Tests were conducted using kaolin clay, then a mixture of kaolin clay and rock flour at varying concentrations and finally using a mixture of kaolin clay, rock flour and No. 2 Foundry Sand from Consol at varying concentrations.

3.6.1 Kaolin clay

Kaolin clay was obtained from the Serina Kaolin (Pty) Ltd which is currently mining a kaolin deposit at Brakkekloof in Fish Hoek, Cape Town. The kaolin was delivered in the form of pellets. To obtain a homogenous slurry the pellets were thoroughly mixed using the hopper recirculating pipe on the East Rig. The recirculating pipe is located directly after the pump and it re-directs the slurry back into the hopper. This procedure is carried out until the slurry is thoroughly mixed before circulating the slurry through the four pipelines.
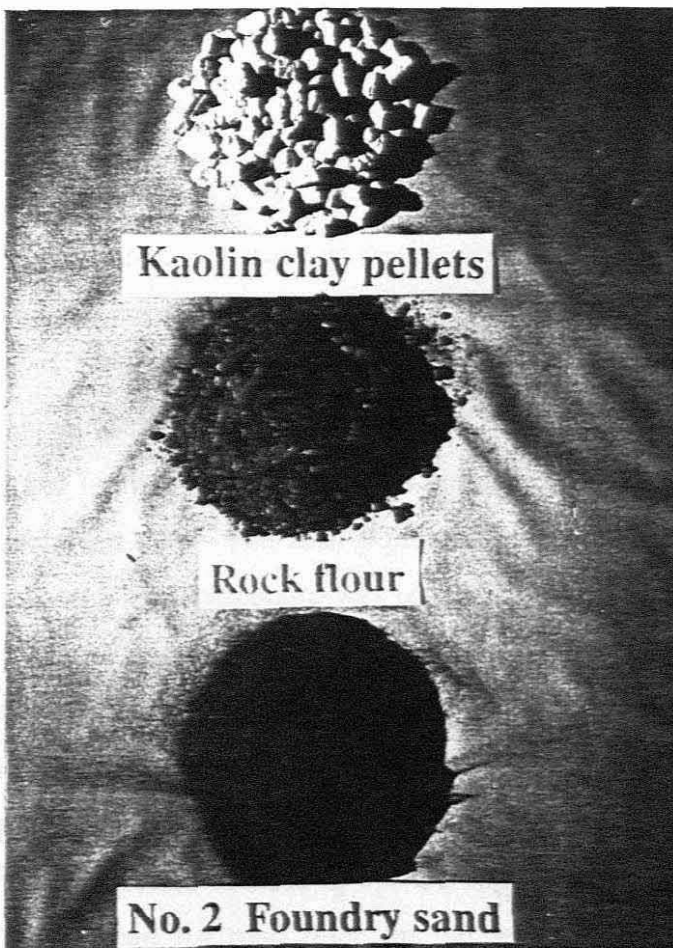
Figure 3.17: Solids materials used for testing purposes

3.6.2 Rock Flour

Rock Flour was obtained from Hippo Quarries from their quarry called Peninsula.

3.6.3 Sand

Sand was obtained from Consol in 25kg bags called No. 2 Foundry Sand. The particle size of the sand was between 75 and 350 μm.

3.7 MIXTURES

3.7.1 Mixture Kaolin Clay and Rock Flour

The rock flour was found to form a settling slurry when mixed with water. In order to obtain a homogeneous slurry kaolin clay was used as a suspending agent for the rock flour. Tests were therefore conducted to determine the amount of kaolin clay needed to suspend the rock flour.

Twenty sample bottles each containing 200g of water were used for the tests. For Test A, 10 of the sample bottles contained rock flour at a relative density of 1,1 and for Test B, the remaining ten sample bottles contained rock flour at a relative density of 1,2.

Kaolin clay was then added to the sample bottles in Test A, starting at 5g of kaolin clay for the first sample bottle and increasing in 5g amounts per sample bottle until the last sample bottle contained 50g of kaolin clay. The rock flour and kaolin clay were then thoroughly mixed and allowed to stand. This procedure was repeated for Test B.

It was found that in both Test A and Test B that 30g of kaolin clay was required to suspend the rock flour and form a homogeneous slurry. At 25g of kaolin clay added, the mixture formed a slow settling slurry and hence the critical point lay between these two limits ie. 25g and 30g of kaolin. It was therefore decided to use the concentration ratio of 30g of kaolin clay per 200g water to suspend the rock flour for the tests in the pipelines or a kaolin concentration of at least $C_v = 5\%$.

3.7.2 Mixture Kaolin Clay and Sand

In order to achieve a higher representative particle size tests were conducted using a mixture of kaolin clay, rock flour and silica sand. Tests were conducted to determine the amount of kaolin clay needed to suspend the rock flour and the No. 2 Foundry Sand.

Twenty Sample bottles each containing 200g of water were used for the tests. For Test C, 10 of the sample bottles contained rock flour and silica sand at a relative density of 1,1 and for Test D, the remaining ten sample bottles contained rock flour and silica sand at a relative density of 1,2.

Kaolin clay was then added to the sample bottles in Test C, starting at 5g of kaolin clay for the first sample bottle and increasing in 5g amounts per sample bottle until the last sample bottle contained 50g of kaolin clay. The rock flour, silica sand and kaolin clay were then thoroughly mixed and allowed to stand. This procedure was repeated for Test D.

It was found that in both Test C and Test D 35g of kaolin clay was required to suspend the rock and silica sand and form a homogeneous slurry. At 30g of kaolin clay added the mixture was a slow settling slurry and hence the critical point lay between these two limits. It was therefore decided to use the concentration ratio of 35g kaolin clay per 200g water to suspend the sand for the tests in the pipelines or a kaolin concentration of at least $C_v = 6\%$.

3.8   EXPERIMENTAL PROCEDURE

3.8.1 Start-up Procedure

The following should be carried out to complete a test run.

1.   First check that there is enough slurry in the hopper to carry out a test. The hopper should be at least half full. Add water or solids to achieve a desired density.

2.   All supplies are switched on and slurry is pumped at the highest pump speed through all the pipes simultaneously to ensure thorough mixing. The slurry

is allowed to flow through the system for sufficient time so as to allow air in the system to escape.

3.   The DPT is calibrated and slurry relative density tests performed.

4.   The data logging programme is loaded and initialised.

5.   The desired flow rate for a test is achieved by controlling the pump speed. The data logging routine is started and the magnetic flow meter and DPT outputs logged for three to five minutes (Sive, 1988). Check for drift.

The calibration of the magnetic flow meter is performed during a test run using timed weigh test samples at different time intervals.

A test is completed by repeating the run at different pump speeds and the data collected is then processed.

When a test is performed on the Mini Rig, slurry continuously empties into the weigh tank and timed weigh test samples are taken at intervals during the test for the calibration of the magnetic flow meter.

After a test set has been completed a slurry relative density test is performed again to ensure that the slurry density has remained constant.

3.9   CONCLUSIONS

The test apparatus used for the experimental investigation has been fully described and the calibration and test procedures to enable the collection of accurate pipeline data have been presented.

The test results of the non-Newtonian slurries that were tested using the apparatus and testing procedures are presented in Appendix A. The results are reviewed in Chapter 4 and discussion arising from the results is presented in Chapter 5.

CHAPTER 4

CHAPTER 4

RESULTS AND ANALYSIS

4.1 INTRODUCTION

The results and analysis are presented in this chapter and in Appendix A. The measured variables of head loss and velocity for each pipe test were used to plot a pseudo-shear diagram. The theoretical model lines are also shown on the data, providing a visual appraisal of the performance of each model.

4.2 PIPELINE TESTS

A typical pseudo-shear diagram for the four combined diameters ie. 25mm, 80mm, 150mm and 200mm is shown in Figure 4.1.
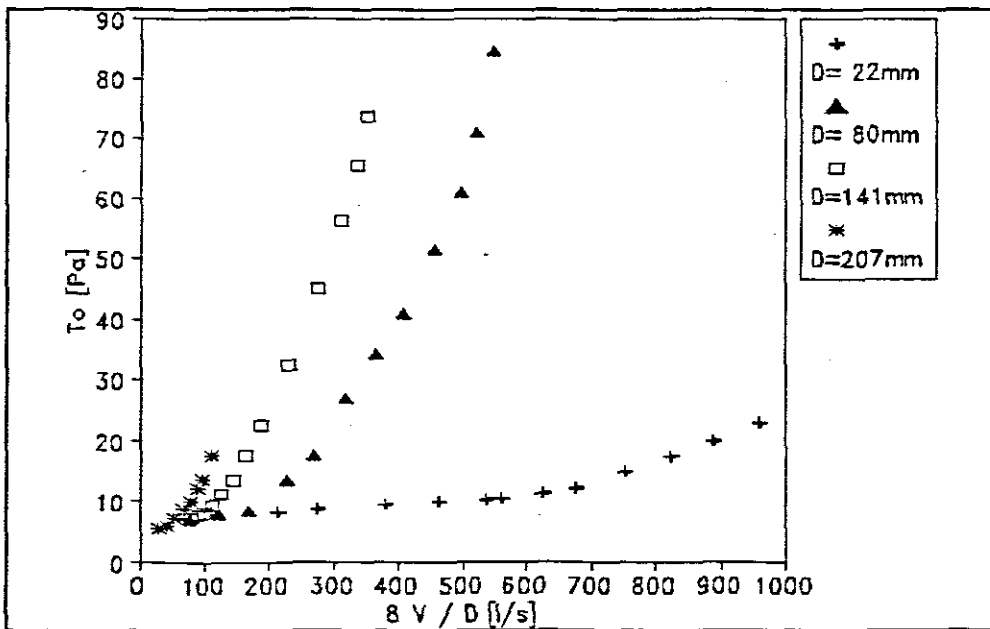
Figure 4.1: Kaolin clay: second data test set: $\tau_y=5,8$; K=0,0176; n=0,815

The change in flow behaviour from laminar to turbulent flow can be seen in the above diagram. The diagram shows agreement with the analysis of Rabinowitsch (1929) and

Mooney (1931) (Section 2.6.2 - Figure 2.5) in that the relationship between the shear stress and shear rate is independent of the diameter in laminar flow. This was true for all tests conducted, where pipe diameter had no influence on wall shear stress at a given pseudo-shear rate in the laminar regime. This indicates that the slurry properties were time independent. In laminar flow, on physical observation of the slurries in the transparent sections of the pipeline, the slurry particles near the tube wall could be seen to be travelling in straight lines. As the velocity increased the particles took on a more random, swirling or eddy motion and the transition from laminar to turbulent flow could clearly be seen. The differential transducer output reading showed more variation in the transition region and confirms the physical observation. This evidence also supports the fact that true turbulence is occurring. Settling of particles was not observed at any of the concentrations tested. The intersection of the laminar and turbulent data can be taken as the critical point at which turbulence begins and hence the critical velocity can be determined.

The 25mm pipeline only shows the first few data points for the onset of turbulence. This is due to the fact that the back pressure of the 150mm pipeline was used as the driving force for the 25mm pipe. Hence, there was insufficient driving force to enable the recording of the full turbulent range. Low velocities were also recorded in the 200mm pipeline due to the set-up of the pipeline system. In a looped pipeline system one is normally limited to two pipeline diameters due to the available head capacity. Using the looped pipeline system at UCT, testing was conducted using as wide a range of diameters as was possible on the one system, but in doing so low velocities in the 200mm pipeline were inevitable.

4.2.1 Pipe Roughness

There is quite a marked difference in the pipe roughness for the three smaller pipelines as opposed to the 200mm pipeline (Table 3.II). The smaller pipelines (ie. 25mm, 80mm & 150mm pipelines) are PVC tubing whereas the 200mm pipeline is constructed of steel. The inside of the 200mm pipe was corroded thus accounting for the high pipe roughness value.

4.2.2 Particle Roughness Effect

The effect of particle roughness on turbulence can be seen in Figure 4.2, a graph of the Roughness Reynolds Number vs the Roughness Function. The turbulent data from the test sets has been used in Figure 4.2, together with the curves and asymptotes for the Nikuradse and Colebrook White loci. The top curve is the locus of data of Nikuradse for sand roughened pipes with uniform roughness. The lower curve is the Colebrook (1939) and White equation (Equation 2.49) which represents the locus of data for randomly rough pipes.
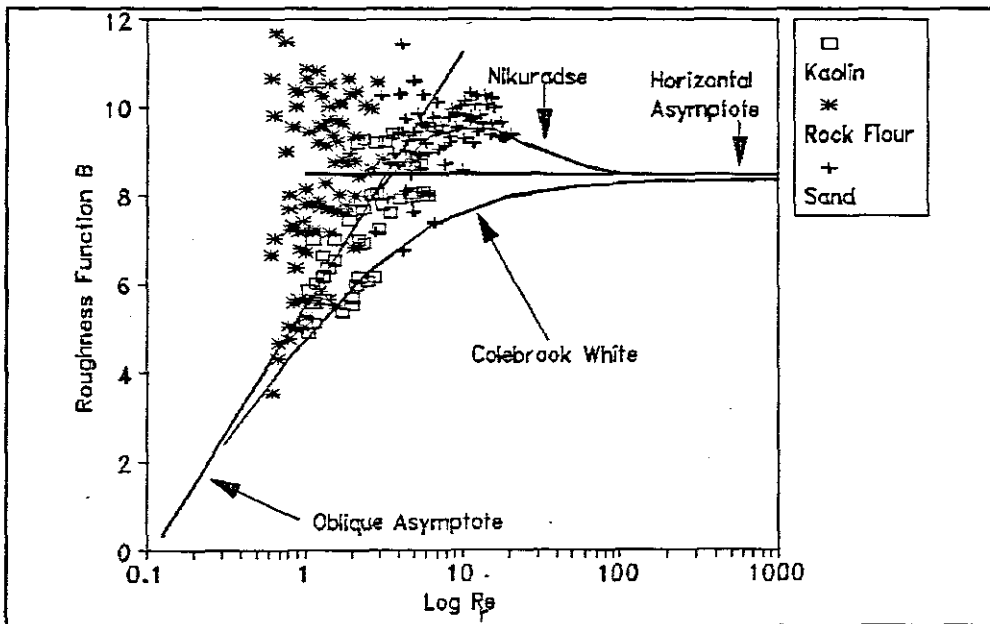
Figure 4.2: Roughness function correlation for non-Newtonian slurries

The turbulent data points used in Figure 4.2 have been classified as those coming from either kaolin test sets, mixture 1 - rock flour test sets or mixture 2 - sand test sets. The highest roughness Reynolds number obtained was 19,6. The data points for the kaolin tend to lie on the line for the law of the wall for smooth pipes, with the rock flour data points lying to the left. The data points for the sand tend to lie on or near the curve of Nikuradse.

4.2.3 Kaolin Clay

Two sets of kaolin clay tests were first conducted to confirm the results already obtained by

Slatter (1994). The results obtained supported the existing data set. (See Appendix A).

4.2.4 Mixtures

Three test sets using a mixture of kaolin clay & rock flour (Mixture 1) and a mixture of kaolin clay, rock flour & sand (Mixture 2) were conducted in order to obtain a higher representative particle size and different PSD to the existing data set.

4.2.5 Representative Particle Size

The Slatter model is the only theoretical model of the five models under consideration to incorporate a representative particle size of the slurry. As determined by Slatter (1994) the d_{85} size was found to be a good representation of the turbulent roughness size effect of the solid particles in the slurry. This representative particle size has been used in all calculations for the Slatter model. However, the d_{85} size for the slurries that were tested does not always give the best representation of the particle roughness effect. Hence, the optimum representative particle sizes for the Slatter model for the data of all the test sets were determined according to the sum of squares error function (SSE - equation 4.1)

$$SSE = \Sigma \ (\ \tau_{0 \ calc} - \tau_{0 \ obs} \ )^2 \ . \qquad\qquad (4.1)$$

$\tau_{0 \ calc}$ is determined from equation 2.73 and equation 2.74 (see section 2.11.5)
The results are tabulated in Table 4.I and can be seen graphically in Figure 4.3 to Figure 4.10.

Table 4.I: Optimum and Experimental Representative Particle Size

Data Test Set	Optimum RPS (μm)	d_{85} (μm)
K_10	33 = d_{87}	30
K_20	44 = d_{95}	25

Table 4.1 cont.

Table 4.I: Optimum and Experimental Representative Particle Size

Data Test Set	Optimum RPS (μm)	d_{85} (μm)
RF_10	0.001	52
RF_20	4E-09	77
RF_30	3E-11	84
S_10	80 = d_{65}	137
S_20	114 = d_{70}	159
S_30	148 = d_{78}	170
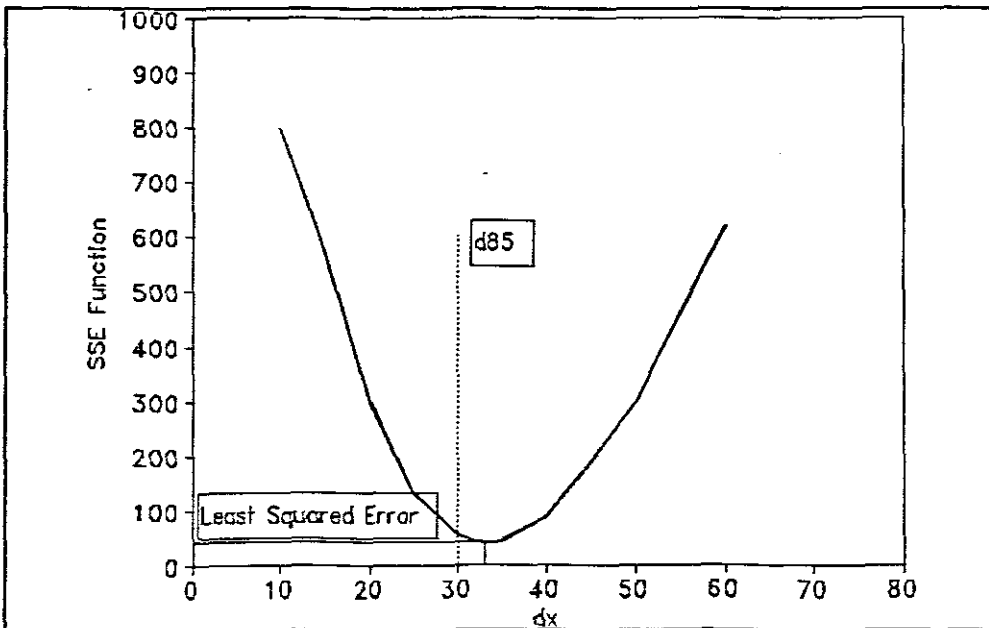
Figure 4.3: Optimum representative particle size for test set K_10
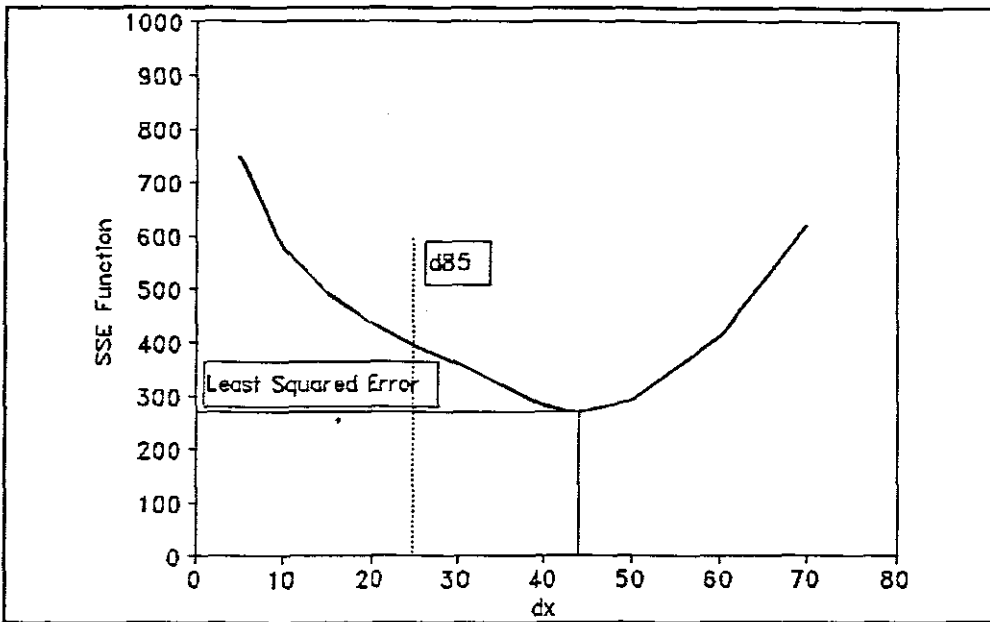
Figure 4.4: Optimum representative particle size for test set K_20
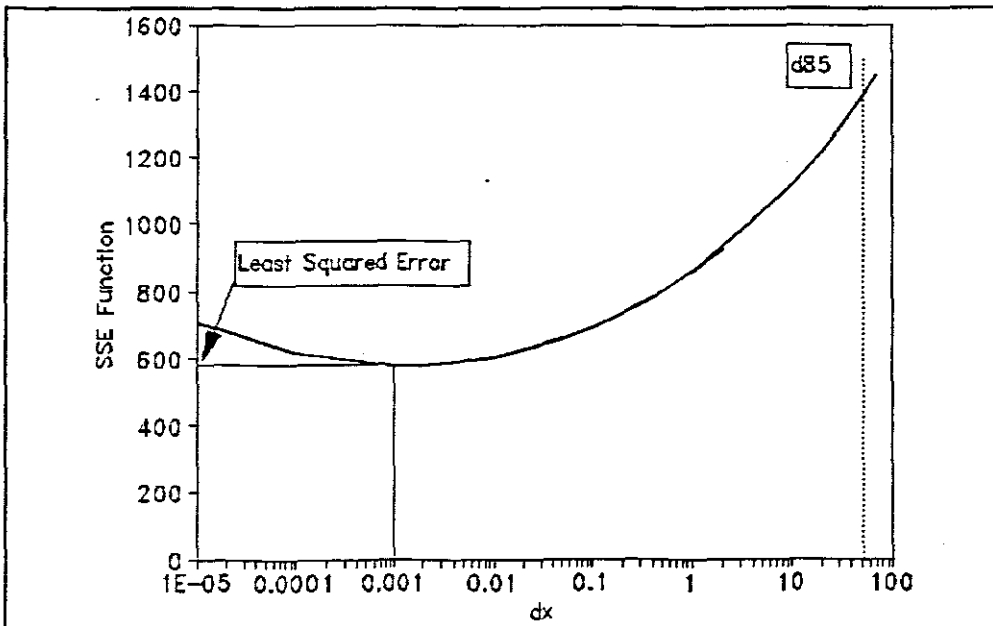
Figure 5 Figure 4.5: Optimum representative particle size for test set RF_10
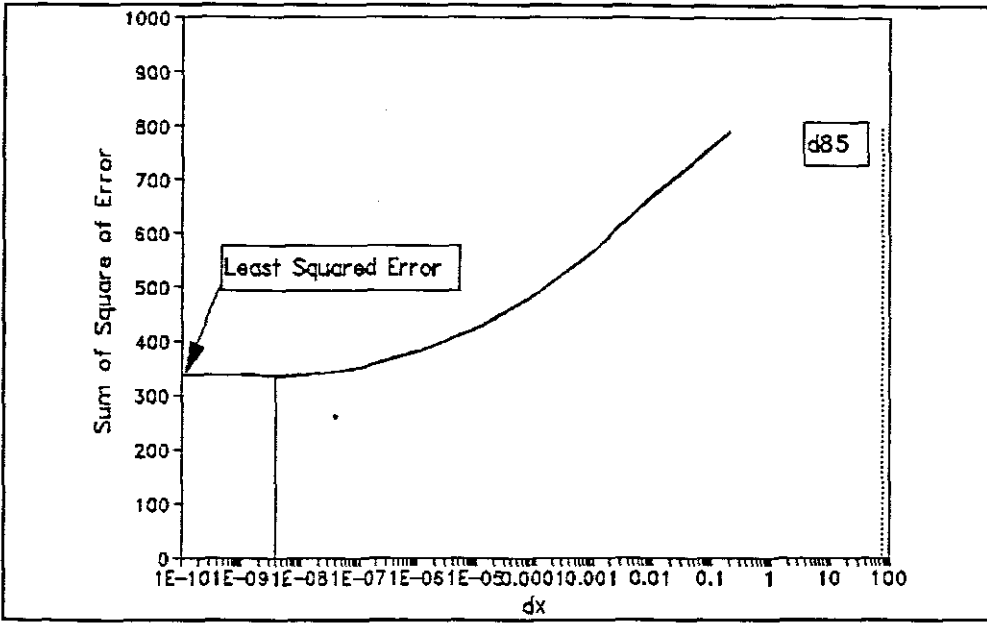
Figure 4.6: Optimum representative particle size for test set RF_20
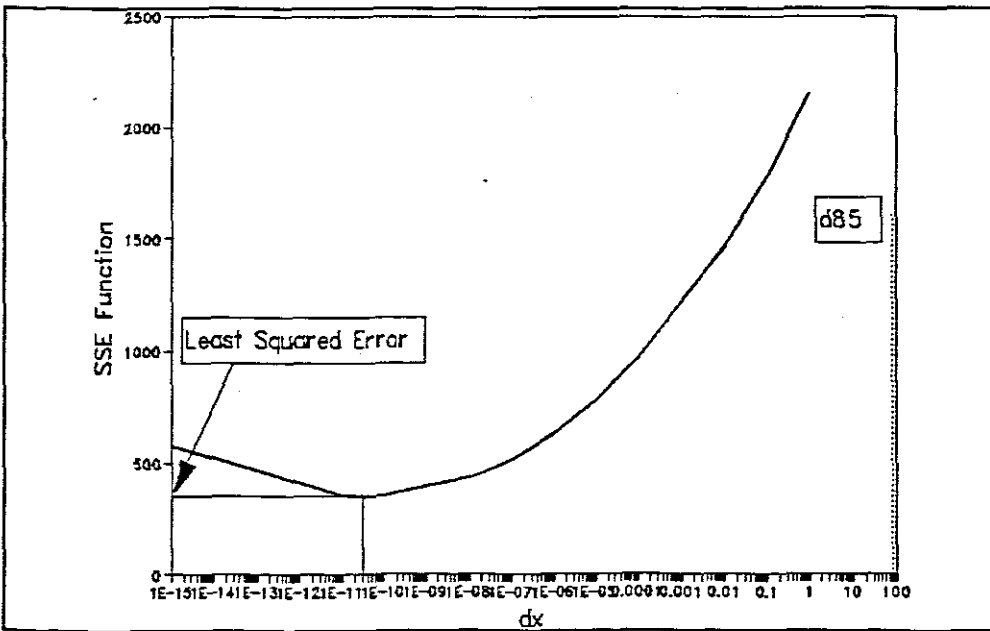
Figure 4.7: Optimum representative particle size for for test set RF_30
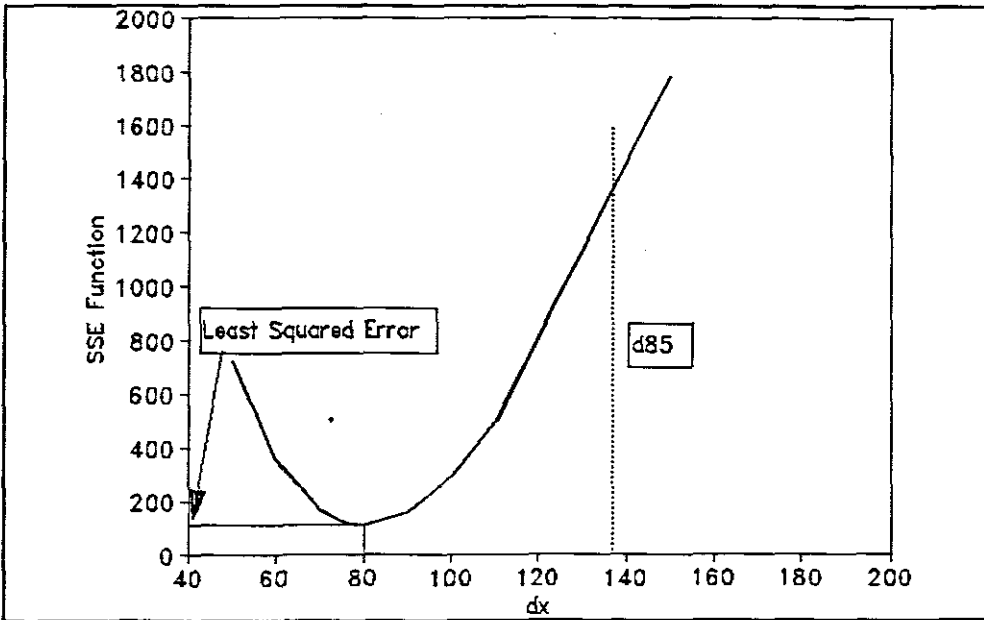
Figure 4.8: Optimum representative particle size for test set S_10
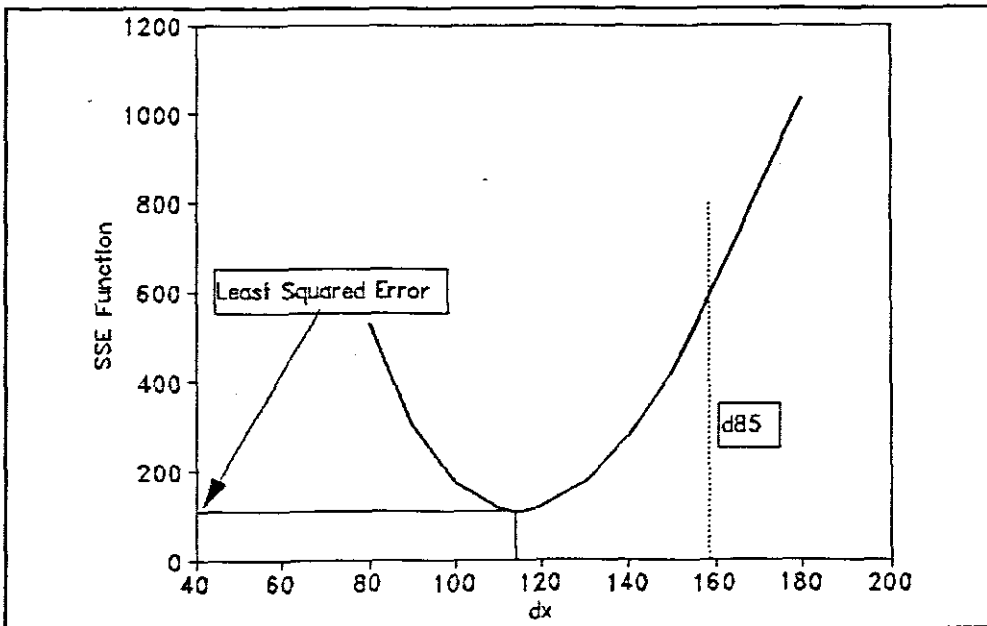
Figure 4.9: Optimum representative particle size for test set S_20
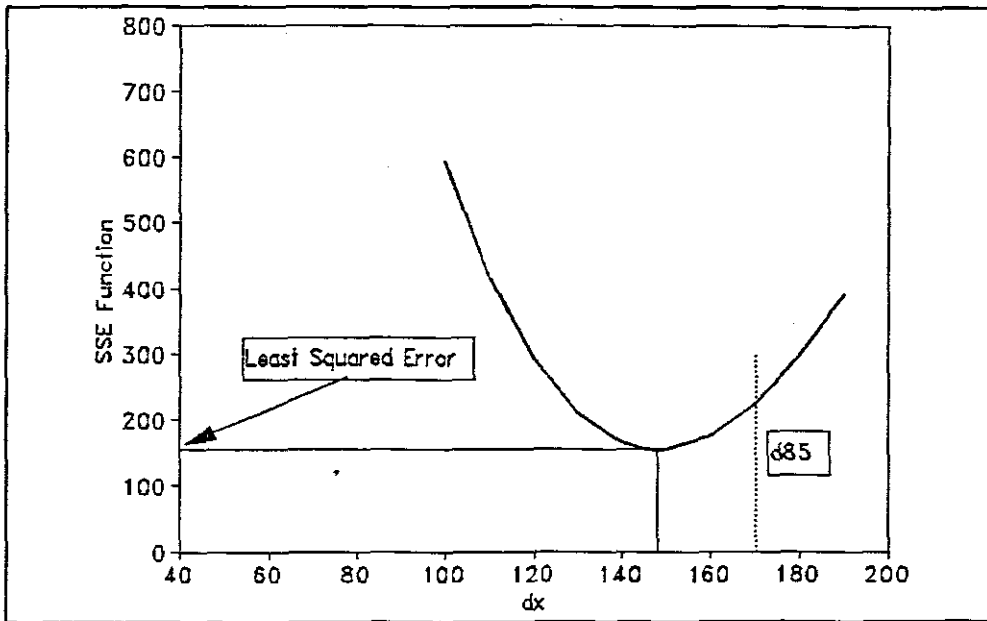
Figure 4.10: Optimum representative particle size for test S_30

4.2.6 Roughness Function Correlation Using Optimum Particle Sizes

The turbulent data points plotted in Figure 4.2 showing the effect of the particle roughness on turbulence are re-plotted in Figure 4.11 using the optimum particle sizes for the data test sets. The data test points of mixture 1 were not used as the optimum sizes obtained did not yield meaningful results.

4.2.7 Slurry Temperature

The temperature of the slurry was measured using a mercury thermometer. The thermometer was dipped into the slurry in the hopper and the temperature recorded at regular intervals during a test set. Essentially the temperature was maintained at approximately 19°C. During a test set the temperature would rise in the region of 2°C to 4°C. However, there were times when the temperature rise would be in the region of 8°C to 10°C. When such a rise in temperature was experienced data points for the 25mm pipeline at the extreme temperatures were taken.
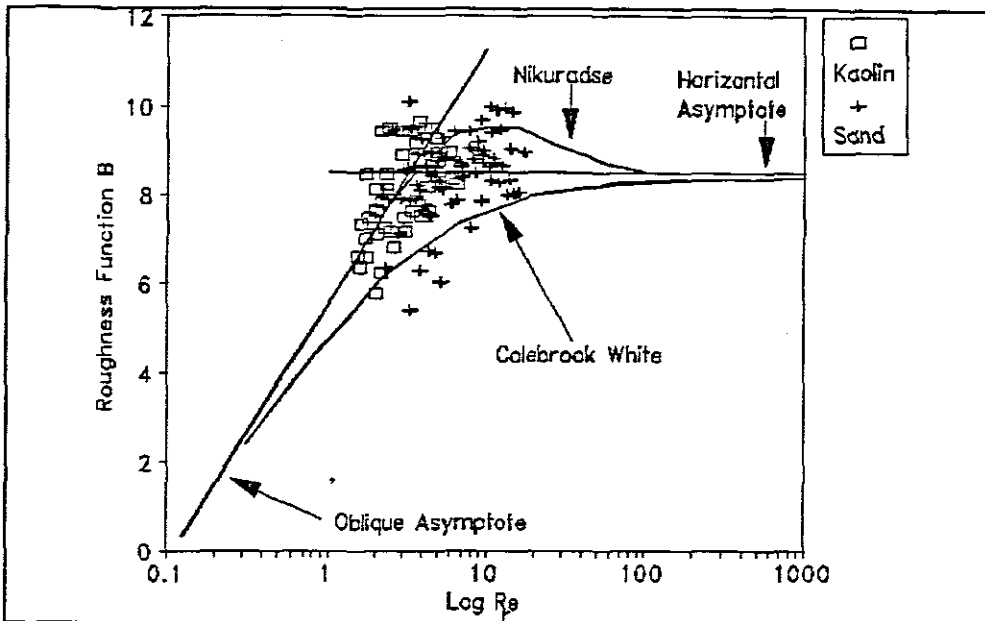
Figure 4.11: Roughness function correlation using optimum particle sizes

The 25mm pipeline was always the first test during a test set and thus data points at the normally maintained temperature of 19°C could be compared with data points at the extreme temperatures. The 25mm pipeline data is used to determine the rheology of the slurry and hence data points for the 25mm pipeline at the extreme temperatures were collected to see if the temperature rise in any way affected the rheology of the slurry.

There appears to be little rigorous detail of temperature effects reported in the literature. Metzner (1956) states that although the complexity of some non-Newtonian systems leads to unusual changes in fluid properties with temperature, most non-Newtonian fluids do not show unusual effects. The following has been reported on how temperature affects the rheology of a suspension:

●   For small changes, the flow behaviour index (n) may be assumed independent of temperature (Reed, 1954); for larger changes, Vaughn (1956) has reported that flow behaviour index increases towards unity ie. many pseudoplastic materials tend to approach Newtonian behaviour.

- The consistency index (K) frequently changes as rapidly with temperature as the viscosity of the solvent or suspending medium (Reed, 1954).

- The changes in τ_y with temperature for Bingham plastics have been reported to resemble changes of the flow behaviour index (Metzner, 1956).

These estimates of temperature effects have been evaluated for slurries containing up to 25% of volume of suspended solids.

However, even with these reported possible effects of temperature, as can be seen from Figure 4.12, a typical pseudo-shear diagram including data points at the extreme temperatures, no temperature effects were found.
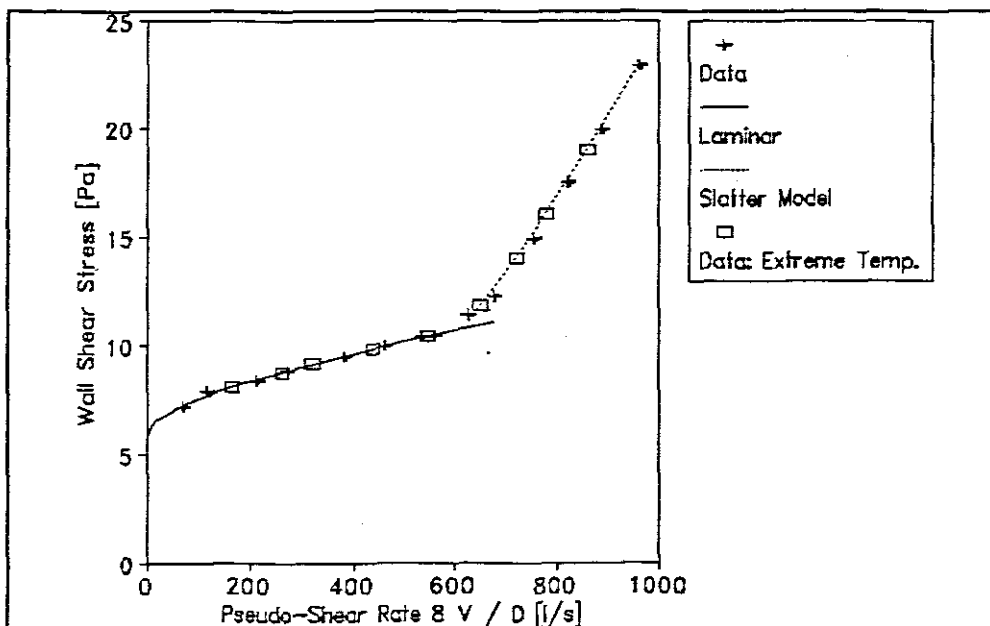
Figure 4.12:   Pseudo-shear diagram for test KMRL20 including data points at extreme temperatures

4.3 RHEOLOGICAL CHARACTERIZATION

The viscous data in the laminar region is coincident for the different diameters of a test set. The rheological constants (τ_y, K and n) were determined from the laminar region of the

25mm pipeline (as outlined in Chapter 2) and are presented in Table 4.II together with the pseudo-shear diagram of the rheology of the test sets for kaolin clay, mixture 1 and mixture 2 in Figure 4.13 to Figure 4.15.

The rheological parameters obtained were used to analyze the test data using the theoretical models mentioned in the literature review.

Table 4.II: Summary of Slurry Properties

No	Test Set	Slurry	$C_v(\%)$	$\tau_y(Pa)$	$K(Pa.s^n)$	n	S_s
1	Sive1 *	Kaolin/Quartz	7,17	4,89	0,2991	0,4840	2,22
3	K_10	Kaolin	7,00	9,14	0,0676	0,6456	2,60
4	K_20	Kaolin	6,16	5,80	0,0176	0,8154	2,60
5	RF_10	Kaolin/Rock Flour	9,67	3,68	0,0132	0,9474	2,60
6	RF_20	Kaolin/Rock Flour	11,00	3,91	0,0105	0,9720	2,60
7	RF_30	Kaolin/Rock Flour	13,29	5,53	0,0194	0,9646	2,60
8	S_10	Kaolin/Rock Flour/Sand	16,47	5,82	0,1413	0,5577	2,65
9	S_20	Kaolin/Rock Flour/Sand	19,43	5,48	0,1239	0,6363	2,65
10	S_30	Kaolin/Rock Flour/Sand	23,86	8,02	0,1350	0,5911	2,65

* - Sive rheology for kaolin only

4.4   VISCOUS SUB-LAYER

The viscous sub-layer thickness can be predicted using the Newtonian approximation and the Wilson & Thomas (1985,1987) and Slatter (1994) models. Figure 4.16 to Figure 4.18 show the relationship between wall shear stress and viscous sub-layer thickness for the first test sets of kaolin clay, mixture 1 and mixture 2 respectively. The Maude & Whitmore (1958) prediction of the viscous sub-layer thickness has been included in the figures. Figure 4.18 shows that at the higher wall shear stress values, the viscous sub-layer thickness is less than the diameter of the larger particles. As discussed in Chapter 2, the particles must therefore have an obstructing effect on the viscous sub-layer thus influencing the turbulent flow behaviour.
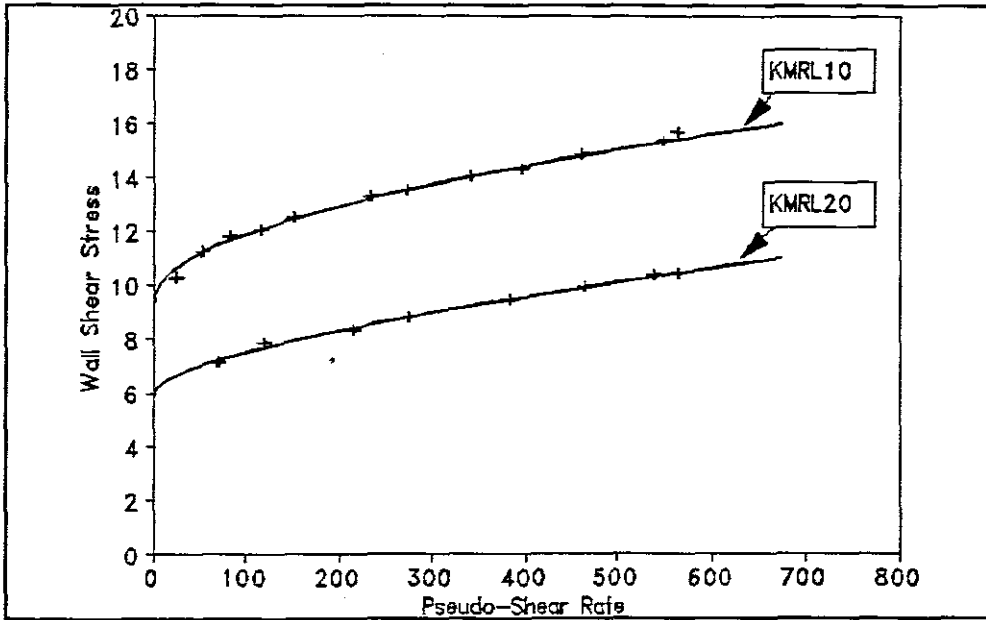
Figure 4.13:   Pseudo-shear diagram showing rheological characterization
for kaolin test sets
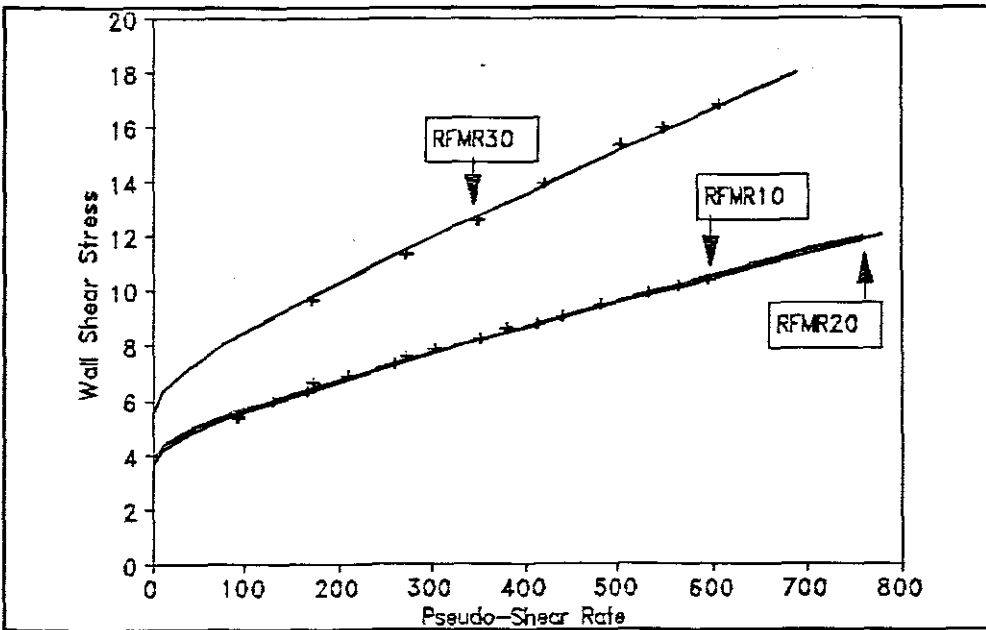
Figure 4.14:   Pseudo-shear diagram showing rheological characterization
for mixture 1 test sets
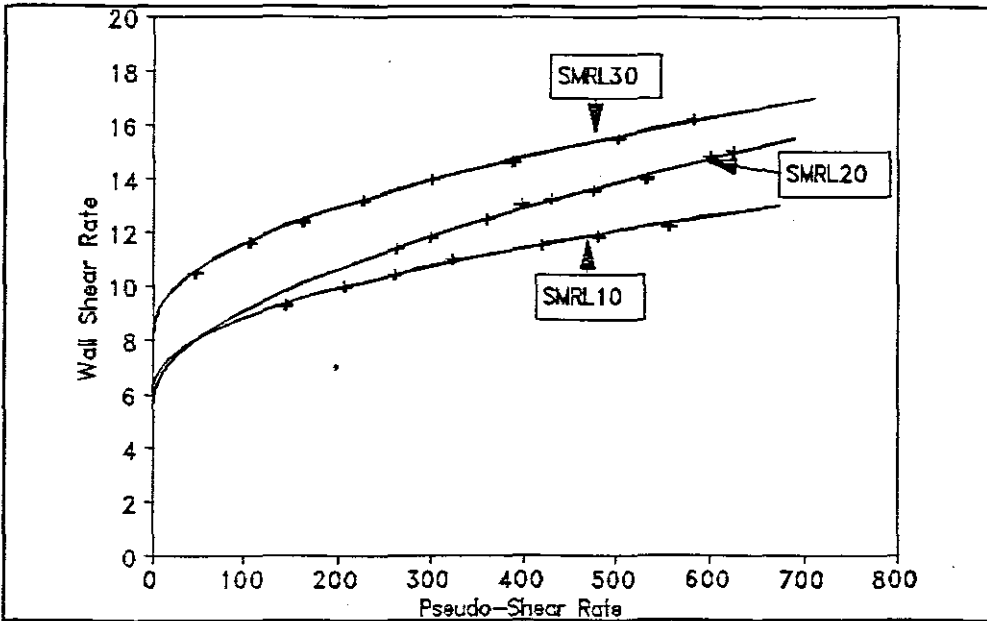
Figure 4.15:   Pseudo-shear diagram showing rheological characterization
               for mixture 2 test sets
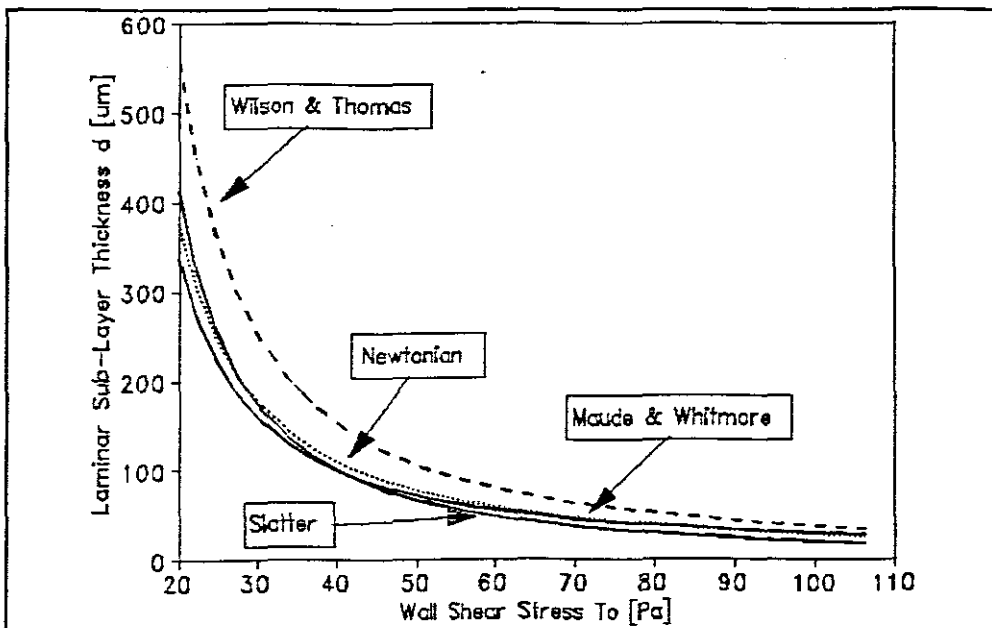
Figure 4.16:   Viscous sub-layer thickness predictions for kaolin clay
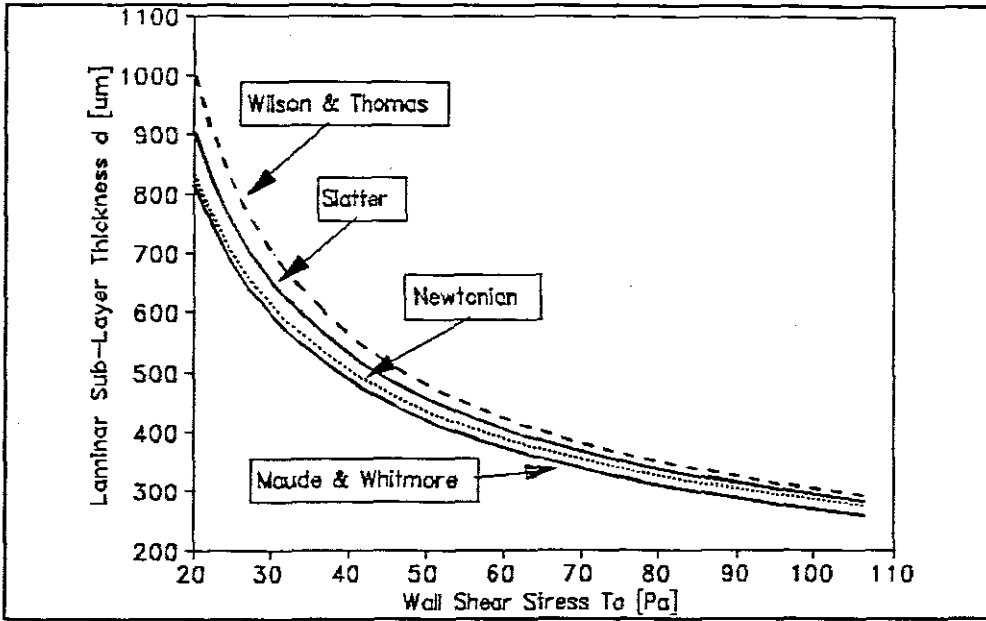
Figure 4.17:   Viscous sub-layer thickness predictions for mixture 1
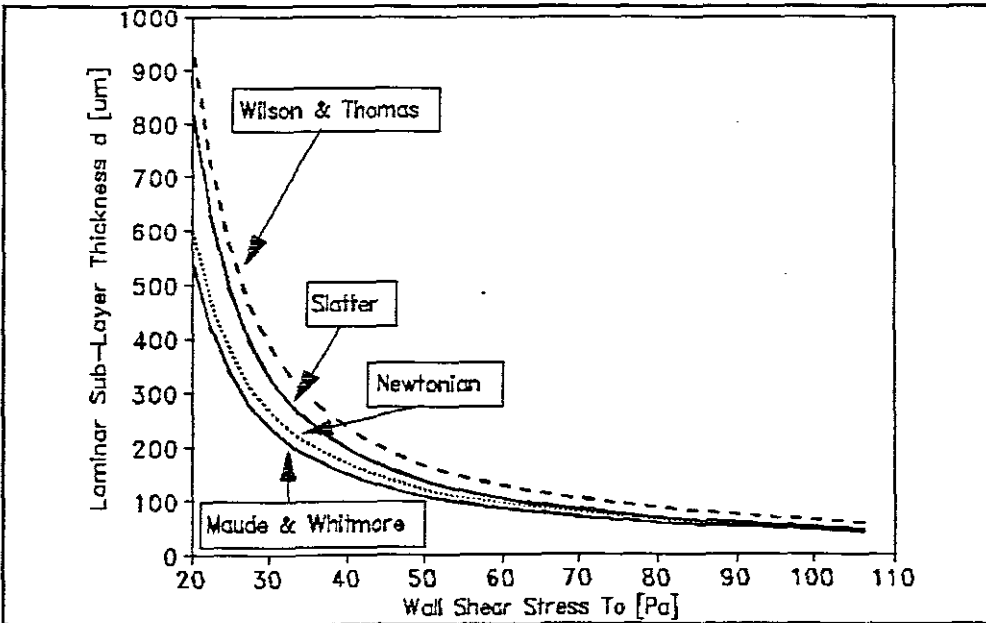
Figure 4.18:   Viscous sub-layer thickness predictions for mixture 2

4.5   INFLUENCE OF PARTICLE SIZE

Figure 4.19 to Figure 4.21 show the effect of increase in concentration and coarse fraction

for kaolin clay, mixture 1 and mixture 2. The clear water line is also included (Colebrook White).

As can be seen from Figure 4.19 an increase in concentration of the kaolin in the laminar flow region increases the wall shear stress. This is due to the increase in viscous forces when concentration is increased. In the turbulent flow region of Figure 4.19 an increase in concentration produces no significant increase in the wall shear stress. This observation confirmed similar findings by Bowen (1961), Harris & Quader (1971) and Slatter (1994). Figure 4.20 and Figure 4.21 appéar to contradict these findings in that there is an observed increase in turbulent flow wall shear stress with concentration. However, it should be noted that concentration was not the only parameter that was changing but that the representative particle size was also increased from an initial 30μm (kaolin) to 170μm (mixture 2) as coarser particles were added. It is therefore surmised that the increase as depicted in Figure 4.20 and Figure 4.21 is due to the increase in representative particle size, and not due to the increase in concentration. This observation is discussed in Chapter 5.
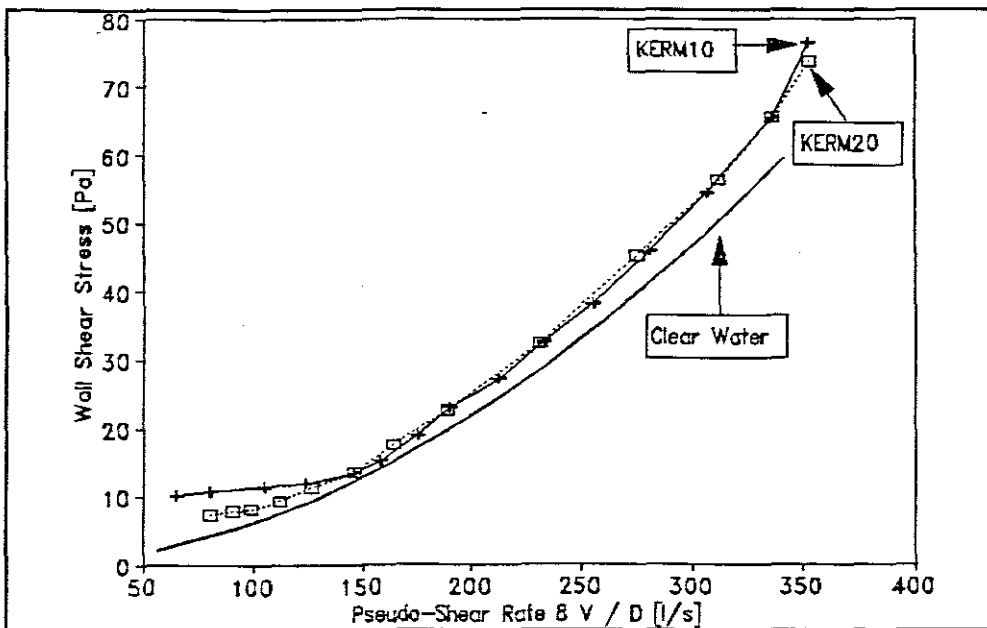
Figure 4.19:   Pseudo-shear diagram for the 150mm pipe showing the data
              for the kaolin tests sets
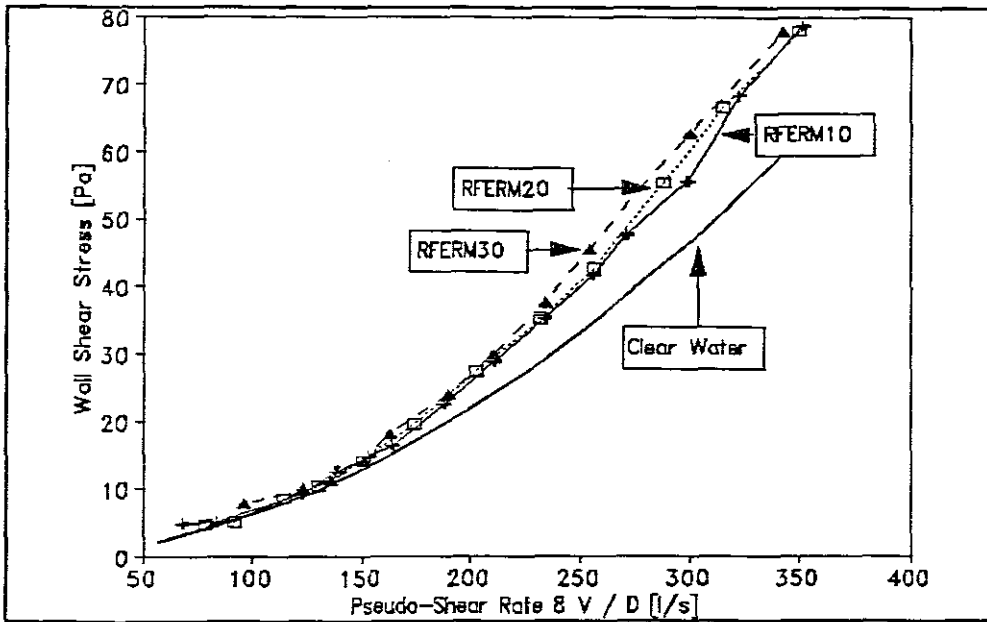
Figure 4.20:   Pseudo-shear diagram for the 150mm pipe showing the data
for the mixture 1 test sets
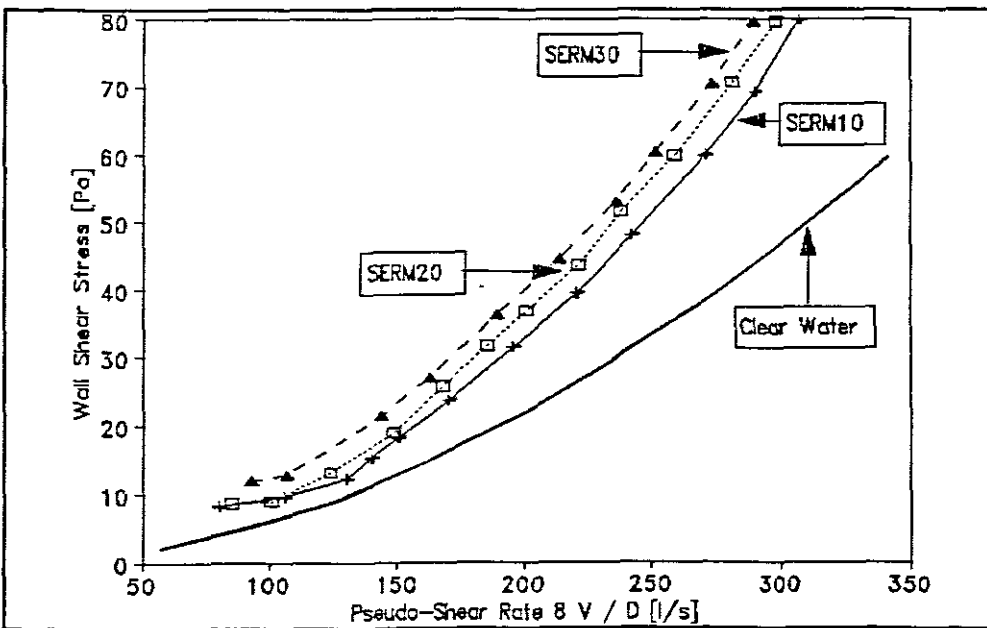
Figure 4.21:   Pseudo-shear diagram for the 150mm pipe showing the data
for mixture 2 test sets

4.6   THEORETICAL MODELS

Figure 4.22 to Figure 4.24 show the experimental results of a typical test for kaolin clay,

mixture 1 and mixture 2, together with the predictions of the five theoretical models under consideration. (Full results of the pipeline tests are given in Appendix A).

4.6.1 Turbulent Model Performance

The turbulent model performance of the theoretical models is tabulated in Appendix A showing the average percentage error (APE) from the turbulent experimental data. The Log Standard Error (LSE) for the turbulent data in each test is also tabulated. The LSE has been found to be useful for model comparisons by Lazarus & Nielson (1978) and is defined as

$$LSE = \frac{\sqrt{\Sigma \left[\log \left(\tau_{0\,obs} \right) - \log \left(\tau_{0\,calc} \right) \right]}}{N - 1} \quad . \tag{4.1}$$

The overall turbulent model performance and the LSE for all the turbulent data points in the data base is shown in Table 4.III and Table 4.IV respectively. The accuracy can also be gauged by the respective lines shown on the pseudo-shear diagrams for each pipe test in Appendix A.
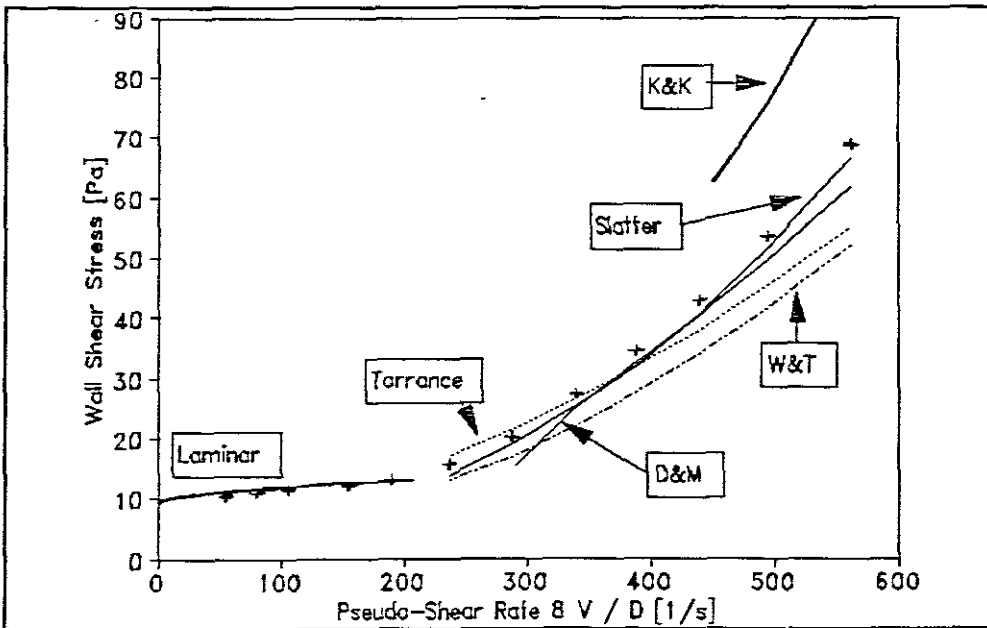
Figure 4.22: Pseudo-shear diagram of the 80mm pipeline: KERS10:
           $d_{85} = 30\mu m$
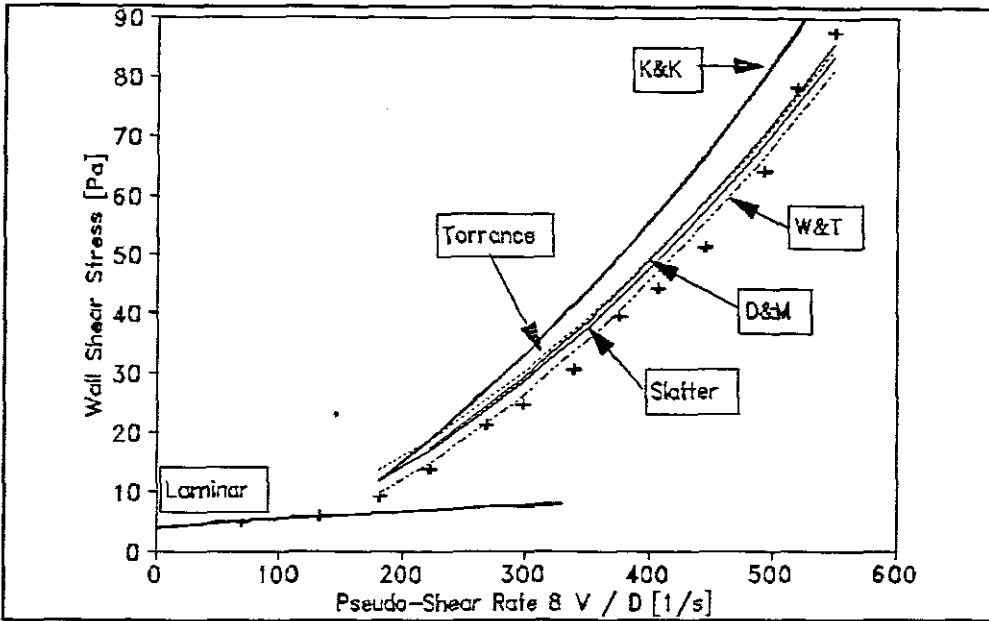
Figure 4.23:   Pseudo-shear diagram of the 80mm pipeline: RFERS10: $d_{85}=52\mu m$
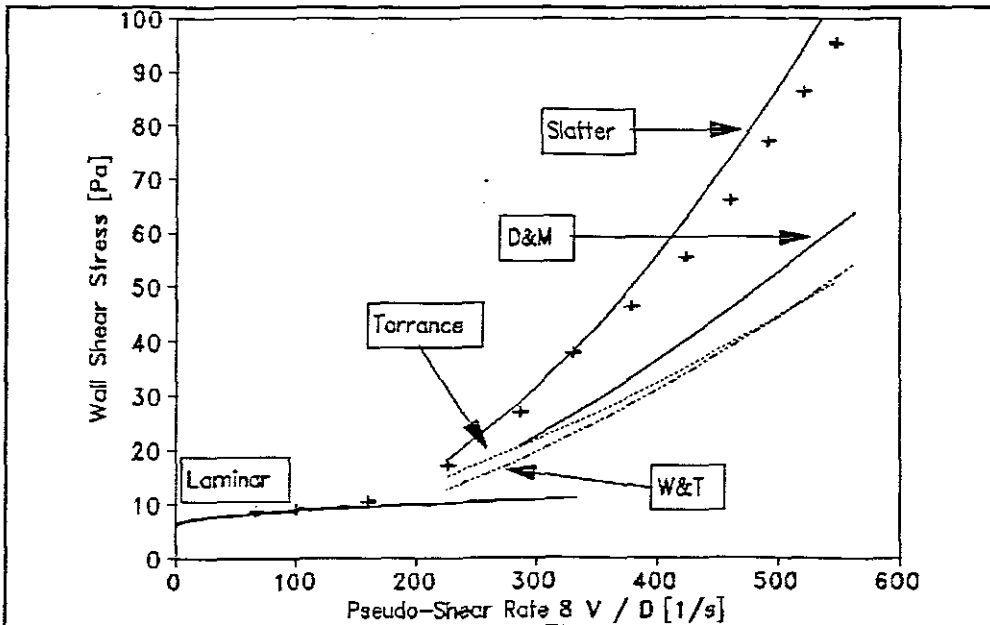
Figure 4.24:   Pseudo-shear diagram of the 80mm pipeline: SERS10: $d_{85}=137\mu m$

Table 4.III: Turbulent Model Performance - Average Percentage Error

Slurry	Torrance	W&T	D&M	K&K	Slatter
Kaolin	17.41	24.66	25.54	145.89	11.98
Mixture 1	28.95	17.49	23.71	102.14	21.97
Mixture 2	11.10	16.83	18.70	168.13	7.75
Overall	19.15	19.66	22.65	138.72	13.90

Table 4.IV: Turbulent Model Performance - Log Standard Error

Slurry	Torrance	W&T	D&M	K&K	Slatter
Kaolin	0.0424	0.0631	0.0678	0.2053	0.0305
Mixture 1	0.0594	0.0374	0.0492	0.1600	0.0454
Mixture 2	0.0274	0.0433	0.0563	0.2207	0.0217
Overall	0.0431	0.0479	0.0577	0.1953	0.0325

Of the theoretical models under consideration Slatter's model best predicted the test data for the kaolin test sets (APE - 11.98%, LSE - 0.0305) and the mixture 2 test sets (APE - 7.75%, LSE - 0.0217). For these two test sets the Wilson & Thomas and Torrance models yielded good results in the early turbulent region but under predicted head loss regularly at higher flow rates. This confirms the findings as reported by Mun (1988) and Xu *et al* (1993). The Kemblowski & Kolodziejski model was also considered however, it did not produce accurate results, consistently over predicting the head loss for kaolin clay, mixture 1 and mixture 2 test sets.

On the whole all theoretical models under consideration performed poorly when modelled with the test data of the mixture 1 test sets. The only exceptions were the 80mm pipeline test data where all the theoretical models closely modelled the test data (especially the Wilson & Thomas model) and the 200mm pipeline test data where the Torrance and Slatter models closely modelled the test data.

Overall the Slatter model (APE - 13.9%, LSE - 0.0325) best modelled the test data. Although the Torrance model (19.15%) and the Wilson & Thomas model (19.66%) are both below an average percentage error of 20%, which is acceptable in engineering practice (Cheng, 1970), the fact still remains that these models diverge from the data at higher shear stresses, indicating that they do not accurately describe the turbulent flow behaviour of the solid-liquid suspensions.

The turbulent model performance can also be seen in Figure 4.25 to Figure 4.29 which shows a log-log plot of $\tau_{0\,obs}$ vs $\tau'_{0\,calc}$ for the five theoretical models which were considered. A 20% error line is included in the plot. It can be seen from the five figures that the Slatter model yields the best results with virtually all the data points within the 20% error lines. Large discrepancies for mixture 1 for all models can be seen.

From the performance of the various theoretical models (visual appraisal of the model lines, average percentage error, log standard error and the log-log plots) it would appear that the Slatter model provides better predictions than the other models for the slurries tested.
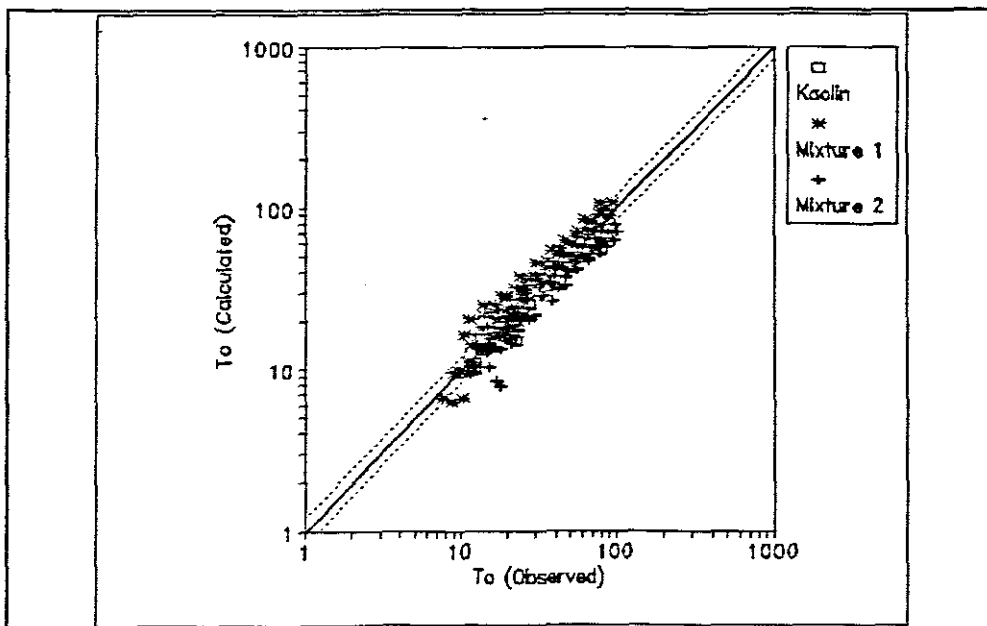
Figure 4.25: A log-log plot of $\tau_{0\,obs}$ vs $\tau_{0\,calc}$ for the Dodge & Metzner model
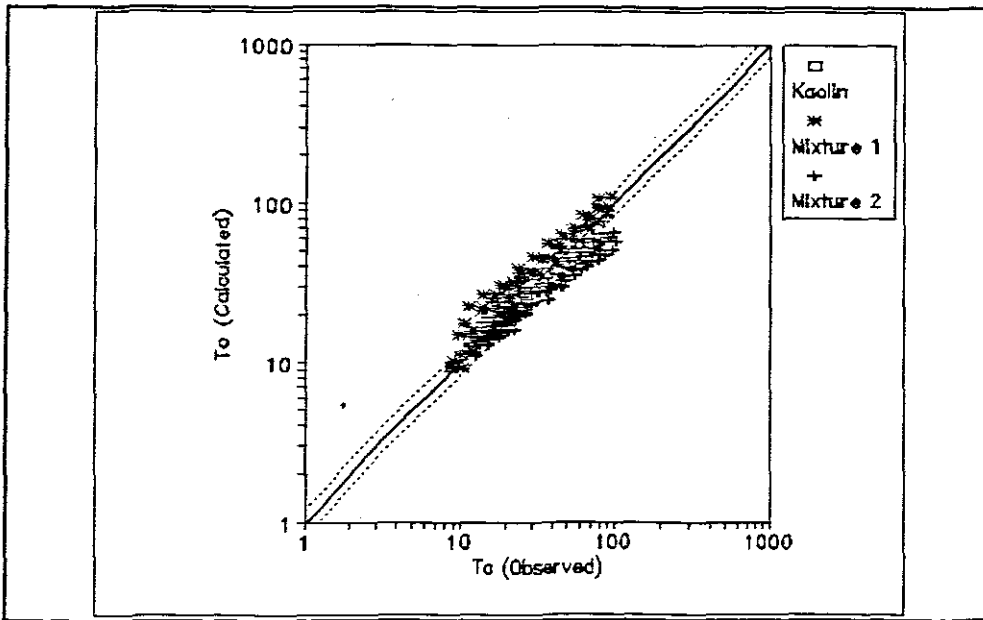
Figure 4.26: A log-log plot of $\tau_{0\,obs}$ vs $\tau_{0\,calc}$ for the Torrance model
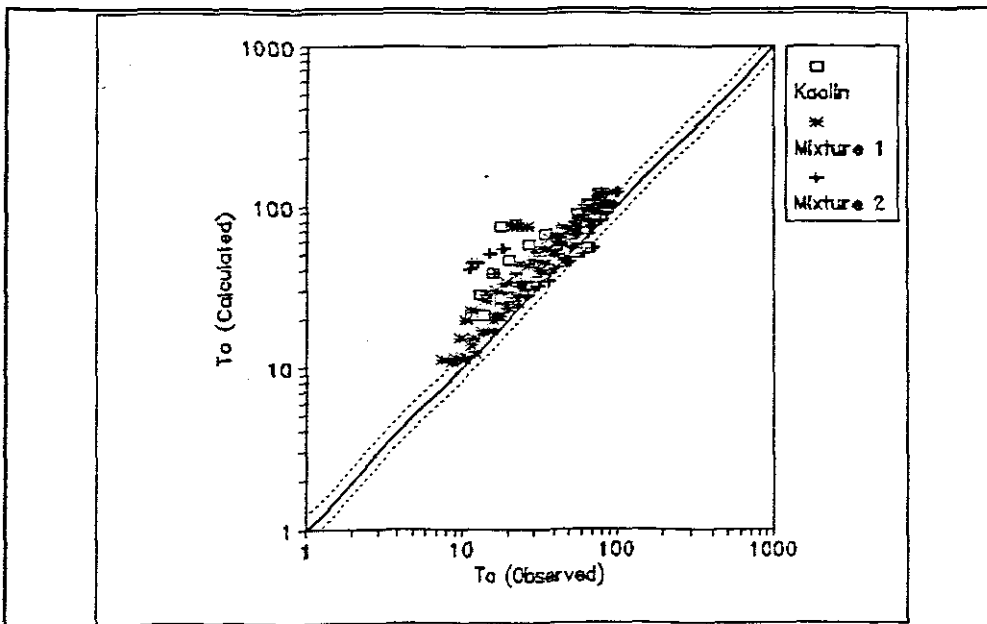
Figure 4.27: A log-log plot of $\tau_{0\,obs}$ vs $\tau_{0\,calc}$ for the Kemblowski &
            Kolodziejski model
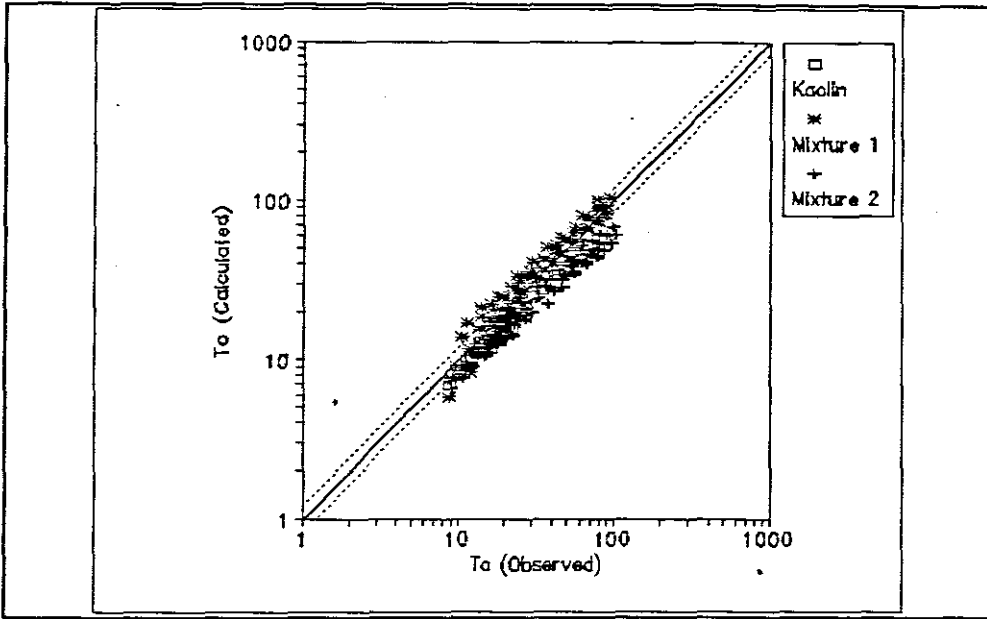
Figure 4.28: A log-log plot of $\tau_{0\,obs}$ vs $\tau_{0\,calc}$ for the Wilson & Thomas model
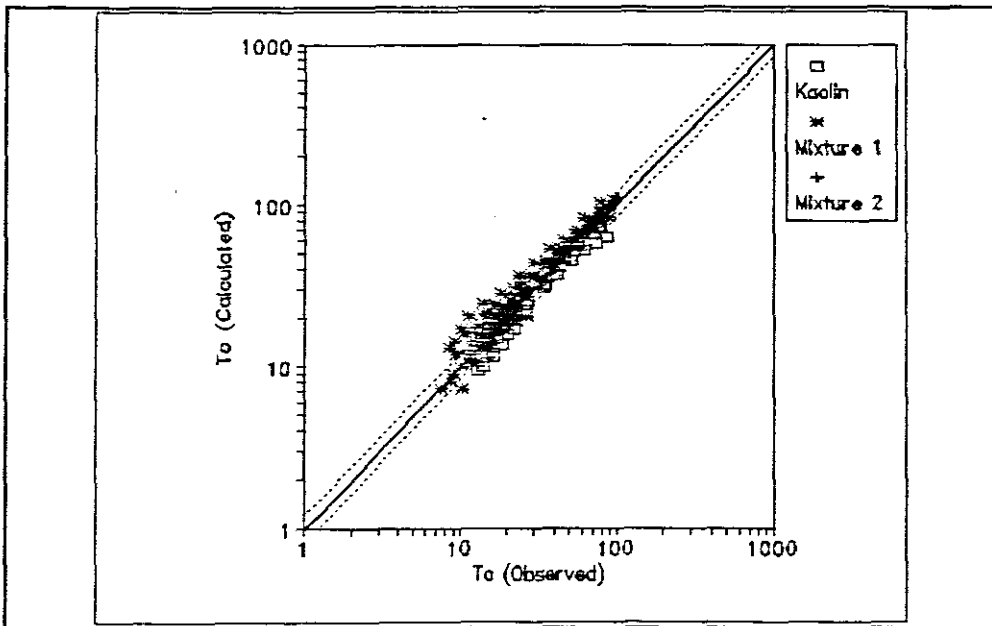
Figure 4.29: A log-log plot of $\tau_{0\,obs}$ vs $\tau_{0\,calc}$ for the Slatter model

4.7.2 Maude & Whitmore Correlation

Maude & Whitmore (1956, 1958) are a few of the researchers to include particle size in their turbulent flow calculations (Chapter 1, Chapter 2). Figure 4.30 shows a typical result of their correlation for a test and as can be seen from the figure it is unable to accurately predict turbulent flow. Mun (1988) also reported the Maude & Whitmore correlation's inability to accurately predict turbulent flow data.
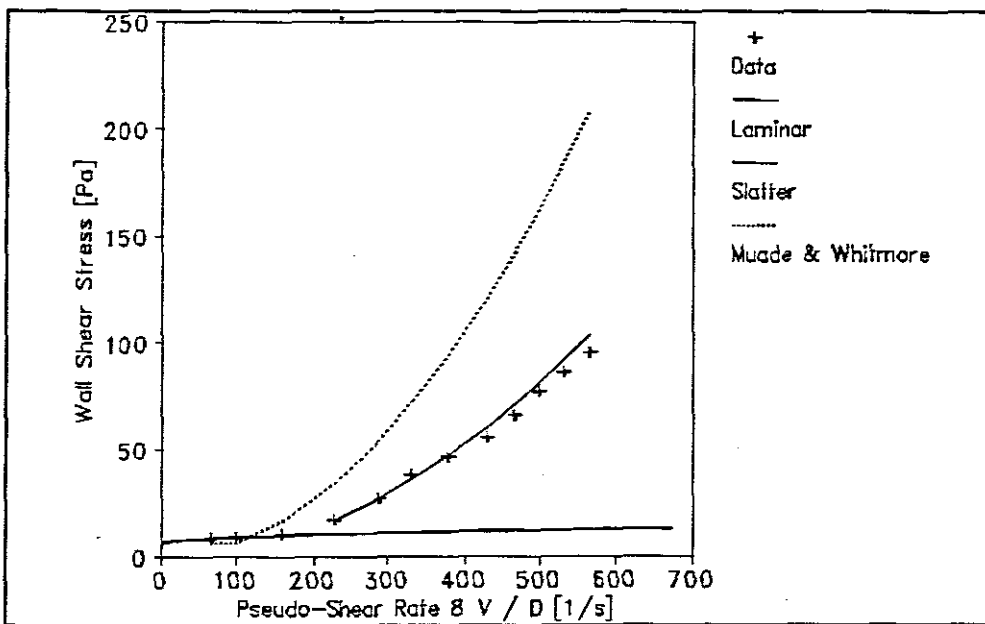
Figure 4.30: Turbulent flow prediction of the Maude & Whitmore correlation for test SERS10

4.7.3 Bowen Correlation

Figure 4.31 depicts the modelling of the Bowen correlation (1961) to the test data for a typical test set. The correlation produces good results for turbulent flow predictions. This confirms the findings of many researchers (eg Harris 1967, Harris 1968, Harris & Quader 1971, Harris & Wilkinson 1971 and Quader & Wilkinson 1980), who advocate that Bowen's correlation should be used due to it's superiority and usefulness. However, it should be noted that the correlation does not provide an explanation of the behaviour of the slurry in terms of the physical properties of the slurry (section 2.10.7).
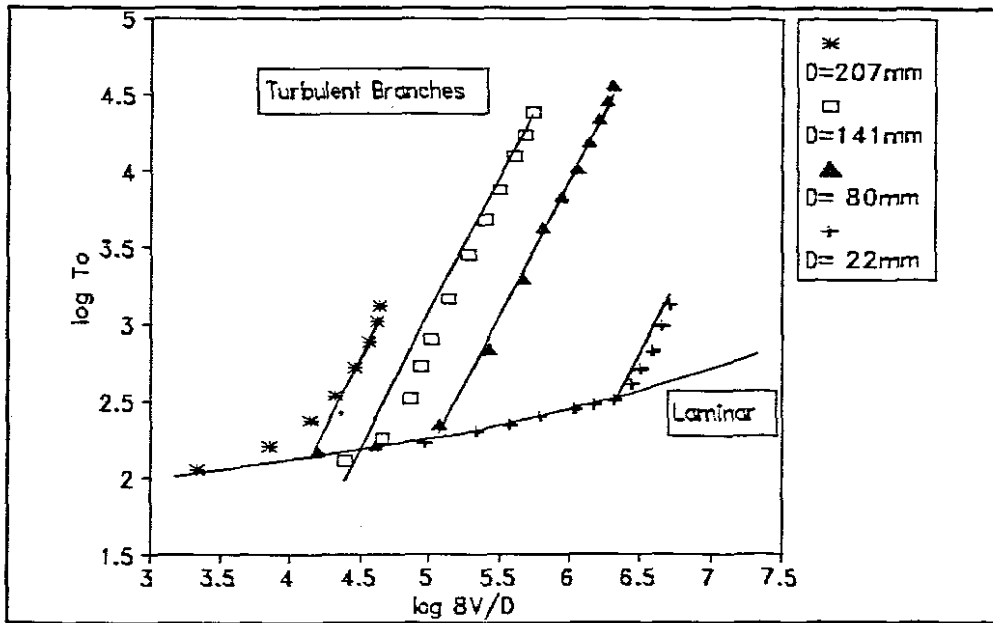
Figure 4.31:   Turbulent flow predictions for the Bowen correlation for test
               set K_20

The Bowen constants for test set K_20, as shown in Figure 4.31, are k=10.13 and b=0.22.

4.8   DATA FROM THE LITERATURE

Experimental data obtained by Sive (1988) were used in the analysis of the various models under consideration. The tests conducted by Sive (1988) were done using a mixture of kaolin clay and a relatively coarse quartz sand which resulted in a non-homogeneous settling slurry with a high representative particle size. The purpose of using this data was to see if the coarse, settling particles contributed to the turbulent flow headloss, as proposed by the Slatter model.

As can be seen from a typical result in Figure 4.32 taken from Sive (1988), Slatter's model was unable to predict the test data of Sive.
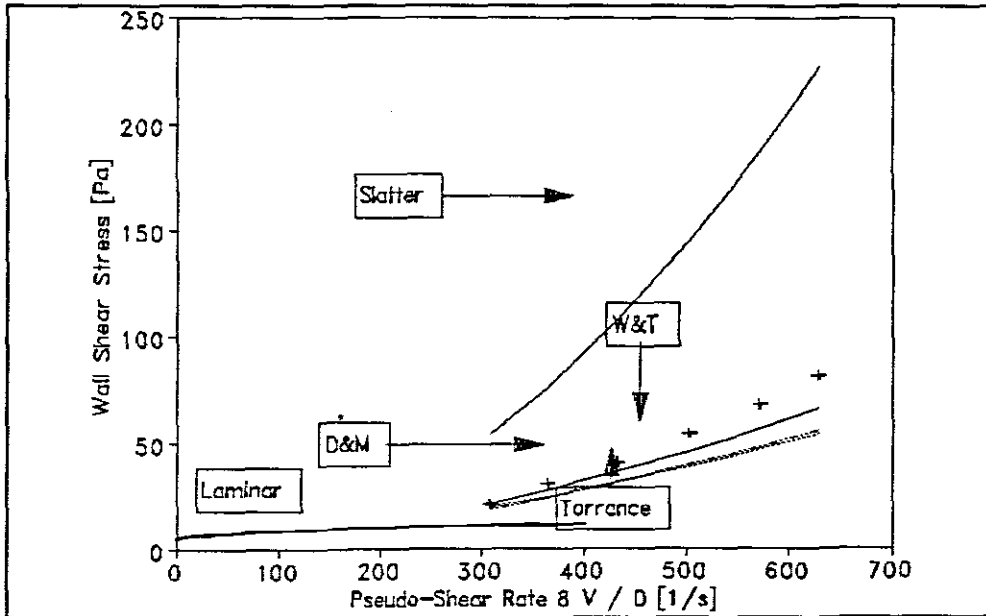
Figure 4.32:   Turbulent flow predictions using Sive test 1 data

4.9   CONCLUSIONS

The results and analysis of the experimental work have been presented. The following can be summarized:

- Pseudo-shear diagrams including laminar and turbulent data together with the predictions of the theoretical models are presented (Appendix A) for all tests conducted.

- No temperature effects were found when the temperature rise of the slurry during a test set was at a maximum.

- The rheological constants (τ_y, K and n) were successfully determined from the laminar flow data of the 25mm pipeline.

- At the higher wall shear stress values for mixture 2 the viscous sub-layer thickness is less than the diameter of the larger particles.

- An increase in the representative particle size caused an increase in the wall shear stress in the turbulent flow region.

- The Slatter model best predicted the test data and becomes more accurate with increasing particle size.

- The Maude & Whitmore correlation is unable to accurately predict turbulent flow behaviour.

- The Bowen correlation produces good results but does not provide an explanation of the behaviour of the slurry in terms of the physical properties of the slurry.

- Slatter's model is unable to predict the turbulent flow behaviour of the Sive data for a non-homogeneous settling slurry.

The results and analysis are discussed in Chapter 5.

CHAPTER 5

CHAPTER 5

DISCUSSION

5.1 INTRODUCTION

This chapter deals with discussing the results and analysis of the test data as presented in Chapter 4 and Appendix A.

5.2 PARTICLE ROUGHNESS EFFECT

In Figure 4.2 it is noted that the data points for the kaolin tend to lie on the line for the law of the wall for smooth pipes, with the rock flour data points lying to the left. The data points for the sand tend to lie on or near the curve of Nikuradse. This is not in line with what Slatter's model anticipates. The data points according to the Slatter model should lie on or near the horizontal asymptote (roughness function B=8,5) since the particles in the suspensions that were tested were neither fixed nor uniform in size, as they were for Nikuradse's experiments. And yet it can be seen from Figure 4.2 that the roughness effect of the solid particles for mixture 2 is as great and even greater than for Nikuradse's experimental data.

For smooth wall turbulent flow the Slatter model predicts that the data should lie on or near the oblique asymptote (line for the law of the wall for smooth pipes) and for the kaolin clay test sets this is certainly the case but yet the data points for mixture 1 lie to the left. In fact most of the data points lie well outside the two asymptotes which describe the limits of behaviour of Newtonian turbulent flow. There are many reported instances of similarities between the turbulent flow of Newtonian and non-Newtonian fluids (section 2.12) and Slatter's findings confirmed this trend. The data of Slatter (1994) matched the limits of the behaviour of Newtonian turbulent flow closely and hence for his correlation of the roughness function for his model the two asymptotes were chosen. However, these test data points contradict the findings of Slatter and would indicate that d_{85} size does not give the best representation of the particle roughness effect.

Further investigation needs to be conducted and a large data base established to determine whether the roughness effect will:

● follow the Nikuradse trend;

● continue increasing, following more closely the oblique asymptote;

● or if it does follow the horizontal asymptote as proposed by Slatter.

5.3   ROUGHNESS FUNCTION CORRELATION USING OPTIMUM PARTICLE SIZES

If, however, the optimum particle sizes are used to plot the roughness function correlation as shown in Figure 4.11 the data points for mixture 2 tend to lie just above the horizontal asymptote. On the whole the data points tend to follow more closely the assumptions on which the Slatter model is based. What this does bring into question is that the d_{85} size does not necessarily give the best representative particle size. These optimum particle sizes indicate that the representative particle size will vary depending on the PSD of the slurry being transported. In fact it would seem from Table 4.I, looking at the optimum sizes for kaolin clay and mixture 2, that a slurry with a steep PSD for the smaller particles (eg. kaolin clay test sets) would have a higher representative particle size than a slurry which has a PSD shape that is less steep from small to large particles. In Table 4.I the kaolin clay test sets have an average particle size of $d_x=d_{91}$ as opposed to mixture 2 tests sets which have an average representative particle size of $d_x=d_{71}$. Therefore the higher fraction of larger particles present in the slurry the lower the representative particle size, as the best representation of the roughness effect is reached at a lower d_x value.

5.4   SLURRY TEMPERATURE

As reported in section 4.2.7 an increase in temperature of between 8°C to 10°C made no significant difference and no temperature effects were found. It is surprising to see this trend since this would cause a decrease in the viscosity for water of approximately 20%. This could influence the rheology of the slurry and might lead one to question the method of

characterising the rheology.   However, a change in concentration was depicted in the rheologies of the various slurries so there is no reason to assume that it would not have detected any changes in rheology due to temperature effects. The occurrences of the slurries reaching these extreme temperatures were few and more data at higher temperatures would be needed to determine the effect of temperature increase, if any.

5.5   VISCOUS SUB-LAYER

The viscous sub-layer as described in section 2.9.1 is a thin layer next to the wall where turbulent mixing is suppressed and where viscous forces predominate. Although the viscous sub-layer is one of the cornerstones of classical turbulence analysis it cannot exist if it is thinner than the particles which comprise the slurry and the continuum approximation must be compromised in turbulent flow analysis (section 2.9.3).   The only other known researchers to have taken account of this were Maude & Whitmore (1956, 1958) who encountered this phenomena in their test work (section 2.11.6).   They found that as the Reynolds number increased the viscous sub-layer became thinner to the extent that the mean particle diameter was greater.   They stated that hence the viscous sub-layer consisted only of the suspending medium.

As can be seen from Figure 4.16 to Figure 4.18, viscous sub-layer thickness predictions for kaolin clay, mixture 1 and mixture 2, the viscous sub-layer exists in the early turbulent region (ie. the viscous sub-layer thickness is greater than the representative particle sizes for all the tests sets).   In this particular region all models under consideration performed well for the test sets, except the Kemblowski & Kolodziejski model. The only exception was the mixture 1 test sets where all the models did not perform well in this region. The reasons for this are considered later in this section.

Using the Slatter model we find that the viscous sub-layer breaks down for $Re_r > 3,32$ which is at a viscous sub-layer thickness of approximately $\delta = 3*d_{85}$ (Slatter, 1996). However, Maude & Whitmore (1956, 1958) postulated that the viscous sub-layer breaks down when the particle diameter is greater than half the thickness of the viscous sub-layer.

Whatever the point is at which the viscous sub-layer breaks down the fact still remains that the viscous sub-layer of a homogeneous slurry cannot exist if it is smaller than the particles which comprise the slurry. As can be seen from Figure 4.18 (mixture 2) the viscous sub-layer thickness is smaller than the particles which comprise the slurry at higher wall shear stresses. The thickness of the viscous sub-layer for kaolin clay (Figure 4.16) is smaller than the particles which comprise the slurry at higher shear stresses but a much smaller fraction than mixture 2. At these higher wall shear stress values the Slatter model best models the test data for the kaolin clay and mixture 2 test sets. This could be ascribed to the fact that Slatter's model accounts for the particles affecting the viscous sub-layer.

To confirm that the particles will affect the viscous sub-layer and are relevant for turbulent flow analysis the number concentration of large particles in the viscous sub-layer was calculated. In order to calculate the number concentration a few assumptions had to made. The assumptions were as follows:

- the particles comprising the slurry are spherical in shape;
- the large particles were taken to be greater than one half of the thickness of the viscous sub-layer in turbulent flow;
- one metre of pipe tubing was considered for calculations;
- an average radius is assumed for the large particles.

From Figure 4.16 to Figure 4.18 we can determine the thickness of the viscous sub-layer in turbulent flow. The thickness of the viscous sub-layer for kaolin clay, mixture 1 and mixture 2 is approximately 40μm, 300μm and 55μm respectively. The percentage of large particles present in the viscous sub-layer can therefore be determined from the PSD (ie. percentage of particles greater than one half the viscous sub-layer thickness). From the diameter and viscous sub-layer thickness the volume of the viscous sub-layer can be determined and knowing the percentage of large particles the volume taken up by the particles in the viscous sub-layer can be calculated. The mass of particles can be obtained from the volume and density and similarly by considering one particle present in the viscous sub-layer, it's mass can be calculated and hence the number of particles. The results obtained are shown in

Table 5.I.

Table 5.I: Number Concentration of Large Particles in Viscous Sub-layer

Test	% Large Particles	No. Particles per m²
K_10	22	163
K_20	20	296
RF_10	4	24
RF_20	5	36
RF_30	6	57
S_10	47	336
S_20	55	463
S_30	62	540

From Table 5.I it can be seen that the highest number of particles per square meter was 540. This indicates that if the particles were evenly spaced that approximately one large particle would be found every 5cm. This is fairly low for one would expect for a particle roughness effect for there to be at least one large particle per millimetre (Slatter, 1996) and yet even with a low number concentration there is evidence of a particle roughness effect. In fact, Slatter (1994) detected a particle roughness effect even when testing slurries with a volumetric concentration as low as 2%. It would therefore appear from tests conducted by Slatter (1994) and test conducted for this thesis that the large particles have a dominant effect on turbulence even when the number concentration is extremely. This would indicate that the particle roughness effect is due to the mere fact that particles are present in the slurry *per se* but it is strange that a small number produce the same effect as a large number.

The number of particles per square meter for the mixture 1 test sets were considerably lower than the other test sets. This could be due to the fact that the viscous sub-layer thickness of mixture 1 is relatively large compared to the kaolin and mixture 2 viscous sub-layer thickness and hence the percentage of large particles present (due to the definition of a large particle) is low. It is interesting to note that number of particles per meter square of viscous sub-layer for the 25mm, 80mm, 150mm and 200mm pipelines is the same per test set due to the number concentration being independent of diameter.

What would strengthen the case of particle roughness turbulence is if the turbulent flow headloss in a vertical test section was found to be the same as the horizontal. There is evidence to suggest (eg. Maude & Whitmore, 1956, Wilson, 1996) that particles have a tendency in vertical pipes to move inward away from the wall (ie. away from the viscous sub-layer). If this is indeed the case then it could affect the effectiveness of the particle roughness effect. Further test should be conducted to confirm if the horizontal headloss and vertical headloss are in agreement.

5.6   INFLUENCE OF PARTICLE SIZE

In Chapter 4, it was stated that an increase in wall shear stress with an increase in concentration for the 150mm pipeline tests for mixture 2 was due to an increase in the representative particle size. The d_{85} particle sizes for the three 150mm pipeline tests were 137μm, 158μm and 170μm and the increase in wall shear stress can clearly be seen in Figure 4.21. Slatter's model best predicted the turbulent flow data for mixture 2 as it is based on the particle roughness effect and is able to account for the increase in wall shear stress. The greater the representative particle size of a homogeneous slurry the greater will be the increase in the wall shear stress and the greater will be the possibility of the other theoretical models being unable to predict the turbulent flow data.

However, this phenomenon could also be ascribed to the fact that there is an increase in the rheology and the density of the slurry. To confirm that the increase in wall shear stress is due to an increase in the particle size, the sensitivity to changes in wall shear stress due to

changes in rheology, density and particle size for the Slatter model was investigated. Considering first the change in wall shear stress due to the change in rheology (from $\tau_y=5,8$ K$=0,1413$ n$=0,5577$ to $\tau_y=8,02$ K$=0,1350$ n$=0,5911$)and density (from 1,2717 to 1,3937) for mixture 2, it was found that Slatter's model produced an increase of 9,6% in the wall shear stress values. This is shown in Figure 5.1. However, when taking into consideration all three parameters (ie. changes in rheology, density and particle size - from 137μm to 170μm) Slatter's model produced an increase of 16.1% in the wall shear stress values as shown in Figure 5.2. The increase of 16,1% due to all three parameters is more in line with what is seen in Figure 4.21 which depicts an average increase in the order of 20% over the test range.

If the increase in wall shear stress was solely due to the influence of the particle size then one would expect the rheologies to be virtually the same. As it is the rheologies are similar (Figure 4.13 to Figure 4.15) however, there is definitely a change in rheology and therefore the increase in wall shear stress cannot be taken to be caused solely due to the influence of particle size.

Where Slatter's model fails to accurately model Sive's data it is felt the reason is that the slurries tested by Sive were settling slurries and not homogenous slurries on which his theoretical model was originally based. However, further investigation is required to determine the limit of validity of the particle roughness effect as it appears that the roughness effect is limited to homogenous flow only. One way of determining the limit of validity of the particle roughness effect would be, in this particular case, to conduct test runs with diluted concentrations of slurry (ie. mixture 1 and mixture 2) until settling does occur. Kaolin clay was used as a suspending agent so if the slurry is continuously diluted with water settling of the particles will occur. From the turbulent flow headloss of the test runs at progressively diluted concentration the limit of the roughness effect should become apparent. The other alternative would be add more rock flour and/or sand particles (as the case may be) and to continue doing so until settling occurs. In fact, the limit of validity of the particle roughness effect could provide a more logical basis for vehicle/load cut-off in mixed regime slurries than is used at present.
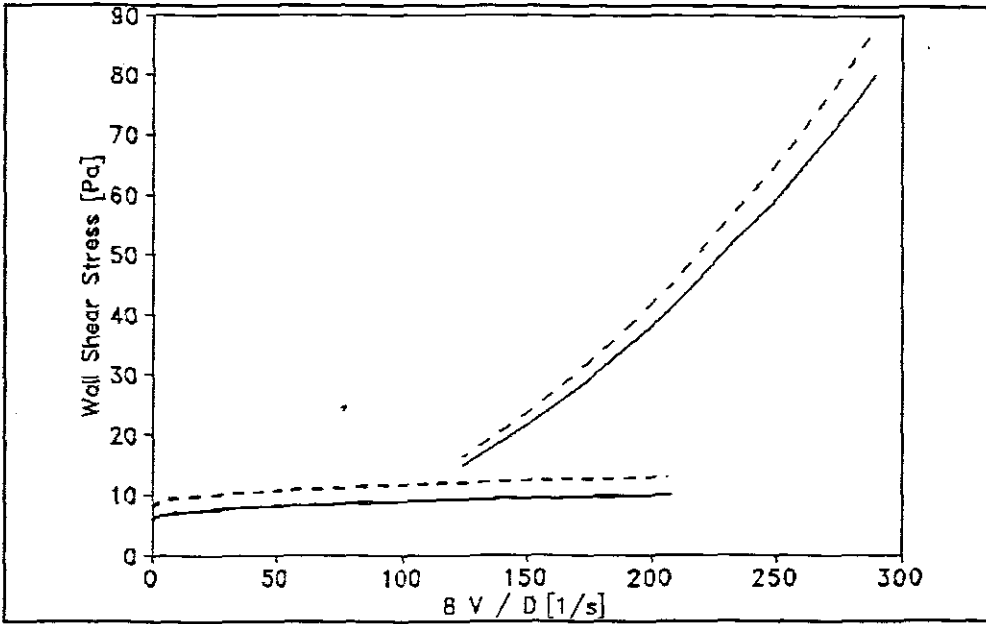
Figure 5.1:   Sensitivity of Slatter model to changes in rheology and density for mixture 2
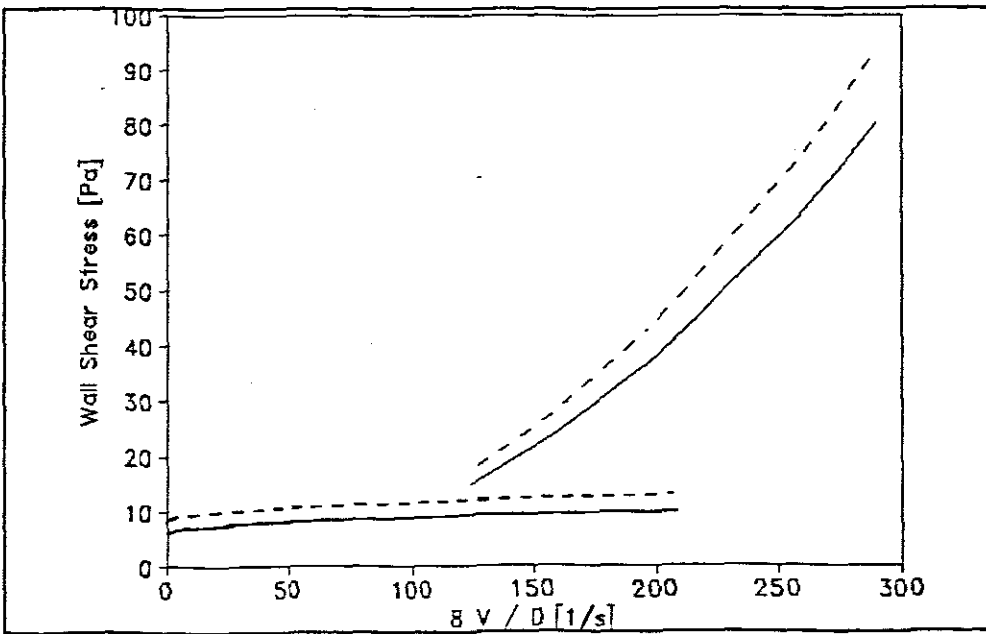
Figure 5.2:   Sensitivity of Slatter model to changes in rheology, density and particle size for mixture 2

5.7   THEORETICAL MODELS

As stated Slatter's model was consistently the best model for the kaolin test sets and for mixture 2 with increasing representative particle size. This is attributed to the fact that his model is able to account for the roughness effect whereas the other models do not. Where Slatter's model fails to predict the turbulent flow data of the mixture 1 test sets, it could be for the following reasons. Firstly, it should be noted that the viscous sub-layer thickness is relatively large in turbulent flow ($\pm$ 300μm) as opposed to the possible effects of the pipe and particle roughness effects. In other words the viscous sub-layer is suppressing the roughness effect and Slatter's model which is over predicting the shear stress values is over compensating for a roughness effect which is not that significant. It is interesting to note for the test data of the large pipes (ie. 200mm pipes) for mixture 1, when the roughness effect could be a factor, the turbulent prediction of the Slatter model is fairly good - an average percentage error of 2.59%, 2,98% and 15,48% for the three tests. Also, from Table 5.I it can be seen that there are relatively fewer larger particles present in the viscous sub-layer as opposed to the other test sets due to the thickness of the viscous sub-layer (see section 5.5). Another reason is that the rheology is tending towards being a Bingham plastic (ie. the value for n is approaching n=1) and under these conditions the Slatter model tends to over predict the shear stress values. At high shear rate values for a Bingham plastic as opposed to yield pseudoplastic the shear stress values will be greater as the viscous forces predominate in this region for Bingham plastics.

Although Slatter's model is the best model overall, the data presented on the particle roughness effect (Figure 4.2) does bring into question the validity of the assumptions on which the Slatter model is based. However, because Slatter's model is based on the particle roughness effect it proves very useful when undertaking for example scale-up from a smooth-walled small bore (eg. PVC pipe) to a rough wall large-scale pipe (eg. galvanised iron), or vice versa. Normally, for example, if the pressure drop in turbulent flow is predicted by the scale-up method of Bowen, a corrected pressure gradient would have to be estimated for the change in roughness. This could be done by using the Govier & Aziz (1972) approach of multiplying the predicted pressure gradient by a ratio of friction factors obtained from the

Moody chart. This is another downfall of the Bowen method. However, if using the Slatter method you would simply select the appropriate roughness effect for the Roughness Reynolds Number (ie. the representative particle size or the pipe hydraulic roughness, whichever is the greater). It is suggested however, that test work is first conducted in smooth pipes to ensure that particle roughness turbulence is indeed occurring. If testing takes place in a pipe with pipe hydraulic roughness higher than the representative particle size the particle roughness effect will not be detected.

This investigation does highlight the fact that the particle roughness effect is valid for the slurries tested and must be used in turbulent flow modelling. The particle roughness effect should be incorporated in the turbulent analysis of non-Newtonian slurries, as has been used in the theory for Slatter's analysis, to account for rough wall turbulent flow and to predict the change from smooth wall to rough wall turbulent flow.

5.8   REYNOLDS NUMBER VS FRICTION FACTOR PLOTS

Figure 5.3 to Figure 5.5 shows the plot of Reynolds number vs friction factor, also called Moody plots, for the Newtonian approximation Reynolds Number, Metzner & Reed Reynolds Number, and a Reynolds number published by Slatter & Lazarus (1993) of the form

$$Re = \frac{8 \rho V^2}{\tau_y + K \left[\dfrac{8V}{D} \right]^n} , \qquad\qquad (5.1)$$

which can be derived by considering the Newtonian approximation and substituting the bulk shear rate in place of true shear rate (Slatter, 1994). Included in the plots are the laminar flow line (ie. $f=16/Re$) and the Prandtl line (Newtonian smooth wall).

The Moody chart shows that for the turbulent flow of Newtonian fluids, pipe roughness can have an appreciable effect. As can be seen from Figure 5.3 the turbulent flow data tends to lie in straight horizontal lines for the various slurries and does not follow the oblique Prandtl line as suggested by Kemblowski & Kolodziejski (1973). This indicates that f is constant with increasing Reynolds numbers and hence it is independent of rheology. This trend is

therefore reminiscent of Newtonian fully developed rough wall turbulent flow the only difference as can be seen from Figure 5.4 and Figure 5.5 is that in the Newtonian case, where the transition spans several orders of magnitude of Reynolds number, the change is abrupt (Slatter, 1994). This does further vindicate the particle roughness approach adopted by Slatter.

This trend where f is constant is however, in contradiction to the relationship of Dodge & Metzner (see Figure 2.11) and the findings of Caldwell & Babbitt (1941) which shows that f continuously decreases with increasing Reynolds Number. This would indicate that their model would not be able to account for particle roughness turbulence which has been shown to occur.

Bowen (1961b) states that if f is constant (ie. a zero slope) this means that the slope through the data points on the pseudo shear diagram plot must equal 2. Thus, in the case of Newtonian turbulent flow, the turbulent branch will have a slope that increases steadily until it reaches a value of 2. For the various test sets the slope of the data points is between 1,7 and 2. The reason it perhaps at times does not reach a value of 2 is that there may not be enough data points in fully rough wall turbulence due to the viscous nature of the slurries that were tested.
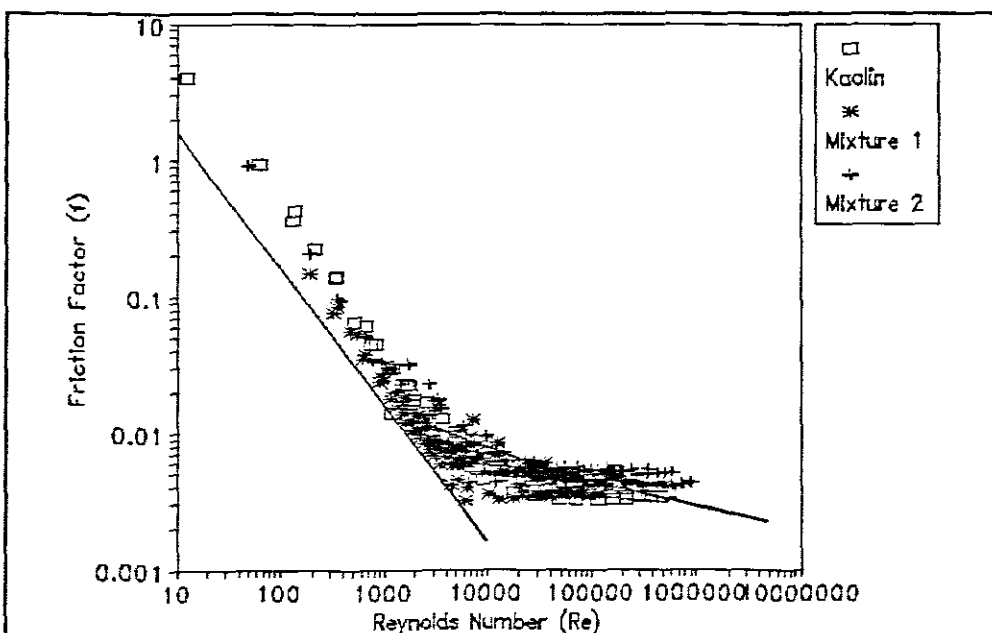
Figure 5.3: Re vs f using the Newtonian approximation
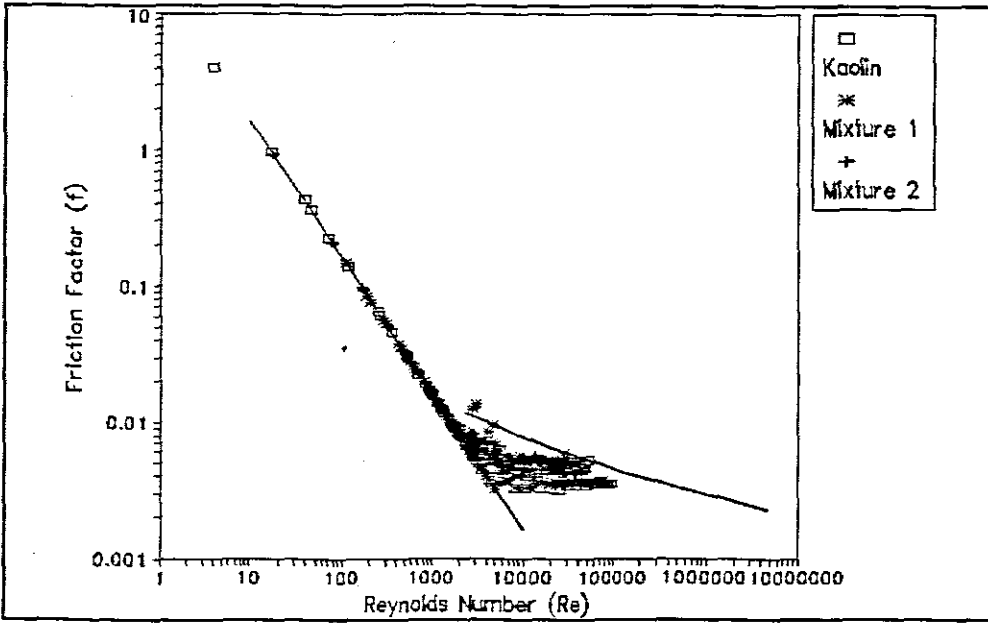
Figure 5.4: Re vs f using the Metzner & Reed Reynolds number
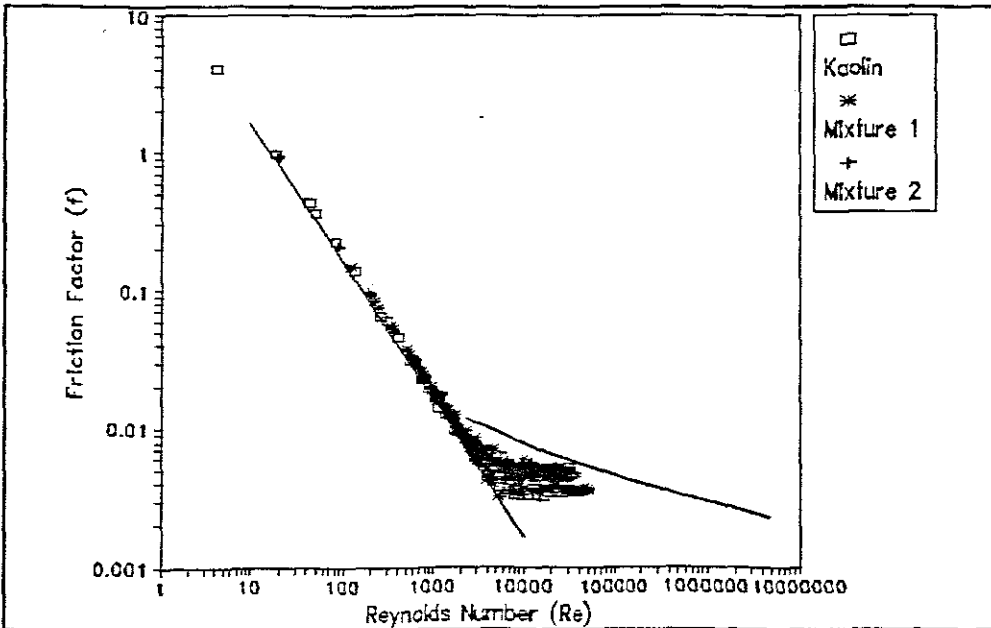
Figure 5.5: Re vs f using the Slatter & Lazarus Reynolds number

5.7   CONCLUSIONS

Experimental work has been conducted using homogeneous non-Newtonian slurries and the analysis and discussion of the results has been presented. As can be seen from the results Slatter's model best predicts the turbulent flow of the theoretical models which were considered. From the evidence it can be concluded that theoretical models based on the particle roughness effect are justified in adopting the approach and in fact the particle roughness effect which does exist should be considered in turbulent flow analysis. There is room for improving on the Slatter model and further test work should be conducted to further vindicate or disprove the assumption on which the model is based but the particle roughness effect is definitely a viable starting point to consider in the turbulent flow of homogeneous non-Newtonian suspensions. The following conclusions can be drawn from the discussion of the results and analysis of the test data:

● A particle roughness effect does exist.

● Further investigation is required and a large data base should be established to accurately determine the limit of validity of the particle roughness effect

● The d_{85} size does not necessarily give the best representative particle size for the particle roughness effect but will depend on the shape of the PSD.

● The viscous sub-layer cannot exist if it is smaller than the particles which comprise the slurry and the continuum approximation must be compromised in turbulent flow analysis.

● The viscous sub-layer breaks down for $Re_r > 3,32$ which is at a viscous sub-layer thickness of approximately $\delta = 3*d_{85}$ for the Slatter model. For the Maude & Whitmore (1956, 1958) correlation the viscous sub-layer breaks down when the particle diameter is greater than half the thickness of the viscous sub-layer. Further investigation is required to accurately predict the exact point at which the viscous sub-

layer does break down.

- There are fewer large particles present in the viscous sub-layer per square meter than would be anticipated for a particle roughness effect.

- Slatter's model can be used for scale-up of pipes with different roughnesses without having to use an estimated pressure gradient which a downfall of the Bowen method.

- The friction factor is constant with increasing Reynolds Numbers and vindicates the particle roughness approach adopted by Slatter.

- The solids Particle Size Distribution is an important property of a slurry for turbulent flow behaviour and should be used to determine the particle roughness effect. The particle roughness effect should be incorporated in the turbulent analysis of non-Newtonian slurries.

CHAPTER 6

CHAPTER 6

SUMMARY AND CONCLUSIONS

6.1 INTRODUCTION

This thesis is a continuation of work conducted by Slatter (1994) and highlights the fact that the particle size distribution is a vitally important property of the suspension and that it does influence turbulent flow behaviour. It shows that turbulence modelling using the particle roughness effect (eg Slatter, 1994) is valid and can be adopted for non-Newtonian slurries.

6.2 SUMMARY AND CONCLUSIONS

There are many non-Newtonian fluids and suspensions encountered in the chemical and processing industries and although there are well established theoretical models in the literature for design, virtually all previous models have failed to adequately address the problem areas of turbulent flow behaviour of suspensions. One of the problem areas is that theoretical models tend to ignore the fact that solid particles are present in homogeneous suspensions and yet they are an inherent part of the fluid. The main aim of this thesis has been to use Slatter's model (which includes both the rheology of the suspension and the particle size distribution of the solids) and other well established theoretical models to model experimental data and to observe and analyze the effect particle size has on turbulent flow behaviour.

The yield pseudoplastic model has been used to model and predict the laminar flow of the suspensions that were tested and the method adopted by Neill for determining the rheology has been verified. The Newtonian turbulent flow model as well as the non-Newtonian models of Dodge & Metzner, Torrance, Kemblowski & Kolodziejski, Wilson & Thomas and Slatter have been reviewed. The correlations of Maude & Whitmore and Bowen were also considered. Other points of note from the literature is that a particle roughness effect has

been reported (which is supported by data from Park *et al* and Pokryvalio & Grozberg), that the continuum approximation must be compromised and that the viscous sub-layer cannot exist if it is smaller than the particles which comprise the slurry.

Test work was conducted at the University of Cape Town's Hydrotransport Research Facility using a pumped recirculating pipe test rig. The test apparatus has been fully described and calibration and test procedures to enable collecting of accurate pipeline data has been presented. Three slurries were used in test work namely kaolin clay, mixture 1 and mixture 2 with a d_{85} particle size ranging from 24μm to 170μm.

From the experimental data it can be seen that a roughness effect does exist and that Slatter's model best predicts the data. This is ascribed to the fact that his model does account for the particle roughness effect whereas the other theoretical models which were considered for this thesis are not able to account for this phenomenon. The particle size has a direct influence on increasing the wall shear stress and at higher wall shear stress values the Torrance and Wilson & Thomas models consistently under predicted the head loss. At lower wall shear stress values when the viscous sub-layer still exists all models apart from the Kemblowski & Kolodziejski model perform well. It can be concluded that the particle size distribution must be used to determine the particle roughness effect and this effect must be incorporated in the turbulent flow analysis of non-Newtonian slurries.

6.3   FUTURE RESEARCH RECOMMENDATIONS

A number of points for future research work have been highlighted by this study:

● Further investigation is required to accurately determine the limit of validity of the particle roughness effect which could serve as the criterion for vehicle/load cut-off in mixed regime flow.

● Although turbulence modelling using the particle roughness effect has been successful

in this investigation and Slatter's model best predicts the test data, the test data does bring into question assumptions made by Slatter for his model. The data points of Roughness Reynolds number vs Roughness Function B for this study do not follow the asymptotes which Slatter assumed non-Newtonian slurries would follow ie. the limits which describe the behaviour of Newtonian turbulent flow. Further investigation is needed to determine what trend the roughness effect will follow and to determine what representative particle size gives the best representation of the roughness effect.

● Further investigations needs to be conducted to determine exactly when the viscous sub-layer will break down as there is contradiction in the literature. For example using the Slatter model we find that the viscous sub-layer breaks down for Re_r > 3,32 which is at a viscous sub-layer thickness of approximately $\delta = 3*d_{85}$ (Slatter et al, 1996). However, Maude & Whitmore (1956, 1958) postulated that the viscous sub-layer breaks down when the particle diameter is greater than half the thickness of the viscous sub-layer.

The viscous sub-layer exists in the early turbulent flow region and all theoretical turbulent flow models used to model the data for this thesis (apart from the Kemblowski & Kolodziejski model) perform well. However, at the point of breakdown of the viscous sub-layer there is at times large discrepancies between the Slatter model and the other models which were considered (Dodge & Metzner, Torrance, Kemblowski & Kolodziejski and Wilson & Thomas models). The particle size will also affect the viscous sub-layer and needs to taken into consideration for the point of breakdown.

6.4   FINAL CONCLUSIONS

An experimental and analytical investigation has been conducted to determine the effect of particle size and PSD on turbulent flow of non-Newtonian slurries. The following final conclusions can be made:

- The relevant literature on slurry flow has been reviewed, including a new approach based on particle roughness turbulence.

- An experimental investigation covering wide ranges of flow conditions and slurry properties has been conducted and the results analyzed.

- Analysis of these results shows that the particle roughness turbulence approach adopted by Slatter (1994) has been validated.

- Recommendations for further research have been made.

REFERENCES

REFERENCES

ALVES G E (1949), Flow of non-Newtonian suspensions, *Chem. Eng.*, May, 107-109.

ALVES G E, BOUCHER D F and PIGFORD R L (1952), *Chem. Eng Progr.*, 48, 385.

AUDE T C, COWPER N T, THOMPSON T L and WASP E J (1971), Slurry Piping Systems: Trends, Design Methods, Guidelines, Chem. Eng., June 28, 74-90.

BENEDICT R P (1980), *Fundamentals of Pipe Flow*, John Wiley & Sons, New York.

BINDER R C and BUSHER J E (1946), *J. Appl. Mech.*, 13, A101.

BLASIUS H (1913), *Mitt. Forschungsarb*, 131, 1.

BOWEN R LeB (1961a), How to handle slurries, *Chem. Eng.*, August 7, 129-132.

BOWEN R LeB (1961b), Designing turbulent flow systems, *Chem. Eng.* 68 143-150.

BS 1377 (1975), *Methods of test for soils for civil engineering purposes*, British Standards Institution, London.

BS 5168, British Standards Institution, London.

BUNKER H L (1954), Pipe Line Design, *Fluid and Particle Mechanics*, University of Delaware Newark, Delaware, 161-170.

CALDWELL D H and BABBITT H E (1941), The flow of muds, sludges and suspensions in circular pipes, *Trans. Am. Inst. Chem. Eng.*, 37, 237-266.

CHARLES M E and KENCHINGTON J M (1976), *Solid Pipeline Course*, Banff, Alberta, Canada, May.

CHENG D C-H (1970), A design procedure for pipeline flow of non-Newtonian dispersed systems, *1ˢᵗ Int. Conf. on the hydraulic transport of solids in pipes*, Hydrotransport 1 Paper J5.

CHENG D C-H (1975), Pipeline Design for non-Newtonian Fluids, *Chem Engnr.*, 301, 525-532, 587-588.

CLAPP R M (1961), Turbulent heat transfer in pseudoplastic non-Newtonian fluids, *International developments in heat transfer*, ASME Part III, Section A, 652.

COLEBROOK C F (1939), Turbulent flow in pipes, with particular reference to the transition region between the smooth and rough pipe laws, *J. Instn. Civil Engrs.*, No. 4, Paper 5204.

DODGE D W and METZNER A B (1959), Turbulent flow of non-Newtonian systems, *AIChE Journal*, Vol. 5, No. 2, 189-204.

DUNCAN T (1982), *Physics - A Textbook for Advanced Level Students*, John Murray Publishers, London.

EDWARDS M F and SMITH R (1980), The turbulent flow of non-Newtonian fluids in the absence of anomalous wall effects, *Journal of non-Newtonian fluid mechanics*, 7, 77-90.

GOVIER G W and AZIZ K (1972), The Flow of Complex Mixtures in Pipes, *van Nostrand Reinhold Co.*

GRUNBERG L and NISSAN A H (1945), Viscosity of Ordinary Liquids at High Rates of Shear, *Nature*, 156, 241.

HANKS R W (1963), The laminar/turbulent transition for fluids with a yield stress, *AIChE Journal*, Vol 9 No 3.

HANKS R W and RICKS B L (1974), Laminar-transition in flow of pseudoplastic fluids with yield stress, *J. Hydronautics*, Vol. 8, No. 4.

HANKS R W and RICKS B L (1975), Transitional and turbulent pipeflow of pseudoplastic fluids, *J. Hydronautics*, Vol. 9, No. 1.

HARRIS J (1967), Letter to the Editor, *Chem. Engnr. (LN)*, Jan/Feb, 30.

HARRIS J (1968), The correlation of non-Newtonian Turbulent pipeflow data, *Rheol. Acta.*, 7, 3, 228-235.

HARRIS J and QUADER A K M A (1971), Design procedures for pipelines transporting non-Newtonian fluids and solid liquid systems, *Brit. Chem. Engrg.*, Vol 16 No 4/5.

HARRIS J and WILKINSON W L (1971), Momentum, heat and mass transfer in non-Newtonian turbulent flow in pipes, *Chem. Engng*, 16, 301-311.

HEDSTRÖM B O A (1952), Flow of plastics materials in pipes, *Industrial and engineering chemistry*, v.44 No.3.

HERSCHEL W H and BULKLEY R (1926), Measurement of consistency as applied to rubber-benzene solutions, *Proc ASTM*, 26 Part 2 621-633.

HEYWOOD N I (1980), Pipeline Design for Non-Newtonian Fluids, *Interflow 80*, IChemE, 33-53

HEYWOOD N I, MEHTA K B and POPLAR D (1993), Evaluation of seven commercially available electromagnetic flowmeters with Newtonian and non-Newtonian china clay slurry in pipeflow, *12th Int. Conf. on slurry handling and pipeline transport*, Hydrotransport 12, BHR Group, p353.

HOLLAND F A (1973), *Fluid flow for chemical engineers*, Edward Arnold, London.

JANNA, W S (1983), *Introduction to fluid mechanics*, Brooks/Cole Engineering Division.

KEMBLOWSKI Z and KOLODZIEJSKI J (1973), Flow resistances of non-Newtonian fluids in transitional and turbulent flow, *Int. Chem. Eng.* 13 265-279.

KNUDSEN J G and KATZ D L (1958), *Fluid Dynamics and Heat Transfer*, McGraw Hill, New York.

LAZARUS J H (1992), The hydraulic transport of solids in pipes. *Course notes*, University of Cape Town.

LAZARUS J H and NEILSON I D (1978), A generalised correlation for friction head losses of settling mixtures in horizontal smooth pipelines, *5th Int. Conf. on the hydraulic transport of solids in pipes*, Hydrotransport 5, Paper B1.

LUMLEY J L (1978), In *Topics in applied physics; Volume 12; Turbulence*, Ed P Bradshaw 2nd edition, Springer-Verlag, New York.

MAUDE A D and WHITMORE R L (1956), The wall effect and the viscometry of suspensions, Brit. Jou. Appl. Phys., 7, 98-102.

MAUDE A D and WHITMORE R L (1958), The turbulent flow of suspensions in tubes, *Trans. I. Chem Eng.*, 36 296-310.

METZNER A B (1956), Non-Newtonian Technology: Fluid Mechanics, Mixing, and Heat Transfer, *Advances in Chemical Engineering*, Vol 1, 77-153, Academic Press Inc, New York.

METZNER A B and REED J C (1955), Flow of non-Newtonian fluids - correlation of the laminar, transition and turbulent flow regions, *AIChE Journal*, v.1 n.4.

MICHIYOSHI I, MATSUMOTO R, MIZUNO K and NAKAI M (1966), Flow of slurry through a circular tube. Friction factor for tubes. Part II., *Int Chem Eng*, 6,2.

MILLER R W (1989), *Flow Engineering Handbook - Second Edition*, McGraw-Hill Publishing Company, New York.

MOODIE L, G S THORVALDSEN, P T SLATTER and F W PETERSEN, The Balanced Beam Tube Viscometer, *Hydraulic Conveying Association of SA Conference*, 14 November, 1994.

MOODY L F (1944), Friction factors for pipe flow, *Trans ASME*, November, 1944.

MOONEY M (1931), Explicit Formulas for Slip and Fluidity, *J. Rheology*, 2, 210-222.

MUN R (1988), Turbulent pipe flow of yield stress fluids, M Eng Sci Thesis, University of Melbourne.

NEILL R I G (1988), The rheology and flow behaviour of high concentration mineral slurries, Msc Dissertation, University of Cape Town.

NIKURADSE J (1932), Gesetzmassigkeiten der turbulenten Stromung in glatten Rohren, *Forschungsheft No. 356*, VDI Verlag, Berlin, 32.

NIKURADSE J (1933), Stromungsgesetze in rauhen Rohren, *Forschungsheft No. 361*, VDI Verlag, Berlin, 22.

ORR C and BLOCKER H G (1955), *Journal Colloid Sci.*,10, 24.

PARK J T, MANNHEIMER R J, GRIMLEY T A, MORROW T B (1989), Pipe flow measurements of a transparent non-Newtonian slurry, *Journal of fluids engineering*, Vol. 111, 331-336.

PARKER S P (1994), *McGraw-Hill Dictionary of Scientific and Technical Terms - Fifth Edition*, International McGraw-Hill Publishing Company, New York.

PHILIPPOFF W (1944), *Viskositat Der Kolloide*, Lithoprinted by J W Edwards, Ann Arbor, Mich.

POKRYVAILO N A and GROZBERG Yu G (1995), Investigation of structure of turbulent wall flow of clay suspension in channel with electrodiffusion method, *Proc. 8th Int. Conf. on Transport and sedimentation of solid particles*, Prague, Czech Republic.

PRANDTL L (1926), *2nd Int. Congress on Applied Mechanics*, Proc pg. 62.

QUADER A K M A and WILKINSON W L (1980), Correlation of turbulent flow rate-pressure drop data for non-Newtonian solutions and slurries in pipes, *Int. J. Multiphase Flow*, 6, 553-561.

RABINOWITSCH B (1929), Über die viskosität und elastizität van solen, *Z. phisikal. Chem.*, 145,1.

REED J C (1954) Master of Chemical Engineering thesis, University of Delaware, Newark.

ROBERTSON G (1996), Private Communication, GeoScience Laboratories, Cape Town, South Africa.

RYAN N W and JOHNSON M M (1959), Transition from laminar to turbulent flow in pipes, *AIChE Journal*, 5 433-435.

SABERSKY R H and ACOSTA A J (1966), *Fluid Flow in Fluid Mechanics: A First Course*, Collier-Macmillan Limited, London.

SCHLICHTING H (1968), *Boundary layer theory*, 5th edition, McGraw-Hill, New York.

SHOOK C A and ROCO M C (1991), *Slurry flow: principles and practice*, Butterworth-Heinemann.

SIVE A W (1988), *An analytical and experimental investigation of the hydraulic transport of high concentration mixed regime slurries*, PhD thesis, University of Cape Town.

SLATTER P T (1994), *Transitional and Turbulent Flow of Non-Newtonian Slurries in Pipes*, PhD Thesis, University of Cape Town. ·

SLATTER P T (1995), Private communication, Cape Technikon, Cape Town, South Africa.

SLATTER P T (1996), Private communication, Cape Technikon, Cape Town, South Africa.

SLATTER P T, LAZARUS J H (1993), Critical flow in slurry pipelines, 12th Int. Conf. on slurry handling and pipeline transport, HYDROTRANSPORT 12, BHR Group, p639.

SLATTER P T, G S THORVALDSEN and F W PETERSEN (1996), Particle Roughness Turbulence, British Hydromechanics Research Group 13th International Conference on Slurry Handling and Pipeline Transport HYDROTRANSPORT 13, Johannesburg, 3-5 September, 1996.

SPIEGEL M R (1972), *Theory and problems of statistics in SI units, McGraw-Hill*, New York.

THOMAS A D (1976), Scale-up methods for pipeline transport of slurries, *Int. J. Min. Proc*, 3, 51-69.

THOMAS A D (1983), Turbulent Pipe Flow of Bingham Plastics, *Proc. 3rd Nat. Cong. Rheol.*, Brit. Soc. Rheol.(Aust), Melbourne, 83-87.

THOMAS D G (1963), Non-Newtonian Suspensions Part II: Turbulent Transport Characteristics, *Ind. Eng. Chem.*, 55, 12, 27-35.

TOMITA Y (1959), A study on non-Newtonian flow in pipes, *Bull JSME*, Vol 2 No 5.

TORRANCE B M^{c}K (1963), Friction factors for turbulent non-Newtonian flow in circular pipes, *S. A. Mechanical Engineer*, v.13.

VAUGHN R D (1956), PhD thesis in Chemical Engineering, University of Delaware, Newark.

VON KARMEN T (1930), *Nachr. Ges. Wiss. Gottingen. Math Physik. Kl.*, 58.

WELTMAN R N (1948), Consistency and Temperature of Oils and Printing inks at High Shearing Stresses, *Ind. Eng. Chem.*, 40, February, 272-280.

WELTMAN R N (1956), Friction Factors for Flow of Non-Newtonian Materials in Pipelines, *Ind. Eng. Chem.*, 48, 3, 386-387.

WILSON K C (1986), Modelling the effects of non-Newtonian and time-dependent slurry

behaviour, *10th Int. Conf. on the hydraulic transport of solids in pipes*, Hydrotransport 10 Paper J1.

WILSON K C (1996), Comments on paper "Particle Roughness Turbulence", HYDROTRANSPORT 13, Johannesburg, 3-5 September, 1996

WILSON K C and THOMAS A D (1985), A new analysis of the turbulent flow of non-Newtonian fluids. *Can. J. Chem. Eng.*, 63, 539-546.

WILSON K C and WILSON K C (1987), New analysis of non-Newtonian flow- yield-power-law fluids, *Can J Chem Eng*, 65 335-338.

XU J, GILLIES R, SMALL M and SHOOK C A (1993), Laminar and turbulent flow of kaolin slurries, *12th Int. Conf. on slurry handling and pipeline transport*, Hydrotransport 12, BHR Group, p595.

ZETTLEMOYER A C and LOWER G W (1955), *Journal Colloid Sci*, 10, 29.

APPENDICES

APPENDIX A

A.1   DETAILED PIPE TEST RESULTS

The detailed pipe test results are presented in this section.

Each test set (ie. 25mm, 80mm, 150mm and 200mm) is preceded by the particle size distribution for that particular test set.

A table of the data points of wall shear stress and velocity precedes each pipeline test sheet.

Each test sheet contains the test apparatus, material, slurry properties, turbulent model performance and the test data plotted on a pseudo-shear diagram.

The test code (eg. SERS10) indicates the following:

S	This describes the material ie. sand (mixture 2) or K=kaolin or RF=rock flour (mixture 1)
ER	This describes the apparatus ie East Rig or Mini Rig
S	This indicates the pipe size = small, medium or large
10	This indicates the test identifier

Kaolin Test Set 10
Particle Size Distribution
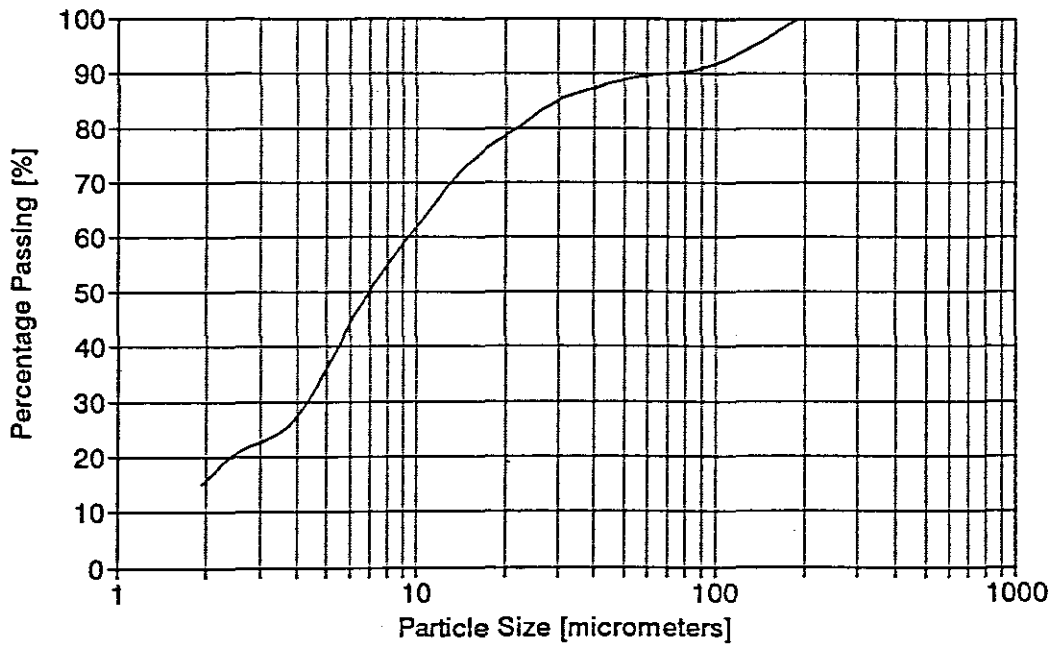
TEST: KMRL10

SLURRY: Water
            Kaolin Clay

CRITICAL VELOCITY: 1.88 m/s

No.	Wall Shear Stress [Pa]	Velocity [m/s]
1.	19.11	2.47
2.	18.07	2.29
3.	17.15	2.10
4.	15.66	1.52
5.	15.35	1.48
6.	14.85	1.24
7.	14.29	1.07
8.	14.04	0.92
9.	13.53	0.74
10.	13.27	0.63
11.	12.52	0.40
12.	12.07	0.31
13.	11.82	0.22
14.	11.24	0.15
15.	10.27	0.07

DATA FROM TEST	KMRL10
APPARATUS	
Facility	Mini Rig
Diameter	22 mm
Material	Kaolin
Operator	GST
Supervisor	PTS

SLURRY PROPERTIES	
Solids Relative Density	2.6000
Slurry Relative Density	1.1121
Volumetric Concentration	7.0 %
Yield Stress	9.140 Pa
Fluid Consistency Index	0.0676 Pa s^n
Flow Behaviour Index	0.6456
Representative Particle size	30 um

TURBULENT MODEL PERFORMANCE		
Model	Avg %	Avg LSE
Torrance	14.20	0.0510
Wilson & Thomas	15.75	0.0667
Dodge & Metzner	64.31	0.2168
Kemblowski & Kolodziejski	294.96	0.5162
New Model	6.38	0.0303

Legend:
+ Data
— Laminar / K&K
— Torrance
— Wilson & Thomas
— New Model
— Dodge & Metzner

X-axis: Pseudo-Shear Rate 8 V / D [1/s]
Y-axis: Wall Shear Stress [Pa]
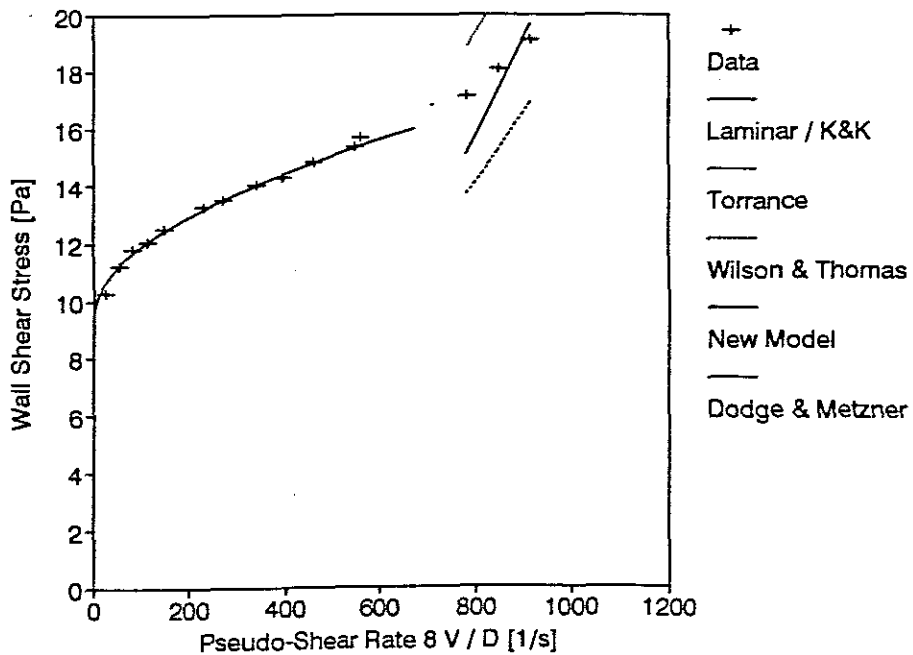
TEST: KERS10

SLURRY: Water
         Kaolin Clay

CRITICAL VELOCITY: 2.32 m/s

No.	Wall Shear Stress [Pa]	Velocity [m/s]
1.	68.82	5.55
2.	53.50	4.88
3.	42.89	4.34
4.	34.48	3.84
5.	27.30	3.36
6.	20.09	2.84
7.	15.64	2.34
8.	13.01	1.87
9.	12.03	1.52
10.	11.38	1.04
11.	10.99	0.80
12.	10.56	0.54

DATA FROM TEST	KERS10
APPARATUS	
Facility	East Rig
Diameter	79 mm
Material	Kaolin
Operator	GST
Supervisor	PTS

SLURRY PROPERTIES	
Solids Relative Density	2.6000
Slurry Relative Density	1.1121
Volumetric Concentration	7.0 %
Yield Stress	9.140 Pa
Fluid Consistency Index	0.0676 Pa s^n
Flow Behaviour Index	0.6456
Representative Particle size	30 um

TURBULENT MODEL PERFORMANCE		
Model	Avg %	Avg LSE
Torrance	10.25	0.0241
Wilson & Thomas	20.26	0.0439
Dodge & Metzner	16.53	0.0394
Kemblowski & Kolodziejski	87.26	0.1229
New Model	6.56	0.0145

Legend:
+ Data
Laminar / K&K
Torrance
Wilson & Thomas
New Model
Dodge & Metzner

X-axis: Pseudo-Shear Rate 8 V / D [1/s]
Y-axis: Wall Shear Stress [Pa]
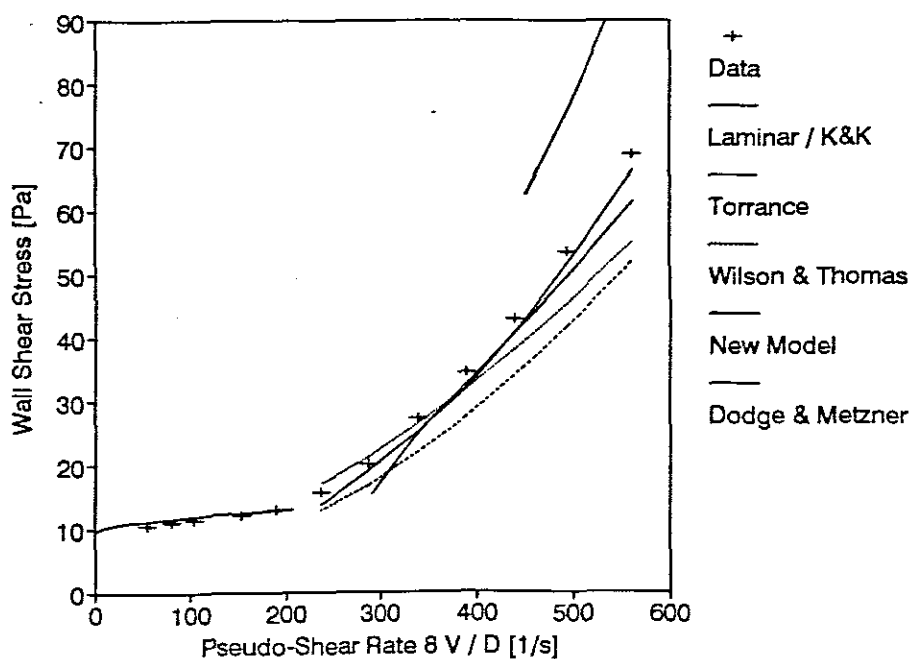
TEST: KERM10

SLURRY: Water
        Kaolin Clay

CRITICAL VELOCITY: 2.94 m/s

No.	Wall Shear Stress [Pa]	Velocity [m/s]
1.	76.46	6.20
2.	65.48	5.91
3.	54.43	5.38
4.	45.77	4.93
5.	38.04	4.56
6.	32.65	4.14
7.	27.17	3.77
8.	22.99	3.36
9.	18.83	3.11
10.	14.95	2.77
11.	13.41	2.57
12.	11.97	2.18
13.	11.47	1.85
14.	10.79	1.42
15.	10.16	1.15

DATA FROM TEST	KERM10
APPARATUS	
Facility	East Rig
Diameter	141 mm
Material	Kaolin
Operator	GST
Supervisor	PTS

SLURRY PROPERTIES	
Solids Relative Density	2.6000
Slurry Relative Density	1.1121
Volumetric Concentration	7.0 %
Yield Stress	9.140 Pa
Fluid Consistency Index	0.0676 Pa s ^ n
Flow Behaviour Index	0.6456
Representative Particle size	30 um

TURBULENT MODEL PERFORMANCE		
Model	Avg %	Avg LSE
Torrance	9.71	0.0206
Wilson & Thomas	14.88	0.0283
Dodge & Metzner	3.88	0.0084
Kemblowski & Kolodziejski	21.71	0.0401
New Model	2.49	0.0049

Legend:
+ Data
— Laminar / K&K
— Torrance
— Wilson & Thomas
— New Model
— Dodge & Metzner

X-axis: Pseudo-Shear Rate 8 V / D [1/s]
Y-axis: Wall Shear Stress [Pa]
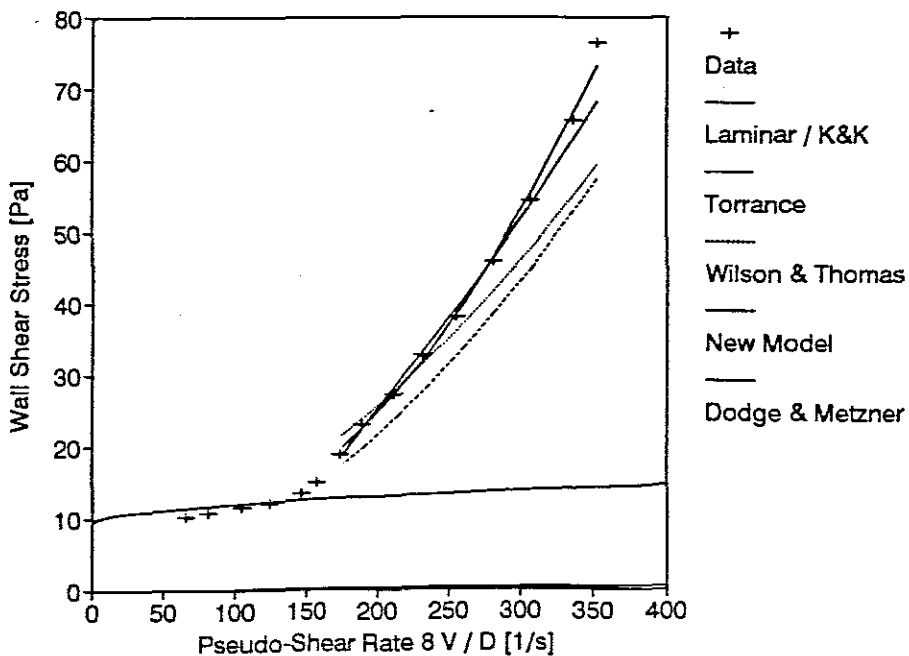
TEST: KERL10

SLURRY: Water
            Kaolin Clay

CRITICAL VELOCITY: 2.21 m/s

No.	Wall Shear Stress [Pa]	Velocity [m/s]
1.	22.12	2.98
2.	20.03	2.84
3.	18.57	2.76
4.	16.30	2.60
5.	13.82	2.36
6.	13.19	2.16
7.	12.82	2.00
8.	11.88	1.81
9.	11.65	1.63
10.	10.89	1.45
11.	10.79	1.24
12.	10.54	1.07
13.	10.33	0.91
14.	9.33	0.67

DATA FROM TEST	KERL10
APPARATUS	
Facility	East Rig
Diameter	207 mm
Material	Kaolin
Operator	GST
Supervisor	PTS

SLURRY PROPERTIES	
Solids Relative Density	2.6000
Slurry Relative Density	1.1121
Volumetric Concentration	7.0 %
Yield Stress .	9.140 Pa
Fluid Consistency Index	0.0676 Pa s^n
Flow Behaviour Index	0.6456
Representative Particle size	130 um

TURBULENT MODEL PERFORMANCE		
Model	Avg %	Avg LSE
Torrance	6.55	0.0197
Wilson & Thomas	21.78	0.0631
Dodge & Metzner	34.57	0.1115
Kemblowski & Kolodziejski	210.64	0.2751
New Model	4.53	0.0168

Legend:
+ Data
— Laminar / K&K
— Torrance
— Wilson & Thomas
— New Model
— Dodge & Metzner
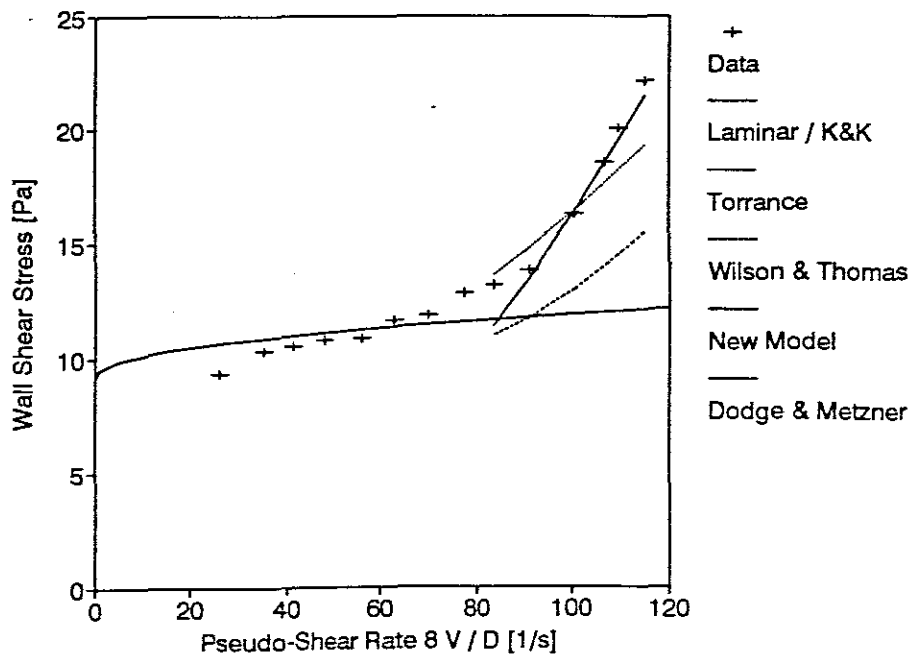
Kaolin Test Set 20
Particle Size Distribution
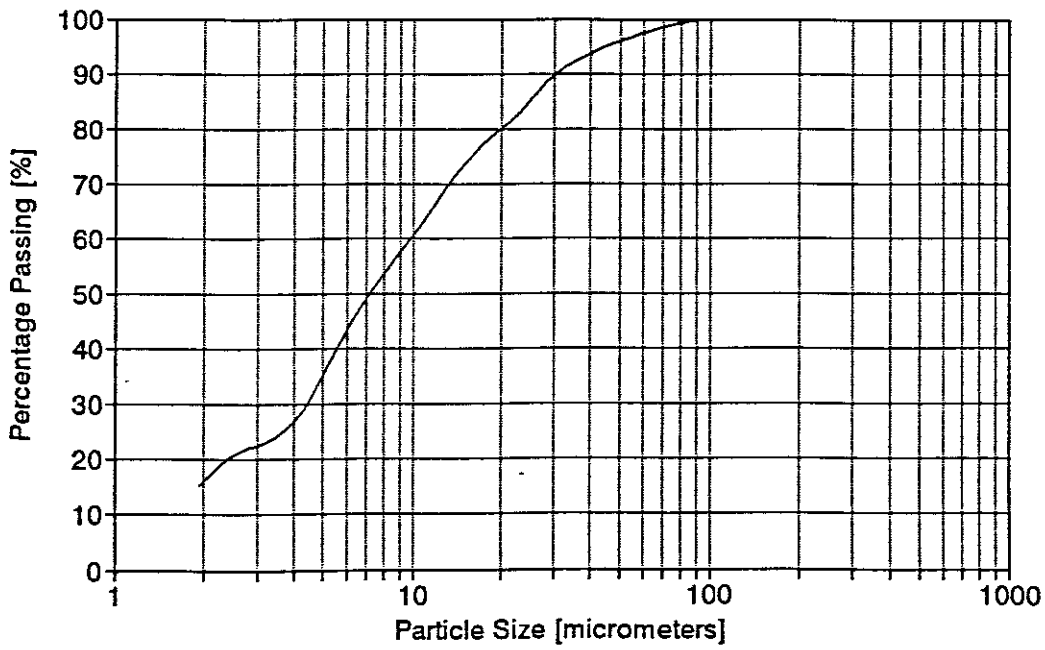
TEST: KMRL20

SLURRY: Water
          Kaolin Clay

CRITICAL VELOCITY: 1.67 m/s

No.	Wall Shear Stress [Pa]	Velocity [m/s]
1.	22.89	2.60
2.	19.92	2.40
3.	17.51	2.22
4.	14.90	2.03
5.	12.21	1.83
6.	11.38	1.69
7.	10.43	1.52
8.	10.37	1.45
9.	9.94	1.25
10.	9.47	1.03
11.	8.83	0.74
12.	8.35	0.58
13.	7.87	0.32
14.	7.15	0.19

DATA FROM TEST	KMRL20
APPARATUS	
Facility	Mini Rig
Diameter	22 mm
Material	Kaolin
Operator	GST
Supervisor	PTS

SLURRY PROPERTIES	
Solids Relative Density	2.6000
Slurry Relative Density	1.0985
Volumetric Concentration	6.2 %
Yield Stress	5.800 Pa
Fluid Consistency Index	0.0176 Pa s^n
Flow Behaviour Index	0.8154
Representative Particle size	25 um

TURBULENT MODEL PERFORMANCE		
Model	Avg %	Avg LSE
Torrance	17.87	0.0413
Wilson & Thomas	15.22	0.0402
Dodge & Metzner	5.30	0.0199
Kemblowski & Kolodziejski	333.73	0.3541
New Model	1.74	0.0049

Legend:
+ Data
— Laminar / K&K
— Torrance
— Wilson & Thomas
— New Model
— Dodge & Metzner
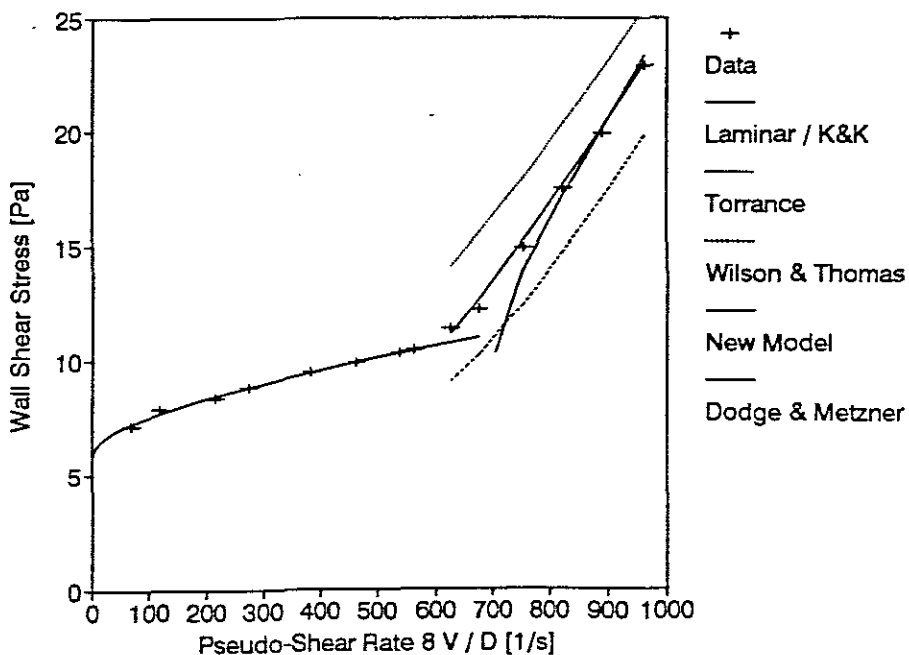
TEST: KERS20

SLURRY: Water
     Kaolin Clay

CRITICAL VELOCITY: 1.95 m/s

No.	Wall Shear Stress [Pa]	Velocity [m/s]
1.	84.69	5.42
2.	71.01	5.14
3.	61.12	4.92
4.	51.53	4.49
5.	40.97	4.03
6.	34.38	3.61
7.	26.94	3.14
8.	17.60	2.64
9.	13.58	2.25
10.	8.44	1.69
11.	7.95	1.21
12.	7.00	0.75

DATA FROM TEST	KERS20
APPARATUS	
Facility	East Rig
Diameter	79 mm
Material	Kaolin
Operator	GST
Supervisor	PTS

SLURRY PROPERTIES	
Solids Relative Density	2.6000
Slurry Relative Density	1.0985
Volumetric Concentration	6.2 %
Yield Stress .	5.800 Pa
Fluid Consistency Index	0.0176 Pa s^n
Flow Behaviour Index	0.8154
Representative Particle size	25 um

TURBULENT MODEL PERFORMANCE		
Model	Avg %	Avg LSE
Torrance	13.78	0.0273
Wilson & Thomas	20.43	0.0390
Dodge & Metzner	8.96	0.0191
Kemblowski & Kolodziejski	26.84	0.0404
New Model	11.87	0.0256

Legend:
+ Data
— Laminar / K&K
— Torrance
— Wilson & Thomas
— New Model
— Dodge & Metzner

X-axis: Pseudo-Shear Rate 8 V / D [1/s]
Y-axis: Wall Shear Stress [Pa]
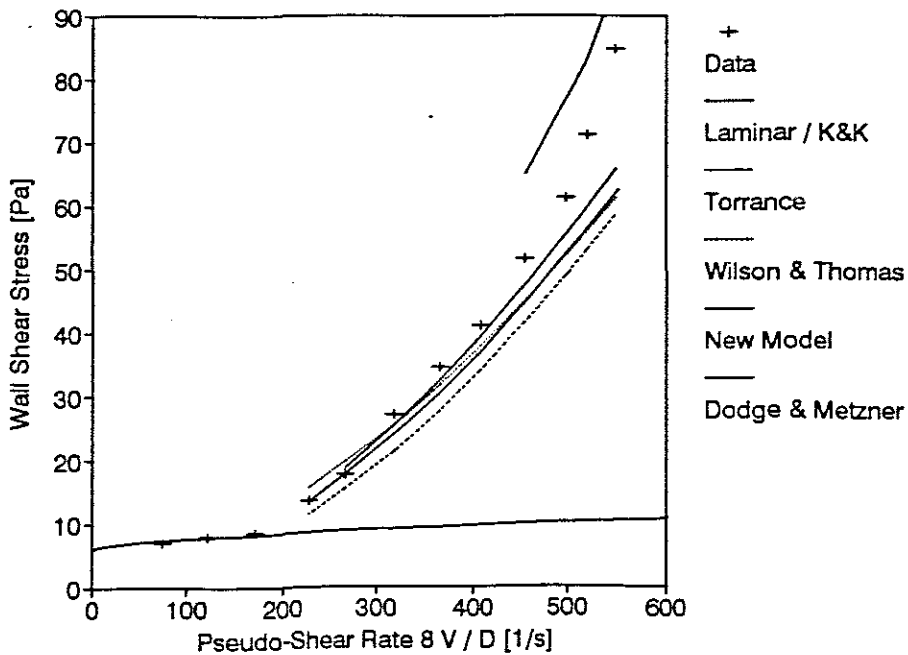
TEST: KERM20

SLURRY: Water
     Kaolin Clay

CRITICAL VELOCITY: 2.22 m/s

No.	Wall Shear Stress [Pa]	Velocity [m/s]
1.	73.65	6.19
2.	65.48	5.90
3.	56.23	5.47
4.	45.10	4.83
5.	32.36	4.05
6.	22.57	3.32
7.	17.58	2.88
8.	13.50	2.56
9.	11.33	2.23
10.	9.39	2.00
11.	8.18	1.75
12.	7.82	1.59
13.	7.32	1.42

DATA FROM TEST	KERM20
APPARATUS	
Facility	East Rig
Diameter	141 mm
Material	Kaolin
Operator	GST
Supervisor	PTS

SLURRY PROPERTIES	
Solids Relative Density	2.6000
Slurry Relative Density	1.0985
Volumetric Concentration	6.2 %
Yield Stress ,	5.800 Pa
Fluid Consistency Index	0.0176 Pa s ^{n}
Flow Behaviour Index	0.8154
Representative Particle size	25 um

TURBULENT MODEL PERFORMANCE		
Model	Avg %	Avg LSE
Torrance	9.14	0.0179
Wilson & Thomas	7.28	0.0130
Dodge & Metzner	8.90	0.0150
Kemblowski & Kolodziejski	58.87	0.0757
New Model	3.46	0.0071

Legend:
+ Data
— Laminar / K&K
— Torrance
— Wilson & Thomas
— New Model
— Dodge & Metzner
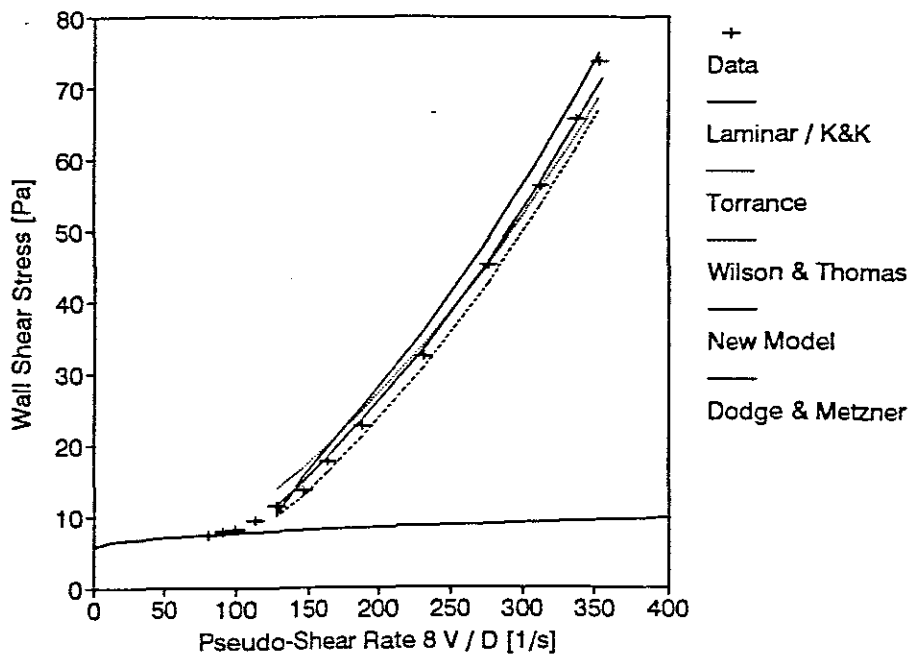
TEST: KERL20

SLURRY: Water
             Kaolin Clay

CRITICAL VELOCITY: 1.55 m/s

No.	Wall Shear Stress [Pa]	Velocity [m/s]
1.	7.64	2.89
2.	13.76	2.49
3.	12.22	2.32
4.	10.08	2.00
5.	8.82	1.74
6.	7.25	1.37
7.	5.99	1.05
8.	5.44	0.72

DATA FROM TEST	KERL20
APPARATUS	
Facility	East Rig
Diameter	207 mm
Material	Kaolin
Operator	GST
Supervisor	PTS

SLURRY PROPERTIES	
Solids Relative Density	2.6000
Slurry Relative Density	1.0985
Volumetric Concentration	6.2 %
Yield Stress	5.800 Pa
Fluid Consistency Index	0.0176 Pa s ^ n
Flow Behaviour Index	0.8154
Representative Particle size	25 um

TURBULENT MODEL PERFORMANCE		
Model	Avg %	Avg LSE
Torrance	7.29	0.0176
Wilson & Thomas	19.06	0.0519
Dodge & Metzner	7.12	0.0199
Kemblowski & Kolodziejski	311.02	0.3410
New Model	9.00	0.0295
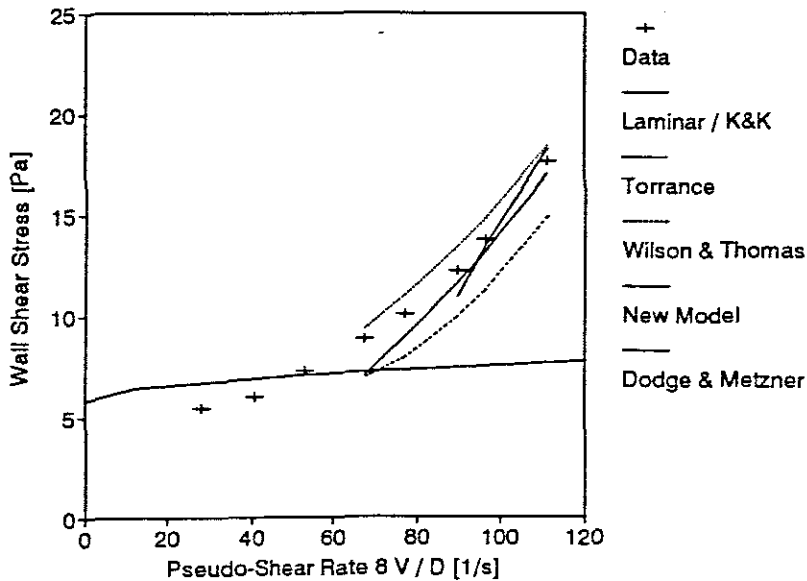
Legend:
+ Data
— Laminar / K&K
— Torrance
— Wilson & Thomas
— New Model
— Dodge & Metzner

GEOSCIENCE

LABORATORIES (PTY) LTD

14A KLOOF STREET CAPE TOWN 8001 PO BOX 16634 VLAEBERG 8018
TELEPHONE (021) 4699111 FAX (021) 245571

LABORATORY TEST RESULTS

PROJECT: **UCT KAOLIN**
PROJECT NO: **15000K**
DATE: **30-05-96**

LABORATORY SAMPLE NO	6	
FIELD REFERENCE NO	RF 1	
DESCRIPTION	LIGHT GREY KAOLIN	
SIEVE ANALYSIS		
% Passing Screens		
106.0mm		
75.0		
53.0		
37.5		
26.5		
19.0		
13.2		
9.5		
4.75		
2.0		
0.85		
0.6		
0.425		
0.3	100	
0.25	99	
0.15	96	
0.075	88	
.0753	90	
.0519	85	
.0209	77	
.0120	71	
.0087	63	
.0062	·56	
.0056	53	
.0025	40	
.0023	36	
ATTERBERG LIMITS		
Liquid Limit		
Plasticity Index		
Linear Shrinkage %		
Specific Gravity (est.)		
MOISTURE/DENSITY		
Max. Dry Density (kg/m^3)		
Optimum Moisture Content (%)		
CALIFORNIA		
BEARING RATIO		
100 % Compaction		
98 %		
95 %		
93 %		
90 %		
Maximum Swell (%)		

REMARKS:

PARTICLE SIZE DISTRIBUTION

PROJECT: UCT KAOLIN **PROJECT NO: 15000**

FIELD SAMPLE NO: RF1

LAB SAMPLE NO: 6

PERCENTAGE RETAINED BY MASS

PERCENTAGE PASSING BY MASS

DEPTH

+
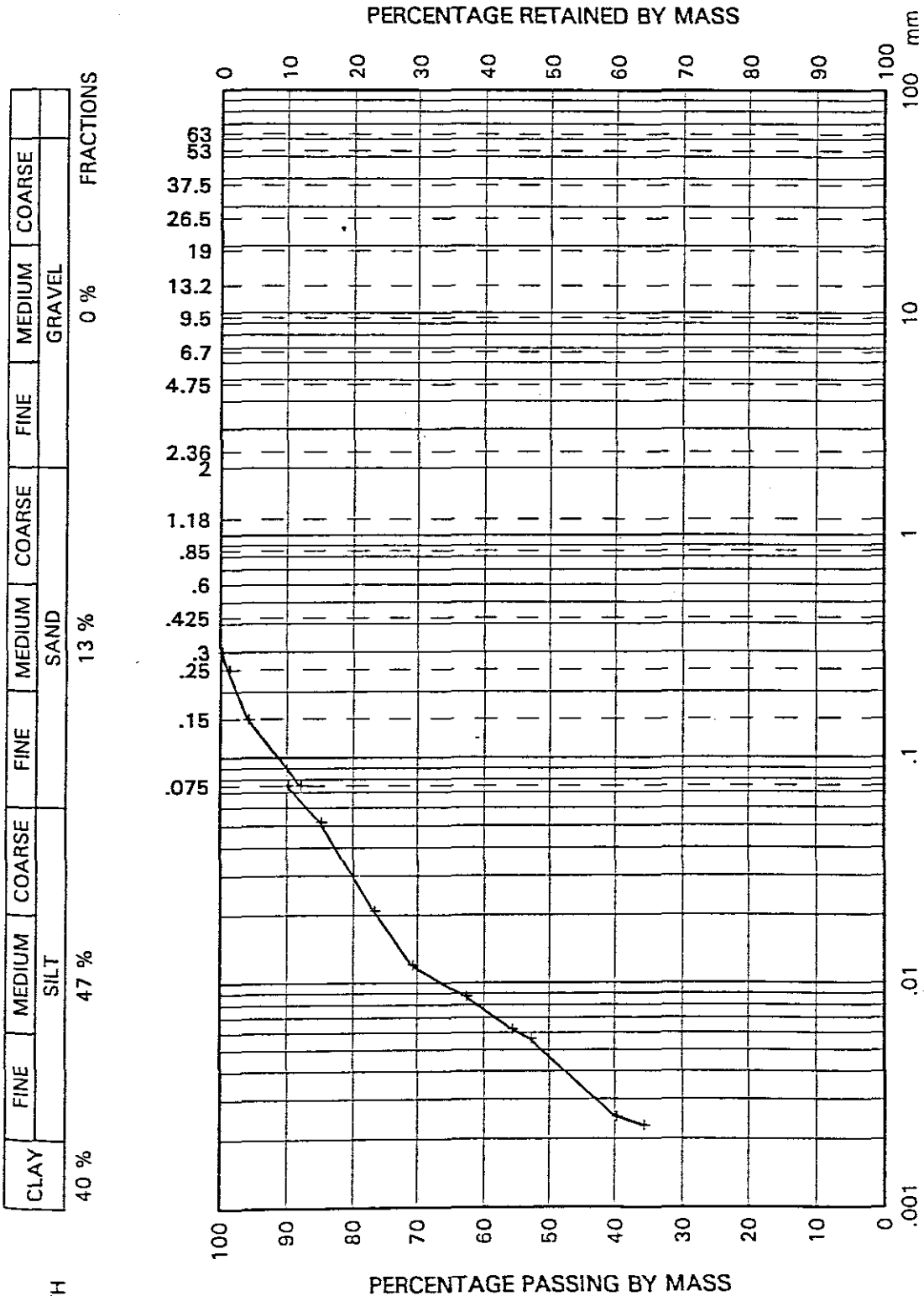
TEST: RFMRL10

SLURRY: Water
        Kaolin Clay
        Rock Flour

CRITICAL VELOCITY: 1.71 m/s

No.	Wall Shear Stress [Pa]	Velocity [m/s]
1.	25.25	2.48
2.	19.58	2.19
3.	17.00	2.03
4.	14.72	1.91
5.	13.47	1.87
6.	11.24	1.71
7.	10.36	1.60
8.	9.91	1.44
9.	9.47	1.30
10.	8.77	1.11
11.	8.22	0.95
12.	7.60	0.74
13.	6.88	0.56
14.	6.33	0.44

DATA FROM TEST	RFMRL10
APPARATUS	
Facility	Mini Rig
Diameter	22 mm
Material	Mixture 1
Operator	GST
Supervisor	PTS

SLURRY PROPERTIES	
Solids Relative Density	2.6500
Slurry Relative Density	1.1547
Volumetric Concentration	9.4 %
Yield Stress	3.680 Pa
Fluid Consistency Index	0.0132 Pa s^n
Flow Behaviour Index	0.9474
Representative Particle size	52 um

TURBULENT MODEL PERFORMANCE		
Model	Avg %	Avg LSE
Torrance	41.57	0.0853
Wilson & Thomas	8.53	0.0209
Dodge & Metzner	23.94	0.0529
Kemblowski & Kolodziejski	321.61	0.3476
New Model	24.37	0.0540

Legend:
+ Data
— Laminar / K&K
— Torrance
---- Wilson & Thomas
— New Model
— Dodge & Metzner
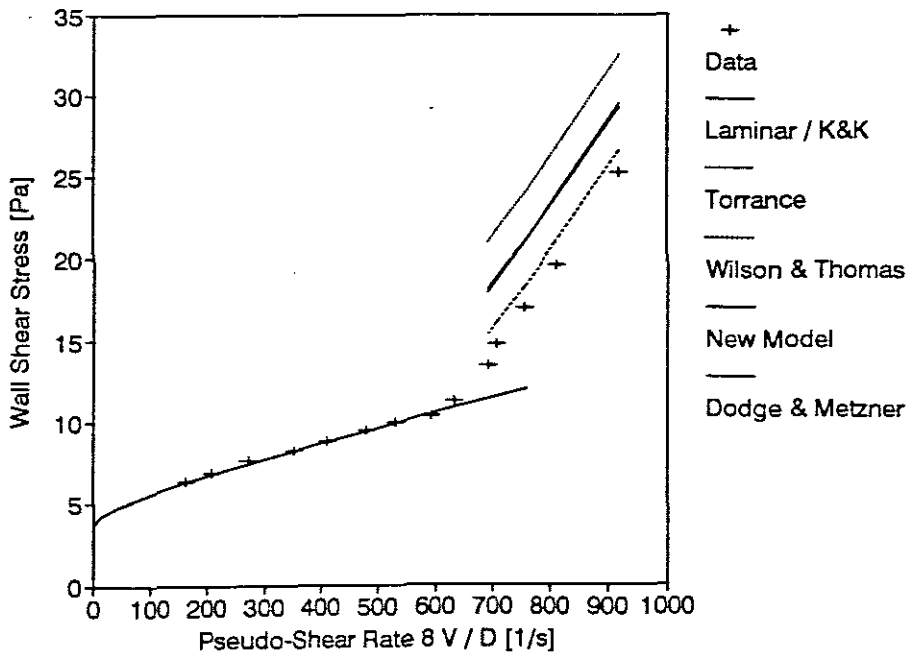
TEST: RFERS10

SLURRY: Water
        Kaolin Clay
        Rock Flour

CRITICAL VELOCITY: 1.96 m/s

No.	Wall Shear Stress [Pa]	Velocity [m/s]
1.	87.50	5.43
2.	78.45	5.13
3.	64.13	4.86
4.	51.25	4.39
5.	44.36	4.02
6.	39.63	3.71
7.	30.61	3.35
8.	24.78	2.94
9.	21.17	2.65
10.	13.84	2.20
11.	9.31	1.78
12.	5.88	1.30
13.	4.91	0.68

DATA FROM TEST	RFERS10
APPARATUS	
Facility	East Rig
Diameter	79 mm
Material	Mixture 1
Operator	GST
Supervisor	PTS

SLURRY PROPERTIES	
Solids Relative Density	2.6000
Slurry Relative Density	1.1547
Volumetric Concentration	9.7 %
Yield Stress .	3.680 Pa
Fluid Consistency Index	0.0132 Pa s ^ n
Flow Behaviour Index	0.9474
Representative Particle size	52 um

TURBULENT MODEL PERFORMANCE		
Model	Avg %	Avg LSE
Torrance	13.10	0.0221
Wilson & Thomas	5.52	0.0098
Dodge & Metzner	11.66	0.0198
Kemblowski & Kolodziejski	25.96	0.0385
New Model	9.74	0.0162
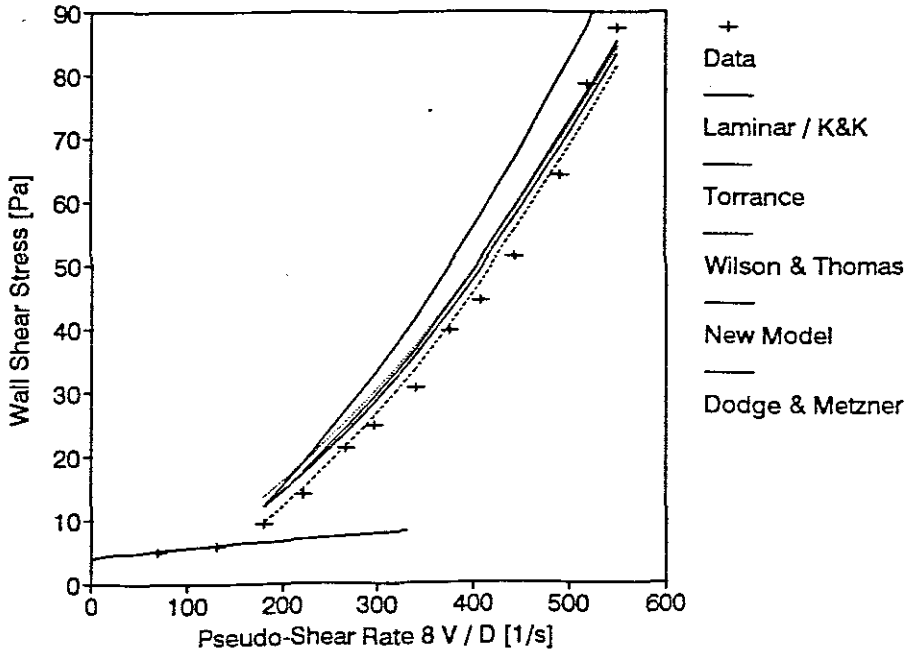
TEST: RFERM10

SLURRY: Water
        Kaolin Clay
        Rock Flour

CRITICAL VELOCITY: 2.24 m/s

No.	Wall Shear Stress [Pa]	Velocity [m/s]
1.	78.79	6.17
2.	68.44	5.66
3.	55.61	5.25
4.	47.58	4.77
5.	41.72	4.50
6.	35.36	4.10
7.	28.87	3.71
8.	22.43	3.31
9.	16.33	2.89
10.	14.72	2.69
11.	12.45	2.42
12.	9.17	2.15
13.	5.01	1.49
14.	4.88	1.21

DATA FROM TEST	RFERM10
APPARATUS	
Facility	East Rig
Diameter	141 mm
Material	Mixture 1
Operator	GST
Supervisor	PTS

SLURRY PROPERTIES	
Solids Relative Density	2,6500
Slurry Relative Density	1,1547
Volumetric Concentration	9,4 %
Yield Stress .	3,680 Pa
Fluid Consistency Index	0,0132 Pa s^n
Flow Behaviour Index	0,9474
Representative Particle size	52 um

TURBULENT MODEL PERFORMANCE		
Model	Avg %	Avg LSE
Torrance	30,14	0,0446
Wilson & Thomas	22,20	0,0335
Dodge & Metzner	31,89	0,0462
Kemblowski & Kolodziejski	54,44	0,0716
New Model	27,66	0,0410

Legend:
+ Data
— Laminar / K&K
— Torrance
— Wilson & Thomas
— New Model
— Dodge & Metzner

Y-axis: Wall Shear Stress [Pa]
X-axis: Pseudo-Shear Rate 8 V / D [1/s]
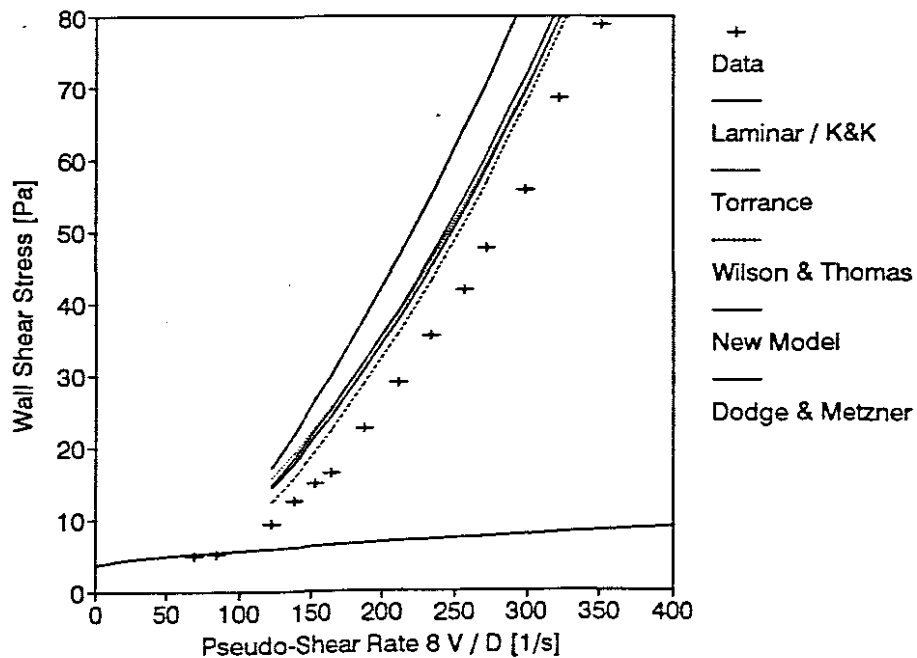
TEST: RFERL10

SLURRY: Water
          Kaolin Clay
          Rock Flour

CRITICAL VELOCITY: 1.27 m/s

No.	Wall Shear Stress [Pa]	Velocity [m/s]
1.	21.22	2.79
2.	16.23	2.40
3.	13.40	2.16
4.	10.11	1.83
5.	8.69	1.63
6.	6.47	1.34
7.	4.97	0.91
8.	4.62	0.71

DATA FROM TEST	RFERL10
APPARATUS	
Facility	East Rig
Diameter	207 mm
Material	Mixture 1
Operator	GST
Supervisor	PTS

SLURRY PROPERTIES	
Solids Relative Density	2,6500
Slurry Relative Density	1,1547
Volumetric Concentration	9,4 %
Yield Stress .	3,680 Pa
Fluid Consistency Index	0,0132 Pa s ^{n}
Flow Behaviour Index	0,9474
Representative Particle size	130 um

TURBULENT MODEL PERFORMANCE		
Model	Avg %	Avg LSE
Torrance	7,76	0,0170
Wilson & Thomas	21,14	0,0574
Dodge & Metzner	13,86	0,0442
Kemblowski & Kolodziejski	70,15	0,1255
New Model	2,59	0,0092
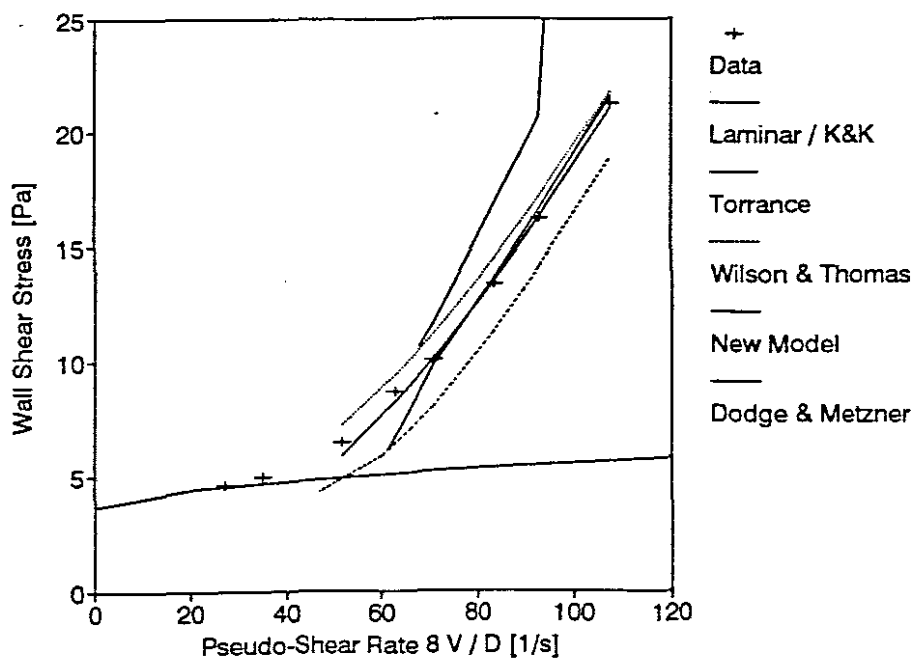
Legend:
+ Data
— Laminar / K&K
— Torrance
— Wilson & Thomas
— New Model
— Dodge & Metzner

GEOSCIENCE
LABORATORIES (PTY) LTD

LABORATORY TEST RESULTS

PROJECT: UCT KAOLIN
PROJECT NO: 15000K
DATE: 30-05-96

LABORATORY SAMPLE NO	7	
FIELD REFERENCE NO	RF 2	
DESCRIPTION	LIGHT GREY KAOLIN	
SIEVE ANALYSIS		
% Passing Screens		
106.0mm		
75.0		
53.0		
37.5		
26.5		
19.0		
13.2		
9.5		
4.75		
2.0		
0.85		
0.6		
0.425		
0.3	100	
0.25	99	
0.15	95	
0.075	86	
.0774	85	
.0527	82	
.0214	74	
.0121	65	
.0088	60	
.0063	53	
.0057	50	
.0026	37	
.0024	34	
ATTERBERG LIMITS		
Liquid Limit		
Plasticity Index		
Linear Shrinkage %		
Specific Gravity (est.)		
MOISTURE/DENSITY		
Max. Dry Density (kg/m^3)		
Optimum Moisture Content (%)		
CALIFORNIA		
BEARING RATIO		
100 % Compaction		
98 %		
95 %		
93 %		
90 %		
Maximum Swell (%)		

REMARKS:

PARTICLE SIZE DISTRIBUTION

PROJECT: UCT KAOLIN **PROJECT NO: 15000**

FIELD SAMPLE NO: RF2

LAB SAMPLE NO: 7

PERCENTAGE RETAINED BY MASS

PERCENTAGE PASSING BY MASS
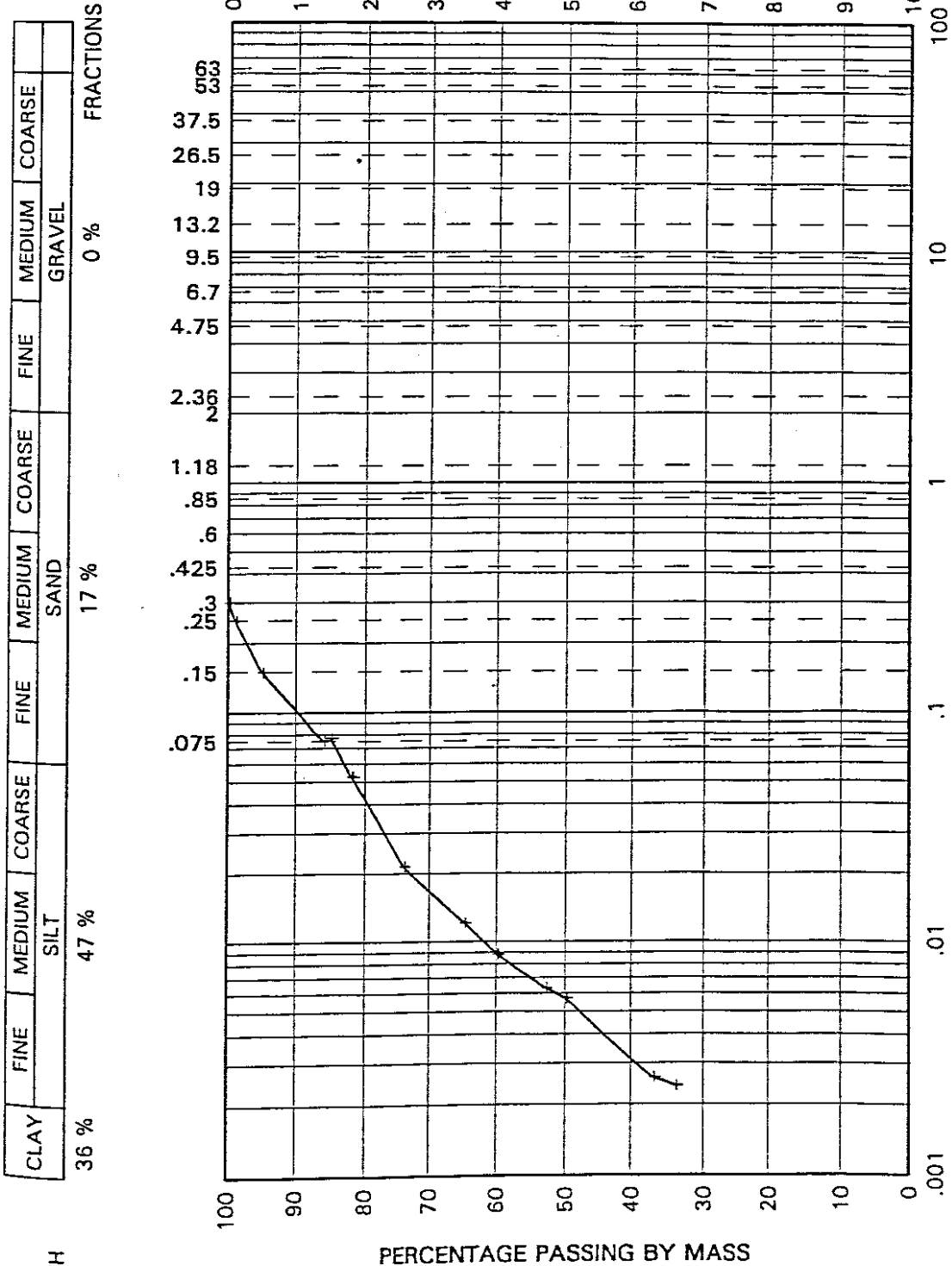
DEPTH

+

TEST: RFMRL20

SLURRY: Water
        Kaolin Clay
        Rock Flour

CRITICAL VELOCITY: 1.81 m/s

No.	Wall Shear Stress [Pa]	Velocity [m/s]
1.	24.49	2.64
2.	19.49	2.36
3.	16.78	2.17
4.	14.98	2.05
5.	11.40	1.82
6.	10.12	1.52
7.	9.05	1.19
8.	8.63	1.02
9.	7.89	0.82
10.	7.35	0.70
11.	6.65	0.46
12.	5.97	0.35
13.	5.39	0.25

DATA FROM TEST	RFMRL20
APPARATUS	
Facility	Mini Rig
Diameter	22 mm
Material	Mixture 1
Operator	GST
Supervisor	PTS

SLURRY PROPERTIES	
Solids Relative Density	2,6000
Slurry Relative Density	1,1759
Volumetric Concentration	11,0 %
Yield Stress	3,910 Pa
Fluid Consistency Index	0,0105 Pa s^n
Flow Behaviour Index	0,9720
Representative Particle size	77 um

TURBULENT MODEL PERFORMANCE		
Model	Avg %	Avg LSE
Torrance	55,31	0,1658
Wilson & Thomas	24,36	0,0820
Dodge & Metzner	39,18	0,1244
Kemblowski & Kolodziejski	260,83	0,4817
New Model	40,30	0,1275
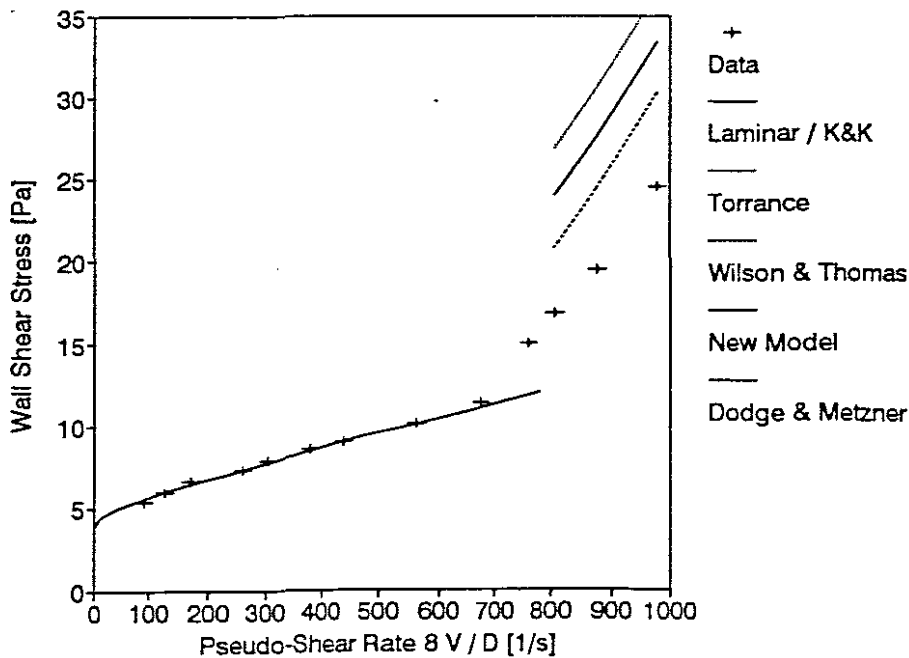
TEST: RFERS20

SLURRY: Water
Kaolin Clay
Rock Flour

CRITICAL VELOCITY: 1.48 m/s

No.	Wall Shear Stress [Pa]	Velocity [m/s]
1.	90.31	5.73
2.	66.13	4.85
3.	53.70	4.35
4.	45.21	3.98
5.	40.27	3.67
6.	32.40	3.23
7.	24.48	2.81
8.	18.47	2.45
9.	11.58	1.96
10.	6.13	1.35
11.	5.64	1.08

DATA FROM TEST	RFERS20
APPARATUS	
Facility	East Rig
Diameter	79 mm
Material	Mixture 1
Operator	GST
Supervisor	PTS

SLURRY PROPERTIES	
Solids Relative Density	2,6000
Slurry Relative Density	1,1759
Volumetric Concentration	11,0 %
Yield Stress ,	3,910 Pa
Fluid Consistency Index	0,0105 Pa s ^{n}
Flow Behaviour Index	0,9720
Representative Particle size	77 um

TURBULENT MODEL PERFORMANCE		
Model	Avg %	Avg LSE
Torrance	14,44	0,0248
Wilson & Thomas	1,58	0,0031
Dodge & Metzner	10,88	0,0180
Kemblowski & Kolodziejski	23,17	0,0343
New Model	9,50	0,0166
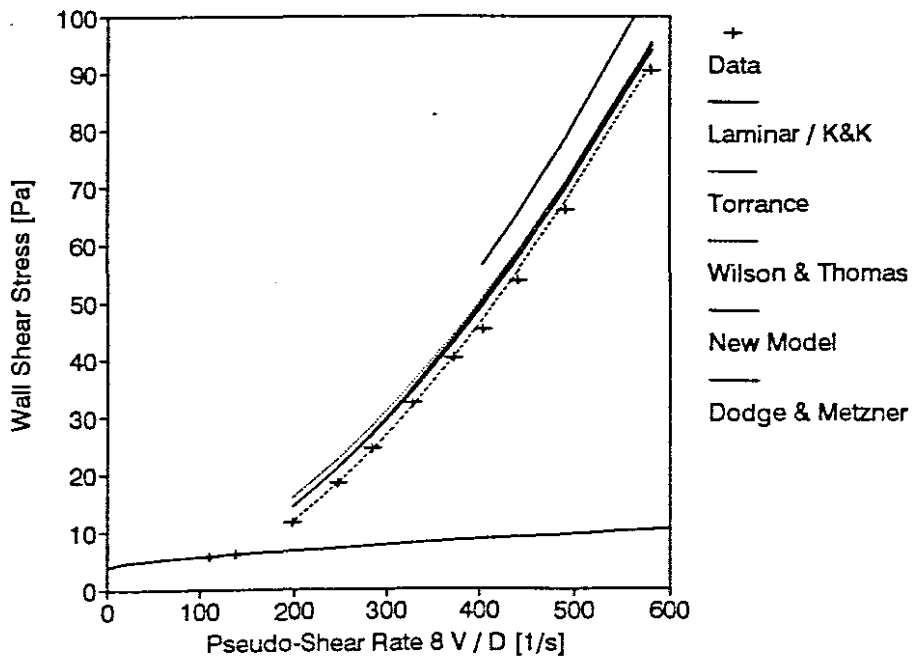
TEST: RFERM20

SLURRY: Water
          Kaolin Clay
          Rock Flour

CRITICAL VELOCITY: 2.22 m/s

No.	Wall Shear Stress [Pa]	Velocity [m/s]
1.	77.92	6.14
2.	66.64	5.53
3.	55.30	5.06
4.	42.66	4.51
5.	35.04	4.07
6.	27.36	3.57
7.	19.49	3.07
8.	14.07	2.64
9.	10.45	2.28
10.	8.53	2.01
11.	4.95	1.63
12.	4.76	1.39

DATA FROM TEST	RFERM20
APPARATUS	
Facility	East Rig
Diameter	141 mm
Material	Mixture 1
Operator	GST
Supervisor	PTS

SLURRY PROPERTIES	
Solids Relative Density	2,6000
Slurry Relative Density	1,1759
Volumetric Concentration	11,0 %
Yield Stress .	3,910 Pa
Fluid Consistency Index	0,0105 Pa s ^ n
Flow Behaviour Index	0,9720
Representative Particle size	77 um

TURBULENT MODEL PERFORMANCE		
Model	Avg %	Avg LSE
Torrance	35,83	0,0524
Wilson & Thomas	23,43	0,0351
Dodge & Metzner	35,18	0,0507
Kemblowski & Kolodziejski	56,22	0,0741
New Model	32,36	0,0474

Legend:
+ Data
— Laminar / K&K
— Torrance
— Wilson & Thomas
— New Model
— Dodge & Metzner
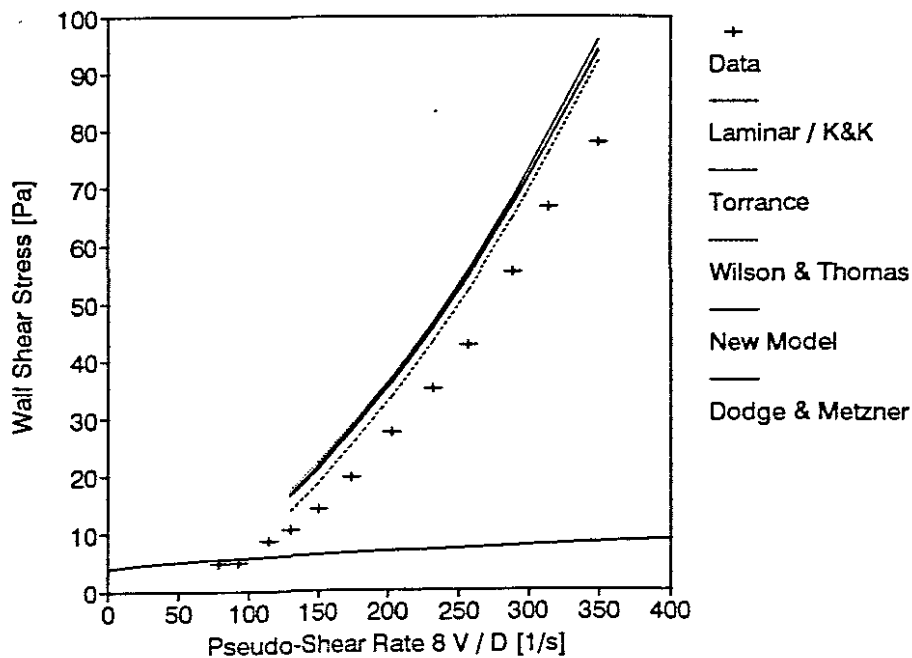
TEST: RFERL20

SLURRY: Water
Kaolin Clay
Rock Flour

CRITICAL VELOCITY: 1.38 m/s

No.	Wall Shear Stress [Pa]	Velocity [m/s]
1.	22.93	2.76
2.	19.47	2.56
3.	15.61	2.32
4.	13.61	2.13
5.	11.21	1.94
6.	9.03	1.71
7.	7.59	1.51
8.	6.49	1.15
9.	5.68	0.88

DATA FROM TEST	RFERL20
APPARATUS	
Facility	East Rig
Diameter	207 mm
Material	Mixture 1
Operator	GST
Supervisor	PTS

SLURRY PROPERTIES	
Solids Relative Density	2,6000
Slurry Relative Density	1,1759
Volumetric Concentration	11,0 %
Yield Stress	3,910 Pa
Fluid Consistency Index	0,0105 Pa s^n
Flow Behaviour Index	0,9720
Representative Particle size	130 um

TURBULENT MODEL PERFORMANCE		
Model	Avg %	Avg LSE
Torrance	7,60	0,0161
Wilson & Thomas	18,93	0,0413
Dodge & Metzner	4,39	0,0122
Kemblowski & Kolodziejski	54,86	0,0952
New Model	2,98	0,0076
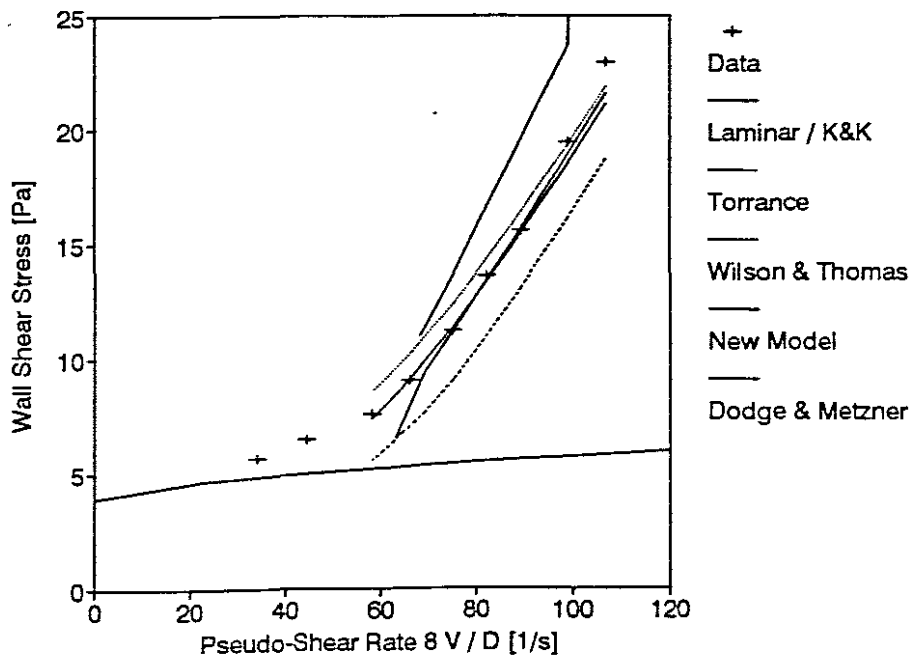
LABORATORY TEST RESULTS

PROJECT: UCT KAOLIN
PROJECT NO: 15000K
DATE: 30-05-96

LABORATORY SAMPLE NO	8	
FIELD REFERENCE NO	RF 3	
DESCRIPTION	LIGHT GREY KAOLIN	
SIEVE ANALYSIS		
% Passing Screens		
106.0mm		
75.0		
53.0		
37.5		
26.5		
19.0		
13.2		
9.5		
4.75		
2.0		
0.85		
0.6		
0.425		
0.3	100	
0.25	99	
0.15	94	
0.075	83	
.0774	84	
.0535	77	
.0217	71	
.0123	61	
.0088	56	
.0063	50	
.0056	47	
.0026	36	
.0024	32	
ATTERBERG LIMITS		
Liquid Limit		
Plasticity Index		
Linear Shrinkage %		
Specific Gravity (est.)		
MOISTURE/DENSITY		
Max. Dry Density (kg/m^3)		
Optimum Moisture Content (%)		
CALIFORNIA		
BEARING RATIO		
100 % Compaction		
98 %		
95 %		
93 %		
90 %		
Maximum Swell (%)		

REMARKS:

PARTICLE SIZE DISTRIBUTION

PROJECT: UCT KAOLIN　　　　**PROJECT NO: 15000**

FIELD SAMPLE NO: RF3

LAB SAMPLE NO: 8

PERCENTAGE RETAINED BY MASS

PERCENTAGE PASSING BY MASS

	FRACTIONS	
COARSE	GRAVEL	0 %
MEDIUM		
FINE		
COARSE	SAND	21 %
MEDIUM		
FINE		
COARSE	SILT	45 %
MEDIUM		
FINE		
CLAY		34 %
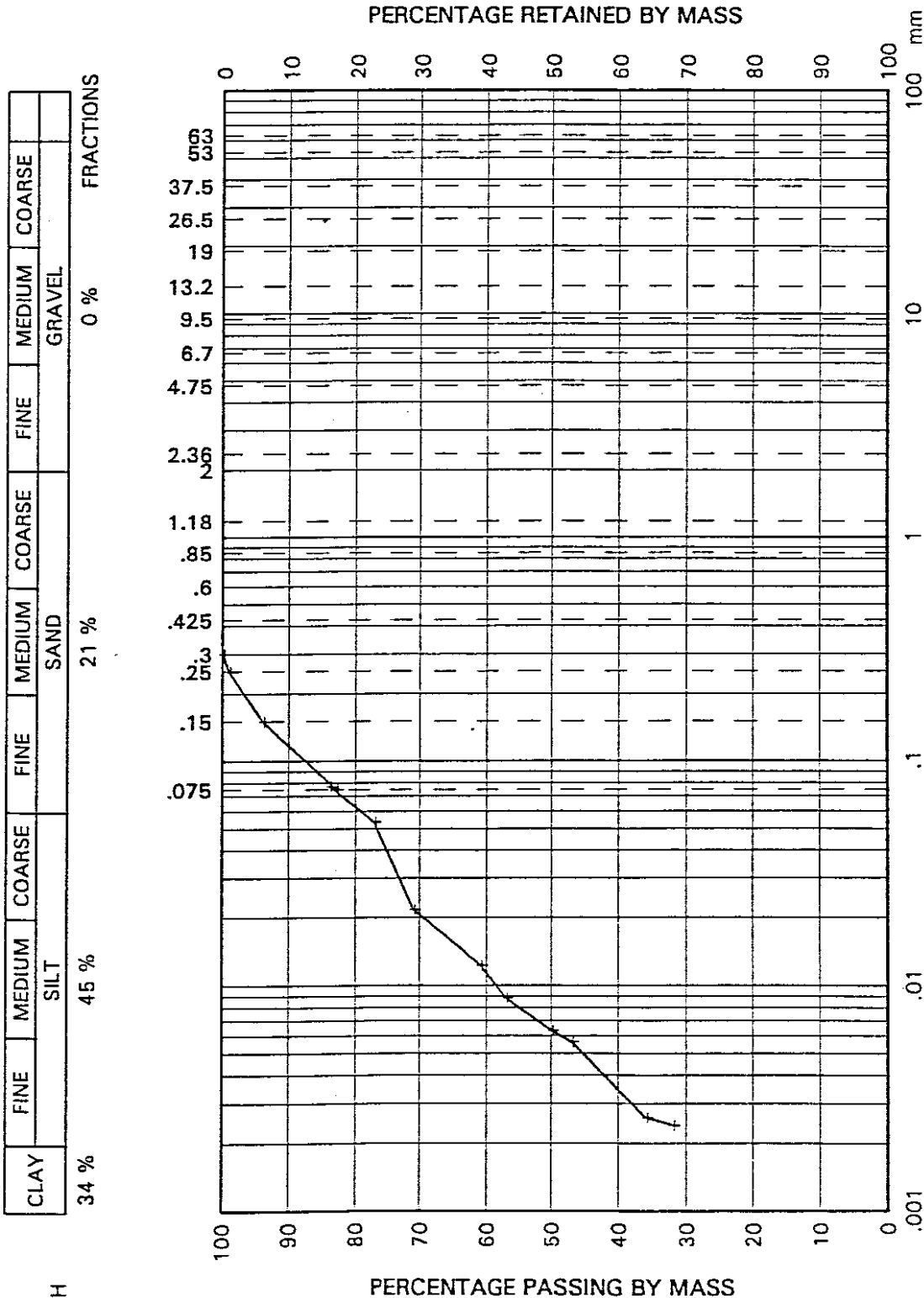
DEPTH

+

TEST: RFMRL30

SLURRY: Water
Kaolin Clay
Rock Flour

CRITICAL VELOCITY: 1.69 m/s

No.	Wall Shear Stress [Pa]	Velocity [m/s]
1.	24.60	2.31
2.	22.37	2.15
3.	21.00	2.00
4.	18.8	1.84
5.	16.80	1.64
6.	15.94	1.48
7.	15.30	1.36
8.	13.90	1.13
9.	12.60	0.94
10.	11.32	0.74
11.	9.62	0.46

DATA FROM TEST	RFMRL30
APPARATUS	
Facility	Mini Rig
Diameter	22 mm
Material	Mixture 1
Operator	GST
Supervisor	PTS

SLURRY PROPERTIES	
Solids Relative Density	2,6000
Slurry Relative Density	1,2127
Volumetric Concentration	13,3 %
Yield Stress .	5,530 Pa
Fluid Consistency Index	0,0194 Pa s ^ n
Flow Behaviour Index	0,9646
Representative Particle size	84 um

TURBULENT MODEL PERFORMANCE		
Model	Avg %	Avg LSE
Torrance	44,71	0,1392
Wilson & Thomas	6,21	0,0248
Dodge & Metzner	20,47	0,0716
Kemblowski & Kolodziejski	217,31	0,4341
New Model	24,26	0,0825

Legend:
+ Data
— Laminar / K&K
— Torrance
— Wilson & Thomas
— New Model
— Dodge & Metzner

X-axis: Pseudo-Shear Rate 8 V / D [1/s]
Y-axis: Wall Shear Stress [Pa]
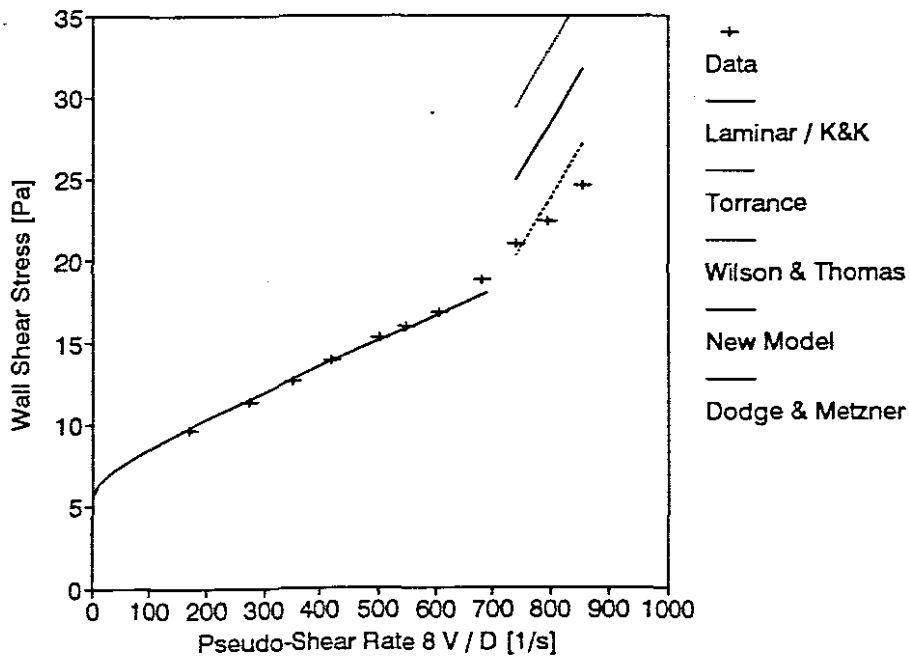
TEST: RFERS30

SLURRY: Water
        Kaolin Clay
        Rock Flour

CRITICAL VELOCITY: 1.87 m/s

No.	Wall Shear Stress [Pa]	Velocity [m/s]
1.	93.29	5.70
2.	76.66	5.12
3.	66.45	4.79
4.	53.79	4.30
5.	41.64	3.69
6.	34.18	3.28
7.	24.34	2.80
8.	15.82	2.24
9.	9.71	1.64
10.	8.58	1.03
11.	7.83	0.66

DATA FROM TEST	RFERS30
APPARATUS	
Facility	East Rig
Diameter	79 mm
Material	Mixture 1
Operator	GST
Supervisor	PTS

SLURRY PROPERTIES	
Solids Relative Density	2,6000
Slurry Relative Density	1,2127
Volumetric Concentration	13,3 %
Yield Stress	5,530 Pa
Fluid Consistency Index	0,0194 Pa s^n
Flow Behaviour Index	0,9646
Representative Particle size	84 um

TURBULENT MODEL PERFORMANCE		
Model	Avg %	Avg LSE
Torrance	29,35	0,0466
Wilson & Thomas	12,13	0,0203
Dodge & Metzner	23,40	0,0374
Kemblowski & Kolodziejski	33,13	0,0503
New Model	21,81	0,0354
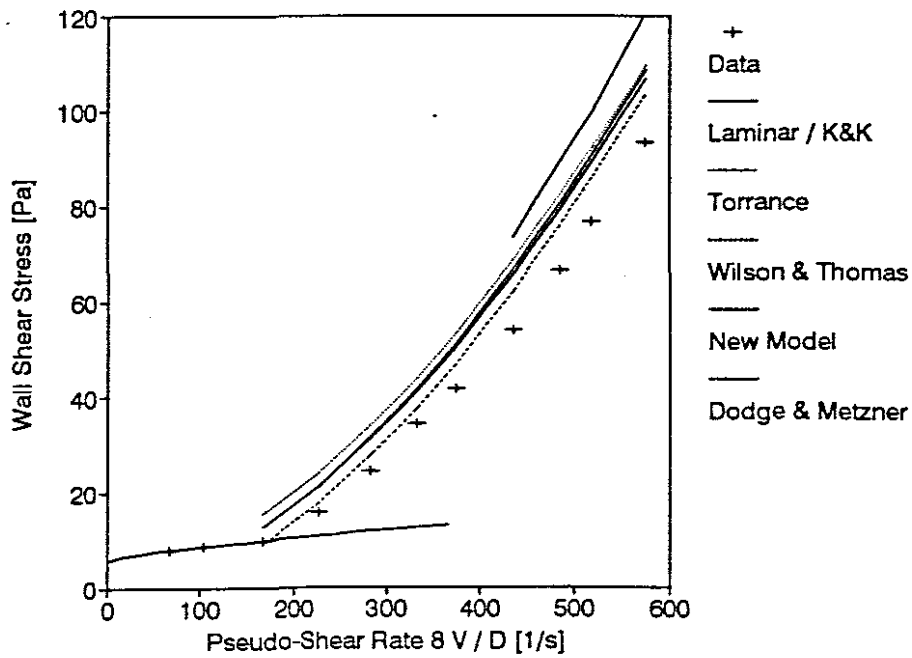
TEST: RFERM30

SLURRY: Water
          Kaolin Clay
          Rock Flour

CRITICAL VELOCITY: 2.26 m/s

No.	Wall Shear Stress [Pa]	Velocity [m/s]
1.	77.82	6.02
2.	62.69	5.26
3.	45.36	4.46
4.	37.51	4.10
5.	29.93	3.70
6.	23.89	3.33
7.	18.06	2.86
8.	14.09	2.65
9.	11.22	2.38
10.	10.00	2.16
11.	7.81	1.70

DATA FROM TEST	RFERM30
APPARATUS	
Facility	East Rig
Diameter	141 mm
Material	Mixture 1
Operator	GST
Supervisor	PTS

SLURRY PROPERTIES	
Solids Relative Density	2,6000
Slurry Relative Density	1,2127
Volumetric Concentration	13,3 %
Yield Stress .	5,530 Pa
Fluid Consistency Index	0,0194 Pa s ^ n
Flow Behaviour Index	0,9646
Representative Particle size	84 um

TURBULENT MODEL PERFORMANCE		
Model	Avg %	Avg LSE
Torrance	58,86	0,0771
Wilson & Thomas	37,03	0,0520
Dodge & Metzner	53,61	0,0711
Kemblowski & Kolodziejski	73,91	0,0908
New Model	50,53	0,0680
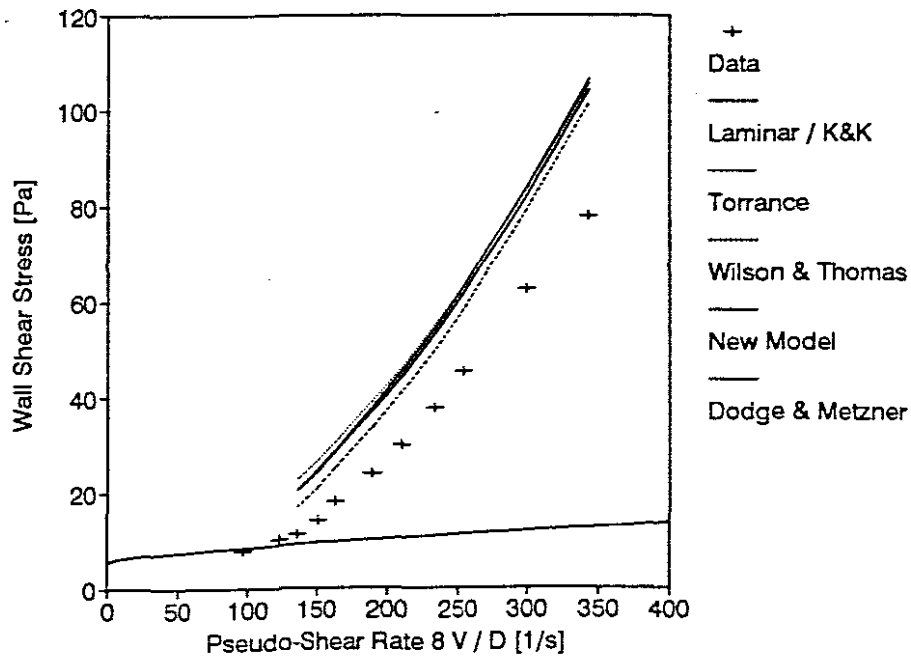
TEST: RFERL30

SLURRY: Water
　　　　Kaolin Clay
　　　　Rock Flour

CRITICAL VELOCITY: 1.42 m/s

No.	Wall Shear Stress [Pa]	Velocity [m/s]
1.	26.58	2.71
2.	22.94	2.62
3.	20.00	2.53
4.	17.60	2.36
5.	15.39	2.15
6.	11.97	1.86
7.	10.30	1.59
8.	8.65	1.22
9.	6.89	0.92

DATA FROM TEST	RFERL30
APPARATUS	
Facility	East Rig
Diameter	207 mm
Material	Mixture 1
Operator	GST
Supervisor	PTS

SLURRY PROPERTIES	
Solids Relative Density	2,6000
Slurry Relative Density	1,1759
Volumetric Concentration	11,0 %
Yield Stress ,	3,910 Pa
Fluid Consistency Index	0,0105 Pa s ^{n}
Flow Behaviour Index	0,9720
Representative Particle size	130 um

TURBULENT MODEL PERFORMANCE		
Model	Avg %	Avg LSE
Torrance	8,70	0,0217
Wilson & Thomas	28,77	0,0682
Dodge & Metzner	16,09	0,0419
Kemblowski & Kolodziejski	34,14	0,0763
New Model	15,48	0,0350
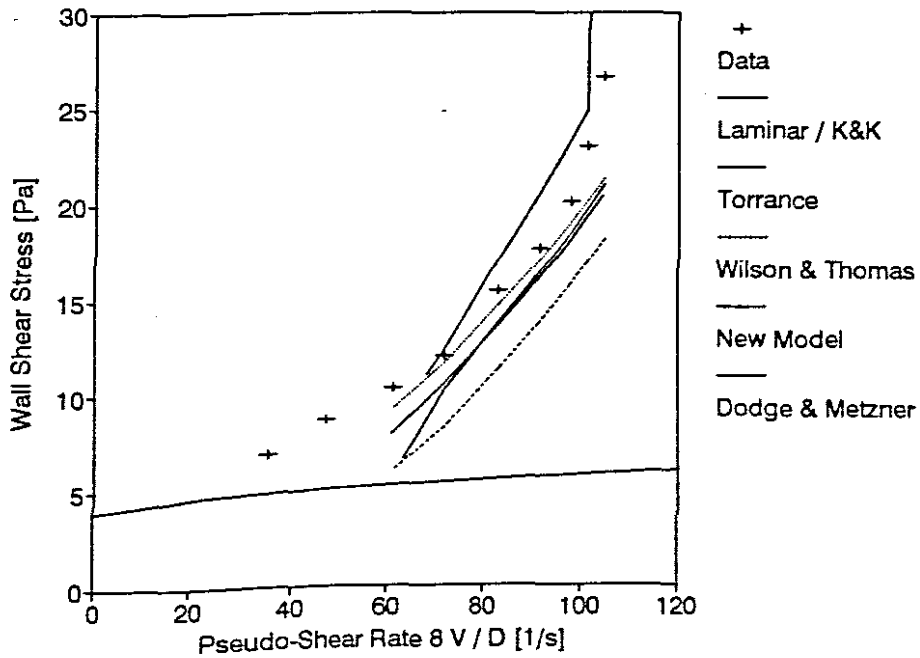
Legend:
+ Data
— Laminar / K&K
— Torrance
—— Wilson & Thomas
— New Model
— Dodge & Metzner

Wall Shear Stress [Pa] vs Pseudo-Shear Rate 8 V / D [1/s]

LABORATORY TEST RESULTS

PROJECT: UCT KAOLIN
PROJECT NO: 15000K
DATE: 30-05-96

LABORATORY SAMPLE NO	1	
FIELD REFERENCE NO	SAND 1	
DESCRIPTION	LIGHT GREY KAOLIN	
SIEVE ANALYSIS		
% Passing Screens		
106.0mm		
75.0		
53.0		
37.5		
26.5		
19.0		
13.2		
9.5		
4.75		
2.0		
0.85		
0.6		
0.425	100	
0.3	99	
0.25	98	
0.15	88	
0.075	60	
.0825	68	
.0574	58	
.0229	51	
.0128	45	
.0091	43	
.0065	39	
.0058	37	
.0026	27	
.0024	26	
ATTERBERG LIMITS		
Liquid Limit		
Plasticity Index		
Linear Shrinkage %		
Specific Gravity (est.)		
MOISTURE/DENSITY		
Max. Dry Density (kg/m^3)		
Optimum Moisture Content (%)		
CALIFORNIA		
BEARING RATIO		
100 % Compaction		
98 %		
95 %		
93 %		
90 %		
Maximum Swell (%)		

REMARKS:

PARTICLE SIZE DISTRIBUTION

PROJECT: UCT KAOLIN   **PROJECT NO: 15000**

FIELD SAMPLE NO: SAND 1

LAB SAMPLE NO: 1

PERCENTAGE RETAINED BY MASS

PERCENTAGE PASSING BY MASS

		FRACTIONS	
COARSE	GRAVEL	0 %	
MEDIUM			
FINE			
COARSE	SAND	41 %	
MEDIUM			
FINE			
COARSE	SILT	33 %	
MEDIUM			
FINE			
CLAY		27 %	

DEPTH

+
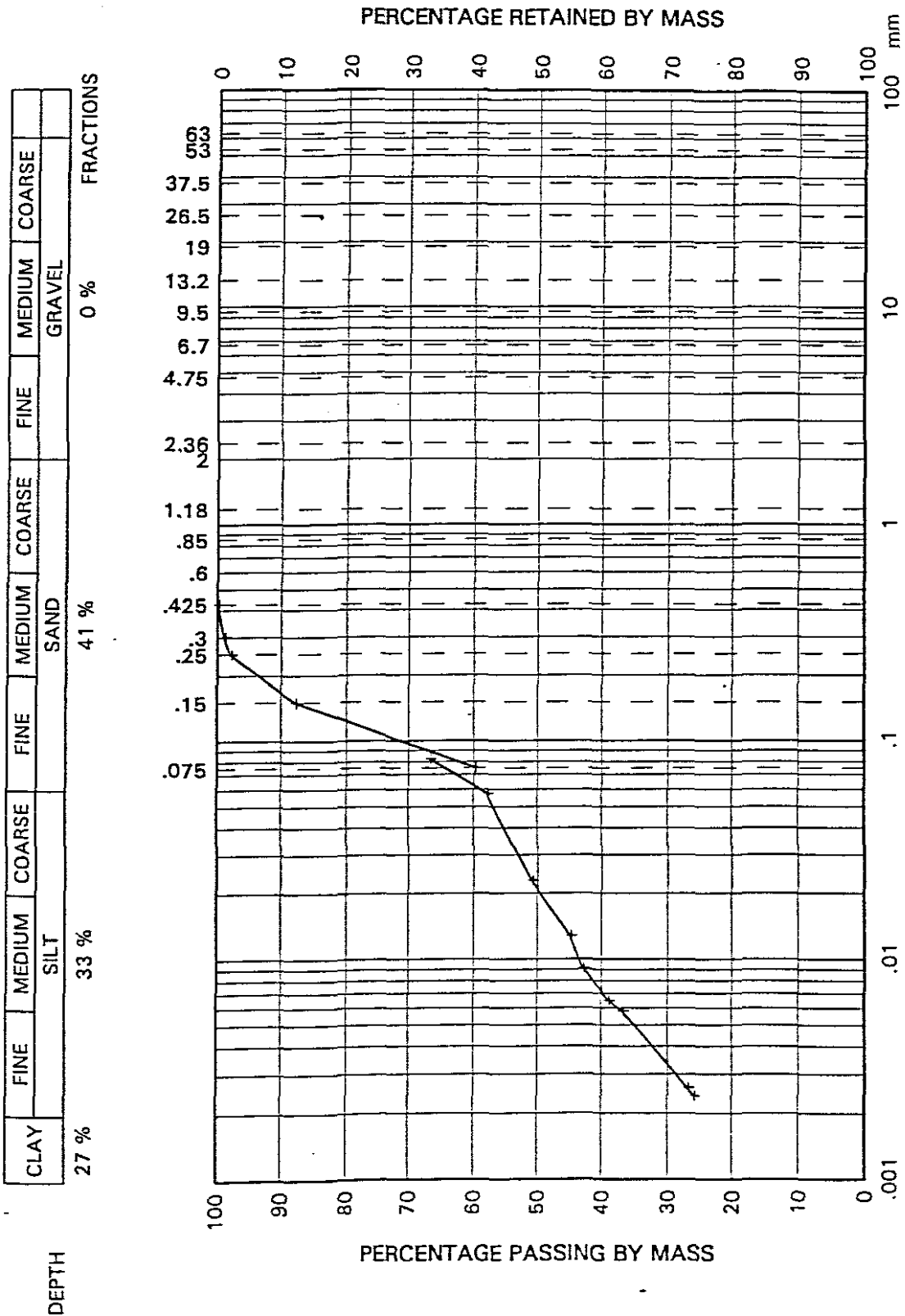
TEST: SMRL10

SLURRY: Water
　　　　Kaolin Clay
　　　　Rock Flour
　　　　Silica Sand

CRITICAL VELOCITY: 1.69 m/s

No.	Wall Shear Stress [Pa]	Velocity [m/s]
1.	22.78	2.23
2.	19.86	2.10
3.	16.87	1.96
4.	14.99	1.80
5.	13.57	1.70
6.	12.24	1.51
7.	11.85	1.29
8.	11.52	1.13
9.	11.00	0.88
10.	10.41	0.70
11.	9.97	0.56
12.	9.27	0.39

DATA FROM TEST	SMRL10
APPARATUS	
Facility	Mini Rig
Diameter	22 mm
Material	Mixture 2
Operator	GST
Supervisor	PTS

SLURRY PROPERTIES	
Solids Relative Density	2,6500
Slurry Relative Density	1,2717
Volumetric Concentration	16,5 %
Yield Stress ·	5,820 Pa
Fluid Consistency Index	0,1413 Pa s^n
Flow Behaviour Index	0,5577
Representative Particle size	137 um

TURBULENT MODEL PERFORMANCE		
Model	Avg %	Avg LSE
Torrance	7,73	0,0267
Wilson & Thomas	21,51	0,0599
Dodge & Metzner	65,68	0,1441
Kemblowski & Kolodziejski	324,83	0,3497
New Model	13,74	0,0318
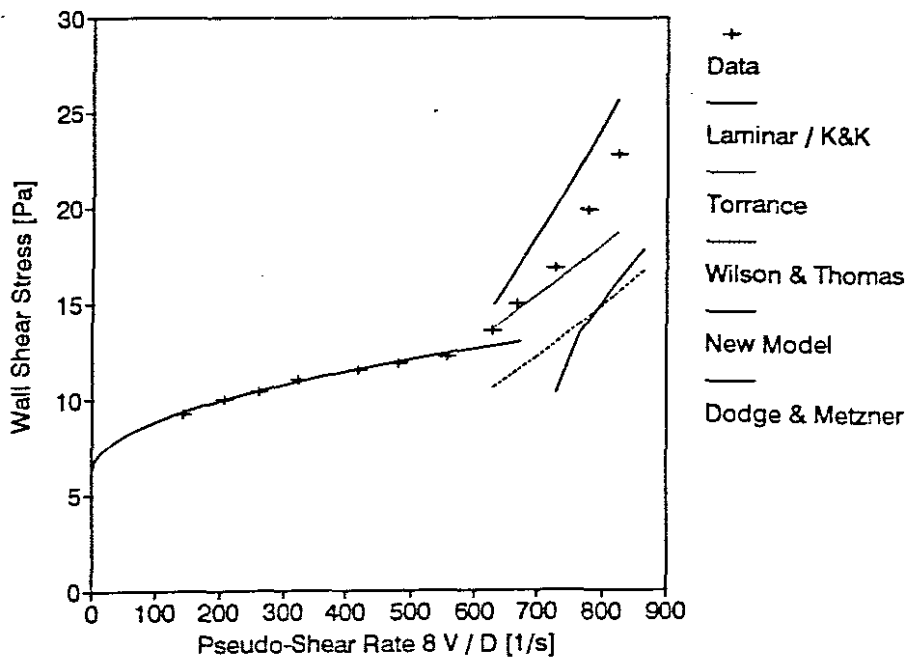
TEST: SERS10

SLURRY: Water
Kaolin Clay
Rock Flour
Silica Sand

CRITICAL VELOCITY: 2.10 m/s

No.	Wall Shear Stress [Pa]	Velocity [m/s]
1.	95.43	5.42
2.	86.31	5.15
3.	76.92	4.86
4.	65.80	4.55
5.	55.38	4.19
6.	46.20	3.73
7.	37.72	3.27
8.	26.76	2.83
9.	17.03	2.24
10.	10.42	1.57
11.	9.10	0.99
12.	8.76	0.65

DATA FROM TEST	SERS10
APPARATUS	
Facility	East Rig
Diameter	79 mm
Material	Mixture 2
Operator	GST
Supervisor	PTS

SLURRY PROPERTIES	
Solids Relative Density	2,6500
Slurry Relative Density	1,2717
Volumetric Concentration	16,5 %
Yield Stress	5,820 Pa
Fluid Consistency Index	0,1413 Pa s^n
Flow Behaviour Index	0,5577
Representative Particle size	137 um

TURBULENT MODEL PERFORMANCE		
Model	Avg %	Avg LSE
Torrance	35,49	0,0774
Wilson & Thomas	38,46	0,0807
Dodge & Metzner	31,85	0,0664
Kemblowski & Kolodziejski	12,99	0,0336
New Model	8,01	0,0135

Legend:
+ Data
Laminar / K&K
Torrance
Wilson & Thomas
New Model
Dodge & Metzner

X-axis: Pseudo-Shear Rate 8 V / D [1/s]
Y-axis: Wall Shear Stress [Pa]
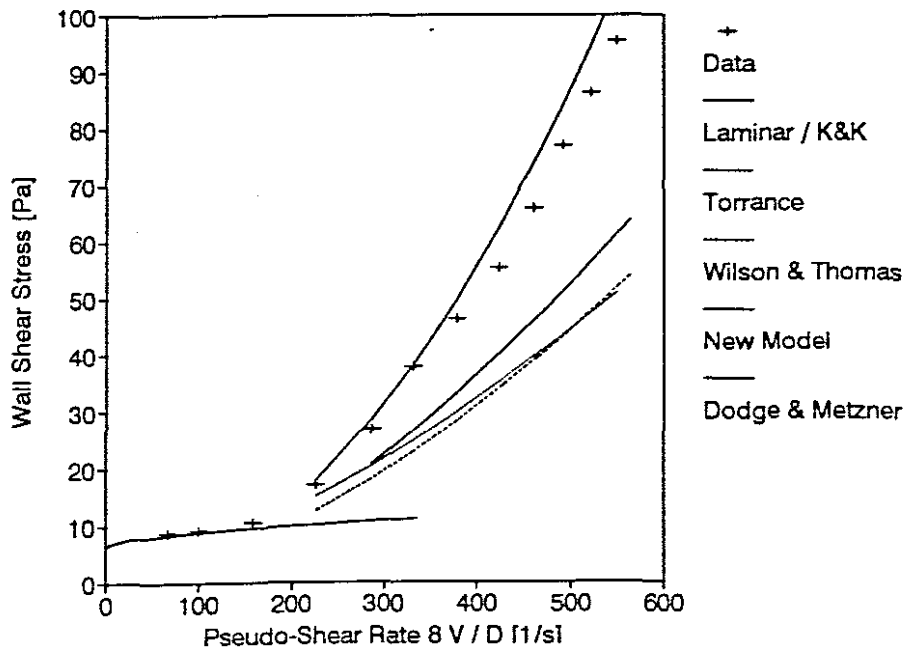
TEST: SERM10

SLURRY: Water
Kaolin Clay
Rock Flour
Silica Sand

CRITICAL VELOCITY: 2.31 m/s

No.	Wall Shear Stress [Pa]	Velocity [m/s]
1.	79.91	5.40
2.	69.15	5.09
3.	59.87	4.75
4.	48.00	4.26
5.	39.42	3.87
6.	31.47	3.43
7.	23.62	2.99
8.	18.18	2.65
9.	15.26	2.46
10.	12.27	2.29
11.	9.54	1.86
12.	8.26	1.41

DATA FROM TEST	SERM10
APPARATUS	
Facility	East Rig
Diameter	141 mm
Material	Mixture 2
Operator	GST
Supervisor	PTS

SLURRY PROPERTIES	
Solids Relative Density	2,6500
Slurry Relative Density	1,2717
Volumetric Concentration	16,5 %
Yield Stress .	5,820 Pa
Fluid Consistency Index	0,1413 Pa s^n
Flow Behaviour Index	0,5577
Representative Particle size	137 um

TURBULENT MODEL PERFORMANCE		
Model	Avg %	Avg LSE
Torrance	24,65	0,0561
Wilson & Thomas	24,89	0,0521
Dodge & Metzner	12,77	0,0277
Kemblowski & Kolodziejski	32,69	0,0549
New Model	16,35	0,0249

Legend:
+ Data
— Laminar / K&K
— Torrance
— Wilson & Thomas
— New Model
— Dodge & Metzner

X axis: Pseudo-Shear Rate 8 V / D [1/s]
Y axis: Wall Shear Stress [Pa]
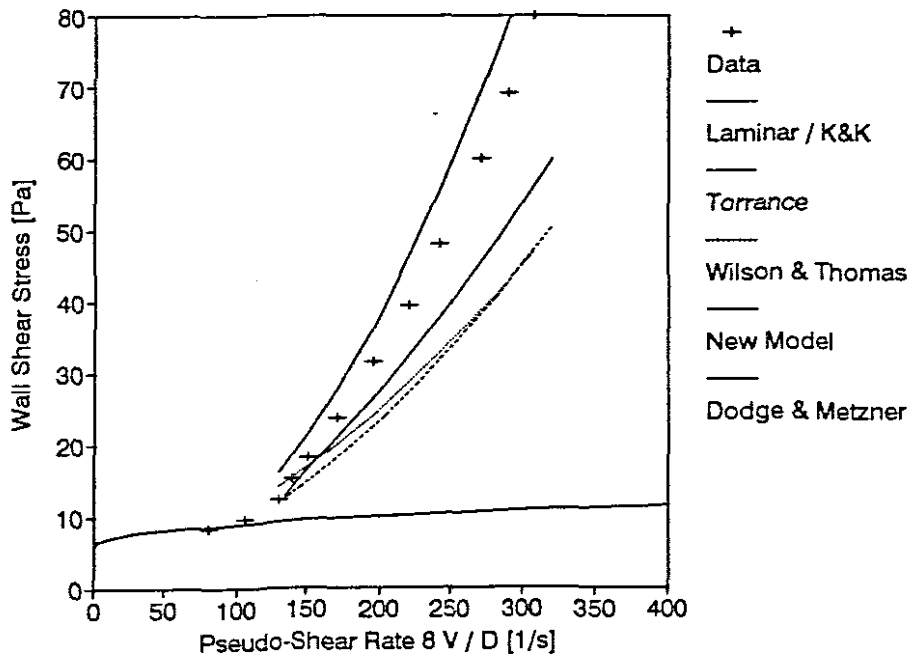
TEST: SERL10

SLURRY: Water
Kaolin Clay
Rock Flour
Silica Sand

CRITICAL VELOCITY: 1.27 m/s

No.	Wall Shear Stress [Pa]	Velocity [m/s]
1.	22.54	2.69
2.	20.30	2.63
3.	17.85	2.47
4.	15.10	2.23
5.	12.59	1.94
6.	10.74	1.63
7.	9.06	1.22
8.	7.75	0.73

DATA FROM TEST	SERL10
APPARATUS	
Facility	East Rig
Diameter	207 mm
Material	Mixture 2
Operator	GST
Supervisor	PTS

SLURRY PROPERTIES	
Solids Relative Density	2,6500
Slurry Relative Density	1,2717
Volumetric Concentration	16,5 %
Yield Stress .	5,820 Pa
Fluid Consistency Index	0,1413 Pa s ^{n}
Flow Behaviour Index	0,5577
Representative Particle size	137 um

TURBULENT MODEL PERFORMANCE		
Model	Avg %	Avg LSE
Torrance	18,05	0,0404
Wilson & Thomas	30,27	0,0697
Dodge & Metzner	26,18	0,0774
Kemblowski & Kolodziejski	232,41	0,2295
New Model	16,85	0,0549

LABORATORY TEST RESULTS

PROJECT: UCT KAOLIN
PROJECT NO: 15000K
DATE: 30-05-96

LABORATORY SAMPLE NO	2	
FIELD REFERENCE NO	SAND 2	
DESCRIPTION	LIGHT GREY KAOLIN	
SIEVE ANALYSIS		
% Passing Screens		
106.0mm		
75.0		
53.0		
37.5		
26.5		
19.0		
13.2		
9.5		
4.75		
2.0		
0.85		
0.6		
0.425	100	
0.3	99	
0.25	98	
0.15	83	
0.075	51	
.0867	55	
.0594	50	
.0231	45	
.0129	42	
.0092	40	
.0066	35	
.0058	34	
.0026	26	
.0024	24	
ATTERBERG LIMITS		
Liquid Limit		
Plasticity Index		
Linear Shrinkage %		
Specific Gravity (est.)		
MOISTURE/DENSITY		
Max. Dry Density (kg/m^3)		
Optimum Moisture Content (%)		
CALIFORNIA BEARING RATIO		
100 % Compaction		
98 %		
95 %		
93 %		
90 %		
Maximum Swell (%)		

REMARKS:

PARTICLE SIZE DISTRIBUTION

PROJECT: UCT KAOLIN   **PROJECT NO: 15000**

FIELD SAMPLE NO: SAND 2

LAB SAMPLE NO: 2

PERCENTAGE RETAINED BY MASS

PERCENTAGE PASSING BY MASS

DEPTH
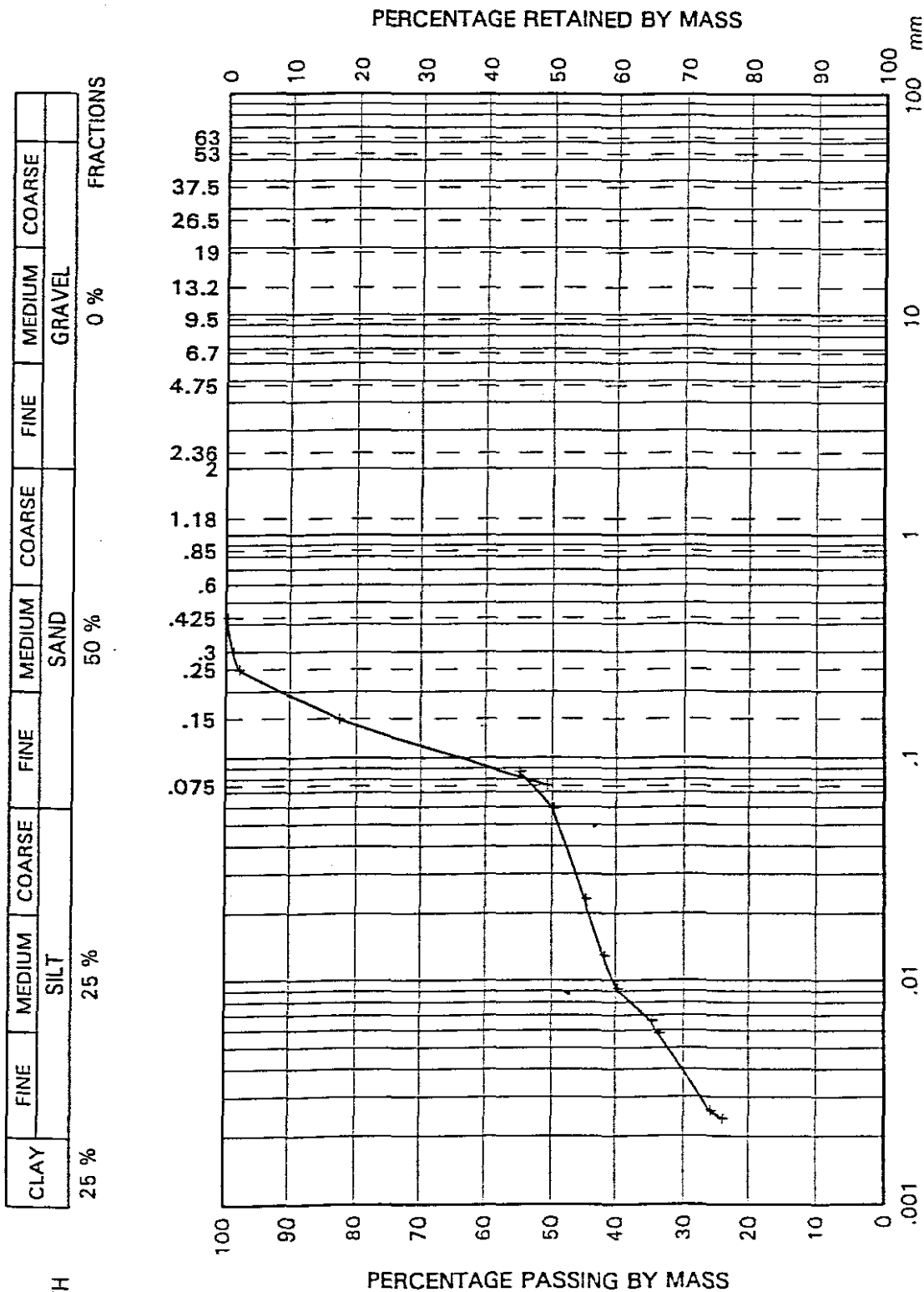
TEST: SMRL20

SLURRY: Water
          Kaolin Clay
          Rock Flour
          Silica Sand

CRITICAL VELOCITY: 1.66 m/s

No.	Wall Shear Stress [Pa]	Velocity [m/s]
1.	21.65	2.12
2.	19.94	2.00
3.	18.03	1.90
4.	16.21	1.79
5.	15.00	1.69
6.	14.81	1.62
7.	13.98	1.43
8.	13.55	1.28
9.	13.22	1.16
10.	13.04	1.07
11.	12.46	0.97
12.	11.80	0.81
13.	13.39	0.71

DATA FROM TEST	SMRL20
APPARATUS	
Facility	Mini Rig
Diameter	22 mm
Material	Mixture 2
Operator	GST
Supervisor	PTS

SLURRY PROPERTIES	
Solids Relative Density	2,6500
Slurry Relative Density	1,3205
Volumetric Concentration	19,4 %
Yield Stress	5,480 Pa
Fluid Consistency Index	0,1239 Pa s ^{n}
Flow Behaviour Index	0,6363
Representative Particle size	159 um

TURBULENT MODEL PERFORMANCE		
Model	Avg %	Avg LSE
Torrance	6,16	0,0194
Wilson & Thomas	13,11	0,0414
Dodge & Metzner	7,03	0,0288
Kemblowski & Kolodziejski	283,85	0,3888
New Model	13,45	0,0369
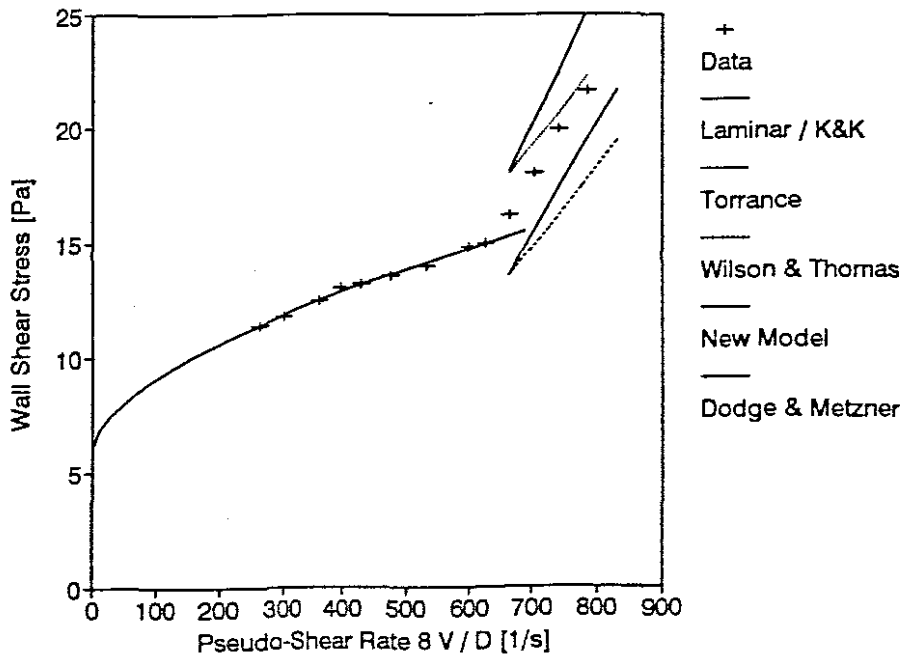
TEST: SERS20

SLURRY: Water
Kaolin Clay
Rock Flour
Silica Sand

CRITICAL'VELOCITY: 2.02 m/s

No.	Wall Shear Stress [Pa]	Velocity [m/s]
1.	98.13	5.37
2.	89.52	5.07
3.	76.39	4.75
4.	67.33	4.37
5.	51.14	3.79
6.	46.64	3.52
7.	32.99	3.01
8.	23.49	2.47
9.	15.33	2.02
10.	11.85	1.46
11.	10.68	0.96

DATA FROM TEST	SERS20
APPARATUS	
Facility	East Rig
Diameter	79 mm
Material	Mixture 2
Operator	GST
Supervisor	PTS

SLURRY PROPERTIES	
Solids Relative Density	2,6500
Slurry Relative Density	1,3205
Volumetric Concentration	19,4 %
Yield Stress	5,480 Pa
Fluid Consistency Index	0,1239 Pa s ^{n}
Flow Behaviour Index	0,6363
Representative Particle size	159 um

TURBULENT MODEL PERFORMANCE		
Model	Avg %	Avg LSE
Torrance	22,75	0,0471
Wilson & Thomas	28,06	0,0547
Dodge & Metzner	17,50	0,0319
Kemblowski & Kolodziejski	21,53	0,0388
New Model	7,01	0,0128

Legend:
+ Data
— Laminar / K&K
— Torrance
— Wilson & Thomas
— New Model
— Dodge & Metzner

Y-axis: Wall Shear Stress [Pa]
X-axis: Pseudo-Shear Rate 8 V / D [1/s]
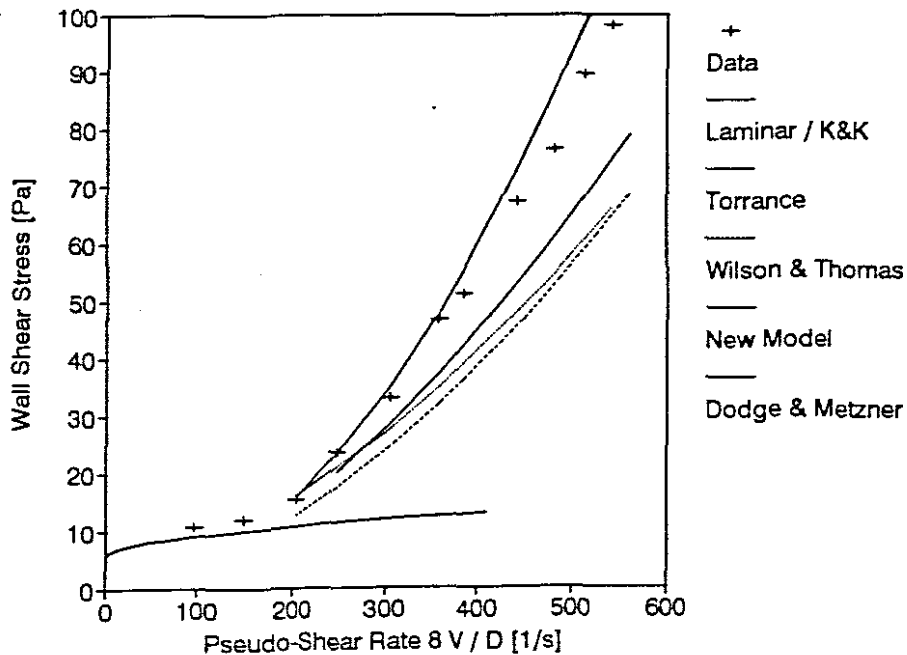
TEST: SERM20

SLURRY: Water
           Kaolin Clay
           Rock Flour
           Silica Sand

CRITICAL VELOCITY: 2.17 m/s

No.	Wall Shear Stress [Pa]	Velocity [m/s]
1.	79.66	5.23
2.	70.60	4.92
3.	59.76	4.54
4.	51.51	4.11
5.	43.55	3.83
6.	36.77	3.52
7.	31.59	3.26
8.	25.62	2.92
9.	18.90	2.61
10.	13.11	2.17
11.	8.89	1.76
12.	8.73	1.50

DATA FROM TEST	SERM20
APPARATUS	
Facility	East Rig
Diameter	141 mm
Material	Mixture 2
Operator	GST
Supervisor	PTS

SLURRY PROPERTIES	
Solids Relative Density	2,6500
Slurry Relative Density	1,3205
Volumetric Concentration	19,4 %
Yield Stress	5,480 Pa
Fluid Consistency Index	0,1239 Pa s^n
Flow Behaviour Index	0,6363
Representative Particle size	159 um

TURBULENT MODEL PERFORMANCE		
Model	Avg %	Avg LSE
Torrance	17,99	0,0361
Wilson & Thomas	14,95	0,0292
Dodge & Metzner	6,55	0,0121
Kemblowski & Kolodziejski	33,64	0,0525
New Model	12,42	0,0195
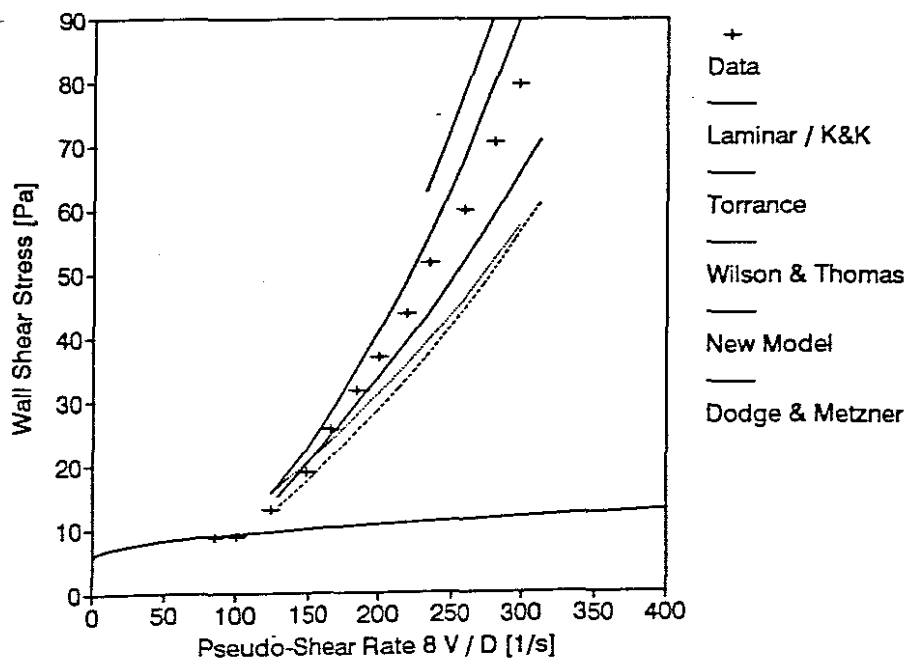
TEST: SERL20

SLURRY: Water
Kaolin Clay
Rock Flour
Silica Sand

CRITICAL VELOCITY: 1.55 m/s

No.	Wall Shear Stress [Pa]	Velocity [m/s]
1.	21.20	2.72
2.	18.51	2.50
3.	14.90	2.17
4.	11.50	1.83
5.	8.97	1.29
6.	8.01	0.90

DATA FROM TEST	SERL20
APPARATUS	
Facility	East Rig
Diameter	207 mm
Material	Mixture 2
Operator	GST
Supervisor	PTS

SLURRY PROPERTIES	
Solids Relative Density	2,6500
Slurry Relative Density	1,3205
Volumetric Concentration	19,4 %
Yield Stress ·	5,480 Pa
Fluid Consistency Index	0,1239 Pa s ^{n}
Flow Behaviour Index	0,6363
Representative Particle size	159 um

TURBULENT MODEL PERFORMANCE		
Model	Avg %	Avg LSE
Torrance	3,65	0,0116
Wilson & Thomas	19,51	0,0629
Dodge & Metzner	10,72	0,0390
Kemblowski & Kolodziejski	244,33	0,3577
New Model	4,90	0,0158
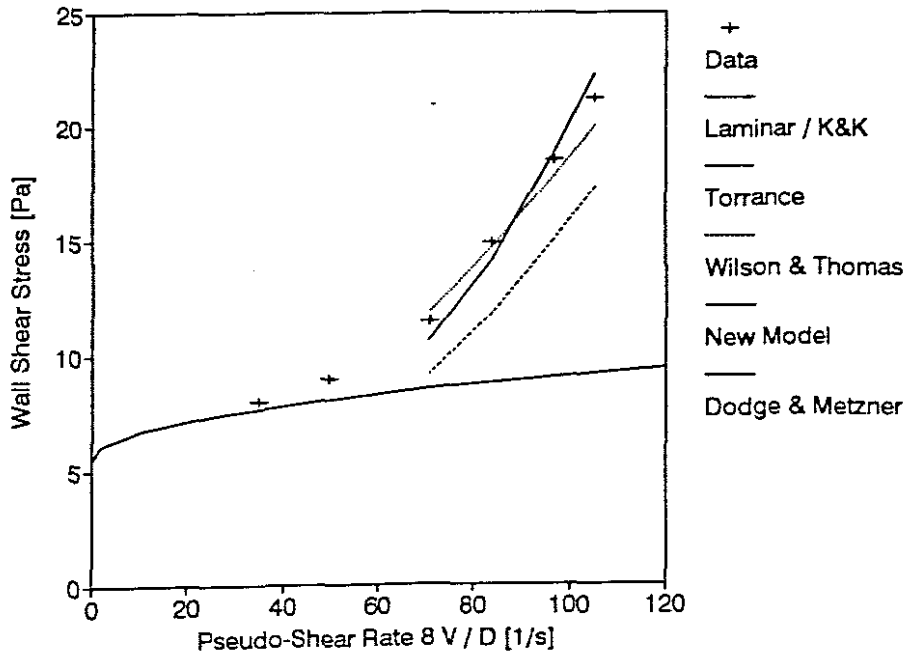
LABORATORY TEST RESULTS

PROJECT: UCT KAOLIN
PROJECT NO: 15000K
DATE: 30-05-96

LABORATORY SAMPLE NO	3	
FIELD REFERENCE NO	S 3	
DESCRIPTION	LIGHT GREY KAOLIN	
SIEVE ANALYSIS		
% Passing Screens		
106.0mm		
75.0		
53.0		
37.5		
26.5		
19.0		
13.2		
9.5		
4.75		
2.0		
0.85		
0.6		
0.425	100	
0.3	99	
0.25	98	
0.15	80	
0.075	41	
.0896	47	
.0613	40	
.0239	37	
.0132	34	
.0094	32	
.0067	29	
.0059	29	
.0027	23	
.0025	21	
ATTERBERG LIMITS		
Liquid Limit		
Plasticity Index		
Linear Shrinkage %		
Specific Gravity (est.)		
MOISTURE/DENSITY		
Max. Dry Density (kg/m^3)		
Optimum Moisture Content (%)		
CALIFORNIA		
BEARING RATIO		
100 % Compaction		
98 %		
95 %		
93 %		
90 %		
Maximum Swell (%)		
REMARKS:		

PARTICLE SIZE DISTRIBUTION

PROJECT: UCT KAOLIN   **PROJECT NO: 15000**

FIELD SAMPLE NO: S3

LAB SAMPLE NO: 3

PERCENTAGE RETAINED BY MASS

PERCENTAGE PASSING BY MASS

DEPTH

+

TEST: SMRL30

SLURRY: Water
Kaolin Clay
Rock Flour
Silica Sand

CRITICAL VELOCITY: 1.68 m/s

No.	Wall Shear Stress [Pa]	Velocity [m/s]
1.	22.78	2.02
2.	20.87	1.95
3.	19.09	1.82
4.	17.60	1.73
5.	16.18	1.57
6.	15.48	1.35
7.	14.61	1.05
8.	13.96	0.81
9.	13.18	0.61
10.	12.36	0.44
11.	11.60	0.28
12.	10.47	0.13

DATA FROM TEST	SMRL30
APPARATUS	
Facility	Mini Rig
Diameter	22 mm
Material	Mixture 2
Operator	GST
Supervisor	PTS

SLURRY PROPERTIES	
Solids Relative Density	2,6500
Slurry Relative Density	1,3937
Volumetric Concentration	23,9 %
Yield Stress ·	8,020 Pa
Fluid Consistency Index	0,1350 Pa s ^ n
Flow Behaviour Index	0,5911
Representative Particle size	170 um

TURBULENT MODEL PERFORMANCE		
Model	Avg %	Avg LSE
Torrance	7,59	0,0315
Wilson & Thomas	19,54	0,0818
Dodge & Metzner	64,41	0,2138
Kemblowski & Kolodziejski	242,87	0,4631
New Model	8,63	0,0318
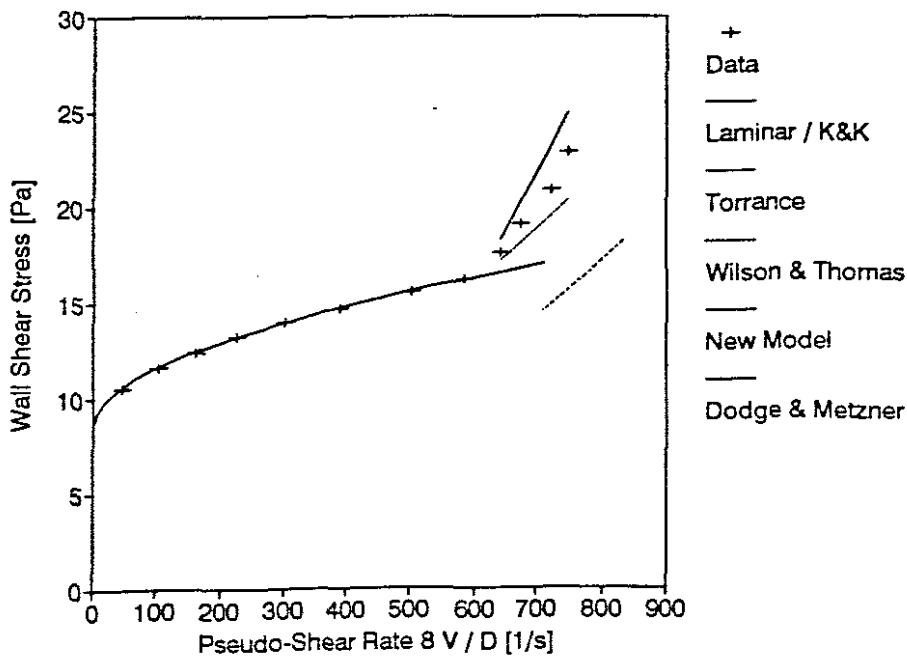
TEST: SERS30

SLURRY: Water
Kaolin Clay
Rock Flour
Silica Sand

CRITICAL VELOCITY: 2.10 m/s

No.	Wall Shear Stress [Pa]	Velocity [m/s]
1.	101.92	5.19
2.	77.39	4.53
3.	64.57	4.24
4.	54.48	3.88
5.	41.09	3.33
6.	29.37	2.75
7.	16.10	1.93
8.	12.17	1.01

DATA FROM TEST	SERS30
APPARATUS	
Facility	East Rig
Diameter	79 mm
Material	Mixture 2
Operator	GST
Supervisor	PTS

SLURRY PROPERTIES	
Solids Relative Density	2,6500
Slurry Relative Density	1,3937
Volumetric Concentration	23,9 %
Yield Stress ·	8,020 Pa
Fluid Consistency Index	0,1350 Pa s^n
Flow Behaviour Index	0,5911
Representative Particle size	170 um

TURBULENT MODEL PERFORMANCE		
Model	Avg %	Avg LSE
Torrance	28,37	0,0736
Wilson & Thomas	34,70	0,0830
Dodge & Metzner	24,24	0,0545
Kemblowski & Kolodziejski	45,72	0,0798
New Model	9,97	0,0192

Legend:
+ Data
— Laminar / K&K
— Torrance
— Wilson & Thomas
— New Model
— Dodge & Metzner

Y-axis: Wall Shear Stress [Pa]
X-axis: Pseudo-Shear Rate 8 V / D [1/s]
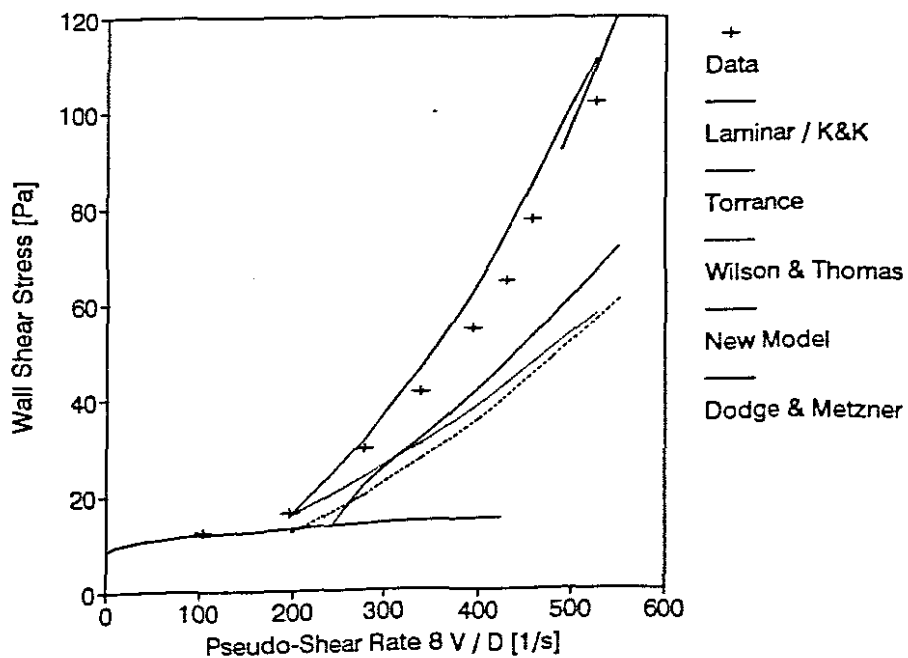
TEST: SERM30

SLURRY: Water
       Kaolin Clay
       Rock Flour
       Silica Sand

CRITICAL VELOCITY: 2.13 m/s

No.	Wall Shear Stress [Pa]	Velocity [m/s]
1.	79.66	5.15
2.	70.44	4.85
3.	60.32	4.49
4.	53.04	4.22
5.	44.58	3.82
6.	36.25	3.40
7.	26.89	2.93
8.	21.44	2.60
9.	12.76	1.94
10.	11.98	1.64

DATA FROM TEST	SERM30
APPARATUS	
Facility	East Rig
Diameter	141 mm
Material	Mixture 2
Operator	GST
Supervisor	PTS

SLURRY PROPERTIES	
Solids Relative Density	2,6500
Slurry Relative Density	1,3937
Volumetric Concentration	23,9 %
Yield Stress ,	8,020 Pa
Fluid Consistency Index	0,1350 Pa s ^{n}
Flow Behaviour Index	0,5911
Representative Particle size	170 um

TURBULENT MODEL PERFORMANCE		
Model	Avg %	Avg LSE
Torrance	24,10	0,0504
Wilson & Thomas	23,21	0,0472
Dodge & Metzner	12,50	0,0234
Kemblowski & Kolodziejski	34,71	0,0594
New Model	14,88	0,0234

Legend:
+ Data
— Laminar / K&K
— Torrance
— Wilson & Thomas
— New Model
— Dodge & Metzner
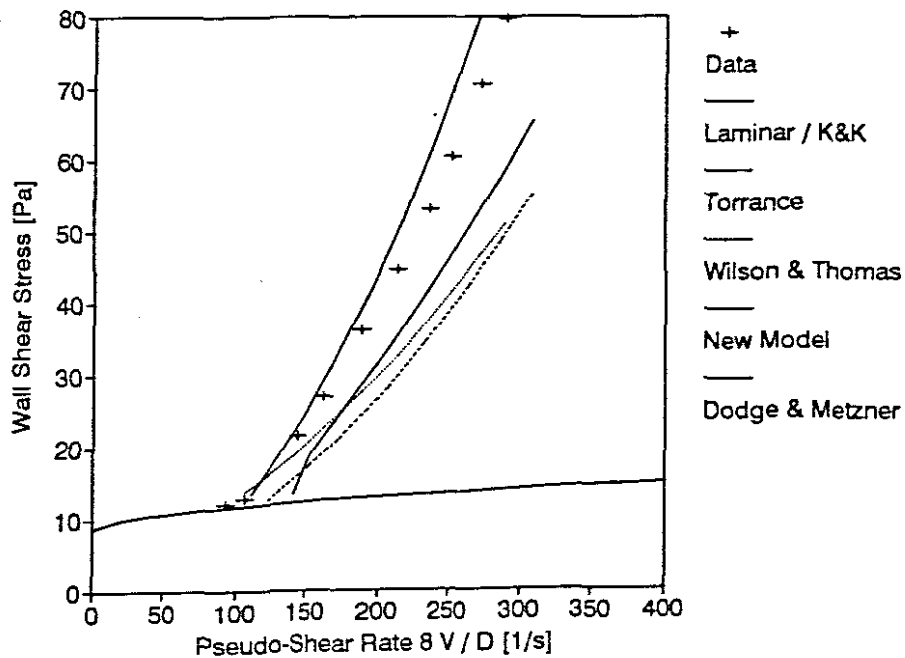
TEST: SERL30

SLURRY: Water
        Kaolin Clay
        Rock Flour
        Silica Sand

CRITICAL VELOCITY: 1.27 m/s

No.	Wall Shear Stress [Pa]	Velocity [m/s]
1.	20.94	2.56
2.	17.96	2.29
3.	14.90	1.87
4.	12.36	1.48
5.	11.05	1.19
6.	10.42	0.94

DATA FROM TEST	SERL30
APPARATUS	
Facility	East Rig
Diameter	207 mm
Material	Mixture 2
Operator	GST
Supervisor	PTS

SLURRY PROPERTIES	
Solids Relative Density	2,6500
Slurry Relative Density	1,3937
Volumetric Concentration	23,9 %
Yield Stress ·	8,020 Pa
Fluid Consistency Index	0,1350 Pa s ^{n}
Flow Behaviour Index	0,5911
Representative Particle size	170 um

TURBULENT MODEL PERFORMANCE		
Model	Avg %	Avg LSE
Torrance	12,34	0,0383
Wilson & Thomas	27,74	0,0943
Dodge & Metzner	27,07	0,0944
Kemblowski & Kolodziejski	241,05	0,3551
New Model	17,54	0,0817

Legend:
+ Data
— Laminar / K&K
— Torrance
— Wilson & Thomas
— New Model
— Dodge & Metzner

Y-axis: Wall Shear Stress [Pa]
X-axis: Pseudo-Shear Rate 8 V / D [1/s]
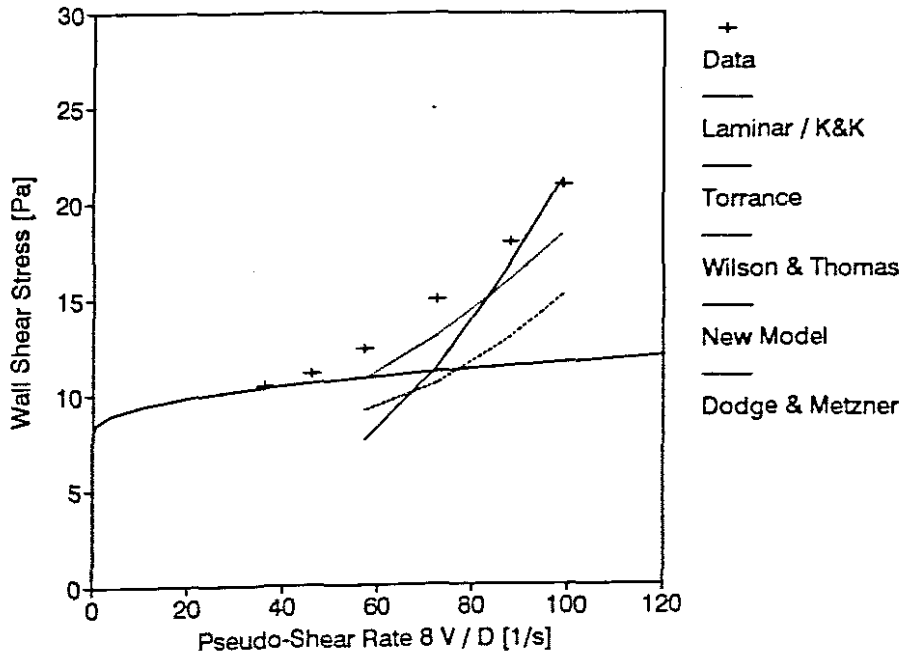
APPENDIX B

B.1   CONFERENCE PAPER - PARTICLE ROUGHNESS TURBULENCE

The conference paper that was presented by the author at HYDROTRANSPORT 13 in support of this thesis is presented in this appendix.

The details of the conference paper are as follows:

"Particle Roughness Turbulence", 13th International Conference on Slurry Handling and Pipeline Transport, Johannesburg, South Africa, September 1996, BHR Group Conference Series - edited by J F Richardson, Mechanical Engineering Publication Limited, UK, pg 237-257.

PARTICLE ROUGHNESS TURBULENCE

by

P T SLATTER, G S THORVALDSEN & F W PETERSEN
Cape Technikon, Cape Town, South Africa

ABSTRACT

The turbulent flow of non-Newtonian slurries has remained a problem, despite much research in this area. The successful resolution of this problem is vitally important not only for hydrotransport applications involving fine slurries, but also for mixed regime slurries, where the vehicle component is usually a non-Newtonian slurry. Two major problem areas are that the turbulent behaviour of these slurries appears unrelated to their laminar behaviour and yet has been found to be strikingly similar to Newtonian turbulent behaviour, in spite of the obvious difference in rheology.

This paper explores these and other problem areas in the literature and shows how previous theoretical models have failed to address them adequately. A new approach to turbulence modelling is reviewed which does address these problem areas. This approach is based on the particle roughness effect, but is as yet relatively untested outside the range of slurries and particle sizes on which it was originally evaluated.

An experimental programme has been initiated to investigate and accumulate a data base of the behaviour of a wider range of non-Newtonian slurries, including slurries with a bimodal particle size distribution. These new data are analysed and the results are presented and discussed. It is concluded that the new approach to turbulence modelling using the particle roughness effect is valid for the slurries tested.

1. INTRODUCTION

The prediction of turbulent flow or pipe flow energy requirements from only the viscous properties of non-Newtonian suspensions has over the years been questioned by researchers. It has been found that the flow behaviour and rheology of these suspensions is influenced by such factors as particle size, shape, weight and distribution (Philippoff 1944, Hedstrom 1952, Orr & Blocker 1955, Zettlemoyer & Lower 1955, Maude & Whitmore 1956, Thomas 1963, Thomas 1983, Mun 1988, Slatter 1994).

The turbulent flow of non-Newtonian suspensions is complex and is often considered problematic to design. However, in many situations it has beneficial characteristics,

preventing suspensions settling and enabling higher throughputs (Mun, 1988). Many theoretical models have therefore been proposed to try and explain and predict turbulent flow behaviour. However, two major problem areas are that the turbulent behaviour of non-Newtonian slurries appears unrelated to their laminar behaviour and yet has been found strikingly similar to Newtonian turbulent flow behaviour, in spite of the obvious difference in rheology.

This paper explores these and other problem areas in the literature and shows how previous models have failed to address them adequately. Slatter's (1994) approach to turbulence modelling, based on his findings on the particle roughness effect, is reviewed. This model addresses these problem areas - however the model was initially evaluated on a limited number of slurries and particle sizes.

Experimental work was conducted at the University of Cape Town's (UCT) Hydrotransport Department, South Africa, using a pumped recirculating pipe test rig of pipe diameters 25mm, 80mm, 150mm and 200mm. Non-Newtonian slurries with varying particle size distributions (PSD's) were tested and analysed, and the results are presented and discussed.

2. LITERATURE REVIEW

2.1 The Yield Pseudoplastic Model

Non-Newtonian slurries can often be modelled as yield pseudoplastics (Govier & Aziz, 1972 and Hanks, 1979) and the laminar flow of all the slurries tested have been successfully characterized using this model. The constitutive rheological equation is

$$\tau = \tau_y + K \left[-\frac{du}{dr} \right]^n , \tag{1}$$

where Ty is the yield stress, K is fluid consistency index and n is the flow behaviour index.

2.2 Laminar Pipe Flow

For laminar pipe flow, volumetric discharge, Q, and average velocity, V, can be determined using the equation

$$\frac{32Q}{\pi D^3} = \frac{8V}{D} = \frac{4n}{K^{\frac{1}{n}} \tau_0^3} (\tau_0 - \tau_y)^{\frac{1+n}{n}} \left[\frac{(\tau_0 - \tau_y)^2}{1+3n} + \frac{2\tau_y(\tau_0 - \tau_y)}{1+2n} + \frac{\tau_y^2}{1+n} \right] , \tag{2}$$

where $\tau_0 = D\Delta p/4L$ and $V = Q/A$.

2.3 Rheological Characterization

Rheological characterization involves choosing a rheological model which best fits the data (the yield pseudoplastic model is used for this study) and then determining the values of τ_y, K and n for a particular slurry. The viscous flow data in the laminar region is coincident for the different tube diameters and the rheological constants (Ty, K and n) were determined using the method proposed by Lazarus & Slatter (1988) and Neill (1988).

2.4 Turbulent Flow

Turbulence is a natural form of fluid motion which is characterized by large, random swirling or eddy motions both parallel and transverse to the direction of the main flow. Particle paths cross and velocity (both direction and magnitude) and pressure, fluctuate on a continuous random basis. The flow behaviour becomes extremely complex and full rigorous analysis becomes impossible (Tennekes & Lumley, 1972).

The turbulent flow of the non-Newtonian slurries that were tested were modelled using Slatter's model as well as the following models which are already well established in the literature,

- Newtonian approximation
- Dodge and Metzner (1959)
- Torrance (1963)
- Kemblowski & Kolodziejski (1973) .
- Wilson & Thomas (1985)

2.4.1 Newtonian Approximation

In order to make use of standard Newtonian theory, a value for the viscosity of the fluid is required. Usually the term viscosity is meaningless once a non-Newtonian approach has been adopted. However, an apparent or secant viscosity (Holland, 1973 and Wilson, 1986) can be defined as

$$\mu' = \frac{\tau_0}{\left[-\dfrac{du}{dr}\right]_0} \cdot \tag{3}$$

Note that μ' is not a constant for a given fluid and pipe diameter, but must be evaluated at a given value for τ_0.

2.4.2   The Dodge & Metzner Model

Dodge & Metzner (1959) developed a turbulent flow model based on the laminar model of Metzner & Reed (1955). The model was developed along the same lines as Newtonian turbulent flow, and the final relationship is of the same format as Newtonian smooth wall turbulent flow, and reverts to the Newtonian form under Newtonian conditions ($K'=\mu$ and $n'=1$).

The relationship is :-

$$\frac{1}{\sqrt{f}} = \frac{4}{n'^{0.75}} \log \left[Re_{MR} \, f^{\frac{2-n'}{2}} \right] - \frac{0.4}{n'^{1.2}} \, .$$
(4)

2.4.3   The Torrance Model

Using the same mixing length model and method of derivation as for Newtonian turbulent flow, Torrance (1963) derived a model for non-Newtonian turbulent flow in pipes using the yield pseudoplastic rheological model (Equation 1) as the starting point. For this model the mean velocity for turbulent flow in smooth pipes is given by

$$\frac{V}{V_*} = \frac{3.8}{n} + \frac{2.78}{n} \ln \left[1 - \frac{\tau_y}{\tau_0} \right] + \frac{2.78}{n} \ln \left[\frac{V_*^{2-n} \, \rho \, R^n}{K} \right] - 4.17 \, .$$
(5)

2.4.4   The Kemblowski & Kolodziejski Model

Kemblowski & Kolodziejski (1973) found that the Dodge & Metzner model did not accurately describe the behaviour of kaolin slurries. They used an empirical approach to model this behaviour based on the pseudoplastic model (K' and n' constant) and a Blasius type equation

$$4f = \frac{0.3164}{Re_{MR}^{0.25}} \, .$$
(6)

They further postulated that the data would lie on a virtually flat f-Re line between the Dodge & Metzner prediction and the above Blasius line (Equation (6)), which they termed a "transition region".

This was modelled empirically as:

$$4f = \frac{E}{Re_{MR}^m} \, \Phi^{1/Re_{MR}} \, , \qquad (7)$$

where E, m and Φ are rheological parameters which are unique functions of the apparent flow behaviour index n'.

2.4.5   The Wilson & Thomas Model

Wilson & Thomas (1985) (also Wilson, 1986 and Thomas & Wilson, 1987) produced an analysis of the turbulent flow of non-Newtonian fluids based on enhanced micro-scale viscosity effects. This model predicts a thickening of the laminar sub-layer by a factor called the area ratio A_r. This area ratio is defined as the ratio of the integrals of the non-Newtonian and assumed Newtonian rheograms (using the apparent or secant viscosity μ') under identical shear conditions. The thickened laminar sub-layer results in an increase in the mean velocity over that for an equivalent Newtonian fluid.

The mean velocity is given by

$$\frac{V}{V_*} = \frac{V_N}{V_*} + 11,6 \, (A_r - 1) - 2,5 \, \ln A_r - \Omega \, , \qquad (8)$$

where V_N is the mean velocity for the equivalent Newtonian fluid based on a secant viscosity (see section 2.4.1) from the yield pseudoplastic rheogram. Ω is a term to account for the blunting of the velocity profile caused by the yield stress,

$$\Omega = -2,5 \, \ln \left[1 - \frac{\tau_y}{\tau_0} \right] - 2,5 \, \frac{\tau_y}{\tau_0} \left[1 + 0,5 \, \frac{\tau_y}{\tau_0} \right] \, . \qquad (9)$$

A method for scale up of turbulent data, based on the above model, has also been proposed (*op cit*).

Rough wall and partially rough wall turbulent flow can be accommodated in the model by using the appropriate roughness when determining V_N. However, this can only be approximate, since the interaction between the pipe roughness and the laminar sub-layer will clearly be different when the thickened laminar sub-layer is present.

2.4.6   The Slatter Model

One fundamental difference between the model proposed by Slatter (1994,1995) and all others is the challenging of the continuum approximation. Traditionally non-Newtonian slurries have been regarded as homogeneous. Clearly, a slurry is a two phase mixture

and can never be truly homogeneous. Treating them as a continuum is therefore an approximation, which works well in the laminar regime. The term homogeneous, when applied to slurries is taken as meaning uniform, stable, spatial distribution of particles.

2.4.6.1 The Laminar Sub-layer

Velocity components normal to the pipe axis cannot exist at the pipe wall, and turbulence is suppressed in this region. Viscous forces are dominant and a laminar sub-layer exists for some finite thickness δ. It has been shown (Slatter, 1994) that the thickness of the laminar sub-layer is of the same order of magnitude as the larger particles in the slurry over the range of wall shear stresses found in turbulent flow. Since the larger particles will be larger than the thickness of the laminar sub-layer at the higher wall shear stress values, the particles must therefore have an obstructing effect on the shear in the laminar sub-layer. The continuum approximation must therefore be compromised in this region.

2.4.6.2 Wall Roughness and the Effect of Solid Particles

Under microscopic investigation it can be seen that the inner wall of the pipe is not smooth but many protrusions exist. The term wall, pipe or surface roughness is used to describe the complex size, shape and spacing of these protrusions. For a given fluid and velocity, roughness in a pipe increases the pressure drop compared with conditions existing in a "smooth" pipe (Bowen 1961, Cheng 1975). At low Reynolds numbers when the laminar sub-layer is sufficiently thick to cover the protrusions on the pipe wall, the roughness will not be effective. At high Reynolds numbers when the laminar sub-layer is not sufficiently thick to cover the protrusions, roughness will be effective. The progressive penetration of the laminar sub-layer by the wall roughness will generate a wake of eddies, stimulating turbulence. This physical phenomenon is of fundamental importance to the understanding of rough wall turbulent flow.

Particles will also have a similar effect to that of the wall roughness, in causing a decrease in the velocity gradient and should be taken into account in turbulent flow analysis.

The change in velocity as the pipe wall is approached is very rapid, the velocity gradient being in the order of 1m/s over the diameter of a typical particle in the region of the pipe wall. If solid particles are present in the fluid they will resist shear and impede such rapid changes in velocity.

A roughness Reynolds number can be used to determine various regions of turbulent flow in a pipe (Schlichting, 1960). The inadequate formulation of the roughness Reynolds number for non-Newtonian slurries is a problem with previous models eg a formulation excluding the yield stress (Torrance, 1963 and Hanks & Dadia, 1971).

2.4.6.3   Representative Particle Size

The wall roughness and particle effect was taken into account in the roughness Reynolds number as given by Slatter (1994).

The effect of roughness on turbulence can be thought of as an aggravation at the wall which stimulates turbulence. Clearly then the larger particles will have a more dominant effect on turbulence than the smaller particles. Also, the larger particles will shield the smaller ones, reducing their effectiveness in stimulating turbulence (Colebrook, 1939).

For all the slurries tested to date it was found that the d_{85} size was a good representation of the turbulent roughness size effect of the solid particles in the slurry ie $d_x = d_{85}$. Where the pipe roughness exceeds the d_{85} size (ie in the 200mm pipe) then $d_x = k$ (Slatter, 1994 and 1995)

2.4.6.4   Similarity Between Newtonian and non-Newtonian Turbulent Flow

Many researchers report similarity between the turbulent behaviour of Newtonian fluids and non-Newtonian slurries (Caldwell & Babbitt 1941, Hedstrom 1952, Metzner & Reed 1955, Dodge & Metzner 1959, Tomita 1959, Michiyoshi *et al* 1966, Edwards & Smith 1980, Thomas & Wilson 1987 and Sive 1988). However, one of the most convincing pieces of evidence to date on the similarity between Newtonian and non-Newtonian slurry turbulent flow is presented by Park *et al* (1989).

Park *et al* (1989) investigated the turbulent structure of a non-Newtonian slurry using laser doppler anemometry and concluded that the transition region is much narrower than for Newtonian fluids. Their non-Newtonian slurry turbulent flow velocity profile agrees well with measurements with air (Newtonian fluid). Furthermore, they reported higher relative turbulence intensities in the wall region for the slurry, when compared with air. This would support the concept of particle roughness.

Pokryvalio & Grozberg (1995) confirmed the findings of Park et al (1994) using electro-diffusion techniques for measuring the velocity profiles of Bentonite clay suspensions and comparing it with air. They reported a significant increase in turbulence intensities in the wall region for the Bentonite clay suspension, providing further support of the concept of particle roughness.

2.4.6.5   New Analysis

The roughness Reynolds number as formulated by Slatter (1994, 1995) is used in order to determine whether smooth wall turbulent flow or fully developed rough wall turbulent flow exists.

$$Re_r = \frac{8 \rho V_*^2}{\tau_y + K \left[\dfrac{8 V_*}{d_x}\right]^n} \cdot \tag{10}$$

If $Re_r < 3,32$ then smooth wall turbulent flow exists and the mean velocity is given by

$$\therefore \frac{V}{V_*} = 2,5 \ln \left[\frac{R}{d_{85}}\right] + 2,5 \ln Re_r + 1,75 . \tag{11}$$

If $Re_r > 3,32$ then fully developed rough wall turbulent flow exists and the mean velocity is given by

$$\frac{V}{V_*} = 2,5 \ln \left[\frac{R}{d_{85}}\right] + 4,75 , \tag{12}$$

and the friction factor is constant.

This correlation produces a transition from the smooth to the rough flow condition which is abrupt.

Tests conducted by Slatter (1994) confirmed the model to be more accurate than the Torrance (1963) model and Wilson & Thomas (1985, 1987) model, when evaluated against experimental data.

2.4.7 Data from the Literature

Experimental data obtained by Sive (1988) was used in the analysis of the various models under consideration. The tests conducted by Sive (1988) were done using a mixture of kaolin clay and a relatively coarse quartz sand, which resulted in a heterogeneous, settling slurry. The purpose of using this data was to see if the coarse, settling particles contributed to the turbulent flow headloss, as proposed by the Slatter model.

3. EXPERIMENTAL WORK

The test facility at UCT which was used had four different pipe diameters namely 25mm, 80mm, 150mm and 200mm nominal bore and slurries were tested at mean velocities ranging from 0,1m/s to 8m/s. Slurries tested included kaolin clay and mixture of kaolin clay and fine sand at varying ratios.

A test set conducted using the facility is defined as a set of tests using the four different pipe diameters but the same slurry.

3.1 Test Facility

Slurry to be used for a test run is collected in a steel hopper which has a capacity $2m^3$. From there it is pumped by a four bladed Mather and Platt 8x6 solids handling pump, which is driven by a variable speed hydraulic drive, through the pipe circuit. Directly after the pump the 150mm line splits up into a 90mm and 150mm pipeline. These two pipelines have a vertical inverted "U" section of 17m, the flowrate being measured in both downcomer sections by means of magnetic flux flow meters. A horizontal section of approximately 30m follows with the return pipelines passing through an in-line heat exchanger and pneumatic diverter valve before being re-routed back into the hopper.

The 150mm horizontal return pipeline splits into a 150mm line and a 200mm pipeline the two joining together after 12m. The 80mm and 150mm pipelines are PVC with clear viewing and test sections located in the horizontal return pipelines. The 200mm line is steel.

Flowrate can be calibrated by diverting the slurry using of the pneumatic diverter valve into the weigh tank which is located alongside the hopper. The weigh tank, which has a capacity of $1,5m^3$ and is placed on a 1750kg mass scale, is used to calibrate the magnetic flux flow meters. After flowrate determinations the slurry is directed back into the looped circuit.

In order to accurately determine the rheology of the slurry a 25mm tube was used. A tapping is taken from the 150mm horizontal return pipeline and using the back pressure, slurry was circulated through the 25mm pipeline into the weigh tank. The flowrate was measured using a 25mm nominal bore Altometer magnetic flux flowmeter. The flowrate of the slurry was checked by doing a calibration using the weigh tank during a 25mm pipe test.

No external agitation was required to maintain solids suspension in the hopper for the slurries which were tested.

3.2 Measured Variables

Readings of head loss were taken at varying velocities and the data obtained was used to plot a pseudo-shear diagram.

3.3 Water Tests

The hydraulic pipe roughness for each of the four pipe sizes was first determined

through conducting clear water pipeline tests. Mean velocity and wall shear stress were measured for velocities over the test range and roughness was determined using the Colebrook / White (1939) equation.

3.3 Material Used

The solids material used for testing purposes was kaolin clay and sand. Tests were conducted using kaolin clay and then a mixture of kaolin clay and No. 2 Foundry Sand from Consol at varying concentrations.

- Kaolin Clay

Kaolin clay was obtained from the Serina Kaolin (Pty) Ltd which is currently mining a kaolin deposit at Brakkekloof, Fish Hoek, Cape Town, South Africa. The kaolin was delivered in the form of pellets and filter cakes. To obtain a homogenous slurry the pellets or filter cake was thoroughly mixed with water using a recirculating pipe after the pump back into the hopper before circulating the slurry through the pipelines.

- Sand

Sand was obtained from Consol in 25kg bags called No. 2 Foundry Sand. The particle size of the sand was between 75 and 350 μm.

3.3.1 Mixtures of Kaolin Clay and Sand

The sand used was found to form a settling slurry with water. In order to obtain a homogeneous slurry, kaolin clay was used as a suspending agent for the sand. Tests were therefore conducted to determine the amount of kaolin clay needed to suspend the sand. It was found that kaolin clay at a concentration of at least $C_v = 5\%$ was required.

3.4 Particle Size Distribution

The particle size distribution of the kaolin clay/sand mixture was obtained by combining the PSD of the kaolin clay (determined using a Malvern 2600/3600 Particle Sizer VF.6) and the PSD of the sand determined through sieving. The d_{85} was then obtained from the combined PSD's as shown below in Figure 1.

4. ANALYSIS & RESULTS

The measured variables of head loss and velocity were used to plot pseudo-shear diagrams ie wall shear stress vs pseudo-shear rate. A typical pseudo-shear diagram is shown in Figure 2 and the improvement obtained using the new model, is clearly visible, as opposed to the other theoretical models.
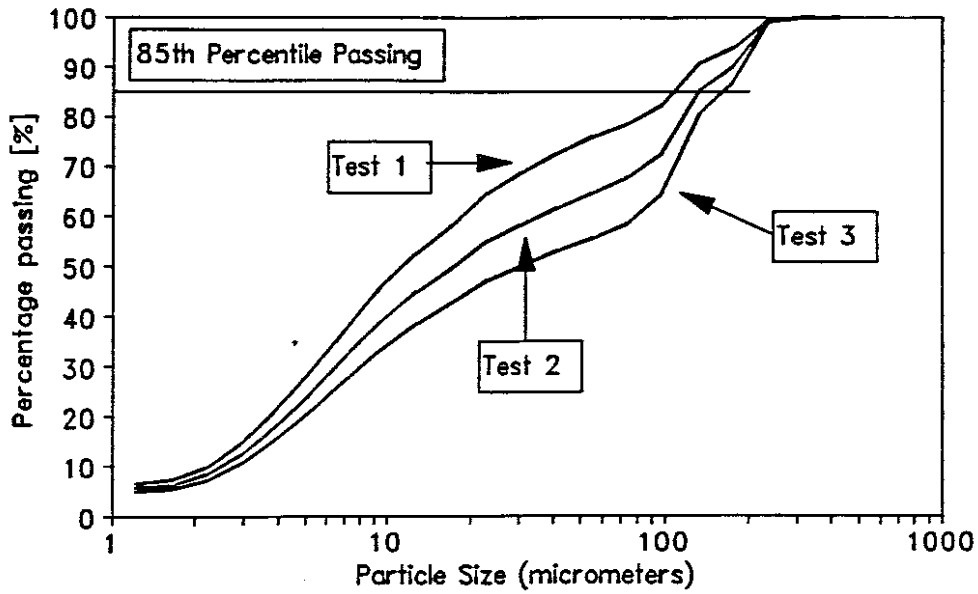
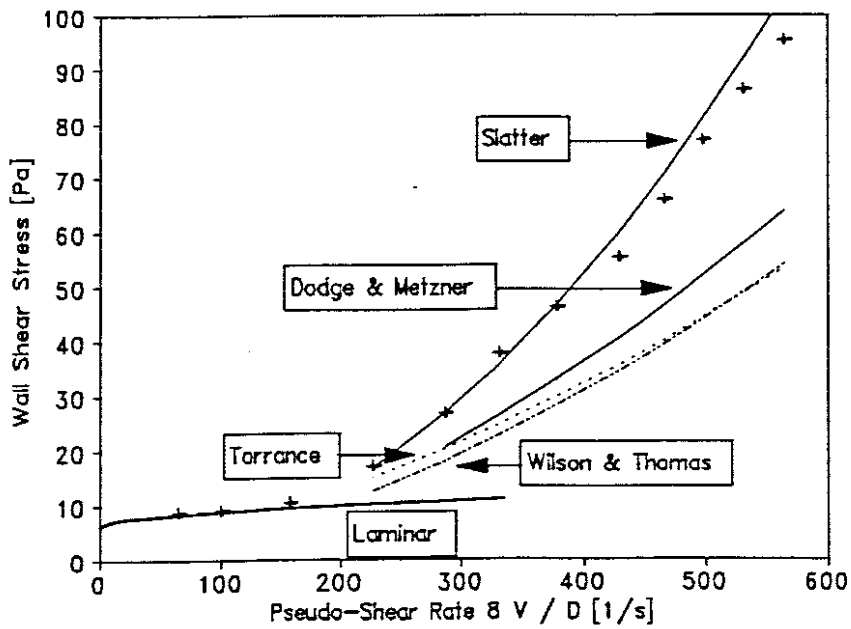**Figure 1: Particle Size Distribution for the Kaolin Clay/Sand Tests**

Figure 2: Pseudo-Shear Diagram of 80mm Pipeline: KSERS10: d_{85} = 109μm

4.1 Rheological characterization

The viscous data in the laminar region is coincident for the different diameters of a test set ie group of tests performed using the same slurry but using a different diameter for each test. The rheological constants (Ty, K and n) were determined from the laminar region of the 25mm pipeline and are presented in Table I together with the pseudo-shear diagram of the rheology of the three sets of sand tests in Figure 3.

The change in behaviour from laminar to turbulent flow is visible by observation of the slurry particles in the transparent tubes during testing. The point at which turbulence begins for each tube size can be clearly seen on the pseudo-shear diagram in each case.

The data obtained was modelled using the theoretical models mentioned in the literature review.

Table I: Summary of Slurry Properties

No	Test	Slurry	$C_v(\%)$	D(mm)	$T_y(Pa)$	$K(Pa.s^n)$	n	S_s	$d_{85}(\mu m)$
1	Sive1 *	Kaolin/Quartz	15.14	79.7	4.89	0.2991	0.484	2.22	1100
2	Sive2 *	Kaolin/Quartz	12.1	139.3	1.99	0.1162	0.5258	2.30	1100
3	KSMRL10	Kaolin/Sand	16.47	21.6	5.82	0.1413	0.5577	2.65	109
4	KSERL10	Kaolin/Sand	16.47	207.0	5.82	0.1413	0.5577	2.65	109
5	KSERM10	Kaolin/Sand	16.47	140.5	5.82	0.1413	0.5577	2.65	109
6	KSERS10	Kaolin/Sand	16.47	79.0	5.82	0.1413	0.5577	2.65	109
7	KSMRL20	Kaolin/Sand	19.43	21.6	5.48	0.1239	0.6363	2.65	131
8	KSERL20	Kaolin/Sand	19.43	207.0	5.48	0.1239	0.6363	2.65	131
9	KSERM20	Kaolin/Sand	19.43	140.5	5.48	0.1239	0.6363	2.65	131
10	KSERS20	Kaolin/Sand	19.43	79.0	5.48	0.1239	0.6363	2.65	131
11	KSMRL30	Kaolin/Sand	23.86	21.6	8.02	0.1350	0.5911	2.65	162
12	KSERL30	Kaolin/Sand	23.86	207.0	8.02	0.1350	0.5911	2.65	162
13	KSERM30	Kaolin/Sand	23.86	140.5	8.02	0.1350	0.5911	2.65	162
14	KSERS30	Kaolin/Sand	23.86	79.0	8.02	0.1350	0.5911	2.65	162

* - Sive rheology for kaolin only

4.2 Laminar Sub-layer Thickness

The laminar sub-layer thickness can be predicted using the Newtonian approximation and the Wilson & Thomas (1985,1987) and Slatter (1994) models. For the first set of kaolin/sand tests, the relationship between wall shear stress and laminar sub-layer thickness is shown in Figure 4. Figure 4 shows that at the higher wall shear stress

values, the laminar sub-layer thickness is less than the diameter of the larger particles.
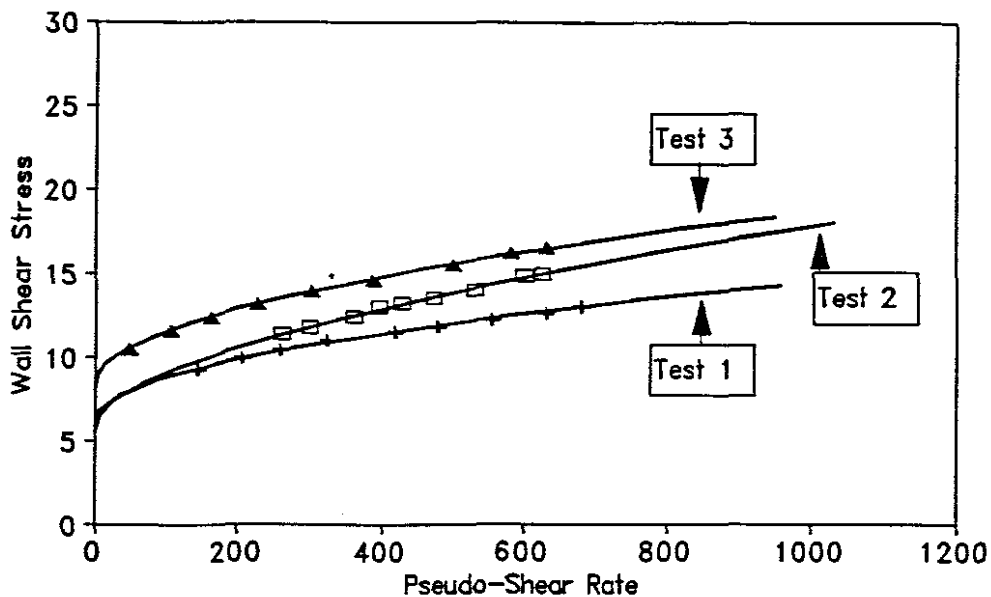

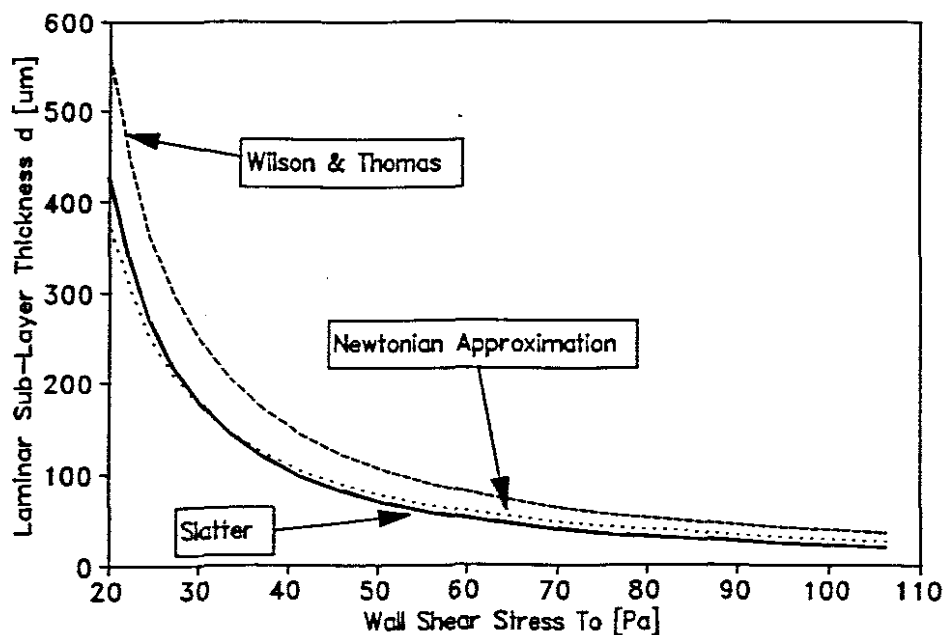**Figure 3: Pseudo-Shear Diagram Showing Rheological Characterization**

Figure 4 : Laminar sub-layer thickness predictions.

4.3 Pipeline Tests

4.3.1 Pipe Roughness

The pipe roughness for the four pipelines is given in Table II.

Table II: Clear Water Test Results

Pipe Diameter (mm)	Pipe Roughness (μm)
25	3
80	6
150	9
200	130

4.3.2 Particle Size Distribution

Figure 5 shows the effect of increasing the representative particle size on the wall shear stress for the 150mm pipeline.
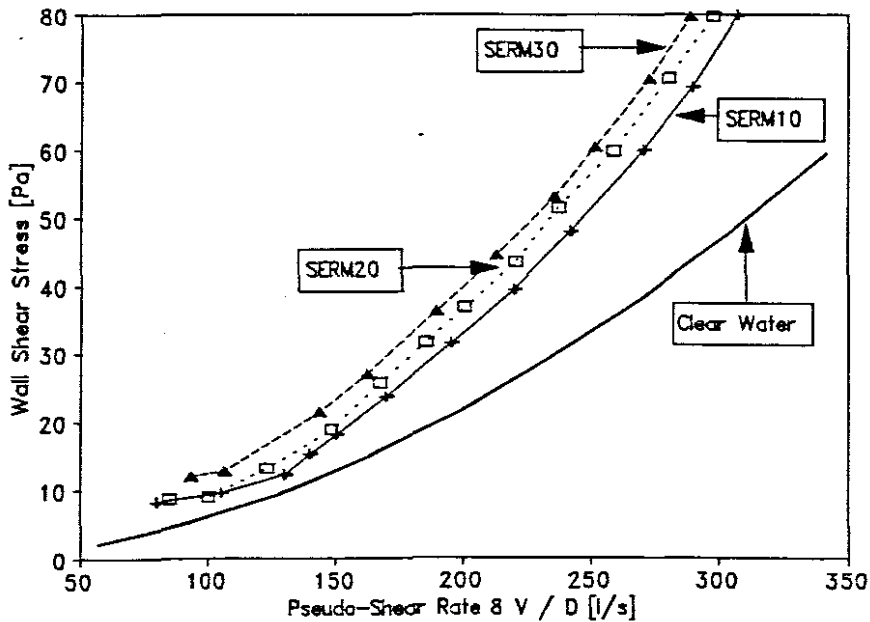

Figure 5: Pseudo-shear diagram for the 150mm pipe showing the data for all three kaolin/sand tests.

4.3.3 Kaolin Clay

Four sets of kaolin clay tests were first conducted to confirm the results already obtained by Slatter (1994). The results obtained supported the existing data set.

4.3.4 Mixture Kaolin Clay & Sand

Tests using a mixture of kaolin clay and sand were conducted in order to obtain a higher representative particle size and different PSD to the existing data set.

4.3.5 Theoretical Models

The turbulent flow performance of the theoretical models is tabulated in Table III showing the average percentage error from the turbulent experimental data. Of the theoretical models under consideration Slatter's model best predicted the test data. The Wilson & Thomas and Torrance models under-predicted head loss regularly. The Kemblowski & Kolodziejski model was also considered, however it did not produce accurate results, significantly over-predicting the head loss.

Table III : Turbulent Model Performance: - Average Percentage Error

No	Test	Slurry	D&M	Torr.	W&T	K&K	Slatter
1	KSMRL10	Kaolin/Sand	65.68	4.89	21.51	324.83	6.60
2	KSERL10	Kaolin/Sand	26.18	18.05	30.27	232.41	17.78
3	KSERM10	Kaolin/Sand	12.77	21.56	24.89	32.69	10.06
4	KSERS10	Kaolin/Sand	31.85	34.66	38.46	12.99	4.86
5	KSMRL20	Kaolin/Sand	7.22	11.60	12.54	286.07	4.18
6	KSERL20	Kaolin/Sand	10.61	3.54	20.85	265.16	11.93
7	KSERM20	Kaolin/Sand	6.55	12.01	14.95	33.64	6.63
8	KSERS20	Kaolin/Sand	17.50	21.72	28.06	21.53	7.89
9	KSMRL30	Kaolin/Sand	64.79	4.25	18.79	246.03	4.63
10	KSERL30	Kaolin/Sand	23.56	12.54	26.56	245.00	24.69
11	KSERM30	Kaolin/Sand	12.50	19.85	23.21	34.71	5.43
12	KSERS30	Kaolin/Sand	24.94	27.55	35.32	44.25	8.32

4.1.5 Data from the Literature

Data from Sive (1988), who used slurries with high representative particle size, was used to model Slatter's theoretical model. As can be seen from the results depicted in Figure 6 (Sive Test 1) Slatter's model was unable to successfully predict the test data of Sive.
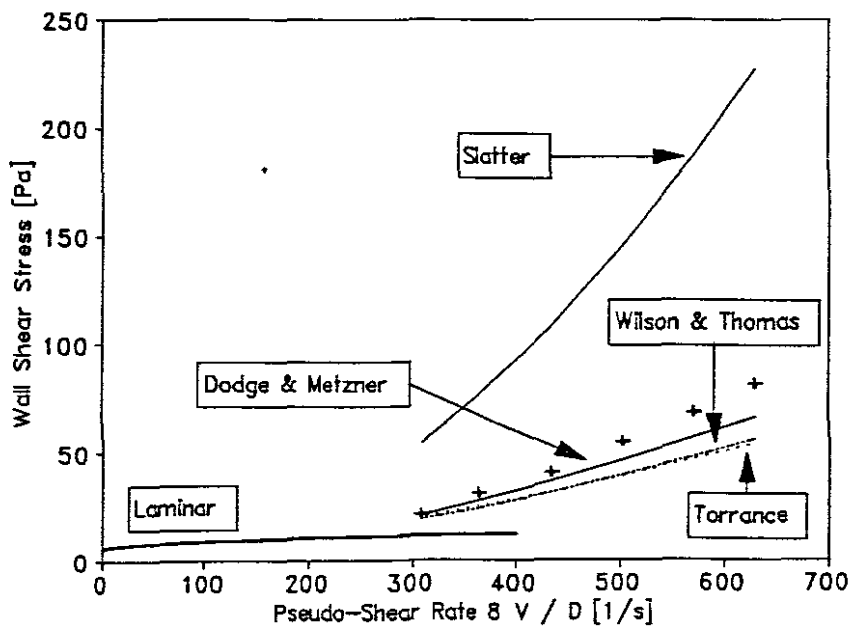

Figure 6: Pseudo-Shear Diagram: Sive Test 1

5. DISCUSSION

Slatter's model was consistently the best model (see Figure 2 and Table III) with increasing representative particle size. This is attributed to the fact that this model is able to account for the particle roughness effect, whereas the other models do not.

Figure 3 and Table 1 show that the rheologies for the three slurry test sets are similar. The increase in wall shear stress shown in Figure 5 is due to the increasing representative particle size as more coarse sand particles were added.

The laminar sub-layer exists in the early turbulent region and in this particular region all models under consideration performed well, except the Kemblowski & Kolodziejski model. For $Re_r > 3,32$ the laminar sub-layer breaks down which is at a laminar sub-layer thickness of approximately $\delta = 3\ d_{85}$. Certainly, a laminar sub-layer cannot exist if it is smaller than the particles which comprise the slurry and the continuum approximation must be compromised.

This investigation highlights the fact that the PSD is a vitally important property of the slurry and should be used for the turbulent flow analysis of non-Newtonian slurries, as has been used in the theory for the new analysis, to account for rough wall turbulent flow and to predict the change from smooth wall to rough wall turbulent flow.

Park *et al* (1989) and Pokryvalio & Grozberg (1995) used very different slurries and experimental techniques, yet both reported significantly higher relative turbulence intensities in the wall region for their slurries, when compared with air. This empirical evidence strongly supports the concept of particle roughness turbulence.

Where Slatter's model fails to accurately predict Sive's data it is felt the reason is that the slurries tested by Sive were settling slurries and not homogenous slurries on which the theoretical model was originally based. Further investigation is required to determine the limit of validity of the particle roughness effect. In fact, the limit of validity of the particle roughness effect could provide a more logical basis for vehicle/load cut-off in mixed regime slurries than is used at present.

Future theoretical modelling of non-Newtonian slurries should take into account both the PSD and the rheology of the slurry.

6. CONCLUSION

Particle roughness turbulence does not apply to settling slurries (as tested by Sive, 1988). Further investigation is required to determine the limit of validity of the particle roughness effect, and this limit could well serve as the criterion for vehicle/load cut-off in mixed regime slurries.

The particle roughness turbulence model is the first model to incorporate the continuum compromise which must arise as the laminar sub-layer thickness is limited, and it is the only model to explain the empirical evidence of increased turbulence intensities in the wall region.

It can be concluded from the test data results that the new approach to turbulence modelling using the particle roughness effect is valid and can be successfully adopted for non-Newtonian slurries.

Acknowledgement

NOMENCLATURE

Symbol	Description	Unit
A	cross sectional area	m^2
A_r	area ratio	
C	concentration	
d	particle diameter	μm
D	internal pipe diameter	m
E	rheological parameter	
f	Fanning friction factor	
k	hydraulic roughness	μm
K	fluid consistency index	$Pa.s^n$
K'	apparent fluid consistency index	$Pa.s^{n'}$
L	pipe length	m
m	rheological parameter	
n	flow behaviour index	
n'	apparent flow behaviour index	
p	pressure	Pa
Q	volumetric flow rate of slurry	m^3/s
r	radius at a point in the pipe	m
R	radius of the pipe	m
Re	Reynolds number	
S	relative density	
u	point velocity	m/s
V	average slurry velocity	m/s
$V_\bullet$	shear velocity	m/s
y	distance from the pipe wall	m
δ	laminar sub-layer thickness	μm
Δ	increment	
μ	dynamic viscosity	Pa.s
μ'	apparent dynamic viscosity	Pa.s
ρ	slurry or fluid density	kg/m^3
τ	shear stress	Pa
τ_y	yield stress	Pa
Φ	rheological parameter	
Ω	velocity function	

Subscripts

0   at the pipe wall
85   85th percentile of the particles passing
r   roughness

s   solids
v   volumetric
x   representative size

REFERENCES

BOWEN R LeB (1961), How to handle slurries, *Chem. Eng.*, August 7, 129-132

CALDWELL D H and BABBITT H E (1941), The flow of muds, sludges and suspensions in circular pipes, *Trans. Am. Inst. Chem. Eng.*, 37, 237-266.

CHENG D C-H (1975), Pipeline design for non-Newtonian fluids, *Chem. Eng.*, September, 525-532.

COLEBROOK C F (1939), Turbulent flow in pipes, with particular reference to the transition region between the smooth and rough pipe laws, *J. Instn. Civil Engrs.*, No. 4, Paper 5204.

DODGE D W and METZNER A B (1959), Turbulent flow of non-Newtonian systems, *AIChE Journal*, Vol. 5, No. 2, 189-204.

EDWARDS M F and SMITH R (1980), The turbulent flow of non-Newtonian fluids in the absence of anomalous wall effects, *Journal of non-Newtonian fluid mechanics*, 7, 77-90.

GOVIER G W and AZIZ K (1972), The Flow of Complex Mixtures in Pipes, *van Nostrand Reinhold Co.*

HANKS R W (1979), The axial laminar flow of yield-pseudoplastic fluids in a concentric annulus, *Ind Eng Chem Process Des Dev*, 18, 3.

HANKS R W and DADIA B H (1971), Theoretical analysis of the turbulent flow of non-Newtonian slurries in pipes, *AIChE Journal*, Vol 17 No 3, 554-557.

HEDSTRÖM B O A (1952), Flow of plastics materials in pipes, *Industrial and engineering chemistry*, v.44 No.3.

HERSCHEL W H and BULKLEY R (1926), Measurement of consistency as applied to rubber-benzene solutions, *Proc ASTM*, 26 Part 2 621-633.

HOLLAND F A (1973), *Fluid flow for chemical engineers*, Edward Arnold, London.

IRELAND, J W (1971), *Mechanics of fluids*, Butterworths.

KEMBLOWSKI Z and KOLODZIEJSKI J (1973), Flow resistances of non-Newtonian fluids in transitional and turbulent flow, *Int. Chem. Eng.* 13 265-279.

LAZARUS J H and SLATTER P T (1988), A method for the rheological characterisation of tube viscometer data, *Journal of pipelines*, v.7.

MAUDE A D and WHITMORE R L (1958), The turbulent flow of suspensions in tubes, *Trans. I. Chem Eng.*, 36 296-310.

METZNER A B and REED J C (1955), Flow of non-Newtonian fluids - correlation of the laminar, transition and turbulent flow regions, *AIChE Journal*, v.1 n.4.

MICHIYOSHI I, MATSUMOTO R, MIZUNO K and NAKAI M (1966), Flow of slurry through a circular tube. Friction factor for tubes. Part II., *Int Chem Eng*, 6,2.

MUN R (1988), Turbulent pipe flow of yield stress fluids, M Eng Sci Thesis, University of Melbourne.

NEILL R I G (1988), The rheology and flow behaviour of high concentration mineral slurries, Msc Dissertation, University of Cape Town.

ORR C and BLOCKER HG (1955), *Journal Colloid Sci*, 10, 24.

PARK J T, MANNHEIMER R J, GRIMLEY T A, MORROW T B (1989), Pipe flow measurements of a transparent non-Newtonian slurry, *Journal of fluids engineering*, Vol. 111, 331-336.

PHILIPPOFF W (1944), Viskositat Der Kolloide, Lithoprinted by J W Edwards, Ann Arbor, Mich.

POKRYVAILO N A and GROZBERG Yu G (1995), Investigation of structure of turbulent wall flow of clay suspension in channel with electrodiffusion method, *Proc. 8th Int. Conf. on Transport and sedimentation of solid particles*, Prague, Czech Republic.

SCHLICHTING H (1960), Chapter XX in *Boundary layer theory*, 4th edition, McGraw-Hill, New York.

SIVE A W (1988), An analytical and experimental investigation of the hydraulic transport of high concentration mixed regime slurries, PhD thesis, University of Cape Town.

SLATTER P T (1994), Transitional and turbulent flow of non-Newtonian slurries in pipes, PhD thesis, University of Cape Town.

SLATTER P T (1995), The turbulent flow of non-Newtonian slurries in pipes, *Proc. 8th Int. Conf. on Transport and sedimentation of solid particles*, Prague, Czech Republic.

TENNEKES H and LUMLEY J L (1972), *A first course in turbulence*, The MIT Press, Cambridge, Massachusetts.

THOMAS A D (1983), Turbulent pipe flow of Bingham plastics, *Proc. 3rd Nat. Conf. Rheol.*, Brit. Soc. Rheol. (Aust), Melb., 83-87.

THOMAS A D and WILSON K C (1987), New analysis of non-Newtonian flow- yield-power-law fluids, *Can J Chem Eng*, 65 335-338.

THOMAS D G (1963), Non-Newtonian suspensions Part III Turbulent transport characteristics, *Industrial and engineering chemistry*, Vol 55, No. 12, December, 27-35.

TOMITA Y (1959), A study on non-Newtonian flow in pipes, *Bull JSME*, Vol 2 No 5.

TORRANCE B M^{c}K (1963), Friction factors for turbulent non-Newtonian flow in circular pipes, *S. A. Mechanical Engineer*, v.13.

WILSON K C (1986), Modelling the effects of non-Newtonian and time-dependent slurry behaviour, *10th Int. Conf. on the hydraulic transport of solids in pipes*, Hydrotransport 10 Paper J1.

WILSON K C, ADDIE G R and CLIFT R (1992), *Slurry transport using centrifugal pumps*, Elsevier Science Publishers Ltd, Essex, England.

WILSON K C and THOMAS A D (1985), A new analysis of the turbulent flow of non-Newtonian fluids. *Can. J. Chem. Eng.*, 63, 539-546.

XU J, GILLIES R, SMALL M and SHOOK C A (1993), Laminar and turbulent flow of kaolin slurries, *12th Int. Conf. on slurry handling and pipeline transport*, Hydrotransport 12, BHR Group, p595.

ZETTLEMOYER A C and LOWER G W (1955), *Journal Colloid Sci*, 10, 29.